Physiological relevance of the E3 ubiquitin ligase HERC1

Arturo Martínez Martínez

UNIVERSITAT DE BARCELONA

DOCTORAL PROGRAM in BIOMEDICINE

Physiological relevance of the E3 ubiquitin ligase HERC1

Doctoral thesis submitted by:

Arturo Martínez Martínez

Thesis conducted under the direction of:

Dr. José Luis Rosa López

Departament de Ciències Fisiològiques
Facultat de Medicina i Ciències de la Salut
Campus Bellvitge - Universitat de Barcelona – 2022

CONTENTS

FIGURE INDEX

INTRODUCTION

MATERIALS AND METHODS

RESULTS

TABLE INDEX

INTRODUCTION

MATERIALS AND METHODS

ABBREVIATIONS AND ACRONYMS

1,25(OH)$_2$D	Active vitamin D
ACC1	Acetyl-CoA carboxylase 1
ACLY	ATP-citrate lyase
Acrp30	Adiponectin gene
ACS	Acetyl-coenzyme A synthetase
ALP	Alkaline phosphatase
Alpha-MEM	Minimum Essential Medium Eagle Alpha Modification
ALPL	Alkaline phosphatase gene
AMPK	Adenosine monophosphate protein kinase
ANCOVA	Analysis of covariance
ATF4	Activating Transcription Factor 4
ATGL	Adipocyte triglyceride lipase
ATP	Adenosine triphosphate
AUC	Area under the curve
BAK	BCL2-antagonist/killer
BAT	Brown adipose tissue
BgAT	Beige adipose tissue
BGLAP	Bone gamma-carboxyglutamic acid-containing protein, Osteocalcin
BMI	Body mass index
BM-MSC	Bone marrow mesenchymal stem cell
BMP	Bone morphogenetic protein
BMR	Basal metabolic rate
bp	Base pairs
BSA	Bovine serum albumin
BV/TV	Bone volume/tissue volume
C/EBP	CCAAT/enhancer binding protein
cAMP	Cyclic adenosine monophosphate
CBL	Casitas B-lineage lymphoma
CHC	Clathrin heavy chain
CHIP	C-terminus of HSC70-interacting protein

ChORE	Carbohydrate response element
ChREBP	Carbohydrate response element binding protein
CIDEA	Cell Death Inducing DFFA Like Effector A
CML	Chronic myeloid leukaemia
COL1A1	Collagen type I alpha 1 chain
CTSK	Cathepsin K
dH_2O	Distilled water
DHT	Dihydrotestosterone
DIO	Diet-induced obesity
DLX5	Distal-less homeobox 5
DMEM	Dulbecco's Modified Eagle's medium
DMP1	Dentin matrix protein 1
DNA	Desoxyribonucleic acid
DSSP	Dentin sialophosphoprotein
DTT	Dithiothreitol
ECL	Enhanced chemiluminescence
ECM	Extracellular matrix
EDTA	Ethylenediaminetetraacetic acid
EE	Energy expenditure
ERK	Extracellular signal-regulated kinase
EtBr	Ethidium Bromide
FASN	Fatty acid synthase
FATP	Fatty acid transporter protein
FBS	Foetal bovine serum
FBW7	F-box/WD repeat-containing protein 7
FBXO25	F-box protein 25
FFA	Free fatty acid
FGF23	Fibroblast growth factor 23
FMOD	Fibromodulin
G3P	Glycerol-3-phosphate
GEF	Guanine-nucleotide exchange factor

GLUT4	Glucose transporter type 4
GRF	Guanine-release factor
GTP	Guanosine triphosphate
GTT	Glucose tolerance test
gWAT	Gonadal white adipose tissue
H&E	Haematoxylin & Eosin
HA	Hydroxyapatite
HCl	Hydrochloric acid
HECT	Homologous to E6-AP carboxy terminus
HERC	RCC1-like domain-containing HECT proteins
HF	Heart failure
HFD	High fat diet
HSC	Hematopoietic stem cell
HSL	Hormone-sensitive lipase
IBSP	Bone sialoprotein 2
IKMC	International Knockout Mouse Consortium
IL	Interleukin
IMPC	International Mouse Phenotyping Consortium
IR	Insulin receptor
ITT	Insulin tolerance test
iWAT	Inguinal white adipose tissue
kDa	Kilo Daltons
KO	Knock-out
LA	Locomotor activity
LD	Loading dye
LDS	Lithium dodecyl sulphate
Lep	Leptin gene
LEPR	Leptin receptor
L-Gln	L-Glutamine
LPL	Lipoprotein lipase
MAPK	Mitogen-activated protein kinase

M-CSF	Macrophage colony stimulating factor
MDFPMR	Macrocephaly, dysmorphic facies, and psychomotor retardation
MEPE	Matrix extracellular phosphoglycoprotein
MGL	Monoacylglycerol lipase
MGP	Mouse Genetics Project
Micro-CT	Micro-computed tomography
MITF	Microphthalmia-associated transcription factor
MK2	MAPK-activated protein kinase 2
MLX	Max-like protein X
MMP-9	Matrix metalloprotease 9
mRNA	Messenger RNA
MSC	Mesenchymal stem cell
MSH2	MutS homolog 2
mTOR	Mammalian target of rapamycin
Myf5	Myogenic factor 5
NAFLD	Non-alcoholic fatty liver disease
$NaNO_2$	Sodium nitrite
NASH	Non-alcoholic steatohepatitis
NBCS	Newborn calf serum
NCP	Non-collagenous protein
NEFA	Non-esterified fatty acid
NFATc1	Nuclear factor of activated T cells 1
NFκB	Nuclear factor kappa B
NMR	Nuclear magnetic resonance
NPY	Neuropeptide Y
Ob	Obese gene (leptin)
OMIM	Online Mendelian Inheritance in Man
OPG	Osteoprotegerin
ORF	Open reading frame
OSX	Osterix
PAGE	Polyacrylamide gel electrophoresis

PBS	Phosphate buffered saline
PCR	Polymerase chain reaction
PDE-3B	Phosphodiesterase 3B
PFA	Paraformaldehyde
PGC1α	PPAR-gamma-coactivator-1-alpha
PKA	Protein kinase A
PML	Promyelocytic leukaemia
PMSF	Phenylmethylsulfonyl fluoride
PP2A	Protein phosphatase 2A
PPARγ	Peroxisome proliferator-activated receptor gamma
PRDM16	PRD1-BF1-RIZ1 homologous domain containing 16
PTH	Parathyroid hormone
PTM	Post-translational modification
PVDF	Polyvinylidene difluoride
PWT	Posterior wall thickness
RANKL	Receptor activator of NFκB ligand
RCC1	Regulator of chromosome condensation 1
RING	Really interesting new gene
RLD	RCC1-like domain
RNA	Ribonucleic acid
RQ	Respiratory quotient
RSK2	Ribosomal protein S6 kinase 2
RUNX2	Runt-related transcription factor 2
SCD1	Stearoyl-CoA desaturase-1
SDS	Sodium dodecyl sulphate
SEM	Standard error of the mean
shH1	Short hairpin RNA against HERC1
shRNA	Short hairpin RNA
SIBLING	Small integrin-binding ligand N-linked glycoproteins
SKP2	S-phase kinase-associated protein 2
SMURF1	SMAD ubiquitination regulatory factor 1

SNS	Sympathetic nervous system
SOST	Sclerostin
SOX18	Sex determining region Y-box 18
Sp7	Osterix
SPRY	SPla and ryanodine receptor domain
SRE	Sterol regulatory element
SREBP-1c	Sterol response element binding protein 1c
sWAT	Subcutaneous white adipose tissue
SWT	Septum wall thickness
TAE	Tris-Acetate EDTA
Tb.N	Trabecular number
Tb.Th	Trabecular thickness
tbl	*Tambaleante*
TG	Triglyceride
TNAP	Tissue non-specific alkaline phosphatase
TNF	Tumour necrosis factor
TRAF6	Tumor necrosis factor receptor-associated factor 6
TRAP	Tartrate-resistant acid phosphatase
TSC1	Tuberous sclerosis complex 1 (hamartin)
TSC2	Tuberous sclerosis complex 2 (tuberin)
UCP1	Uncoupling protein 1
UPS	Ubiquitin proteasome system
UV	Ultraviolet
VEGF	Vascular endothelial growth factor
VLDL	Very low-density lipoprotein
vWAT	Visceral white adipose tissue
WAT	White adipose tissue
WHO	World Health Organization
WT	Wild type
WWP	WW Domain Containing E3 Ubiquitin Protein Ligase
β-HPV5	Beta-human papillomavirus 5

ABSTRACTS

English abstract

HERC1 is a E3 ubiquitin ligase that belongs to the Large HERC family, a group of proteins characterized by the presence of a HECT domain, responsible for their ubiquitin ligase activity, and two or more RLD domains. Mutations in HERC1 gene in humans have been related to different types of cancers and neurological diseases. The study of its physiological relevance using mouse models have been focused on the analysis of the *tambaleante* mice, that carry a recessive missense mutation in Herc1 gene that leads to increased levels of the protein. Although the neurological phenotype of the *tambaleante* mice been extensively investigated, few data is available about the role of HERC1 in other physiological processes.

Bone and adipose tissue are two highly dynamic organs, that are subjected to constant remodelling and have an active role in the secretion of several factors with autocrine, paracrine and endocrine effects. The homeostasis and function of both these tissues are tightly regulated by a plethora of molecular mechanisms, including MAPK signalling and ubiquitylation. Furthermore, these organs are in a continuous crosstalk in which the factors secreted by one are involved in the regulation of the other. Consequently, dysfunction of one of these tissues is usually accompanied by alterations in the homeostasis of both.

The main objective of this thesis has been the characterization of the role of HERC1 in different physiological processes in vivo. With this purpose, a new mouse model has been used, consisting in mice displaying a 191 bp deletion within Herc1 gene. As a result of this deletion, HERC1 protein is absent in all the tissues analysed, thus being a loss-of-function knock-out (KO). Among the physiological processes studied, the focus of the thesis has been set on describing of the alterations of bone homeostasis provoked by *Herc1* knock-out and the role of this gene in the regulation of systemic energy balance and its implications on adipose tissue phenotype.

The first part of the thesis evaluates the effect of the depletion of HERC1 in bone remodelling. The results show that, although silencing of *Herc1* seems to induce osteoblastic differentiation in vitro, knock-out animals display progressive osteopenia

that starts before in young females but finally affects both sexes at an increased age. The analysis of the causes of this bone loss revealed that the absence of Herc1 provokes a significant stimulation of osteoclast differentiation and function, thus increasing bone resorption and unbalancing bone remodelling.

For the second part of the thesis, the modulation of energy balance by HERC1 was assessed. The knock-out of the gene has a sex-dependent effect, as it causes a dysfunction of non-shivering thermogenesis in females that leads to the reduction of energy expenditure and ultimately to the energy disbalance towards increased fat accumulation. As a consequence of this, female *Herc1*-KO mice present symptoms compatible with metabolic syndrome, such as insulin resistance. The switch of the animals a high fat diet revealed that both male and female KO mice were more susceptible to the development of obesity, although the effects of the lack of Herc1 were still more severe in females.

Taken together, all these data stablish a first characterization of the physiological relevance of HERC1 as a regulator of bone and adipose homeostasis and energy balance in vivo, as well as its potential role in other tissues such as the myocardium. Although further research is needed to unveil the molecular mechanisms underlying these effects, these results suggest that dysfunctions of HERC1 could lead to higher susceptibility to diseases such as osteoporosis or diabetes.

Spanish abstract

HERC1 es una E3 ubicuitina ligasa que pertenece a la familia Large HERC, un grupo de proteínas caracterizadas por la presencia de un dominio HECT, responsable de su actividad ubicuitina ligasa, y dos o más dominios RLD. Mutaciones en el gen de *HERC1* en humanos han sido relacionadas con diferentes tipos de cánceres y enfermedades neurológicas. El estudio de su relevancia fisiológica usando modelos murinos se ha centrado en el análisis del ratón tambaleante, que presenta una mutación sin sentido recesiva en el gen *Herc1* que va ligada a un incremento en los niveles de la proteína. Aunque el fenotipo neurológico del ratón tambaleante ha sido extensamente investigado, existe poca información sobre el papel de HERC1 en otros procesos fisiológicos.

El hueso y el tejido adiposo son dos órganos dinámicos, que están sujetos a un constante remodelado y tienen un rol activo en la secreción de diversos factores con efecto autocrino, paracrino y endocrino. La homeostasis y función de ambos tejidos están estrechamente reguladas por una plétora de mecanismos moleculares, que incluyen señalización por MAPK y ubicuitilación, entre otros. Además, estos órganos están continuamente comunicados entre sí, pues los factores secretados por uno están generalmente implicados en la regulación del otro. Consecuentemente, la disfunción de uno de estos tejidos generalmente se acompaña de alteraciones en la homeostasis de ambos.

El principal objetivo de esta tesis ha sido la caracterización del papel de HERC1 en diferentes procesos fisiológicos *in vivo*. Con este propósito, se ha utilizado un nuevo modelo animal, que consiste en ratones con una deleción de 191 pares de bases dentro del gen *Herc1*. Como resultado de esta deleción, la proteína HERC1 está ausente en todos los tejidos analizados, siendo este un modelo *knock-out* de pérdida de función. Entre los procesos fisiológicos estudiados, esta tesis se ha enfocado en describir las alteraciones de la homeostasis ósea provocadas por la eliminación de HERC1 y el papel de este gen en la regulación del balance energético y sus implicaciones en el fenotipo del tejido adiposo.

La primera parte de la tesis se centra en evaluar el efecto de la depleción de HERC1 en el remodelado óseo. Los resultados muestran que, aunque el silenciamiento de *Herc1* parece inducir la diferenciación osteoblástica in vitro, los ratones *knock-out* desarrollan una osteopenia progresiva que empieza antes en las hembras jóvenes pero que finalmente afecta a ambos sexos a una edad más avanzada. El análisis de las causas de esta pérdida de hueso reveló que la ausencia de HERC1 provoca una estimulación significativa de la diferenciación y función de los osteoclastos, lo que conlleva un incremento de la reabsorción de hueso y un desbalance del remodelado óseo.

En la segunda parte de la tesis se estudió la modulación del balance energético por HERC1. La depleción de este gen tiene un efecto dependiente del sexo, ya que causa una disfunción de la termogénesis adaptativa únicamente en hembras, lo cual lleva a una reducción del gasto energético y finalmente a un desbalance energético que provoca un incremento en la acumulación de grasa. Como consecuencia, las hembras *knock-out* de *Herc1* presentan síntomas compatibles con el síndrome metabólico, como la resistencia a la insulina. Cuando estos animales fueron alimentados con una dieta alta en grasa, se reveló que tanto los machos como las hembras deficientes del gen *Herc1* son más susceptibles al desarrollo de obesidad, aunque los efectos de la falta de HERC1 son más severos en las hembras.

Como resumen final, todos estos datos establecen una primera caracterización de la relevancia fisiológica de HERC1 como regulador del balance energético y de la homeostasis del hueso y el tejido adiposo, así como su potencial papel en otros tejidos como el miocardio. Aunque futuros experimentos son necesarios para destapar los mecanismos moleculares que subyacen a estos efectos, estos resultados sugieren que las disfunciones de HERC1 pueden conferir una mayor susceptibilidad a enfermedades como la osteoporosis o la diabetes.

INTRODUCTION

CHAPTER I. UBIQUITYLATION

I.1. Ubiquitylation

Ubiquitylation is one of the most thoroughly studied post-translational protein modifications (PTMs). It is a process that consists in the conjugation of ubiquitin – a 76 amino acid protein – to other proteins in a variety of distributions: monoubiquitylation (in a single residue), multiubiquitylation (in multiples residues) or polyubiquitylation. In the latter, ubiquitylation of one of the seven lysine residues of a substrate-attached ubiquitin leads to the formation of a ubiquitin chain. If the same residue is modified for every molecule of ubiquitin, the homogenous chain is named after the lysine that is being used for polymerization. With these signals, ubiquitylation controls many responses such as protein binding, chromatin condensation, intracellular trafficking or the targeting of proteins for proteasomal or autophagic degradation[1]. Dysregulation of this mechanism has broad effects that range from aberrant activation or deactivation of cellular pathways to accumulation of misfolded proteins. Thus, alterations in the ubiquitylation process are responsible for many physiopathological situations such as cancer, immune pathologies, neurodegenerative diseases and metabolic syndromes[2].

The binding of ubiquitin to the substrate is a 3-step process. First, a ubiquitin-activating enzyme (E1) binds the ubiquitin monomer to a cysteine residue within its structure in an ATP-dependent manner. Then, a ubiquitin-conjugating enzyme (E2) loads the ubiquitin from the E1 and binds the last enzyme, the ubiquitin ligase (E3), which catalyse the covalent union of the ubiquitin to a lysine residue in the target protein (Figure 1A). Substrate specificity in ubiquitylation is determined by its interaction with E3 enzymes, which are in turn responsible for the regulation of their target proteins[3]. In human genome, there are annotated two E1s, around 38 E2s and over 600 E3 enzymes[4].

Ubiquitin ligases can be classified according to their ubiquitin ligase domain. There are two main families: **RING** (Really interesting new gene) and **HECT** (Homologous to the E6-AP carboxyl terminus). E3 ligases with a RING domain act as

scaffolds for the ubiquitylation: they bind the E2 and the target protein and facilitate the transferring of the ubiquitin from the E2 to the substrate (Figure 1). Conversely, ubiquitin ligases with a HECT domain present an active cysteine residue (Cys) that binds the ubiquitin from the E2 forming a thioester bond before transferring it to the substrate (Figure 1C). In humans, there are approximately 600 types of RING and 30 types of HECT E3s[5,6].

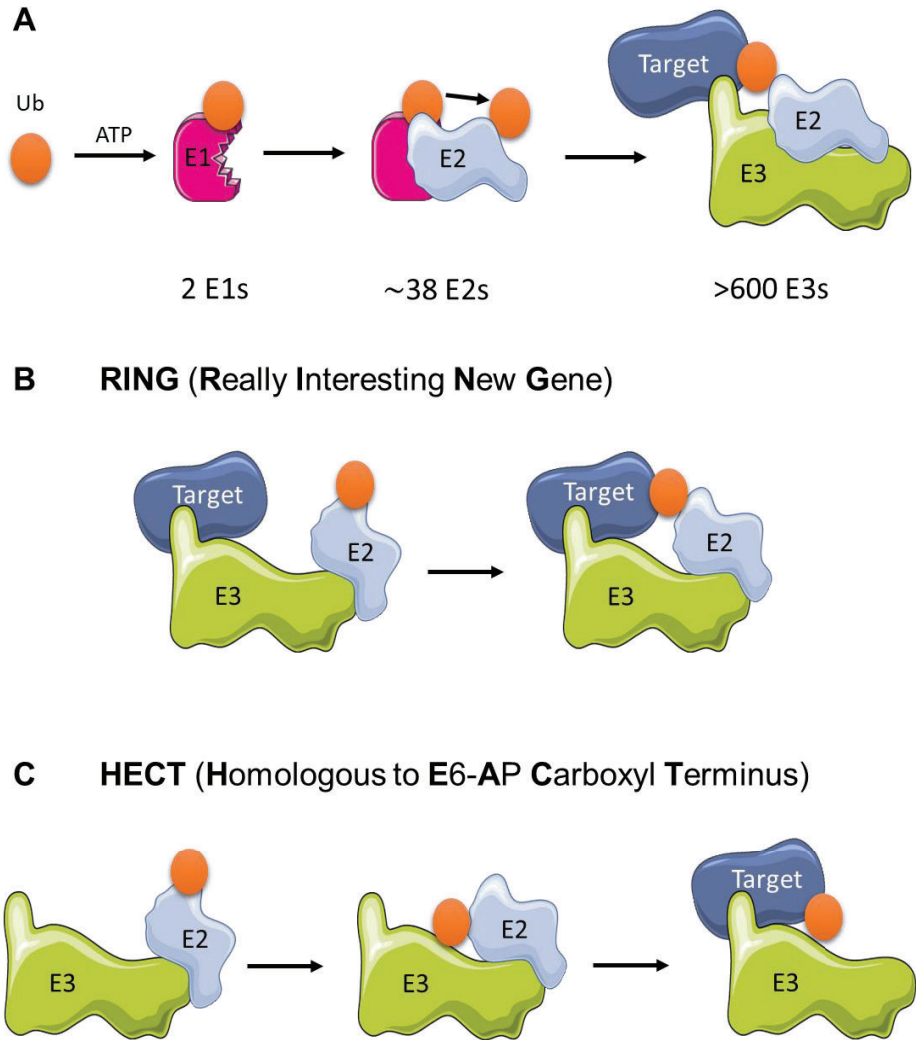

Figure 1. Ubiquitylation process. A) Schematic representation of the ubiquitylation cascade. The ubiquitin is first activated by an E1 enzyme with ATP consumption. Then, ubiquitin is transferred to a E2 enzyme, which in turn binds to an E3 to mediate the ubiquitylation of the target protein. **B) Mechanism of action of the RING ubiquitin ligases**. E3 RINGs bind the target and the E2 and mediate the transferring of the ubiquitin directly from the E2 to the target. **C) Mechanism of action of HECT ubiquitin ligases.** HECT E3s transfer the ubiquitin from the E2 to a residue within its own structure, and then catalyze the ubiquitylation of the target.

HECT ubiquitin ligases are characterized for the presence of a **HECT domain** in their C-terminal region. This domain has approximately 350 amino acids and is named after its high similarity to the carboxyl extreme of the protein E6AP[7]. HECT domain forms a bilobed structure consisting of a helix-turn-helix motif packed with two antiparallel β sheets at the N end and four at the C end. This structure facilitates the transmission of the ubiquitin from the catalytic cysteine in the C-terminal lobe of the domain to the target[8,9]. Even if the HECT domain confers the catalytic activity, substrate specificity is determined by the interaction of the target proteins to their other domains. Depending on the composition and distribution of these different domains, HECT proteins can be divided in several groups.

Classically, human HECTs have been classified in 3 families: tryptophan-tryptophan (WW) domain-containing HECT proteins (**NEDD4-like family**), RCC1-like domain (RLD)-containing HECT proteins (**HERC family**) and HECT proteins lacking both of those domains, named as "**single HECTs**"[3,6]. Nevertheless, sequence comparison analysis yielded a much more complex division of the HECT family into **16 different subgroups**: NEDD4-like proteins, **Small HERCs**, **Large HERCs** and 13 different subfamilies of the miscellaneous classification formerly known as "single HECTs"[10].

I.2. Large HERC family

As stated above, although traditionally classified together with the Small HERC proteins, sequence analysis demonstrated that Small and Large HERCs actually form two distantly related protein families. Classically, the HERC family had been characterized by the presence of and HECT domain and one or more RLD domains within the protein structure[11]. However, it was demonstrated that the RLD domains from Small and Large HERCs had important structural differences[12], and that these domains were acquired by each family in two independent events. Therefore, the similarity between these two protein families is due to convergent evolution rather to a common phylogenetic history[10].

Large HERC protein family is composed of two members, **HERC1** and **HERC2**. They are characterized by the presence of a HECT, more than one RLD and some other

domains. This complexity in their domain structure confers them a huge size. In humans, HERC1 has 4861 amino acids and HERC2 presents 4834 amino acid residues. This equals to a molecular weight of 532 and 528 kDa, respectively. HERC1, besides the HECT domain, possesses two RLD domains, an SPla and ryanodine receptor (SPRY) domain, a BH3 domain and a WD40 region, which is a Trp-Asp (W-D)-rich 40-amino acid repeat. HERC2, in turn, presents a HECT, three RLDs, a cytochrome b5 (Cyt b5) domain, a mind-bomb/HERC2 (M-H) domain, a Cul7, PARC and HERC2 (CPH) domain and other conserved sequences such as ZZ zinc fingers and DOC (Figure 2)[9,11].

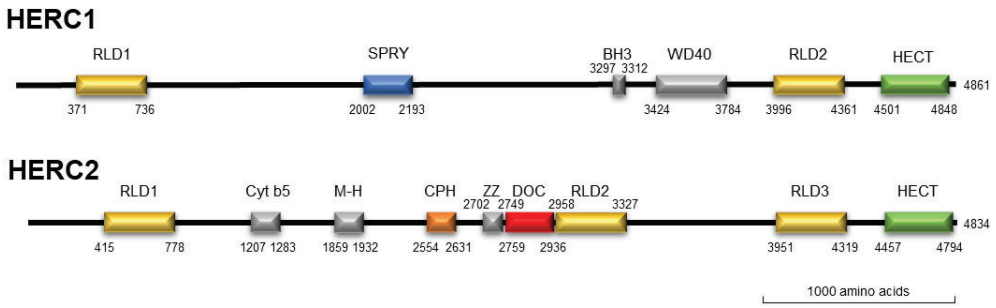

Figure 2. Primary structure of human HERC1 and HERC2. The approximate relative position of each protein domain is depicted as indicated by ScanProsite domain predictions with the amino acid sequences. Adapted from García-Cano *et al.*, 2019[9].

The **RLD domain** was first described in RCC1 protein[13]. Its tertiary structure is composed of seven β blades prone to a radially symmetric distribution that resembles the shape of a propeller[14]. Functionally, RCC1 exerts a double function: it acts as a guanine-nucleotide exchange factor (GEF) for the GTPase Ran and also interacts with chromatin through histones H2A and H2B to participate in the cell cycle regulation, microtubule nucleation, nucleocytoplasmic transport and nuclear envelope and mitotic spindle formation[12,15,16].

The evolutionary origin of the Large HERC family has been tracked to Choanoflagellatea, although they are mainly expressed in animals. In fact, only HERC2 appears in some Choanoflagellatea species, such as *Monosiga brevicollis* and *Salpingoetta rosetta*. The emergence of HERC1 occurred at the Choanoflagellatea – Metazoa split, with both proteins being already present in the metazoan placozoan

Trichoplax adhaerens (Figure 3). Phylogenetic analysis of the amino acid sequences of HERC1 and HERC2 have shown that these proteins segregate in two clusters with higher similarity between orthologues, and that the phylogenetic relationships of the sequences within the clusters coincide with the evolution of the species (Figure 3). This indicates that Large HERCs, since their emergence, have been well conserved in almost all the Metazoa phyla. Remarkable exceptions are the absence of HERC1 in most of the Arthropoda clade, although it is possible to find the protein in some species of insects[9,10]. Curiously, HERC2 sequence from choanoflagellate *S. rosetta* display a SPRY domain, characteristic of HERC1. However, the low degree of similarity between this domain and the SPRY present in *T. adhaerens* HERC1 indicates that this presence is due to convergent evolution, a common event in HECT proteins, rather to homology[9,10].

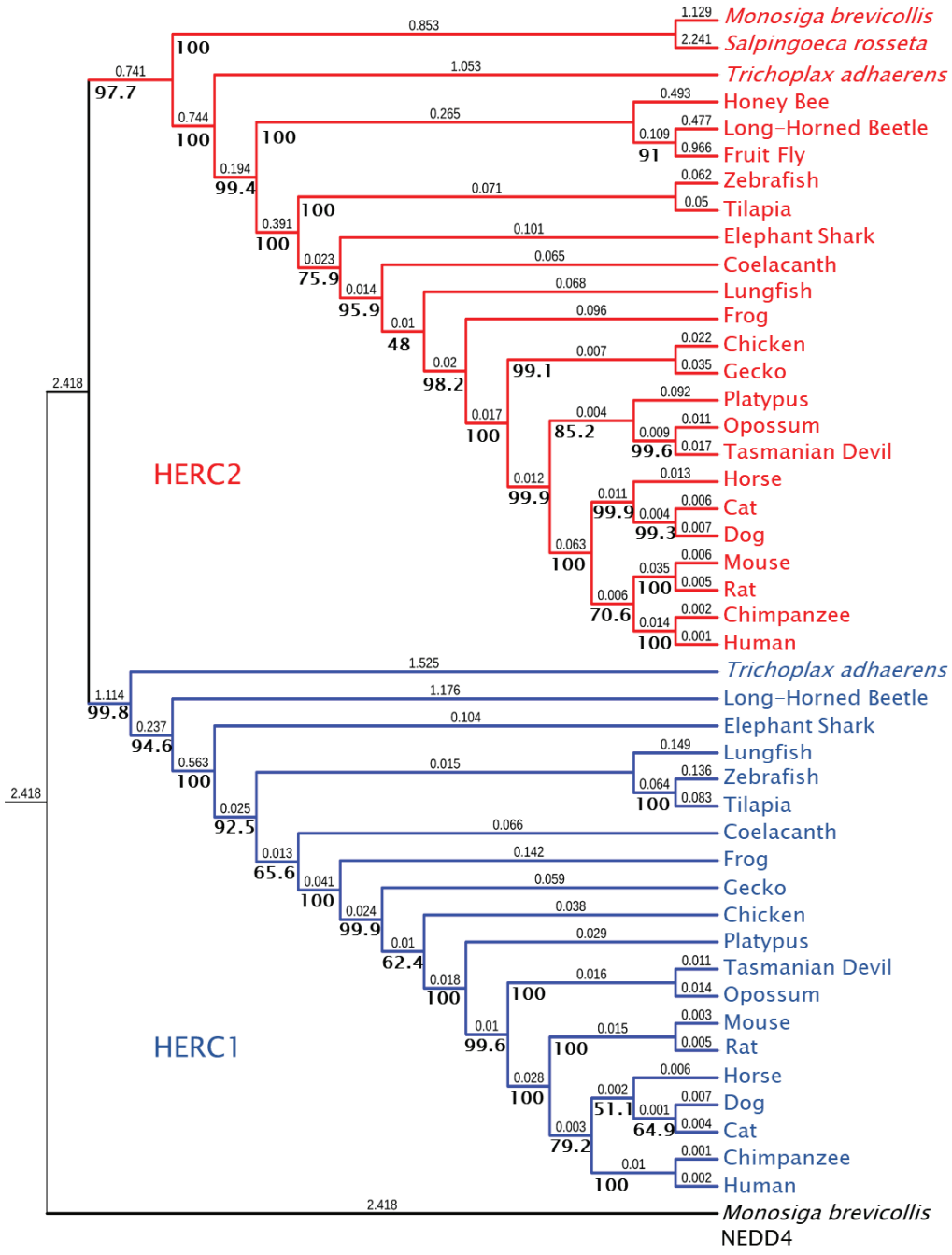

Figure 3. Molecular phylogeny of Large HERCs. The tree shows the clustering of HERC1 (blue) and HERC2 (red) amino acid sequences from significative choanoflagellate and metazoan species. Ultrafast bootstrap support (1,000 replicates) is shown next to the branches in bold. Smaller numbers indicate branch lengths. NEDD4 protein from *Monosiga brevicollis* was used as an outgroup. Adapted from García-Cano et al. 2019[9].

I.3. HERC1

HERC1, initially known as p619 and p532, was the first member discovered of the Large HERC family. It was described in 1996 in a search for oncogenic activity in sequences isolated from human breast adenocarcinoma, using nude mouse tumorigenicity assays. The full-length cDNA clone of this gene was isolated from a human fetal brain cDNA library, with a single open reading frame (ORF) of 14,585 nucleotides that predicted a 4861 amino acid long polypeptide. Its subcellular distribution was found limited to cytoplasm and Golgi/vesicular-like membrane compartments[17]. Human *HERC1* gene contains 78 exons and has been mapped to **chromosome 15q22**[18,19]. This gene is expressed in all mammalian tissues, with higher expression in testis and brain and lower in liver, and it was found overexpressed in several human tumour cell lines[17].

The first study that described HERC1 also proposed that the RLD1 domain acted as a GEF for ARF1 and certain proteins from the Rab family of GTPases[17]. This was supported by the previous role described for RCC1 as a GEF of Ran[15]. Nevertheless, posterior studies found that RLD1 in HERC1 does not function as a GEF but as a **guanine-release factor (GRF)** of ARF proteins. Hence, instead of stimulating GDP/GTP exchange and activate ARF and Rab GTPases, HERC1 stimulates the dissociation of guanine nucleotides from these proteins, thus inhibiting them. This process is also dependent on the binding of phosphatidylinositol-4,5-bisphosphate [PI(4,5)P2] to the RLD1 domain[20]. The RLD2 domain, conversely, exhibit no GEF or GRF activity, but it is able to bind myristoylated ARF1 and to interact with clathrin heavy chain (CHC) and the heat-shock protein HSP70[17,21]. Following the proposed role of HERC1 in membrane trafficking supported by the regulation of ARF and Rab proteins and the interaction with CHC, it was also found that HERC1 is recruited to actin-rich surface protrusions after ARF6 activation by aluminium fluoride. The translocation of HERC1 to these actin-rich structures was proposed to be via its interaction with PI(4,5)P2, since these phospholipids are abundant in these protrusions[22]. A posterior study also identified HERC1 as a putative binding partner of IQAP1, a key interactor centre for GTPase regulators[23].

It has been described that HERC1 binds ubiquitin in a reaction catalysed by the E2 enzyme UbcH5[24]. Through this, the active cysteine of the HECT domain is loaded with a ubiquitin monomer that will be subsequently transferred to a target. The first ubiquitylation substrate that has been validated for HERC1 was the serine/threonine protein kinase **C-RAF**[25]. C-RAF is one of the three isoforms of RAF (A-, B- and C-RAF), which is an important part of the mitogen-activated protein kinase (MAPK) pathway of ERK. In this signalling cascade, upon stimulation of a receptor tyrosine kinase in the cell surface, RAS GTPase is activated, and this in turn activates RAF. Activated RAF phosphorylates and activates MEK, which in turn phosphorylates ERK. This activated ERK is able to phosphorylate hundreds of different substrates, thus coordinating a cellular response to external stimuli. Dysregulation of this pathway has long been associated with human cancers. In fact, in one-third of them, this signalling cascade has been found overactivated[26–28]. HERC1 plays a role in the regulation of this pathway by polyubiquitylating C-RAF with a lysine 48-linked chain, a mark that targets the protein to proteasomal degradation (Figure 4A). Therefore, depletion of HERC1 has been proved to cause a dysregulation of the ERK pathway and consequently an increase in cellular proliferation[25]. Moreover, in a posterior study it was found that HERC1 regulation of C-RAF not only influences ERK activity, but also the p38 MAPK pathway[29]. In this work, Pedrazza *et al.* show that HERC1 act as a modulator of a previously unknown crosstalk between p38 and ERK MAPK pathways by which RAF proteins regulate the levels of MKK3, an upstream kinase of p38. Hence, the rise in C-RAF levels derived of the lack of HERC1 results in an increase of p38 activation coupled with enhanced cell migration. Altogether, these studies reveal that the ubiquitin ligase activity of HERC1 is essential for the regulation of important cellular processes such as proliferation or migration (Figure 4B)[25,29,30]. More recently, a **second ubiquitylation substrate** has been described for HERC1. **PSMC5**, a subunit of the proteasome, has been discovered to be targeted for degradation by HERC1 when unassembled. Through this mechanism, HERC1 acts as a quality control factor monitoring failures in proteasome assembly, as it facilitates the removal of unassembled intermediates[31].

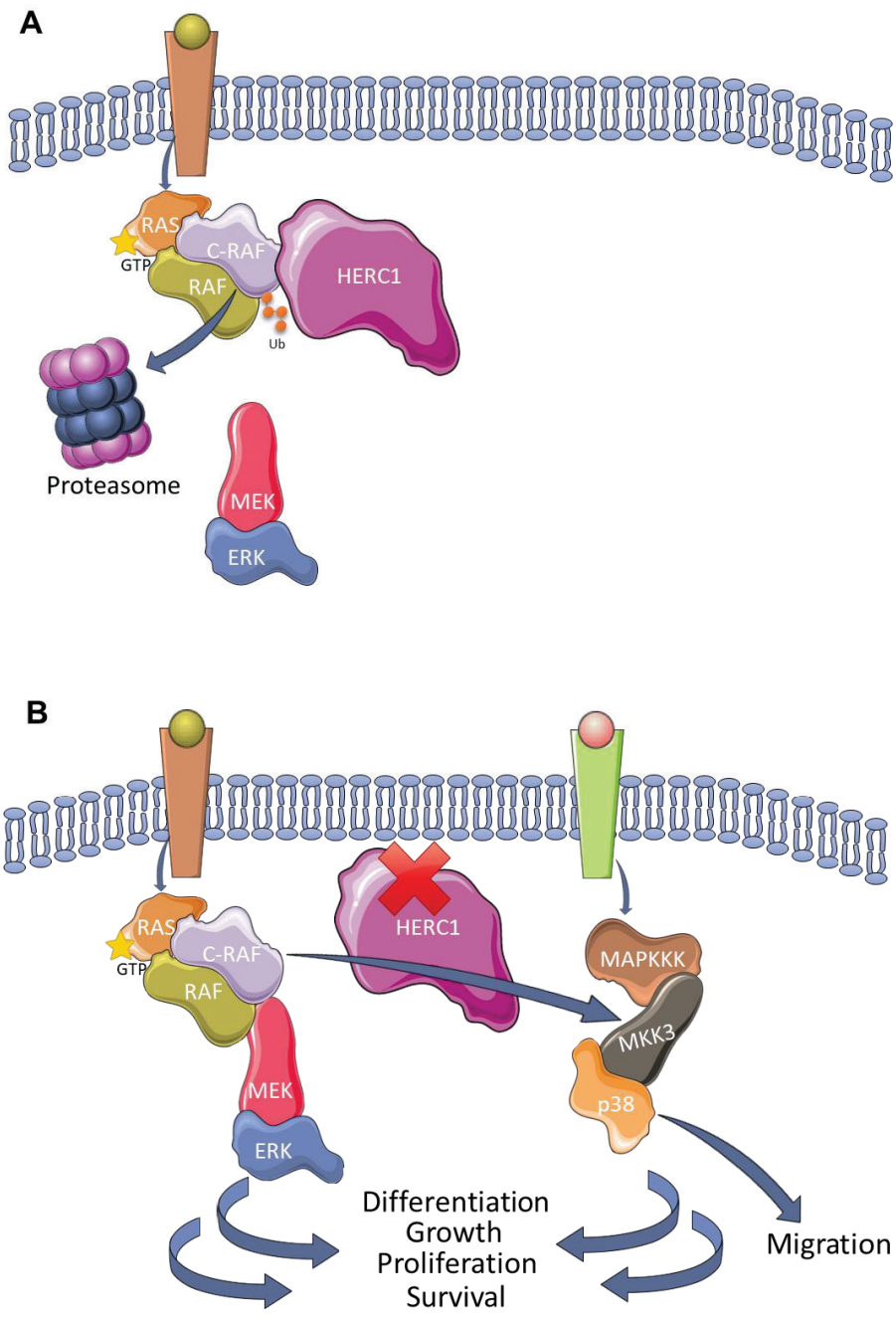

Figure 4. Regulation of MAPK pathways by HERC1. A) HERC1 binds to C-RAF protein and ubiquitylates it in a lysin 48-linked chain, thus marking it for degradation in the proteasome. This interrupts the signalling cascade that leads to ERK. **B**) When HERC1 is absent, C-RAF protein levels are risen and this leads both to an overactivation of ERK signalling and to an increase in MKK3 levels, which in turn causes hyperphosphorylation of p38. The conjunction of ERK and p38 increased activity enhance the cellular responses regulated by these MAPK, including the migration, differentiation, growth, proliferation and survival. Adapted from Sala-Gaston *et al.*, 2020[28].

Besides its ubiquitin ligase activity, the HECT domain has also been found to be necessary for the binding of the glycolytic isoenzyme M2 pyruvate kinase (M2-PK) to HERC1. Although this enzyme is usually related to proliferative tissues and cancer cells, the physiological relevance of this interaction has not been elucidated, as no enzymatic or ubiquitin-ligase activity has been detected as a result[32]. The carboxyl terminus of HERC1 also mediates its binding to the tuberous sclerosis complex 2 protein (TSC2), also called tuberin. This interaction with the C-terminal region of HERC1 prevents TSC2 to bind to hamartin (tuberous sclerosis complex 1: TSC1)[33]. The complex between hamartin and tuberin is needed for the regulation of cell growth through inhibition of the mammalian target of rapamycin (mTOR) pathway[34]. Chong-Kopera *et al.*[33] proposed that HERC1 binding to TSC2 destabilise the complex, giving a role to the ubiquitin ligase as a regulator of the mTOR signalling. This effect of TSC2 stability has been proposed as a mechanism for the regulation of the protein levels of the DNA mismatch repair enzyme MutS homolog 2 (MSH2)[35]. Diouf *et al.* found that somatic mutations in HERC1 were linked to decreased levels of MSH2 protein in leukaemia cells. They suggest that the loss of HERC1 provokes a stabilization of TSC2, which results in a more efficient inhibition of mTOR leading to the overactivation of protein phosphatase 2A (PP2A). The dysregulation of PP2A would be the cause of MSH2 destabilization. By that mechanism, HERC1 plays a role in maintaining genomic integrity in leukaemia cells[35].

The aforementioned works clearly suggest that HERC1 alterations may be related to **cancer**. Actually, there are now many studies that relate HERC1 to different types of human cancers (Table 1)[30]. It is involved in non-melanoma skin cancer through its interaction with the E6 protein of β-human papillomavirus 5 (β-HPV5), which is needed for the degradation of the pro-apoptotic protein BCL2-antagonist/killer (BAK). This prevents the UV-induced apoptosis of damaged epithelial cells[36]. A genomic fusion of *HERC1* with promyelocytic leukaemia (*PML*) gene was found in one patient with acute promyelocytic leukaemia[37]. Moreover, mutations or depletion of *HERC1* gene have been related to other types of leukaemia[38–40], to different types of breast cancer[41–43] and to a rare case of pulmonary sclerosing pneumocytoma[44]. In addition, in osteosarcoma cells there was found a negative correlation of HERC1 mRNA levels with

the expression of Sex determining region Y-box 18 (SOX18), a protein usually overexpressed in this type of tumour[45]. The relation of HERC1 with leukaemia is still widening, as a recent study also found that HERC1 expression was severely downregulated in acute and chronic leukaemia, but also that this expression is restored after remission. Besides, they report that, in chronic myeloid leukaemia (CML) cells, HERC1 interacts with the BCR-ABL1 fusion protein and is phosphorylated by it[46]. As the BCR-ABL1 fusion is the paradigmatic malignant event in CML[47], HERC1 being a substrate of its kinase activity supports its implication in the regulation of the cancerous phenotype.

Table 1. Cancers associated with HERC1 and related molecular mechanisms. Adapted from Sala-Gaston et al., 2020.[30]

Associated cancer	Related molecular mechanism	Reference
Acute lymphoblastic leukaemia	*HERC1* mutation leading to MSH2 destabilization	35
Sporadic colorectal cancer	*HERC1* mutation leading to MSH2 destabilization	35
Non-melanoma skin cancer	Enhanced BAK protein degradation	36
Acute promyelocytic leukaemia	*HERC1-PML* genomic fusion	37
Acute myeloid leukaemia	*HERC1* mutations and *HERC1* mRNA downregulation	38,46
Adult T-cell acute lymphoblastic leukaemia	*HERC1* mutations	39
T-cell prolymphocytic leukaemia	*HERC1* mutations	40
Invasive lobular breast cancer	*HERC1* mutations	41
Metastatic triple-negative breast cancer	*HERC1* mutations and *HERC1* depletion	42,43
Pulmonary sclerosing pneumocytoma	*HERC1* mutations	44
Osteosarcoma	Negative correlation of SOX18 overexpression and HERC1 mRNA levels	45
Chronic myeloid leukaemia	*HERC1* mRNA downregulation. Interaction with BCR-ABL1 fusion protein.	46
Kidney cancer	*HERC1* expression correlates with better prognosis	48,49

Head and neck cancer	*HERC1* expression correlates with better prognosis	48,49
Pancreatic cancer	*HERC1* expression correlates with better prognosis	48,49
Oesophageal cancer	*HERC1* mRNA differently expressed	50
Gastric cancer	*HERC1* mRNA differently expressed	50
Non-small cell lung cancer	*HERC1* expression correlates with poor overall survival	51
Ovarian cancer	*HERC1* expression correlates with poor prognosis	52

Altogether, these studies point to HERC1 as a possible **tumour suppressor protein**. This is also supported by data from the Human Protein Atlas, that show that patients with kidney, head and neck and pancreatic cancers have greater survival when their HERC1 expression levels are higher[48,49]. However, recent genome-wide studies have also related HERC1 to poor prognosis in oesophageal and gastric cancers[50], non-small cell lung cancer[51] and ovarian carcinoma[52]. Future research will be interesting to further unravel the molecular mechanisms by which HERC1 regulates the cell pathways responsible for cancer transformation in different physiological contexts.

Apart from cancer, HERC1 has also been related to **neurological disorders**. Homozygous or compound heterozygous mutations in *HERC1* gene have been detected in patients with common clinical features leading to the describing of the Macrocephaly, dysmorphic facies, and psychomotor retardation (MDFPMR) syndrome (OMIM #617011)[53]. In addition to the common features that share the individuals suffering this syndrome, there has also been described ataxic gait and hypotonia in two of them[54], epilepsy, thick corpus callosum and cerebellar atrophy in another[55], and hypotonia, kyphoscoliosis, epilepsy and autistic features in another[56]. There was also described a pair of siblings with a *HERC1* splice variant mutation with the common features of MDFPMR but no other apparent affectations[57]. Recently, a study also found a gain-of-function mutation of *HERC1* in two sisters that displayed MDFPMR accompanied with epilepsy, somatic overgrowth, seizures, schizoaffective disorder and pyramidal tract signs[58]. Furthermore, HERC1 has also been considered a predictor of

autism risk by several genetic studies that have associated *HERC1* mutations with autism spectrum disorders[59,60]. Hence, there is increasing evidence that reveal the *HERC1* important role in neuropathology in humans. The molecular mechanisms underlying this have been thoroughly studied in the *tambaleante* mouse model, that will be detailed next.

I.3.1. HERC1 mouse models

I.3.1.1. Tambaleante mouse model

The ***tambaleante*** **(*tbl*)** mouse has been the standard model to study the role of HERC1 *in vivo*. These mice carry an autosomal recessive mutation that arose spontaneously in the DW/JPas genetic background at the Institut Pasteur in 1987. It was reported that this mutation was causing progressive degeneration of Purkinje cells after 2 months of age that was paired with a severe ataxic syndrome[61]. Posterior studies with these mice described degenerative changes in Purkinje cells axons and dendrites and demonstrated that increased autophagy was involved in the death of these cells[62,63]. However, it was not until 2009 that this mutation was characterized as a G1448A transition in the *Herc1* gene, mapped at murine chromosome 9[64]. This change of nucleotide results in a Gly483Glu amino acid substitution in the RLD1 domain of HERC1 that presumably alters the structure of the protein and its function, although it also causes an increase in the levels of HERC1 in all analysed tissues. In this study, Mashimo *et al.* corroborated the enhanced autophagy reported in degenerative Purkinje cells and linked it with a decrease in mTORC1 activity, a pathway that had already been described to be regulated by HERC1 through its interaction with TSC2[64]. These authors also describe that *tbl* homozygous animals had significantly reduced growth and lifespan and that they were fertile but poor breeders[64].

Further characterization of the neurological phenotype of *tbl* mice have proved that these animals also present reduced motor learning capacities[65]. Moreover, they also show affectations unrelated with the cerebellum phenotype: In neuromuscular junctions, it has been reported that the neurotransmitter release is impaired[66]. In CA3 hippocampal pyramidal, neocortical pyramidal and spinal cord motor neurons there is a defective ubiquitin-proteasome-driven protein aggregate clearance and an increased

autophagic flux[67]. Besides, HERC1 has been found necessary for the normal axonal myelination in the peripheral nervous system, and consequently *tambaleante* mice display poor myelination and delayed action potential transmission[68]. Furthermore, there have been detected ectopic dendritic spines in *tbl* mice, although the total number of mature spines is decreased. These alterations are consistent to other physiological alterations also detected in these mice: altered long-term potentiation, fewer synaptic vesicles, a decrease in glutamatergic inputs and defects in memory and associative and spatial learning[69,70]. Recently, a study with cultured *tambaleante* hippocampal neurons have shown that HERC1 regulates presynaptic membrane dynamics in central synapses. In this work, they report that the presynaptic terminals of *tbl* mice have fewer docked synaptic vesicles, more endosomes and autophagosomes, reduced active zones and less presynaptic endings over the hippocampal main dendritic trees. Besides, they demonstrate that the mutated RLD1 domain of HERC1 as a result of *tbl* mutation is unable to bind CHC, which could explain part of the affectations observed in synaptic vesicles, since clathrin binding is one of the proposed mechanisms for HERC1 regulation of membrane trafficking[71].

Altogether, the study of the *tambaleante* model has been a great tool for deepen the knowledge about the physiological role that HERC1 plays in the nervous system. However, few data have shed light on the other functions that this protein could have in other organs. Furthermore, it is still not clear how the *tbl* mutation exactly affects HERC1 function. For this motive, the combination of this mouse model with other genetic models would be an interesting strategy for further characterize the physiological relevance of HERC1 *in vivo*.

I.3.1.2. Herc1-*knockout mouse model*

In 2007, the International Knockout Mouse Consortium (IKMC) stablished the aim of generate mutations in every coding gene known in the murine genome. For that, they have developed high-throughput gene trapping and gene-targeting strategies[72–74]. In the line of these efforts, Dr. Chris Tyler-Smith and Dr. Michal Szpak generated a ***Herc1*-knockout (KO) mouse strain** in a C57BL/6N genetic background (C57BL/6N-*Herc1*$^{em3(IMPC)Wtsi}$/Wtsi (EM:10257)), at the Wellcome Trust Sanger Institute. The mutated allele was generated by a Crispr/Cas9 mediated deletion of 191 base pairs (bp)

including the exon 8 on the *Herc1* gene (Figure 5A). The protein encoded by this mutated allele was thus truncated, and western blot analysis revealed that this protein was undetectable in all analysed tissues (Figure 5B). Hence, the *Herc1* KO generated is total for all mice organs.

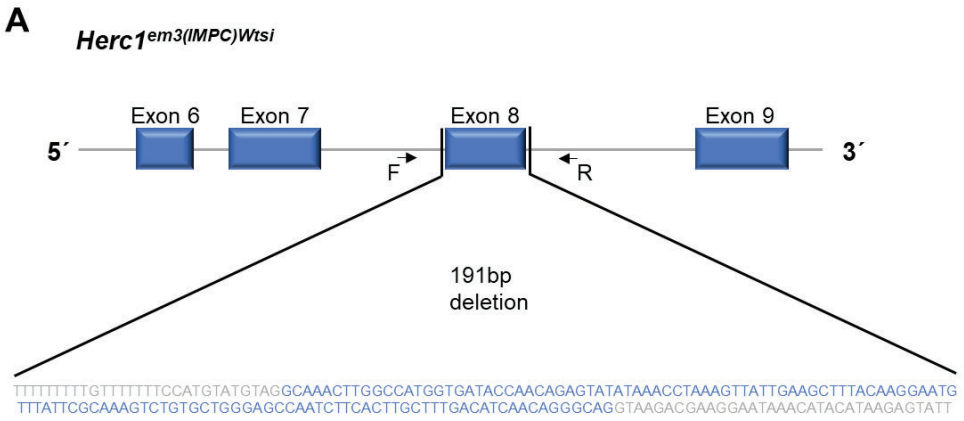

Figure 5. *Herc1* knockout mouse. A) Genetic region of the mutation. A 191 bp deletion eliminates exon 8 of the Herc1 gene, generating the *Herc1*$^{em3(IMPC)Wtsi}$ mutated allele. **B)** Protein expression of HERC1 in liver, kidney, spleen and brain from wild-type (WT) and *Herc1*-KO C57BL/6N mice, analysed by Western Blot. CHC (Clathrin Heavy Chain) was used as a loading control. Abbreviations: WT, wild-type; KO, *Herc1*-knockout.

As a part of the Sanger Mouse Genetics Project (MGP), these mice were subjected to a preliminary phenotyping. Data from these animals is publicly available at the International Mouse Phenotyping Consortium (IMPC) and can be obtained in: https://www.mousephenotype.org/data/genes/MGI:2384589[75]. In comparison with wild types, *Herc1*-KO mice were reported to present increased total body fat amount, decreased lean body mass, impaired glucose tolerance, decreased bone mineral content and male infertility, among other phenotypes. This evidence suggests that HERC1 play a role in many more physiological processes that have not been studied before in the

tambaleante model, and that the *Herc1*-KO mice are a powerful tool for unravelling this physiological relevance. Nevertheless, as this phenotyping was part of a systematic process aimed at the generation of a high number of new mouse mutant strains, the characterization of these phenotypes is limited and preliminary. Hence, the main objectives of this doctoral thesis are focused on the characterization of this mouse model.

CHAPTER II. THE BONE

II. 1. The skeleton

The **skeleton** is a complex system composed of bones and/or cartilages that exerts many physiological functions such as structural support, connection to the muscular system and tendons for locomotion, and protection of soft tissues and inner organs. Bone skeletons also serve as calcium and phosphate storage, regulating their circulating levels and maintaining mineral homeostasis. Bones also house bone marrow and allow haematopoiesis[76–78]. Furthermore, in the lasts decades it has been extensively reported that the skeleton is actually an **endocrine organ** regulating the secretion of important factors such as Fibroblast Growth Factor 23 (FGF23), vitamin D, leptin, insulin, neuropeptide-Y (NPY) or osteocalcin. Hence, bone is in a continuous crosstalk with other organs such as adipose tissue, pancreas or kidney (Figure 6). Through this broad net of organ communications, bone is a key component in the regulation of glucose, lipid and energy metabolism, as well as in testosterone production and male fertility[79–84].

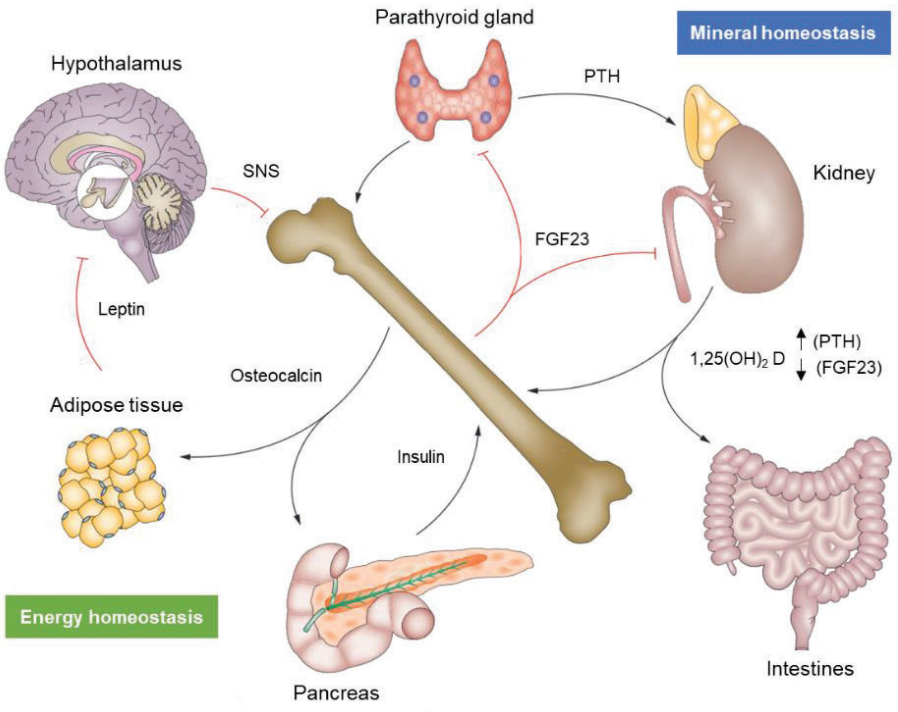

Figure 6. Bone in the crossroads of mineral and energy homeostasis. Through the secretion of different factors, the bone affects mineral and energy homeostasis. Decreased circulating calcium stimulates the parathyroid gland, that release parathyroid hormone (PTH). PTH, in turn, stimulates osteoclastic bone resorption, renal calcium reabsorption and renal production of $1,25(OH)_2D$ (active vitamin D), which acts at an intestinal level increasing calcium absorption. However, the increase in serum phosphate and $1,25(OH)_2D$ stimulate FGF23 production in bone. FGF23 is secreted and affects the parathyroid gland and the kidney, inhibiting PTH and $1,25(OH)_2D$ production, thus stablishing a negative feedback loop. Regarding energy homeostasis, bone is involved in two other loops: a negative bone-hypothalamic loop and a positive bone-pancreas loop. In the latter, osteocalcin stimulates the secretion of insulin by β-cells in the pancreas, which also drives further production of osteocalcin by stimulating osteoblasts. In the former loop, leptin inhibits osteogenesis and the homeostatic function of the skeleton indirectly through the hypothalamus by supressing the sympathetic nervous system (SNS) tone. On the other hand, this enhances the production of osteocalcin which, besides feeding the positive pancreatic loop, also acts together with NPY on adipose tissue increasing the production of adiponectin, an insulin sensitizing hormone. Adapted from DiGirolamo *et al.* 2012[82].

II.2. Bone structure

Bone tissue is characterized by the presence of a hard extracellular matrix mainly composed of hydroxyapatite crystals. Bone cells and vessels are found embedded in this matrix and surrounding its surface. Depending on the structural

organization, two main histological types can be differentiated: cortical and trabecular bone. **Cortical bone**, also known as compact bone, presents a dense, tight and structured organization. It is organized in osteons, or Harvesian systems, which are concentrical layers of matrix and bone cells forming a central channel, the Harvesian canal, which protects nerves and blood vessels (Figure 7). This bone type has a low turnover rate and high resistance. **Trabecular bone**, also named cancellous or spongy bone, is characterized by the organization of its osteons in a mesh or trabecular formation, with cavities between ossified structures. These spaces house the bone marrow and blood vessels, thus being key for haematopoiesis. Furthermore, the trabeculae in cancellous bone are highly interconnected, which is an essential characteristic for the strength of the bone. However, this bone type has a significantly higher turnover rate than the cortical bone, and alterations in this balance are usual markers of bone pathologies such as osteopetrosis or osteoporosis[76,77,85,86]. The main parameters that define the architecture of spongy bone are the number of trabeculae (Tb.N), their thickness (Tb.Th) and the density of trabecular bone (BV/TV: bone volume relativised to total tissue volume). Each of these factors affects differently to the strength of bone structure. For instance, reduction of the number of trabeculae reduces the strength and stiffness of bone by two or three times more than does losing the same amount of bone via trabecular thinning, since the loss of trabecular connectivity reduces the capacity of bone to direct stresses[87].

Globally, cortical bone represents the 80% of the skeleton, while trabecular bone accounts for the 20%. However, this ratio depends on the type of bone and the zone within it. For example, long bones are composed of the hollow central areas called diaphysis, the distal rounded areas called epiphysis and the metaphysis surrounding the growth plate. In the diaphysis, cortical bone represents the 95% of the structure, being the trabecular bone restricted to a marginal 5%. Conversely, in the epiphysis the trabecular bone percentage is increased to a 50:50% ratio with the cortical (Figure 7). Other types of bone present different distributions, like the vertebrae, in which the trabecular bone predominates accounting for a 75% of the bone mass. However, these ratios may also vary in pathological situations[76,77,85].

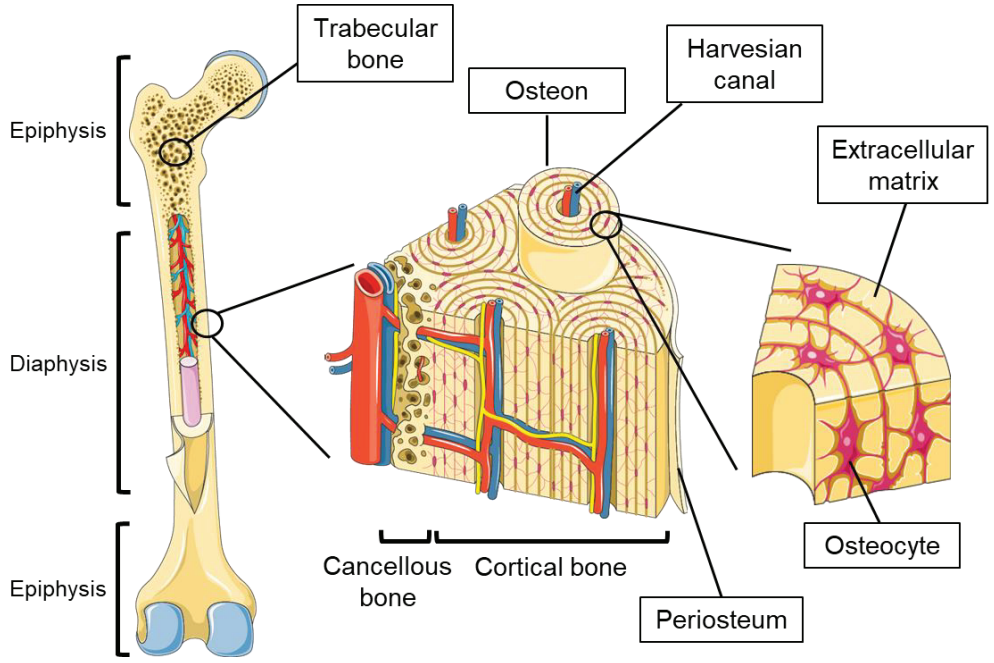

Figure 7. Internal structure of long bones. Long bones are divided in their distal regions, the epiphysis, and the central zones, the diaphysis. The epiphysis is composed of a 50:50% ratio between trabecular and cortical bone. In the diaphysis, the percentage of cortical bone is around 95%. This bone is organized in osteons, that are concentrical layers of osteocytes and extracellular matrix leaving a channel in the middle, the Harvesian canal, where nerves and blood vessels traverse the bone. The surface of the cortical bone is surrounded by the periosteum, an external layer with osteoprogenitor cells. Adapted from *Meng Bao et al.*, 2013[86]

Bone surfaces are covered with the periosteum, an external layer composed of connective tissue and osteoid population including osteoprogenitor cells, that are involved in balancing bone remodelling (Figure 7)[76].

II.2.1. Extracellular matrix

The main characteristic of bone is its hard **extracellular matrix (ECM)**. This consistence is due to the calcification that presents, as the 50-70% of the ECM is composed of inorganic minerals. There is also an organic secreted fraction that accounts for the 20-40% of the matrix, while the water represents the 5-10%. Lipids are also present in the ECM in a smaller portion, not surpassing the 3%[88].

The **inorganic fraction** of the ECM is mainly composed of small crystals of hydroxyapatite (HA) [$Ca_{10}(PO_4)_6(OH)_2$], that bind to collagen scaffolds providing the

bone its characteristic stiffness and also serving as the main reservoir of phosphate and calcium ions[76,78,89].

The main component of the **organic fraction** is the **collagen**, which constitutes the 90-95% of this secreted portion. Collagen fibres are extremely strong and flexible, providing high tensile strength. Besides, they serve as scaffolds for bone mineralization. 28 types of collagens have been described in mammals, being the collagen type I the most abundant in bone. These proteins are synthesized in the osteoblasts and secreted to the ECM, where they bind to other collagen fibres forming triple helix structures. These helix associate with the hydroxyapatite crystals and combine to end up forming lamellar structures that will form the osteons[90–92].

The remaining 5-10% part of the organic fraction is formed by **non-collagenous proteins (NCPs)**. These proteins are also produced and secreted by bone cells, including osteoblasts, osteocytes, osteoclasts and chondrocytes. They exert several functions, being important for the regulation of bone homeostasis[76]. Among the NCPs, the most relevant are the SIBLING family proteins, along with alkaline phosphatase, osteonectin and osteocalcin.

Alkaline phosphatase (ALPL) is a glycoprotein that induce ECM mineralization by degrading extracellular inorganic pyrophosphate (PPi), which is a strong mineralization inhibitor, to inorganic phosphate (Pi). This enzyme is expressed in the early phases of osteoblast differentiation and thus it is a good marker for early osteogenesis[93,94].

Osteonectin is the most abundant NCP in the bone. It is a phosphoprotein that binds both collagen and hydroxyapatite, thus creating a link between organic and inorganic phases of the ECM. Osteonectin also inhibits cellular proliferation and stimulates osteoblast maturation and survival[95].

Osteocalcin (**BGLAP**: Bone γ-carboxyglutamic acid-containing protein) accounts for around 20% of the NCPs in the bone. This protein in synthesized in the osteoblasts and post-translationally modified by γ-carboxylation in a vitamin K-dependent process. This carboxylation increases osteocalcin affinity for hydroxyapatite. Hence, most secreted osteocalcin remains embedded in the calcified matrix. There, it

is an important factor for the regulation of bone mineralization. However, the acidic conditions created during bone resorption promote decarboxylation of osteocalcin, thus being released into the circulation. Uncarboxylated osteocalcin acts as a hormone regulating glucose and lipid metabolism through its interactions with adipose tissue and pancreas (Figure 6). Furthermore, osteocalcin is also recognized by Leydig cells in the testes, where it enhances testosterone synthesis[81,82,96,97].

The small integrin-binding ligand N-linked glycoproteins (SIBLING) are other important members of the ECM. These proteins are also secreted by bone cells and are highly related to the regulation of bone mineralization and homeostasis. Osteopontin is one of the most important members of the family. It acts as an inhibitor of mineralization by binding to HA. Another relevant protein is bone sialoprotein, that enhance osteoblast differentiation and promote ECM mineralization by nucleating HA crystals. Other members of the SIBLING family involved in the regulation of bone mineralization are dentin matrix protein 1 (DMP1), dentin sialophosphoprotein (DSSP) and matrix extracellular phosphoglycoprotein (MEPE)[98].

II.2.2. Bone cells

As stated before, the extracellular matrix is formed by the secretion of the different factors by the bone cells. Because of the production and secretion of this matrix, cells remain embedded within it or surrounding its surface. However, bone is not a static structure, but a **highly dynamic organ** that is subject to constant remodelling during the whole life of the individual. These dynamics are stablished by the bone formation of the **osteoblasts** and the bone resorption activity of the **osteoclasts**. The **osteocytes** act as mechanosensors that orchestrate the process. Deregulation of this balance lead to bone pathologies such as osteoporosis, when bone resorption is increased over bone formation, or osteopetrosis, when the osteoblast function prevails over the osteoclast resorption[76].

II.2.2.1. Bone marrow mesenchymal stem cells

Mesenchymal stem cells (MSCs) are multipotent stem cells present in several proliferative adult tissues that present the capacity of self-renewal while maintaining multipotency. This multipotency allow them to differentiate into different cell lineages

depending on the signalling inputs that they receive, modulated by cytokines, growth factors and other extracellular matrix molecules. This signalling activates concrete transcription programs that will define the differentiation fate of the MSCs, that can derive to chondrogenic, osteogenic, adipogenic or myogenic lineages (Figure 8)[99,100]. These capacities of self-renewal and multipotency that MSCs present makes them a great cellular research model to study the differentiation process of the aforementioned lineages. Additionally, they have also been proposed as a potential therapeutic agent for human pathologies such as skeletal disorders[101].

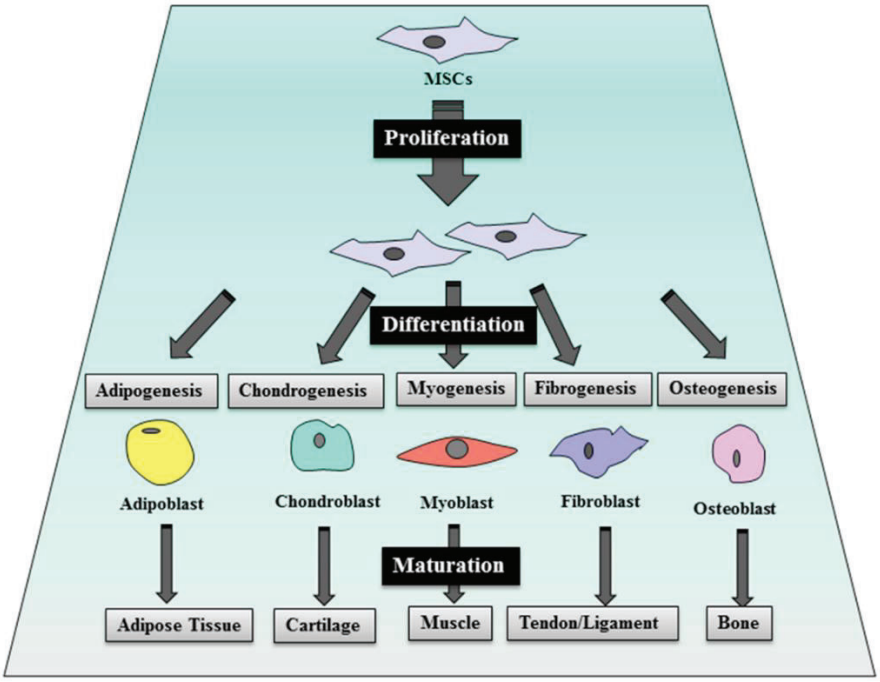

Figure 8. MSCs differentiation potential. Upon activation of concrete transcription factors in a highly regulated process, MSCs may differentiate into several cell types, such as adipocytes, chondroblasts, myoblasts, fibroblasts and osteoblasts. Undifferentiated MSCs keep the capacity of self-renewal. Adapted from Almalki and Agrawal, 2016[100].

The **bone marrow mesenchymal stem cells (BM-MSCs)** are a population of non-haematopoietic MSCs that can be found in adult bone marrow, representing around the 0.01-0.001% of bone cells. They are the resident multipotent cells that confers the bone the ability to regenerate by generating new osteoblasts through osteoblastogenesis[99].

II.2.2.2. Osteoblasts

Osteoblasts are cuboidal cells derived from the osteogenic differentiation of BM-MSCs. These cells are responsible for the synthesis and secretion of factors for the formation and mineralization of the bone matrix. For this, they are equipped with abundant rough endoplasmic reticulum and Golgi apparatus, as well as a large flow of secretory vesicles. The secreted proteins from the osteoblasts form an immature bone matrix called osteoid, that would be mineralized in subsequent steps.

Osteoblastic specialization starts from BM-MSCs that undergo differentiation to osteochondroprogenitors. After this initiation, some of these cells will become preosteoblasts by expressing a series of genes such as *RUNX2*, *COLIA1* and *ALP*, and initiate a proliferative phase, starting to secrete the osteoid. Mature osteoblasts will be characterized by the expression of the transcription factor *OSX* and by the increased secretion of proteins involved in the mineralization of the matrix, such as osteocalcin or osteopontin. In the final step of osteogenic differentiation, mature osteoblasts can undergo apoptosis or differentiate into osteocytes or bone-lining cells. The set of genes involved in the whole process of osteogenic differentiation will be detailed in next sections.

Bone-lining cells are quiescent flat-shaped osteoblasts that remain in the endosteum and do not proliferate. They are interconnected with osteoblasts through adherent junctions, and different functions have been proposed for them, such as endosteum formation, mineral ion transport or the regulation of bone resorption. Nevertheless, their functionality is still poorly understood[76,78,102].

II.2.2.3. Osteocytes

Mature osteoblasts get surrounded by the extracellular matrix that they secret and then engage the final step of osteogenic differentiation to **osteocytes**. Thus, mature osteocytes are located in spaces in the calcified bone matrix, called lacunae. These lacunae present narrow channels between them, the canaliculi, that allow the osteocytes to be interconnected between them through filopodia prolongations and gap junctions. Osteocytes are the most abundant bone cell type, representing the 90-95% of them[103].

Osteocytes are the orchestrators of **bone remodelling**, being able to communicate to both osteoblasts and osteoclasts and regulate their function by secreting factors such as Receptor activator of NFκB ligand (RANKL) or Sclerostin (SOST), that will be detailed later. Furthermore, osteocytes are also important **mechanosensors**, responding to mechanical stresses by secretion of factors involved in bone synthesis. This function allows the activation of fracture repair processes, among other responses[104–107]. Osteocytes also exert important **endocrine functions**, being the cells producing factors like SOST or FGF23, which activity regulating mineral homeostasis has been explained before (Figure 6). Besides this function, these factors have been linked to the regulation of haematopoietic stem cell mobilization, myogenesis and muscle function and adipose tissue differentiation and homeostasis[108–111].

II.2.2.4. Osteoclasts

Osteoclasts are the opposite cells to osteoblasts, both in function and origin. These cells do not arise from MSCs but from the haematopoietic lineage. Monocytes-macrophage precursors located near the bone surface fuse together and are activated by factors mainly produced by osteocytes, which induce their differentiation into the multinucleated osteoclasts. Regarding their function, these cells secrete acids and enzymes that degrade the bone surface, releasing minerals and factors to the circulation. Hence, they stablish a balance with osteoblasts that keeps bone structure and homeostasis[112,113].

Active osteoclasts are located in the surface of the bone. They are polarized cells that reorganise their actin cytoskeleton to create a resorption area in contact with the mineralized bone matrix. This resorption area is acidified by the secretion of ions from the osteoclasts, which also secrete enzymes involved in the digestion of components of the ECM, like cathepsin K (CTSK). All of this leads to the dissolution of the hydroxyapatite crystals and the degradation of the organic matrix in the bone surface. In physiological conditions, this area is sequentially populated with osteoblasts secreting new ECM, completing the remodelling process (Figure 9)[76,78,113,114].

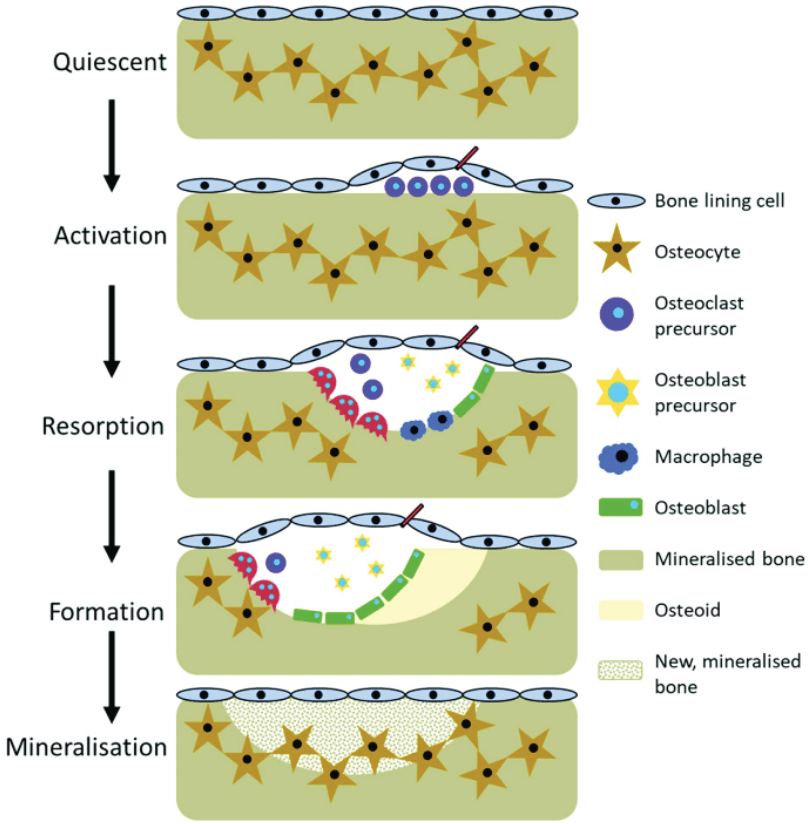

Figure 9. Bone remodelling process. Osteoclast precursors are recruited onto the bone surface and create a resorption area where they degrade the bone matrix. This zone is repopulated with new osteoblasts that secrete a new osteoid that will be subsequently mineralised. Adapted from Owen and Reilly, 2018[114].

II.3. Osteogenic markers

Osteogenic differentiation from MSCs to osteoblasts and osteoclasts is a highly regulated process that requires the expression of a concrete set of transcription factors that in turn modulate the expression of necessary of genes for proper differentiation and function of bone cells. The expression of these genes is a good marker for analysing the osteogenic activity both in cultured MSCs and *in vivo*. During this thesis, some of these markers have been used for monitoring this process (Figure 10).

II.3.1. *RUNX2*

Runt-related transcription factor 2 (RUNX2) is considered the master transcription factor of osteoblastogenesis. It is expressed in condensed MSCs precursors, starting the process of osteogenesis, and its expression is maintained until mature osteoblasts are formed. RUNX2 activity is needed for the expression of key genes in osteoblast differentiation and function, such as *BGLAP*, *Osteopontin*, *COL1A1* or *COL1A2*. It also binds to the promoter of the transcription factor *Osterix*, enhancing its expression that will be necessary for osteogenesis progression. Furthermore, the lack of *Runx2* expression in mice have been proved to totally prevent osteoblast maturation and ossification[115–117].

II.3.2. *COL1A1*

Collagen type 1 alpha chain 1 (*COL1A1*) encodes, together with *COL1A2*, for collagen type I, the most abundant protein in the bone ECM. The expression of *COL1A1* is started in early stages of osteoblast differentiation, detecting moderate levels of *COL1A1* mRNA in MSCs precursors and immature preosteoblasts. Upon osteoblast maturation, the transcription factors RUNX2 and Osterix enhance *COL1A1* expression, so its levels get significantly increased. This is necessary for the secretion of collagen type I from the osteoblasts to the ECM. Hence, *COL1A1* expression is a marker of osteoblast maturation, and it finally decreases in osteocytes. Mutations affecting *COL1A1* and *COL1A2* genes are causative of severe bone pathologies like Osteogenesis imperfecta[118–120].

II.3.3. *ALPL*

Alkaline phosphatase (ALP) is a glycoprotein present in the bone ECM that induce its mineralization by facilitating the formation of hydroxyapatite crystals. This protein presents four isoforms, being the tissue non-specific alkaline phosphatase (TNAP), encoded by the ***ALPL*** gene, the most abundant in bone, as well as in other tissues such as liver and kidney. In osteoblast differentiation, *ALPL* gene is expressed in early stages and is upregulated during osteoblast maturation, being modulated by the osteogenic program coordinated by RUNX2/Osterix transcription factors. In mature osteocytes, mRNA levels of *ALPL* decline[93,94,121]. Mutations in *ALPL* gene in humans lead

to hypophosphatasia, a condition that provokes rickets, osteomalacia and hypomineralization of teeth[122].

II.3.4. *SP7/Osterix*

Transcription factor SP7, also known as **Osterix (Osx),** is another of the main orchestrators of osteoblast differentiation. *SP7* gene is expressed in MSCs precursors and osteochondroprogenitors, where it acts as an inhibitor of chondrogenesis and enhancer of osteoblastogenesis, and its expression is maintained in mature osteoblasts and osteocytes. *SP7* transcription is stimulated by the binding of RUNX2 to its promoter, although it has been proved that DLX5 transcription factor is also able to induce *Osx* expression even in the absence of RUNX2[116,123–125]. Therefore, Osterix is activated in a second step during osteoblast differentiation and then it exerts a key role for osteoblast and osteocyte function, controlling the expression of many ECM proteins such as COL1A1, ALPL, BGLAP, IBSP (bone sialoprotein 2) or FMOD (fibromodulin), and also regulating angiogenesis in bone through Vascular endothelial growth factor (*VEGF)* induction[119,126]. These functions are exerted not only through its transcriptional factor activity but also by promoting chromatin structure modification in its target genes promoters[127]. Osx is thus necessary for bone formation and homeostasis, as *Osx*-knockout mice are not able to form calcified bone, and its inactivation postnatally induces severe bone loss[126,128].

II.3.5. *DLX5*

Distal-less homeobox 5 (DLX5) is part of the DLX family of transcription factors, heavily implicated in embryogenesis. *DLX5*, together with *DLX3* and *DLX6*, are specifically implicated in osteogenesis. *DLX5* is expressed in immature osteoblasts, but its levels increase during maturation and peak at the mineralization phase[129,130]. This transcription factor promotes osteoblastic differentiation upregulating factors such as *RUNX2* and *Osterix,* and it has also a positive effect in bone mineralization[125,129,131,132]. In fact, Dlx5-deficient mice show craniofacial abnormalities and a mild delay in long bones ossification[133].

II.3.6. *BGLAP*

Bone γ-carboxyglutamic acid-containing protein (BGLAP), also named **Osteocalcin**, is another of the main NCPs in the bone matrix. *BGLAP* gene is expressed in several tissues, such as adipose, liver, testis or brain, but its levels are considerably reduced compared to bone, where its expression is induced by factors like RUNX2 during osteoblastogenesis. Within this process, *Osteocalcin* is not expressed until mature osteoblast stage, and a peak in its expression in linked to matrix mineralization. Consequently, *BGLAP* is usually studied as a specific marker of late osteoblastogenesis[123,134–136]. The functions of Osteocalcin in bone homeostasis are not fully defined, although it has been related to the promotion of bone formation, the modulation of the mechanical properties of the skeleton and the facilitation of osteoclasts differentiation[136]. Regarding its endocrine activity, as previously explained Osteocalcin has been found to be an important hormone in the regulation of glucose and lipid metabolism and in male fertility[81,97]. However, recent studies with new *Osteocalcin* KO mouse models do not observe alterations in these functions, so its endocrine rule needs to be further investigated[137].

II.3.7. *DMP1*

Dentin matrix protein 1 (DMP1) is a member of the SIBLING family of glycoproteins, important members of the bone ECM. The expression of *DMP1* gene is detected in mature osteoblasts, although remaining low until the differentiation to osteocytes, when *DMP1* is highly upregulated. Furthermore, it is considered a good marker for late osteogenesis[138]. This expression in late osteogenesis has revealed necessary for osteocyte maturation and mineralization of the matrix, as DMP1 acts as a regulator of hydroxyapatite crystals nucleation[139]. The function of DMP1 in late osteogenesis is corroborated in mouse models, since *Dmp1*-null mice display no gross abnormalities at birth, but these animals develop bone alterations, typically rickets and osteomalacia, starting one week after birth and worsening with age[139,140].

II.3.8. *FGF23*

Fibroblast growth factor 23 (FGF23) is an important hormone highly expressed in bone specifically by the osteocytes, being thus a marker for the last stage

of osteogenesis. The expression of *FGF23* gene is enhanced when serum phosphate levels are increased, and it acts on the kidney and parathyroid gland regulating the mineral homeostasis to reduce the excess of circulating phosphate, thus protecting the organism against the deleterious effects that it has, like chronic kidney disease, alterations in skeletal mineralization or ventricular hypertrophy, among others[82,141,142].

II.3.9. *SOST*

Sclerostin (*SOST*) is a gene only expressed in mature osteocytes after the mineralization of their surrounding ECM. SOST protein is secreted and exerts a paracrine function, preventing new bone formation by inhibiting osteoblast maturation in a mechanism dependent of the inhibition of the Wnt signalling[143,144]. Sclerostin deficiency is a cause of sclerosteosis, a progressive skeletal disorder that is characterized by increased bone mass as a consequence of increased osteoblast activity[104]. Besides this paracrine action, it has also been reported that SOST act as an hormone, being related to enhancing fat mass and adipocyte differentiation[110,145,146].

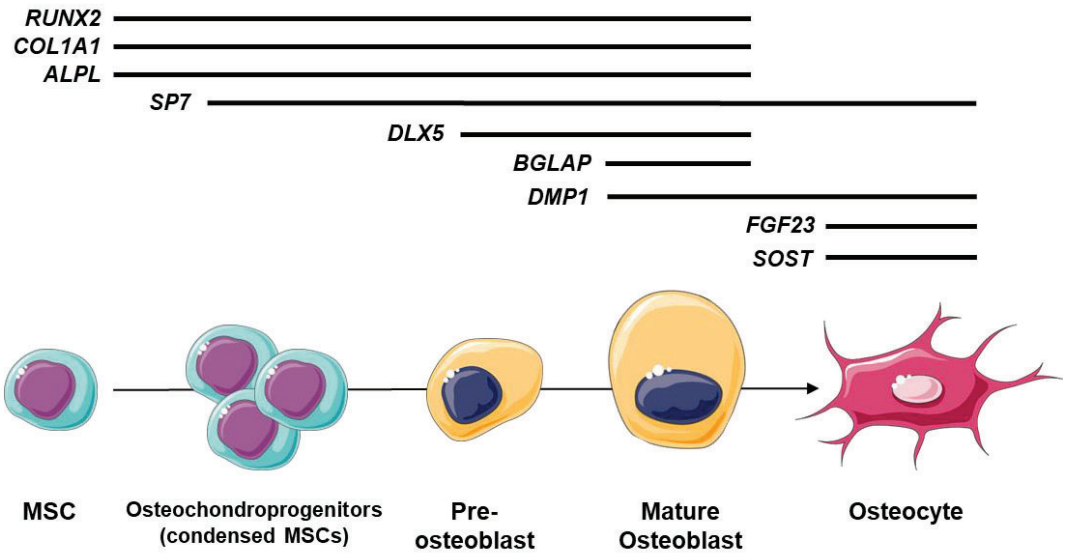

Figure 10. Expression pattern of different osteogenic markers. Main genes involved in osteogenesis that have been used as markers in this thesis for the different stages of differentiation. Schematic lines depict the temporal expression of each gene.

II.4. Osteoclastic markers

Bone remodelling is a highly regulated process, balanced by the osteoblastic bone creation and osteoclastic resorption. As explained in the last section with osteoblastic differentiation, osteoclast formation and activity are also paired with the expression of a concrete set of genes, both from osteoclast and from osteocytes, which function producing factors is necessary for osteoclastogenesis. These genes have been used as molecular markers for measuring osteoclast function (Figure 11).

II.4.1. *RANKL*

Receptor activator of Nuclear factor κB (NFκB) ligand (RANKL) is a member of the tumour necrosis factor (TNF) cytokines. This protein is produced by osteoblasts and osteocytes and can be found both bound to their cellular membrane and soluble, although the membrane-bound form seems to be more effective[105,147]. Therefore, mainly through cell interactions, RANKL is recognized by RANK receptors in the membrane of precursors from the hematopoietic lineage. This interaction provokes RANK activation, which enables a cellular response composed of a plethora of signalling cascades involving NFκB and MAPK pathways, among others. The final output is the activation of a transcription program that promotes osteoclastic differentiation and function[148,149].

Different factors have been shown to influence *RANKL* gene expression in the osteoblastic lineage. Among them, the parathyroid hormone and the $1,25(OH)_2D_3$ are enhancers of *RANKL* expression, thus stimulating bone resorption to regulate mineral homeostasis[82,150]. Interleukin (IL)-6 type cytokines also promote *RANKL* transcription, while the Wnt pathway exerts a negative control[150].

II.4.2. *OPG*

Osteoprotegerin (OPG) is a soluble member of the TNF receptors that lacks the transmembrane domain. This protein is mainly produced and secreted by the osteoblasts and acts as a RANKL decoy receptor. When secreted to the ECM, OPG can bind to RANKL in the surface of osteoblasts and osteocytes and block its interaction with the RANK receptor in the osteoclast precursors. That way, OPG prevents the

osteoclastogenic signalling led by RANK activity thus inhibiting bone resorption[147,151,152]. Although the concrete regulation of *OPG* gene is unclear, *RANKL* overexpression is in general associated with lower levels of *OPG* mRNA, changing the ***RANKL*/*OPG* ratio** in favour of osteoclastogenesis. Therefore, this ratio has been postulated as a marker for osteoclastogenic activity and a major determinant of bone mass[153]. Chronic alterations of the balance of this ratio have been related to the onset of bone and vascular diseases[154].

II.4.3. *TRAP*

Tartrate-resistant acid phosphatase (TRAP) is an iron-containing enzyme that catalyse the hydrolysis of phosphate esters and anhydrides under acidic conditions. *TRAP* gene is expressed by cells from monohistiocytic lineage like macrophages or dendritic cells, although limited expression has also been detected in osteoblasts and osteocytes[155,156]. Hence, the expression of *TRAP* in bone is already detected in mononucleated osteoclast precursors[157]. Mature osteoclasts display high expression of *TRAP*, and therefore it has been used as an indicator for osteoclastic activity, both at mRNA level and as a histochemical marker, since osteoclasts show an intense staining for TRAP in bone sections[158,159]. When secreted to the resorption area by the osteoclasts, TRAP participates in the hydrolysing of components of the ECM such as the osteopontin[158]. Mice lacking *Trap* gene present bone abnormalities such as disrupted ossification and mild osteopetrosis[160].

II.4.4. *CTSK*

Cathepsin K (CTSK) is the major cysteine peptidase involved in the digestion of the ECM components of bone during remodelling. As such, CTSK is mainly produced by mature osteoclasts and secreted to the resorption pit. There, cathepsin K is able to cleavage at multiple sites the triple helices of collagen that scaffold the whole matrix, being the only enzyme described capable of doing it[161–163]. Regarding *CTSK* gene expression, it is influenced by the same factors that decide osteoclast differentiation. Thus, *CTSK* mRNA levels are enhanced by RANKL/RANK signalling and reduced by OPG, besides other regulators also related to osteoclastogenesis[164]. The expression

pattern of *CTSK* gene and the function of the peptidase makes it a great marker for measuring the osteoclastic activity in bones.

The essential function of CTSK in bone resorption is corroborated by the consequences of its deficiency. In humans, mutations in *CTSK* are the cause of Pycnodysostosis, a rare skeletal dysplasia that entails bone alterations such as skull deformities, short stature, increased bone density and fragility or dental abnormalities, among others[165]. In mice, knock-out of *Ctsk* provokes osteopetrosis related to deficits in matrix degradation[166].

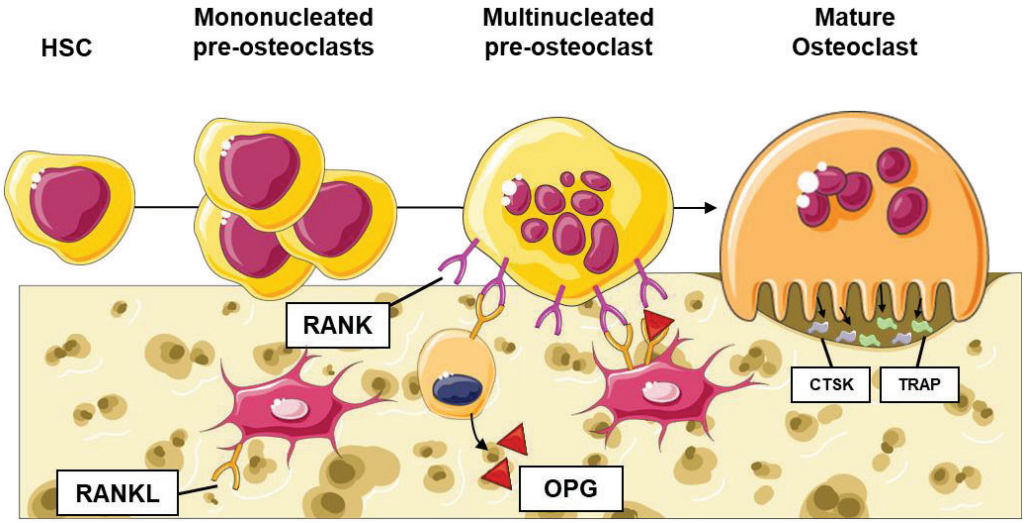

Figure II. Schematic representation of osteoclastogenesis. Osteoclasts precursors from the hematopoietic lineage are recruited to the bone surface. There, they fuse into multinucleated pre-osteoclasts and are differentiated into mature osteoclasts. One of the signals that drives this cell specialization is stimulation of their RANK receptors by RANKL expressed at the membrane of osteoblasts and osteocytes. Nonetheless, OPG secreted by osteoblasts acts as a decoy receptor for RANKL, preventing its binding to RANK. Mature osteoclasts exert their bone digestion function by acidifying the resorption pit and secreting catalytic enzymes such as CTSK or TRAP. HSC: Hematopoietic Stem Cell.

II.5. Signalling in bone homeostasis

Bone formation and remodelling are highly dynamic processes that require the integration of multiple signalling pathways in all the bone cells. Among them, MAPK and ubiquitylation signalling will be briefly reviewed because of their relevance in the current thesis.

II.5.1. MAPK signalling in bone

Mitogen-activated protein kinases (MAPK) are serine/threonine kinases that mediate the cellular response to a wide range of stimuli. Two of the main MAPK pathways, ERK and p38, have been briefly explained in the previous chapter in relation of the regulation that HERC1 exerts on their activation[25,29]. In addition to the functionality previously described for these MAPKs, they are also involved in the regulation of bone mass as mediators of osteoblast and osteoclast differentiation[167,168].

II.5.1.1. MAPK signalling in bone formation

Regarding **osteoblastogenesis**, both ERK and p38 activity have been found as modulators of the process. **ERK** has two isoforms: ERK1 (MAPK3) and ERK2 (MAPK1), both present in osteoblasts exerting similar functions. ERK1/2 bind RUNX2 at its C-terminal proline/serine/threonine-rich domain and phosphorylate the protein at serine residues S43, S301, S319, and S510 (numbering related to murine sequence). S301 and S319 phosphorylation have been proved to enhance RUNX2 transcriptional activity, thus stimulating osteoblastogenesis[169–171]. Furthermore, ERK and p38-dependent phosphorylation of RUNX2 and Osterix is necessary for their cooperative activity as osteoblastogenic transcription factors[172]. Other transcription factor phosphorylated by ERK is Peroxisome proliferator-activated receptor gamma (PPARγ), a master regulator of adipogenic differentiation. However, phosphorylation of PPARγ in Sl12 by ERK has an inhibitory effect, reducing its activity. Therefore, ERK activation leads to facilitate precursor MSCs differentiation to osteoblasts rather than to adipocytes[173,174]. The importance of this MAPK in bone development is endorsed by an *Erk*-depleted mouse model, that presents a substantial impairment in bone mineralization[175].

p38 MAPK pathway has been more thoroughly studied in bone formation. This kinase presents four isoforms: α (MAPK14), β (MAPK11), γ (MAPK12) and δ (MAPK13). Among them, p38α is the predominant form throughout all tissues[176]. p38 potential to modulate osteoblastogenesis is mainly mediated by its capacity to phosphorylate key osteogenic transcription factors, thus enhancing their function (Figure 12)[177]. Hence, similarly to ERK, p38 phosphorylates RUNX2 is several residues, sharing some of them with ERK[178,179]. Furthermore, p38 has also been proved to phosphorylate OSX, at serines

73 and 77, facilitating the recruiting of co-factors needed for its transcriptional activity[119,180]. Moreover, as explained before, the phosphorylation of OSX and RUNX2 mediated by p38 and ERK is essential for their binding, which substantially increases their transcriptional power[172]. Another transcription factor regulated by p38 is DLX5, which is phosphorylated at S34 and S217. This modification also increases its activity, which in turn further enhances the whole osteogenic transcriptional program, given the upregulation that DLX5 exerts on *RUNX2* and *OSX* expression[132]. Besides these classic osteogenic targets, p38, together with ERK, can also phosphorylate Ribosomal protein S6 kinase 2 (RSK2)[181,182], which in turn activates by phosphorylation Activating Transcription Factor 4 (ATF4). This latter transcription factor has also been found to be necessary for bone development at late stages[183].

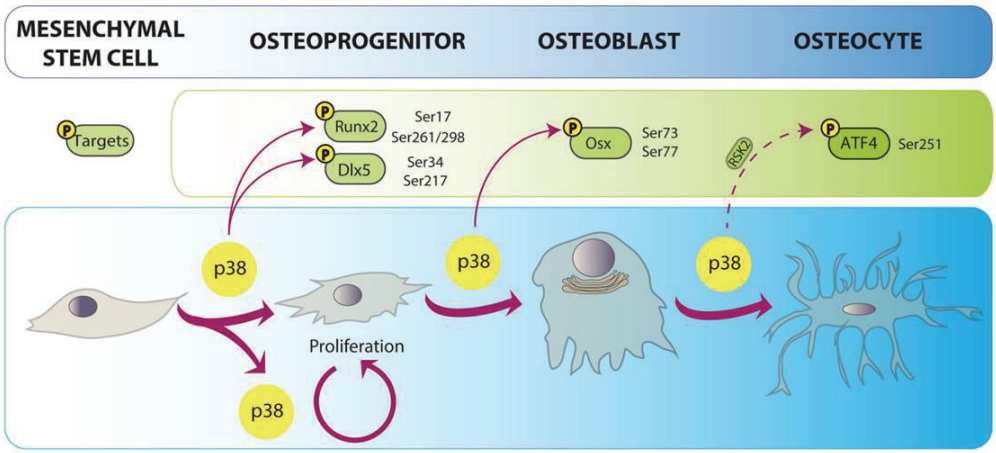

Figure 12. p38 targets in osteogenesis. p38 stimulates osteoblast proliferation and differentiation at different steps by phosphorylating key transcription factors. The concrete serine residues phosphorylated by p38 are depicted. Direct arrows indicate direct targets, while dashed arrows show indirect phosphorylation. Adapted from Rodríguez-Carballo *et al.*, 2016[177].

In addition to the targeting of these key transcription factors, p38 function has also been related to the modulation of bone formation by its control of cell migration and the integration of different signalling cascades as response to a plethora of external stimuli[177]. The key importance of p38 in bone homeostasis is corroborated by *in vivo* models. *Mapk14* (p38α) homozygous deletion causes embryonic lethality[176], so conditional knock-out mouse models have been used to study its physiological relevance. It has been discovered that the depletion of *Mapk14* in the

osteochondroprogenitor lineage generates a significant bone loss, that affected different parts of the bone structure depending on the age on which the gene loss was triggered. These results showed that p38α exerts a complex regulation in bone homeostasis at different stages of osteoblast development throughout the whole life[184]. p38β has also been seen relevant for bone homeostasis *in vivo*, since the *Mapk11* knock-out mouse model, although being totally viable, display substantially reduced bone mass[178].

II.5.1.2. MAPK signalling in bone resorption

MAPKs signalling has also been found necessary for **osteoclast differentiation and activation**. Besides RANKL, Macrophage colony stimulating factor (M-CSF) is the other factor essential for the progression of osteoclastogenesis. It has been described that both M-CSF and RANKL activate MAPK pathways as mediators of their cellular response[168].

ERK phosphorylation is induced by M-CSF and RANKL signalling. Activation of ERK by the former in osteoclast precursors results in an increase in their proliferation and survival[185,186]. These effects are mediated by the phosphorylation of a set of key osteoclastogenic transcription factors such as Microphthalmia-associated transcription factor (MITF) or TFE3[187], and by the indirect induction of other proteins involved in osteoclast survival, like the transcription factor Egr2[188]. On the other hand, the activation of ERK by the RANKL/RANK signalling have been shown to regulate osteoclast differentiation and function by the induction of the expression of several proteins like the Matrix metalloprotease 9 (MMP-9), implicated in osteoclast migration and bone resorption[149,189]. The ERK physiological relevance in osteoclastogenesis have been validated in mouse models that show that depletion of *Erk1* gene reduce osteoclast number and compromise resorption pits formation[190].

p38 regulation of osteoclastogenesis is mainly due to its action as a hub of the RANKL/RANK signalling in osteoclast precursors. Upon induction of RANK receptor, MAPK cascades are engaged involving different MAPK kinase kinases (MAPKKKs) and MKK3/6 as MAPK kinases (MAPKK). These pathways converge in the activation of p38, which in turn phosphorylates and activates a plethora of factors essential for

osteoclastogenesis such as Nuclear factor of activated T cells 1 (NFATc1), MITF, NFκB, ATF2 or MAPK-activated protein kinase 2 (MK2), among others. The activity of these factors results in the production of key osteoclastic proteins like TRAP, CTSK or E-cadherin[168,191–195]. Mouse models have revealed that p38 exerts a complex function in the regulation of osteoclastogenesis in an aging-dependent manner, since ablation of *Mapk14* (p38α) in osteoclasts precursors provokes an increment of bone mass at young age, but 6 months-old mice exhibit an osteoporotic phenotype associated with an increase in osteoclastogenesis and bone resorption[196].

Altogether, the growing literature in the field demonstrates that ERK and p38 MAPK pathways play a key role in the regulation of bone remodelling. Although the concrete modulation is complex, the common consensus is that activation of these MAPKs enhances both the osteoblastic and osteoclastic programs.

II.5.2. Ubiquitylation in bone

Being one of the most important post-translational modifications in the regulation of cell pathways, **ubiquitylation** is also a key mechanism for the modulation of bone remodelling. Consequently, several studies have shown that some ubiquitin ligases play a role in regulating osteoblast and osteoclast differentiation[197,198].

II.5.2.1. Ubiquitylation in bone formation

The **osteoblastogenesis** process is modulated by many PTM of proteins involved in it. Hence, ubiquitylation has proven necessary for the regulation of several signalling pathways and transcription factors related to osteogenesis[197].

Regarding the main transcription factors, RUNX2 and OSX, both have been found to be ubiquitylation substrates. **RUNX2** was first found to be directly ubiquitylated by the SMAD ubiquitination regulatory factor 1 (SMURF1), a E3 ubiquitin ligase with a HECT domain. As a result of this signal, RUNX2 is targeted for proteasomal degradation, inhibiting osteoblast differentiation[199,200]. Another HECT ubiquitin ligase, WWP1, is also recruited to RUNX2 to promote its degradation, thus antagonizing the osteoblast maturation and ECM mineralization, in a process mediated by the zinc finger adapter protein SHN3[201]. The next E3 enzyme related to the promotion of RUNX2

degradation was CHIP (C-terminus of HSC70-interacting protein). This protein interacts with RUNX2 and promotes its ubiquitylation, negatively regulating osteoblast differentiation. Besides, the same study also proved that CHIP has a different expression pattern than SMURF1 and WWP1 during osteoblastogenesis, which suggest that these three proteins cooperate in the fine-tuning of RUNX2 levels during the whole process[202]. The last ubiquitin ligase that has been detected targeting RUNX2 for ubiquitin-mediated proteasomal degradation is the S-phase kinase-associated protein 2 (SKP2). Hence, depletion of this protein increases RUNX2 levels and enhances osteoblast differentiation[203]. However, not all the ubiquitylation found in RUNX2 provokes its degradation. WWP2, another WW domain-containing HECT E3, is able to monoubiquitylate RUNX2 leading to its transactivation, which has a positive effect for osteoblastogenesis[204].

Osterix was also identified as a ubiquitin-regulated factor[205]. In this line of research, CHIP osteoblastogenesis inhibiting activity was endorsed by the discovery that it can also target OSX for ubiquitylation and proteasomal degradation upon chronic stimulation by TNFα[206]. The members of the mammalian Casitas B-lineage lymphoma (CBL) CBL-b and c-CBL are others ubiquitin-ligase proteins that have been shown to promote OSX ubiquitin-mediated degradation, thus reducing the potential for osteoblast differentiation[207]. Finally, two members of the F-box protein family are also related to the control of OSX levels, although in opposite directions. On the one hand, the F-box/WD repeat-containing protein 7 (FBW7) targets OSX for ubiquitylation and degradation, in an interaction that requires the p38-mediated phosphorylation of OSX in S73 and S77[208]. On the other hand, the F-box protein 25 (FBXO25) indirectly enhances *OSX* expression by promoting the monoubiquitylation of histone H2A at lysine 120 (H2AK120), which in turn stimulates the trimethylation of histone 3 at lysine 4 (H3K4). Both histone modifications induce *OSX* transcription. Therefore, FBXO25 has a positive effect on osteoblast differentiation. Nonetheless, FBXO25 levels are also regulated by other E3 ubiquitin ligase, Cullin-3, which promotes FBXO25 ubiquitin-mediated proteasomal degradation, thus inhibiting OSX expression and osteoblastogenesis[209].

II.5.2.2. Ubiquitylation in bone resorption

Ubiquitin ligases play different roles in **osteoclastogenesis** as well. Among them, CBL-b and c-CBL have also been thoroughly studied in this process[198]. These RING ubiquitin ligases interact with the key transcription factor NFATc1 in late stages of osteoclast maturation and promote its degradation, thus exerting a negative regulation of osteoclastogenesis[210]. Consistent with this mechanism is the observation that ablation of *Cbl-b* gene in mice leads to osteopenia because of an increase in bone resorption[211]. However, these two ubiquitin ligases have also been found to be necessary for the survival and function of osteoclasts[212]. In fact, c-CBL is able to ubiquitylate the pro-apoptotic protein BIM in osteoclasts, therefore targeting it for degradation and preventing osteoclast apoptosis[213]. It has also been discovered that c-CBL participates in the integration of RANKL/RANK signalling, and that its loss provokes a decrease in osteoclast activity[214].

Besides the CBL proteins, other ubiquitin ligases have also been related to the regulation of bone resorption. For instance, Tumor necrosis factor receptor-associated factor 6 (TRAF6) is a RING ubiquitin ligase that is recruited to the cytoplasmatic domain of active RANK, and its ubiquitin ligase activity is necessary for the initiation of the signalling cascade that leads to the maturation of osteoclast precursors[215]. Other E3 enzyme that promotes osteoclastogenesis is LNX2, that is upregulated during the process and is key for the regulation of both the M-CSF and the RANKL signalling[216]. Conversely, other ubiquitin ligases exert negative effects on osteoclast differentiation. That is the case of Itch, a E3 ubiquitin ligase that promotes the deubiquitylation of TRAF6 by facilitating the binding of the deubiquitinating enzyme CYLD. Consequently, Itch activity attenuates RANK signalling thus inhibiting osteoclastogenesis[217].

CHAPTER III: THE ADIPOSE TISSUE

Classically considered as an energy storage, nowadays it is well known that, besides that, **adipose tissue** is actually a complex endocrine organ, responsible for many functions in the whole body, like glucose and lipid metabolism, energy balance, insulin sensitivity, thermogenesis, inflammation or tissue repair. This new perspective on adipose tissue started in 1994 with the discovery of leptin[218], an adipocyte-produced hormone that affects both the hypothalamus and peripheral organs. Since then, many other adipose factors have been identified and have expanded the knowledge about the high diversity of physiological functions that adipose tissue exerts in the organism[219,220].

III.1. Adipose tissue structure

Adipose tissue is a connective tissue that offers cohesion and isolation to organs and skin. Adipose or fat mass can account for the 5 to the 60% of total body weight, and this percentage and the distribution of adipose depots are affected by factors like age, sex and ethnicity[221–223]. Adipose tissues are composed of a variety of different cell types, including mesenchymal cells, fibroblasts, pericytes, endothelial cells, blood cells and immune cells. Nevertheless, the major component of adipose tissues are always the **adipocytes**. The adipocytes are lipid-containing cells that are responsible for most of the functions that adipose tissue exerts, from lipid storage and release to the secretion of signalling peptides. However, these functions vary depending on the intracellular structure of these cells, as there have been described different types of adipocytes. Hence, the major type of adipocyte present in an adipose tissue depot allow the differentiation of three main sorts of fat: white, brown and beige[224].

III.1.2. White adipose tissue

White adipose tissue (WAT) is the most abundant kind of fat. This tissue is mainly composed of **white adipocytes**, which are rounded cells characterized by containing a unique and large lipid droplet that occupies almost the whole volume of the cell, restricting the cytoplasm to a thin layer and displacing the nucleus to the periphery (Figure 13)[225]. This cell structure determines the functionality of these

adipocytes, as they are the main reservoir of energy in the body, being able to take up and release lipids responding to energy requirements. Besides that, white adipocytes, together with other cells within WAT, secrete a large number of regulatory factors with both paracrine and endocrine action[220].

Depending on their lipid droplet, white adipocytes size range between approximately 20 to 200 μm[221]. The size and number of white adipocytes is usually determined by the metabolic state of the organism. When there is calorie surplus, WAT mass is enlarged by the stimulation of the formation of new white adipocytes (**hyperplasia**) and by the increase of the size of existing adipocytes by the enlargement of their lipid droplet (**hypertrophy**). However, chronic stimulation of these process leads to pathological situations like obesity, that impairs the structure and functionality of the adipocytes[226].

III.1.3. Brown adipose tissue

Brown adipose tissue (BAT) is a type of fat only present in mammals, being more abundant in small animals and newborns. This tissue is highly vascularized, and its main component are the **brown adipocytes**. These cells, unlike white adipocytes, present multiple small lipid droplets and contain a high number of mitochondria (Figure 13). The high vascularization and the mitochondrial density in BAT confer the tissue its characteristic brown colour[227]. The important differences between WAT and BAT make these two tissues easily distinguishable with optic microscopy (Figure 13).

As also happens in WAT, the structure of BAT allows its unique functions. Brown adipocytes are characterized by performing non-shivering thermogenesis, dissipating energy in form of heat through uncoupling mitochondrial respiration[228]. In addition to this main function, there is increasing evidence that prove that BAT also exerts an endocrine function, being responsible for the production of several regulatory factors that affect both the own BAT and other tissues[229]. Like WAT, BAT has also important plasticity. Hence, upon chronic exposure to stimuli like cold or other catabolic conditions, the BAT mass increases by hypertrophy and hyperplasia. However, it is described that the structure and function of this tissue can also be impaired by factors such as age or obesity[220].

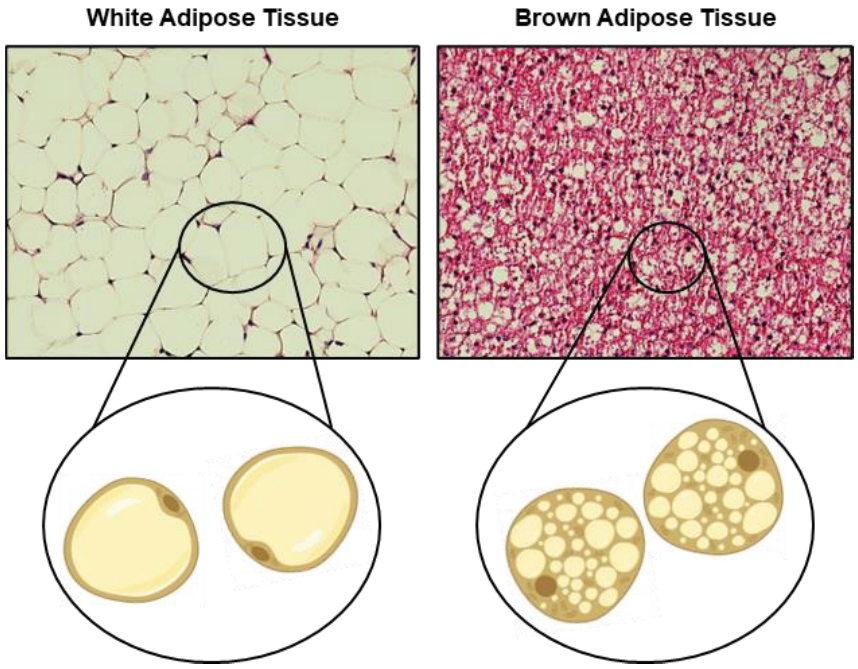

Figure 13. Histological differences of white and brown adipose tissues. Haematoxylin and eosin (H&E) staining of white and brown adipose tissues. Illustrated white and brown adipocytes are shown below each tissue. White adipocytes contain a large lipid vacuole that occupies almost the whole volume of the cell. Conversely, brown adipocytes have a higher non-lipidic cytoplasmatic fraction, with a greater density of mitochondria and smaller lipid droplets.

III.1.4. Beige adipose tissue

White and brown adipose tissues are usually located at separated anatomical locations and derive from different lineage precursors. However, there is a third type of adipocytes, that are closer to the white lineage but share the cell structure and function with brown adipocytes. These are known as **brite** or **beige adipocytes**, and their genesis is inducible by similar factors that stimulate BAT activation, like cold exposure. The name "brite" comes from "brown in white", which refers to the fact that beige adipocytes are found within WAT depots. This appearance of brown-like adipocytes in the white tissue is called "browning", and it has been shown that it can be induced by B_3-adrenergic stimulation[230,231]. The new beige adipocytes can be formed by transdifferentiation from white adipocytes or by proliferation of precursors in WAT[232,233]. Furthermore, it has been described that there can be a bi-directional interconversion between white and beige adipocytes[234].

III.2. Adipose tissue distribution

Adipose tissue is distributed throughout the whole body. It is organized in depots distinguished by their distinct anatomical locations and their adipocyte composition (Figure 14).

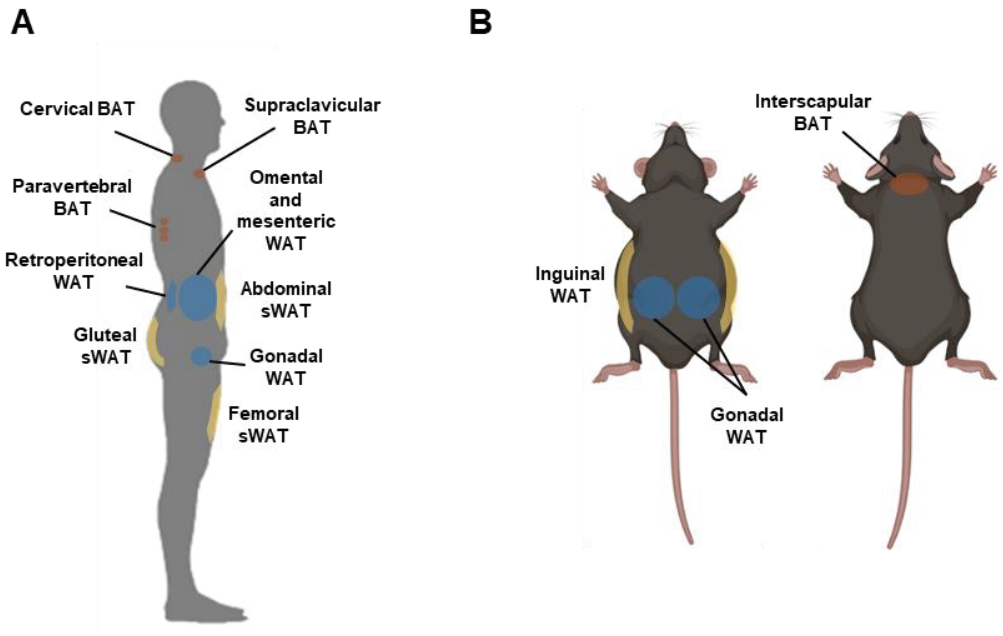

Figure 14. Location of main adipose tissue depots in adult humans (A) and mice (B). BAT depots are depicted in brown, sWAT in yellow and vWAT in blue. In mice representation, left picture corresponds to face up position, whereas right picture depicts a face down mouse. Adapted from Park, 2014[235].

III.2.1. WAT distribution

The most predominant adipose tissue in the body, WAT, can be found throughout the whole organism. Nevertheless, it is possible to distinguish two main subpopulations: subcutaneous and visceral white adipose tissue (sWAT and vWAT, respectively)[236]. **sWAT** is located under the skin in several body regions, acting as a barrier against infections, as a thermal insulator and as a cushion for external mechanical stresses. In humans, the most predominant sWAT depots are found in the abdominal and gluteal-femoral regions[237]. In mice, the classical example of sWAT depot is the inguinal WAT (**iWAT**), which is found anterior to the upper site of the hind limbs (Figure 14)[235]. **vWAT**, conversely, is located inside the peritoneum and surrounds

internal organs such as the stomach, liver, kidneys, gonads and intestines, providing them with protective padding. Depending on the organ that surround, these WATs are known as omental, retroperitoneal, gonadal or mesenteric WAT (Figure 14)[235]. Importantly, many adipose depots do not correlate precisely between human and mice. For instance, the omental WAT represents the principal deposit of visceral adipose tissue in humans while in mice it is almost absent, being the gonadal WAT (gWAT) the major representation of visceral fat of these rodents (Figure 14B)[238]. It is also important to note that in humans there are important sex-related differences as well. Hence, men accumulate more fat mass in vWAT and abdominal sWAT, while in women the gluteofemoral sWAT depots are usually the predominant fat storage[221].

sWAT and vWAT are also known to have important physiological differences in aspects like the endocrine function, the response to insulin and the rate of lipolysis and triglyceride synthesis[239,240]. In fact, preadipocytes express specific gene signatures depending on their depot of origin, and that makes them have different behaviours even after isolation and culture *in vitro* under the same conditions[241]. Probably because of these differences, sWAT and vWAT have been related to opposite effects, since accumulation of vWAT is commonly associated to the onset of metabolic disorders like diabetes, while sWAT mass has even been inversely correlated with disease risk[221]. Apart from the cell-autonomous mechanisms, another hypothesis suggested for this difference in the physiological relevance of both tissues is their specific relationship with the blood circulation. vWAT venous blood is drained directly to the liver through the portal vein, providing this organ a direct access to the free fatty acids (FFAs) and adipokines secreted by visceral adipocytes, which are usually pro-inflammatory[240].

Besides the main sWAT and vWAT depots, there are also other small and discrete WAT depots, usually closely associated with other organs or anatomical structures, where they exert novel tissue-specific functions. Regarding these depots, we can name the **dermal adipose tissue**, separated from sWAT by a striated muscle layer in mice and by the fascia superficialis in humans, that participates in hair development, pathogen resistance and skin wound healing[236]. There is also the **mammary adipose tissue**, that contains a special type of adipocytes, the pink adipocytes, that have a strongly polarized morphology resembling epithelial cells and are involved in milk

production during lactancy[242]. Another important adipose depot is the **bone marrow adipose tissue**. This tissue is composed of primarily white adipocytes derived from BM-MSCs, thus sharing a common origin with osteoblasts. Factors that favour osteogenesis usually inhibit adipogenesis and vice versa. Therefore, bone marrow adipose tissue has been related to the regulation of bone homeostasis[243]. Furthermore, bone marrow adiposity is also increased with aging and in pathological bone situations like osteoporosis[244], and it has also been proposed as an stimulator of osteoclastic activation[245]. Besides this bone-regulating activity, bone marrow adipose tissue has also been described to exert other functions, such as the regulation of haematopoiesis or the secretion of adiponectin[245].

III.2.2. BAT distribution

Brown fat represents only a small portion of all the adipose mass. This is specially marked in humans, where until a relatively short time ago it was believed that BAT depots were restricted to the neonatal and early childhood periods, disappearing in adults. However, although it is true that BAT mass is reduced in an age-dependent manner, adult humans do really present small depots of **constitutive BAT**, located mainly at discrete sites of the upper trunk like the supraclavicular, the cervical or the paravertebral regions (Figure 14A). In mice, there is a major BAT depot in the interscapular area, with a relatively large volume compared to human BAT depots (Figure 14B)[235].

The other type of brown-like cell, the **beige adipocytes**, can be found within WAT depots, as mentioned before. These cells arise upon B_3-adrenergic stimulation as a consequence of stimuli like cold exposure. Classically, beige adipocytes have been found principally in sWAT depots, and have been especially studied in the iWAT of mice, where beige adipocyte maturation is mainly due to transdifferentiation from white adipocytes[232]. Nevertheless, it has also been observed that browning can also occur in vWAT depots, where it seems to be related to proliferation of new adipocyte precursors[233].

III.3. Adipogenesis

Adipose tissues are **highly dynamic**, being in constant remodelling depending on the energy balance and thermogenetic necessities of the organism. In fact, adipose tissue is characterized for being one of the tissues with the higher expansion potential. Thus, in conditions of calorie surplus, WAT increases in size by hypertrophy and/or hyperplasia. The balance between these two forms of fat expansion has important metabolic implications, for hypertrophic adipocytes experience increased mechanical stress and hypoxia, changing their biochemical properties. Hence, when compared to smaller adipocytes, they display elevated lipolysis, increased secretion of inflammatory cytokines and a reduced production of anti-inflammatory adipokines. Conversely, hyperplasia has been seen as a good adaptative mechanism, since it allows good vascularization and the maintaining of a healthy adipocyte function[246].

Adipogenesis is the process of differentiation of new adipocytes. These cells arise from mesenchymal precursors (MSCs) present in proliferative tissues like adipose or bone marrow. As pluripotent as they are, MSCs can commit to different lineages, having the potential to become adipocytes, myocytes, osteoblasts, fibroblasts or chondrocytes (Figure 8). The determination of the cell type that will develop from a MSC depends on the activation of a specific transcription program that will stimulate one lineage while inhibiting the others[100]. The adipogenesis process is divided in two phases: first, MSCs commit to preadipocytes and then they differentiate towards mature adipocytes. During this two-step process, a plethora of signalling pathways coordinate the activation of key transcription factors that promote the expression of adipogenic proteins. Among them, **PPARγ** and CCAAT/enhancer-binding protein alpha (**C/EBPα**) are considered the master regulators of adipogenesis, and their activity is necessary for adipocyte differentiation[247].

In the first step, bone morphogenetic proteins (BMPs) play an essential role in preadipocyte commitment. Concretely, BMP2 and BMP4 have been proved sufficient to start *in vitro* adipogenic differentiation[248]. These proteins start a signalling pathway through recognition by BMP receptors that leads to the activation of SMAD4 by activating its heterodimeric partners SMAD1, SMAD5 and SMAD8. Activated SMAD4

acts as a transcription factor promoting *PPARγ* expression[246]. Other signalling proteins and transcription factors are also involved in the regulation of adipogenesis. Some of them have a positive effect on the differentiation, such as the AP-1 or the STAT transcription factor families, as well as other isoforms of C/EBP, while others exert a negative regulation of the process, like the Wnt signalling or the GATA family of transcription factors. Most of the regulation that all these proteins play in adipogenesis is through the modulation of PPARγ and C/EBPα activity[249].

The second phase of adipogenesis consists in the final differentiation of preadipocytes, when they acquire its characteristic morphology. This is a highly regulated process, although PPARγ and C/EBPα act as the orchestrators. It is described that activation of PPARγ enables a transcriptional cascade that leads to the expression of adipogenic proteins. The most important downstream effect of PPARγ is the activation of C/EBPα. These two transcription factors, when active, induce each other expression in a positive feedback and also synergize to promote the transcription of important genes for adipocyte maturation, such as *AP2*, *GLUT4*, leptin or adiponectin[225,246]. Some of these genes have been used as markers for monitoring the state of adipogenetic induction in this thesis (Figure 15).

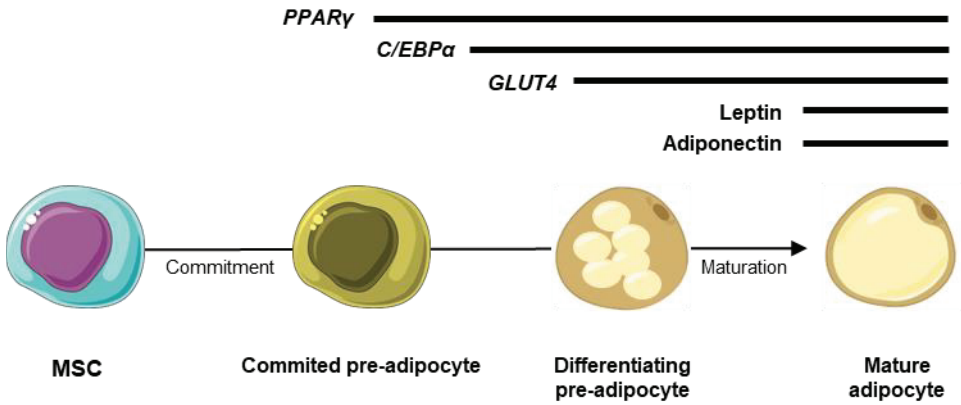

Figure 15. Expression pattern of different adipogenic markers. Adipocytes arise from MSCs upon the sequential induction a set of genes. First, they lose their pluripotency committing to a pre-adipocyte state. These pre-adipocytes conserve the same morphology as MSCs. Then, the expression of PPARγ triggers a transcription cascade, starting with the induction of C/EBPα transcription factor. These two factors cooperate to promote the expression of key proteins for adipocyte function like *GLUT4*, an insulin-dependent glucose transporter. Mature adipocytes also express genes responsible for adipose endocrine function, such as leptin and adiponectin. Adapted from Ghaben and Scherer, 2019[246].

III.3.1. Brown adipogenesis

White and brown adipocytes have **different developmental origins**. Even if both derive from mesenchymal stem cells, the precursors of brown adipocytes are characterized by the expression of the myogenic factor 5 (Myf5), while white pre-adipocytes do not express this marker. Hence, brown adipocytes share a common lineage with the skeletal myogenic cells. This is true for constitutive brown adipocytes found in BAT discrete depots, but not for beige adipocytes that arise from browning upon stimulation in WAT depots. These brite cells, although being morphologically and functionally brown, share the white Myf5-negative lineage (Figure 16)[227,238,250].

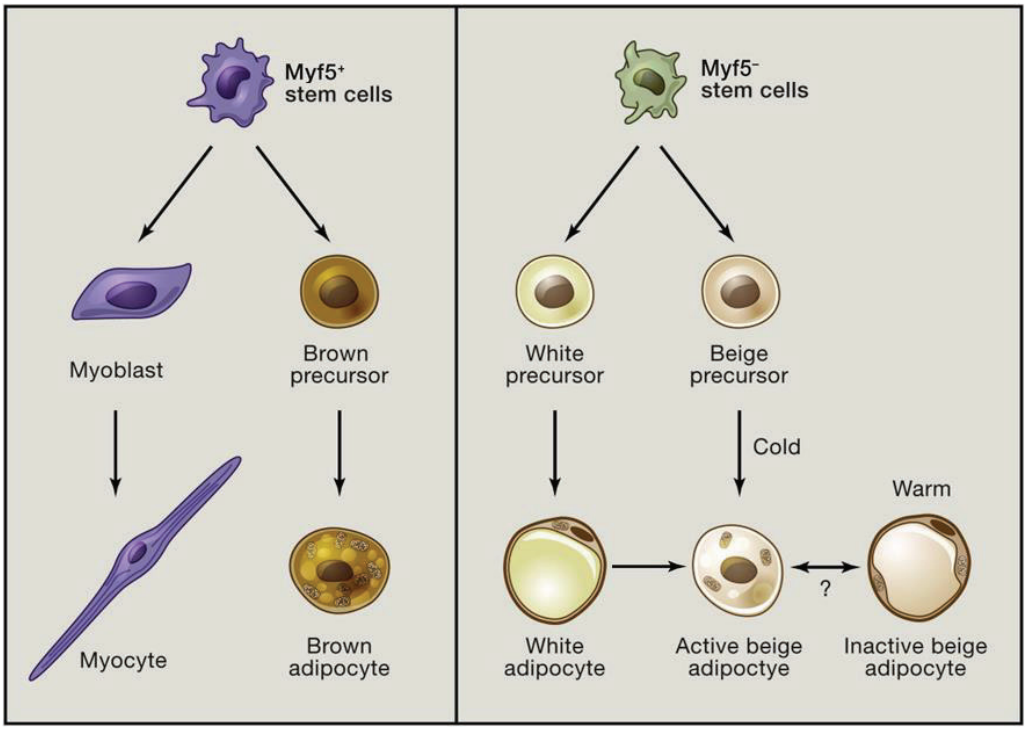

Figure 16. Lineage origin of different adipocytes. Brown adipocytes derive from Myf5-positive stem cells, which also give rise to myocytes. Conversely, white and beige adipocytes arise from Myf5-negative stem cells. It is suggested that beige adipocytes can appear by transdifferentiation of white adipocytes of by proliferation of beige precursors in WAT. Beige adipogenesis is stimulated by cold exposure, and brite adipocytes can adapt a white phenotype upon ceasing of the cold stimulus. Modified from Rosen and Spiegelman[238].

Despite originating from different lineages, both white and brown adipocytes rely on the same PPARγ and C/EBPα-orchestrated transcriptional cascade for adipogenesis[251]. However, there are other factors that have been found necessary for

the specification of the brown phenotype, both in brown and beige adipocytes. One of them is **PGC1α** (PPARγ-coactivator-1α), which is a coactivator of PPARγ that is also involved in mitochondrial biogenesis, modulating oxidative metabolism and thermogenesis. The induction of PGC1α leads to the expression of regulatory enzymes of mitochondrial metabolism and of **UCP1** (Uncoupling protein 1), which is the enzyme that provokes the uncoupling of the mitochondrial respiratory chain, dissipating its energy in the form of heat. Thus, it is responsible for the process of non-shivering thermogenesis, main characteristic of the brown adipocytes[252]. Other transcription factor implicated in conferring brown cell identity is PRDM16 (PRD1-BF1-RIZ1 homologous domain containing 16). PRDM16 co-regulates important factors like PPARγ, C/EBPα and PGC1α, inducing the expression of brown-fat specific genes. PRDM16 plays a pivotal role in the specification of brown cell phenotype, since it is able to induce both the browning process of white adipocytes and the differentiation of myogenic precursors to brown adipocytes[253–255]. Besides these, other factors also regulate brown adipogenesis, both favouring it or inhibiting the process. The latter is the case for some microRNAs like miR-133a/b or miR-155, that impair thermogenic genes expression by targeting the transcription factors implicated in their synthesis[250,251].

The emergence of brown and beige adipocytes is highly stimulated by cold exposure. This stimulus provokes the stimulation of the adipose tissue by the sympathetic nervous system (SNS), that releases catecholamines like norepinephrine. These molecules are recognized by **β-adrenergic** receptors, which enable signalling cascades that lead to the expression of brown adipogenic and thermogenic genes. Concretely, the activation of β1-adrenegic receptors in BAT stimulates brown adipogenesis[256]. In WAT, the browning is linked to β3-adrenergic stimulation, which causes the transdifferentiation from white to beige adipocytes[231,232].

III.4. Adipose tissue functions

Adipose tissue is **a complex organ** that exert a plethora of functions in the whole organism. In addition to the energy storage and regulation of lipid metabolism, it also has important endocrine functions, being responsible for the secretion of several factors that act on many other tissues. Moreover, the heterogeneity of adipose tissues allows the specialization of very different activities, like the thermogenesis of BAT and beige adipose tissue (BgAT). Here, I present a brief review of some of the most relevant functions of adipose tissue.

III.4.1. Energy homeostasis and lipid metabolism

The most classically known function of adipose tissue is the energy storage in the form of triacylglycerols, deposited in the large lipid vacuole that white adipocytes present. These triglycerides (TGs) are lysed and released to the circulation as free fatty acids, that can be used as energy fuel by other organs when glucose is limiting. This function is highly regulated by internal and external factors that are integrated in the white adipose tissue, that hence acts as a master regulator of energy homeostasis[257].

The **accumulation of lipids** in adipocytes is enhanced when there is an energy surplus in the organism. The first sensor for this state is glucose levels, which are usually elevated after high carbohydrate feeding. This increased circulating glucose causes, in healthy individuals, the secretion of insulin from the pancreas. **Insulin**, the key hormone for the regulation of energy homeostasis, is recognized by receptors on the surface of adipose cells and this initiates a signalling cascade that leads to the mobilization to the cell membrane of the insulin-dependent Glucose transporter type 4 (GLUT4). Through this protein, glucose enters the adipocyte where it undergoes glycolysis. As a result, the cells produce glycerol-3-phosphate (G3P), which will serve as the backbone for TGs, and pyruvate, which enters the mitochondria for further oxidation, producing citrate as an intermediate metabolite. This citrate is transformed to acetyl-coenzyme A, which in turn serves as the substrate for the synthesis of new fatty acids in the process of *de novo* **lipogenesis**. Furthermore, the signalling by insulin also induces the expression of genes involved in this process, such as *ACC1* (Acetyl-CoA carboxylase 1) or *SCD1* (Stearoyl-CoA desaturase-1), as they code for the enzymes

responsible for the processing of acetyl-coA to fatty acids. On the other hand, a high fat diet inhibits de novo lipogenesis, since high levels of fat are also recognized by adipocytes, and they repress the expression of the genes upregulated by insulin (Figure 17)[258,259].

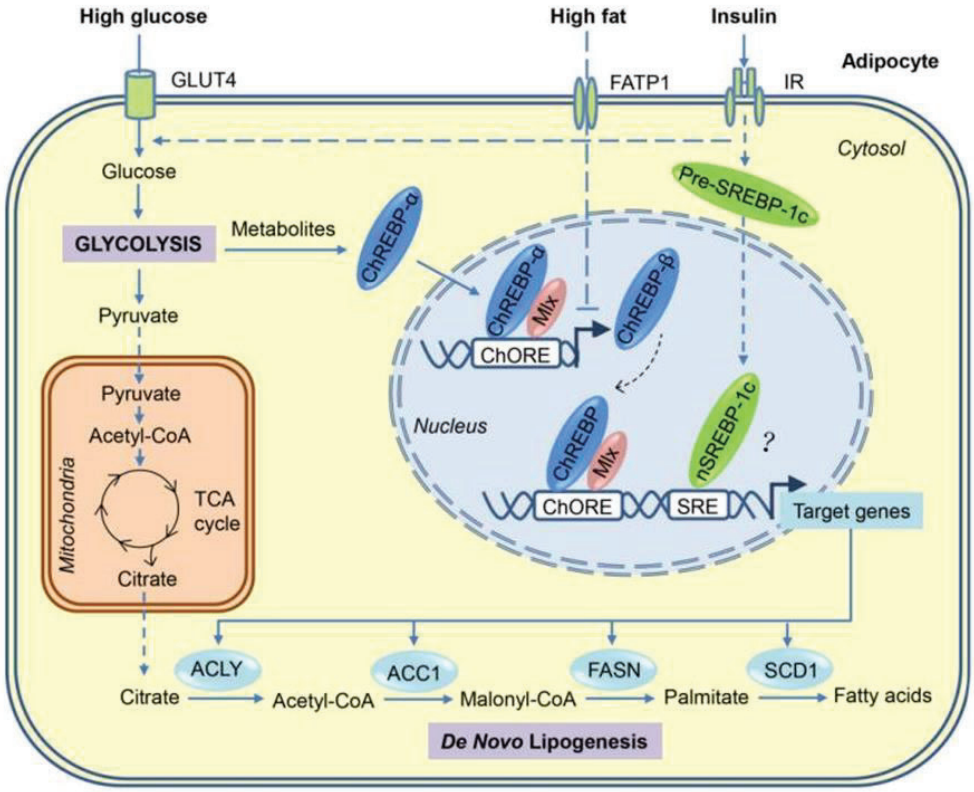

Figure 17. Activation of lipogenesis in adipocytes. Glucose is internalized in the cell by insulin-activated channel GLUT4. Glucose undergoes glycolysis in the cytosol, and the resulting pyruvate enters the mitochondria for the tricarboxylic acid cycle. Citrate is exported to the cytosol where it serves as a substrate for lipogenesis, process in which it is transformed to fatty acids by enzymes coded by genes regulated primarily by the interaction of Carbohydrate response element binding protein (ChREBP) with the carbohydrate response elements (ChORE). The Sterol response element binding protein 1c (SREBP-1c), a transcription factor activated by insulin signalling, may also play a role in the expression of these genes, although its function is not fully elucidated. High fat levels, conversely, inhibit de novo lipogenesis by repressing the activity of ChREBP. This inhibition is mediated by the internalization of fatty acids by the Fatty Acid transport protein 1 (FATP1). ACLY: ATP-citrate lyase; ACC1: Acetyl-CoA carboxylase 1; FASN: Fatty acid synthase; SCD1: Stearoyl-CoA desaturase-1; IR: Insulin receptor; SRE: Sterol regulatory element; Mlx: Max-like protein X. From Song et al. 2018[259].

Other source of lipids for adipocytes are TGs originally synthesized in the intestine or liver that enter the bloodstream bound to chylomicrons or very low-density lipoproteins (VLDL). Insulin plays a key role in the uptake of these lipids by the

adipocytes, for it is responsible for the activation of lipoprotein lipase (LPL) in the vascular endothelium of adipose tissue. LPL hydrolyse the circulating TGs, thus liberating non-esterified fatty acids (NEFA) that can be translocated to the interior of the adipocyte by specific transporters like CD36 or the fatty acid transporter proteins (FATPs). This translocation is also stimulated by insulin action. Once NEFAs are inside the cell, they incorporate acetyl-coA by the acetyl-CoA synthetase (ACS) enzyme, converging with the process of *de novo* lipogenesis to produce TGs for storage[259–261].

Inversely, during states of energy demand, like exercise or fasting, TGs are broken by **lipolysis**, that releases NEFA and glycerol that enter the circulation to serve as an energy supply for other tissues such as muscle and liver. In the process of lipolysis, TGs are sequentially disassembled: first, triglycerides are transformed into diglycerides by the action of the adipocyte triglyceride lipase (ATGL), that release one of the fatty acids. Then, the hormone-sensitive lipase (HSL) converts the diglyceride into a monoglyceride. Last, the monoacylglycerol lipase (MGL) hydrolyse the monoglyceride for the release of the last fatty acid and a glycerol molecule[258].

Different factors **induce lipolysis**. One of the most classical is the stimulation of β-adrenoreceptors of adipocytes by catecholamine secretion from the SNS. The activation of these receptors initiates a lipolytic cascade by the stimulation of cyclic adenosine monophosphate (cAMP) production. Elevated cAMP levels cause the activation of Protein kinase A (PKA), responsible for the phosphorylation of HSL and Perilipin, activating the former and inhibiting the latter. This allows the translocation of HSL to the lipid vacuole, since Perilipin is a lipid droplet-associated protein that protects it from the hydrolysis of HSL. Other factors also cooperate in the induction of lipolysis under energy demands, like circulating glucagon or the signalling by natriuretic peptides or other hormones such as the growth hormone and the thyroid-stimulated hormone. There is also a lipolytic induction produced by adipokines with autocrine and paracrine effects, like leptin. TNF-α is another of the pro-lipolytic factors, acting through the activation of the MAPK pathway of ERK, that leads to the phosphorylation and inhibition of Perilipin, thus facilitating HSL activity[258,262,263].

On the other hand, some factors **negatively regulate lipolysis**. The most important of these factors is insulin. Insulin signalling in adipocytes also leads to the activation of phosphodiesterase 3B (PDE-3B), an enzyme that catalyse the breakdown of cAMP, thus supressing the activity of PKA and inhibiting lipolysis[264]. In this way, insulin coordinates the lipid metabolism in adipocytes depending on the energy state of the organism: when glucose levels are high after feeding, insulin stimulates lipogenesis and inhibits lipolysis. Among the other factors that downregulate lipolysis there is adiponectin, another adipokine produced by the adipocytes that has autocrine and paracrine action. This protein has been shown to inhibit lipolysis through AMPK-mediated mechanism, and to supress HSL activation[263,265].

III.4.2. Endocrine function

In addition to the regulation of lipid metabolism, both white and brown adipose tissues are also responsible for the secretion of a plethora of regulatory factors with autocrine, paracrine and endocrine action. Some of these adipose factors are peptides, which are named **adipokines**, but others are from a lipidic nature, and are known as **lipokines**. Through these regulatory factors, fat targets many other organs such as liver, muscle or brain, thus regulating systemic functions like food appetite, energy expenditure, glucose metabolism, bone homeostasis or insulin sensitivity, among others (Figure 18)[220,266]. The whole adipokine pool in humans is vast, comprising around 600 potential adipokines[267]. However, only two of them, leptin and adiponectin, are selectively expressed in adipocytes. Therefore, the rest of cell types present in adipose tissue, such as immune cells and fibroblasts, also play an important role in the endocrine function of this organ[220,267].

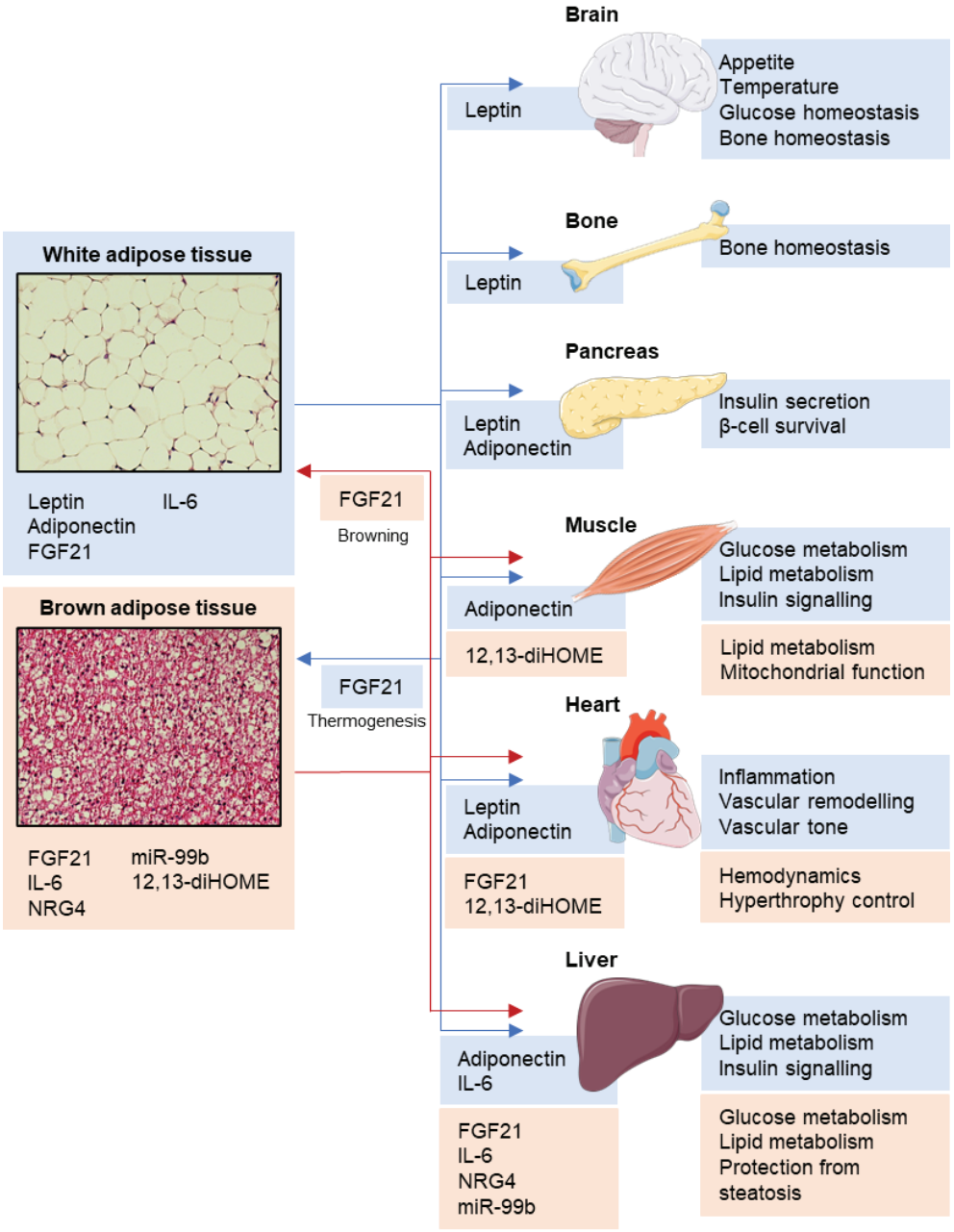

Figure 18. Endocrine effects of adipokines. Representation of the pattern of action of some of the most relevant adipokines secreted from white and brown adipose tissues. Blue lines and boxes represent secretion from WAT, and red lines and light orange boxes represent secretion from BAT. Right to each organ, the functions exerted by WAT adipokines are represented in light blue boxes, while the functions derived from BAT factors are written in light orange boxes. Adapted from Scheja and Heeren, 2019[220].

III.4.2.1. Leptin

Leptin was the first adipokine identified, that changed the paradigm for the study of adipose tissue in 1994. This protein is encoded by the obesity gene (*ob*), also known as *Lep*, and deficiency of this gene in mice provokes an extremely obese phenotype[218]. Nowadays, it is well known that leptin plays a major role in the control of energy balance primarily by the **suppression of appetite**, inhibiting food intake. In healthy humans and rodents, circulating leptin levels positively correlate with adipose mass and are reduced when prolonged fasting. In this fasted state, the SNS stimulate the adipose tissue β-adrenergic receptors, signal that inhibit leptin production. Thus, leptin levels are a sensor for the nutritional state and the energy demands of the organism[220,268].

The appetite suppression function is exerted by passing the blood-brain barrier and targeting the hypothalamus, which cells present leptin receptors (LEPR) on their surface. The stimulation of these receptors in the hypothalamus enables signalling cascades that result in the promotion of the expression of anorexigenic peptides like POMC or BDNF (appetite blockers), and the inhibition of orexigenic factors such as NPY, orexin or galanin (stimulators of appetite)[258,269]. Leptin signalling in the central nervous system has also been related to the promotion of energy expenditure in mice through thermogenesis, although the effect is not clear on humans[270]. However, recent studies have shown that leptin does not seem to elicit a thermogenic effect, but rather regulates heat loss[271].

LEPRs are also present in other peripheral tissues where leptin also exerts important functions. By targeting β-cells in the pancreas, leptin signalling modulates glucose homeostasis by regulating insulin production and secretion through the modulation of β-cell mass and survival[272]. Leptin has also been related to the regulation of reproductive organs[273,274]. Furthermore, leptin is strongly involved in **bone homeostasis**, both from central and peripheral signalling. The central modulation has a catabolic effect and occurs mainly through the activation of the SNS by leptin stimulation. SNS then acts on bone by suppressing osteoblast formation and promoting osteoclastic activity, thus reducing bone mass. Inversely, in the peripheral pathway leptin has an anabolic effect, since it is recognized by receptors on BM-MSCs, resulting

in the facilitation of the osteoblastic differentiation of these cells. Moreover, leptin has also been found to repress osteoclast maturation in vitro. Hence, the peripheral action of leptin on bone causes an increase in bone mass, creating a balance with the opposite effects that the central signalling has. In line with this functions, leptin levels have been related to different bone diseases such as osteoporosis or osteoarthritis[275].

III.4.2.2. Adiponectin

Adiponectin is the other adipokine specifically produced and secreted by the adipocytes. Encoded by the *ADIPOQ* gene in humans and its homologous *Acrp30* in mice, this protein is key for **insulin sensitivity** and has anti-inflammatory and antiapoptotic properties. Contrary to leptin, circulating adiponectin levels are usually negatively correlated with adipose mass, which explain some of the consequences of obesity that lead to the development of metabolic syndrome features such as insulin resistance[276]. Adiponectin signalling is mediated by binding to its receptors AdipoR1, highly expressed in muscle, and AdipoR2, nearly restricted to liver. The activation of these receptors enables a cellular response mediated by the adaptor protein APPL1. Through this protein, adiponectin promotes the phosphorylation of two main signalling cascades: the Adenosine monophosphate protein kinase (AMPK) and the p38 MAPK pathways. AMPK activity causes an increase in mitochondrial biogenesis, primarily in muscle, and decrease gluconeogenesis, while p38 signalling provokes an increase in glucose intake[276-278]. Besides these pathways, APPL1-mediated adiponectin action also stimulates the activity of PPARα, which enhances fatty acid oxidation[279]. Furthermore, APPL1 also facilitates the downstream signalling from the insulin receptor[280]. Altogether, these catabolic effects lead to the decrease in TG content in muscle and liver, improving insulin sensitivity[276].

III.4.3. Thermogenesis

Brown adipose tissue is the main effector of **adaptive non-shivering thermogenesis**. This process consists in the production of heat as a response to environmental temperature and diet, and it is necessary to protect the organism from hypothermia and to regulate the body energy balance[281]. This is especially relevant in newborns, rodents and hibernating animals, in which BAT represents a higher portion

of total adipose mass, with large BAT depots clearly recognizable, although imaging studies have shown that adult humans also possess BAT depots in different locations, although considerably smaller[250].

The thermogenic function executed by brown adipocytes requires **high energy consumption**, for what these cells use glucose and fatty acids as fuel. Glucose uptake is stimulated by the same stimuli that promote thermogenesis, like cold exposure, and it is also accomplished in an insulin-dependent manner, although some insulin-independent pathways have been proposed as well. Fatty acids, the other main energy source of these cells, are easily available by lipolysis of the TGs stored in the multiple lipid droplets that brown adipocytes contain. Nevertheless, brown adipocytes also perform de novo lipogenesis and take up NEFA from the circulation[282].

The high number of mitochondria present in brown adipocytes are responsible for non-shivering thermogenesis. This phenomenon is accomplished by the **uncoupling of the mitochondrial respiratory chain**, which is normally used to produce ATP from the transmission of electrons provided by the oxidation of carbohydrates, lipids and proteins[283]. In brown and beige adipocytes, this electron chain is interrupted by the **UCP1 protein**, that thus prevents the formation of ATP, dissipating the energy accumulated as heat[281]. The extensive vascularization that BAT has facilitates the dissipation of the produced heat through the blood.

BAT is not only extensively vascularized, but also highly innervated by the efferent fibres from the SNS. This allows the central control of adaptive thermogenesis, since the SNS is activated by cold exposure and also by leptin signalling after feeding. Hence, upon these stimuli the SNS release catecholamines in adipose tissue that stimulate both lipolysis and thermogenesis, increasing the energy expenditure and contributing to maintain body temperature. The enhancing of thermogenesis in BAT is mainly mediated by the stimulation of the **β3-adrenergic receptors**, which activation is also a cause of browning in WAT[231,232,281,284]. As explained before, β3-adrenergic stimulation increases the levels of cAMP, which activates PKA. This kinase, apart from the facilitation of lipolysis, is also responsible for the induction of thermogenesis through the phosphorylation of MAPK p38, which upregulates *UCP1* expression by

activating PGC1α and ATF-2 transcription factors[285,286]. In mice, the suppression of the sympathetic tone by the acclimation of the animals to thermoneutrality (30-32°C) results in lipids accumulating and coalescing into larger lipid droplets in brown adipocytes, acquiring a WAT-like morphology. Likewise, beige adipocytes also enter an inactive white form. When mice are moved back to the mild cold (20-22°C), BAT recovers its functional phenotype, and it is further expanded by hyperplasia if the mice are exposed to severe cold temperatures (4-6°C)[251]. The process of lipid droplet fusion is mediated by the Cell Death Inducing DFFA Like Effector A (CIDEA)[287]. The presence of this protein is highly specific for brown adipocytes, and hence it is also used as a marker of brown differentiation[288].

III.5. Energy balance

Energy balance is the relation between the caloric intake and the energy expenditure of an organism. Alterations of this balance causes changes in body mass: when there is a surplus of energy intake, the body weight is risen mainly because of an increase in fat deposition. Conversely, when energy expenditure surpasses energy intake there is a negative energetic balance that leads to a loss of body mass[289]. The intake of calories comes exclusively from feeding, but the total energy expenditure is complex, for it depends on many different processes. Nonetheless, it can be divided in three main components: physical activity, basal metabolic rate and adaptive thermogenesis[290].

The energy consumed by **physical activity** is highly variable, as it depends on many factors like the amount of exercise performed, the energy cost of the activity and the own individual that performs it. In normal conditions, it usually represents between an 8-15% of the total energy expenditure. It is proved that physical activity is inversely proportional to the body weight, although it is a trait influenced by both genetic and environmental factors[291].

The **basal metabolic rate (BMR)** is defined as the energy expenditure of an individual in a resting state in thermoneutrality. There are many variables that can be measured for the calculation of BMR, but the most commonly used is the oxygen consumption rate when there are no differences in the locomotor activity and there is

no thermal stress[292]. The main modulators of this basal metabolism are the thyroid hormones, which have been extensively proved as stimulators of energy expenditure by the increase of BMR[293].

Adaptive thermogenesis is the heat production as a response to environmental temperature and diet. Although it can be executed in the muscle coupled to muscular contraction (shivering thermogenesis), the main effector of adaptive thermogenesis is the BAT, that performs the process of non-shivering thermogenesis that has been detailed in the previous section[281].

III.6. Obesity and metabolic syndrome

The aetiology of **obesity** is very complex, being affected by factors such as socioeconomic status, environment and personal behaviours or genotype-phenotype interactions. However, the convergence of all the different factors results in a chronic energy disbalance, when the energy intake surplus is maintained for a long time causing an excessive accumulation of adipose tissue[294]. Although being an imprecise tool, the body mass index (BMI) is the most commonly used measurement for the diagnosis of obesity[295]. It is based on the quotient between the body mass of the individual in kg and their square heigh in m^2. The World Health Organization (WHO) uses the BMI to define undernutrition when BMI≤18.5 kg/m^2, normal weight when BMI=18.5-24.9 kg/m^2, overweight when BMI=25-29.9 kg/m^2 and obesity when BMI surpass 30 kg/m^2. BMI values over 40 kg/m^2 are considered extreme obesity[294]. Over the last five decades, the prevalence of obesity has dramatically increased in all countries of the world, with a specially alarming affectation of children and adolescents[296].

Obesity constitutes an important risk factor for the development of **metabolic syndrome**. This state is characterized by the combination of different features such as obesity, insulin resistance, dyslipidaemia and hypertension, that together lead to the development of severe comorbidities like type 2 diabetes mellitus, non-alcoholic fatty liver disease (NAFLD) and cardiovascular disease, that reduce the life expectancy and quality of the affected people[297].

III.6.1. Insulin resistance

Insulin is the key hormone for the regulation of systemic glucose and lipid metabolism. Its function is not restricted to the adipose tissue, but in fact there are many insulin-sensitive organs that depend on its signalling. Thus, insulin stimulates glucose-consuming tissues such as skeletal muscle, adipose tissue and liver, to uptake glucose and promote the synthesis of glycogen and lipids, while inhibiting lipolysis and hepatic gluconeogenesis. **Insulin resistance** is defined as the inability by some tissues to respond to physiologically normal levels of insulin, thus impairing the functions exerted by insulin signalling and the capacity for lowering circulating glucose levels after feeding. These consequences make insulin resistance a major component of metabolic syndrome and a prevalent risk factor for type 2 diabetes[298].

Obesity and insulin resistance are closely related[299]. The persistently positive energy balance pushes the plasticity of WAT to its limits. The excess of energy is stored in adipose tissue in the form of TGs, for this tissue needs to expand. The first mechanism for this expansion is adipocyte hypertrophy[300]. However, hypertrophic adipocytes show a pro-inflammatory adipokine secretion pattern, with a reduction of the production of insulin-sensitizers factors like adiponectin. Furthermore, these overloaded cells have a lower lipogenesis-to-lipolysis ratio, provoking the leakage of more NEFA to the bloodstream, thus increasing circulating FFAs[246]. To protect the organism from this state, adipose tissue is also able to expand by hyperplasia, inducing the differentiation of new adipocytes from mesenchymal precursors. However, there is a limited number of precursors cells in adipose tissues, and the hypertrophic tissue also has impairments in the adipogenesis process[300]. Altogether, the persistence of a positive energy balance creates a dysfunctional overloaded WAT incapable of containing all the caloric excess, increasing the circulating lipids that will be deposited in non-adipose tissue organs. This phenomenon is known as **ectopic fat accumulation**, and it is a cause of **lipotoxicity**, which causes metabolic alterations in processes related to fatty acid oxidations and in intracellular signalling. Insulin signalling is one of mechanisms affected by this lipotoxicity, that hence induce the development of insulin resistance. Consequently, ectopic fat accumulation in tissues like liver or skeletal muscle is considered a good predictor for insulin resistance[298–301].

III.7. Signalling in adipose tissue homeostasis

Adipose tissue homeostasis is complex, since it is a highly dynamic tissue that is constantly remodelled and it is also a very active organ, exerting many key functions for systemic homeostasis. Therefore, a multitude of signalling pathways are involved in the regulation of adipose tissue. Next, similarly to the previous chapter, the implication of MAPKs and ubiquitylation will be briefly reviewed.

III.7.1. MAPK signalling in adipose tissue

MAPKs pathways are involved in many cellular processes, especially in those related to cell proliferation, migration and differentiation. Thus, it is not surprising that they have been related to the regulation of adipogenesis[302]. Moreover, some of the pathways have also been found as modulators of adipose tissue function and homeostasis[302,303].

ERK role in adipogenesis is controversial. On the one hand, some studies have shown that ERK activation has a positive effect on adipocyte differentiation as a mediator of insulin signalling, since this kinase is part of its canonical phosphorylation cascade[304]. Furthermore, other works have described that ERK activity is necessary for the expression of the adipogenic key factors PPARγ and C/EBPα, thus corroborating its positive role[305]. Moreover, deletion of *Erk1* in mice causes an impairment in adipogenesis, together with decreased adiposity and protection to the obesity and insulin resistance provoked by a high fat diet. In this study, the authors also show that WT animals fed a high fat diet have increased ERK activity, which supports the role of ERK in the promotion of obesity[306]. Interestingly, adipocytes from human patients with type 2 diabetes also present increased ERK phosphorylation[307]. On the other hand, ERK has also been linked to a negative regulation of adipogenesis. As explained in the bone chapter, PPARγ is phosphorylated in S112 by ERK, with an inhibitory effect on its activity and thus supressing adipogenesis[173,174]. The discrepancy between these results could be explicated by the hypothesis that ERK activity must be timely regulated: activated in the first step of adipogenesis but turned off later to prevent PPARγ from being phosphorylated[308].

p38 MAPK has been thoroughly studied in relation with adipose tissue homeostasis, and therefore it has been related to multiple processes such as differentiation of both white and brown adipocytes, adipokine secretion, browning and BAT thermogenesis[303]. Regarding **adipogenesis**, it has been seen that p38 is also necessary in the first steps of differentiation for the phosphorylation of C/EBPβ, an upstream activator of C/EBPα and PPARγ. Inhibition of p38 impairs the phosphorylation of PPARγ and the accumulation of lipids in primary human preadipocytes, but it has no effect in later stages of differentiation[309,310]. Nevertheless, other studies have reported that p38 activity also has negative effects on adipocyte differentiation through the activation of CHOP, a negative regulator of C/EBPα, and that p38 activity declines during adipocyte differentiation and its deficiency stimulates adipogenesis both *in vitro* and *in vivo*[311,312]. The contradictory results suggest that p38 could also be playing a timing-dependent role in adipogenesis, similarly to ERK. However, a growing body of evidence is supporting the role of p38 as a positive regulator of adipogenesis through the integration of the signalling by various upstream activators, such as BMP proteins[303].

p38 also plays an important role in **thermogenesis**. As commented before, the β3-adrenergic stimulation driven by SNS is a major inducer of the thermal activity, and this function is partly mediated by p38, which is phosphorylated by PKA and contributes to the expression of *UCP1* gene by the activation of the transcription factors PGC1α and ATF-2[285,286]. Moreover, p38 activity as mediator of BMP signalling also has implications in the thermal activity, as it stimulates brown adipogenesis and BAT activation[313,314]. Besides the stimulation of thermogenesis in BAT, the adrenergic stimulation by SNS is also a cause of browning in adipose tissue, following the same cellular mechanisms involving PKA and p38 activity[315]. Browning in WAT is also mediated by BMPs and by many other signalling molecules such as FGF21 or the cardiac natriuretic peptides, by the enabling of pathways that converge in the activation of p38[303]. All this evidence points to the key role that this MAPK plays in the integration of the thermogenic stimuli.

p38 activity in other tissues has also proved relevant for the homeostasis of adipose tissue. Adipose tissue is in constant crosstalk with many other organs, being

both a regulator and regulated by them. A good example of this is the bone, which homeostasis is dependent on a healthy adipose tissue, and its secreted factors have a strong influence in the maintaining of it[97,243,316]. Interestingly, p38 function in osteoblasts has been seen necessary for adipose tissue homeostasis. An osteoblast conditional KO of *p38α* in mice causes a strong decrease in body weight and adiposity that was paired with an increase of energy expenditure through thermogenesis, for *Ucp1* levels were upregulated in WAT and BAT. These alterations were not related to osteocalcin signalling, but rather to a decrease in the bone production of NPY. Furthermore, restoration of NPY circulating levels partially restore the phenotype[83]. These results indicates that bone regulates adipose tissue homeostasis through diverse ways, and that p38 activity in other tissues is also key for the correct adipose functions.

III.7.2. Ubiquitylation in adipose tissue

Among the PTMs involved in the regulation of adipose tissue homeostasis, the role of **ubiquitylation** is not the most extensively explored, although it is a growing field of research with some works that have started shedding light on how ubiquitin ligases can modulate several key processes for adipose tissue formation and function.

Adipogenesis is controlled by many different mechanisms, but in the end most of the signals are integrated into the regulation of two master transcription factors, PPARγ and C/EBPα. **PPARγ** has been the focus of most of the studies intended to elucidate the modulation mechanisms of adipogenesis. This protein has a short half-life in adipocytes and its stability is regulated by the ubiquitin-proteasome system[317]. This is an important feature for this factor, since it has been reported that the same ligands that promote the transcriptional activity of PPARγ also induce its ubiquitin-mediated degradation, highlighting the importance of PPARγ timing regulation[318]. However, the modulation of this transcriptional factor by ubiquitin ligases goes in both directions, as ubiquitylation by some E3 enzymes target PPARγ for degradation, as is the case for TRIM25, while other ubiquitin ligases, like NEDD4, provoke the stabilization of this protein[319,320]. This ambivalence evidences the complexity of the ubiquitin-mediated regulation of PPARγ, which allows the fine-tuning of its protein levels during the process of adipogenesis.

C/EBPα is the other master regulator of adipocyte differentiation. Like PPARγ, its stability is also regulated by ubiquitin ligases. FBW7, an E3 enzyme also involved in the modulation of osteogenesis[208], targets C/EBPα for degradation by direct ubiquitylation, thus reducing its protein levels and inhibiting adipogenesis[321]. Similarly, the HECT ubiquitin ligase E6AP also negatively regulates adipocyte differentiation by promoting the ubiquitylation of C/EBPα, reducing its proteins levels. Interestingly, E6AP expression is downregulated during early adipogenesis, which suggests that the correct regulation of C/EBPα by ubiquitylation is a key mechanism for the control of the first steps of adipocyte differentiation[322]. The essential role of ubiquitin-mediated protein degradation in the modulation of adipogenesis is corroborated by the fact that proteasome dysfunctions disrupt adipocyte differentiation[323]. These impairments in the ubiquitin-proteasome pathway have also been reported as causes of age-related adipogenesis dysfunction[324].

Thermogenesis is another adipose function controlled by ubiquitylation. One example of an E3 ligase involved in this regulation is RNF34, a RING ubiquitin ligase that ubiquitylates PGC1α, targeting it for degradation and reducing the thermal activity of brown adipocytes. Furthermore, the β3-adrenergic stimulation on these cells supresses RNF34 expression. This indicates that this E3 enzyme could be a constitutive repressor of thermogenesis, which inhibition upon thermogenic stimuli is necessary for the proper function of brown adipocytes[325]. Other ubiquitin ligases are involved in the regulation of browning. This is the case of CUL2, another member of the RING family, that catalyses the ubiquitylation of PRDM16, thus suppressing beige fat biogenesis. Inhibition of this E3 enhances the browning process. Interestingly, aging provokes an increase in the expression of CUL2, which can be an important factor for the reduced browning ability that occurs at elevated ages[326].

The ubiquitin-mediated regulation of adipose tissues has important consequences for the energy balance and metabolic health of the organism. The ubiquitylation of different members of the insulin signalling cascade, such as insulin receptors or AKT, reduce their proteins levels and is related to the development of **insulin resistance**. Some members of the Cullin family of RING ubiquitin ligases are involved in the targeting of these proteins. These E3 enzymes are induced by pro-

inflammatory factors, which would partly explain how pro-inflammatory secretions from hypertrophic adipocytes can induce insulin resistance and lead to diabetes[327].

OBJECTIVES

The availability in the laboratory of the *Herc1*-knockout mouse strain gave us a powerful tool to study the role of this gene in an *in vivo* context. Thus, our main aim in this thesis was to characterize the model to evaluate the physiological relevance of HERC1 in different phenotypes. Specifically, we focused on two main goals:

1. Study the modulation of bone homeostasis by HERC1.
2. Analyse the role of HERC1 in metabolic health and adipose tissue.

MATERIALS AND METHODS

I. Animals

The *Herc1*-knockout mouse strain (C57BL/6N-*Herc1*<em3(IMPC)Wtsi>/Wtsi (EM:10257))[75] was produced by Dr. Chris Tyler-Smith and Dr. Michal Szpak in the Wellcome Trust Sanger Institute Mouse Genetics Project (Sanger MGP). These animals display a 191 bp deletion in the exon 8 of *Herc1* gene, producing a truncated and unstable protein. The animals were maintained at 22-24°C on a 12-hour light/12-hour dark cycle and had *ad libitum* access to food and water. Mating pairs or trios were created using only *Herc1*-heterozygous mice, since homozygosis of the *Herc1*-KO allele provokes infertility in males[75] and a very poor breeding efficiency in females (data not shown). For body weight monitoring, mice were weighed weekly using the same weighing scale.

All procedures were approved by the Ethics Committee for Animal Experimentation of the University of Barcelona and the Generalitat de Catalunya.

I.1. Mice identification

Mice littermates were identified with small incisions in their ears, and the tissue removed was used for DNA extraction and genotyping of *Herc1*.

Table 2. Coding system used for mice identification

Mice	Left ear (L) marks	Right ear (R) marks	Code
1	0	1	NR
2	1	0	LN
3	1	1	LR
4	0	2	N2R
5	2	0	2LN
6	1	2	L2R
7	2	1	2LR
8	2	2	2L2R

I.2. DNA extraction from mice

For digestion of mice tissues and purification of DNA, 2 different methods were used:

I.2.1. NucleoSpin Tissue Kit

DNA purification with NucleoSpin Tissue Kit (Macherey-Nagel #740952.250) was performed following the manufacturer instructions:

1. For each sample, mix 180 µL of lysis buffer (T1) with 20 µL of proteinase K solution. Incubate the tissue for 1-3 hours, or overnight, at 56°C.
2. Lyse the samples by adding 200 µL of buffer B3, vortex vigorously and incubate for 10 minutes at 70°C.
3. Adjust DNA binding conditions adding 210 µL of ethanol (96-100%) to the sample and vortex vigorously.
4. Place a column into a collection tube and apply the sample to the column to bind the DNA to the filter. Centrifuge for 1 minute at 11000G and discard the flow-through.
5. Wash twice the silica membrane:
    a. 1st wash: add 500 µL of buffer BW. Centrifuge for 1 minute at 11000G. Discard flow-through.
    b. 2nd wash: add 600 µL of buffer B5. Centrifuge for 1 minute at 11000G. Discard flow-through.
6. Dry the silica membrane by centrifuging again for 1 minute at 11000G.
7. Elute the DNA by adding 50 µL of pre-warmed (70°C) buffer BE. Incubate 1 minute at room temperature and centrifuge 1 minute at 11000G into a new and autoclaved centrifuge tube.

I.2.2. Quick DNA purification protocol

A faster and cheaper method for DNA extraction from mice tissue proved equally good results for our aims, although it should be tested for every new purpose. This protocol was adapted from The Jackson Laboratory[328]:

1. Incubate the tissue with 75 µL of solution A (25 mM NaOH, 0.2 mM EDTA) for 1h. at 98°C.
2. Lower the temperature of the sample by placing it in ice. This only needs to be done once, and the rest of the protocol can be performed at room temperature.
3. Add 75 µL of solution B (40 mM Tris-HCl, pH=5.5).
4. Centrifuge at 6000 rpm for 3 minutes.
5. Separate the supernatant in a new autoclaved tube, avoiding taking rests of tissue. Discard the undigested pellet.

I.3. Genotyping

For genotyping, DNA purified from the tissues was used as template for PCR of a region within the *Herc1* gene. Primers used were:

- Forward primer (DF-1): TGAATGAGCATAAGACACAAATGGC
- Reverse primer (DR-1): TATCGACTTACTTCAAAGAGCAGGG

For the PCR reaction:

Table 3. Reaction mix for genotyping PCR.

Reagent	Volume/reaction
MyTaq Mix 2X (Bioline #BIO-25041)	10 µL
Primers (10 µM)	0.4 µL of each primer
Purified genomic DNA	5 µL
MilliQ water	4.2 µL

The **PCR** reactions were performed in a 2720 Thermal Cycler (Applied Biosystems) using the following conditions for amplification:

1. Denaturalization: 94°C for 5 minutes.
2. 35 cycles of amplification:
    I. Denaturalization: 94°C for 30 seconds.
    II. Annealing: 56°C for 30 seconds.
    III. Elongation: 72°C for 1.5 minutes.

3. Final elongation: 72°C for 7 minutes.
4. Save at 4°C.

The PCR products were then separated by **electrophoresis in 1.5% agarose gels**:

1. For each gel, mix 0.9g. of agarose (Ecogen #AG-0120) in 60 mL of Tris-Acetate-EDTA (TAE) 1X buffer. (TAE buffer 50X: 2M Tris, 50mM EDTA, 57.1 mL glacial acetic acid, pH=8).
2. Heat the solution in the microwave and mix until agarose is dissolved. It is recommended to stop heating, mix and heat again several times to avoid boiling and facilitate dissolving.
3. Let the solution rest for decreasing the temperature. It is possible to use water cooling on the outside of the beaker to fasten the procedure, but it is important not to overcool the solution to avoid solidification.
4. Add 6 µL of Ethidium Bromide (EtBr, Sigma #E1510) in 60 mL of the mix. IMPORTANT: Use protective gloves and laboratory coat for the handling of EtBr, as it has mutagenic effects. It is recommended to only work with this compound under a fume hood to avoid the inhalation of toxic vapours.
5. Prepare the plastic moulds and combs and add the prepared mix.
6. Let it dry for 20 minutes.
7. Prepare the samples by adding loading buffer (LD) 6X (Thermo Scientific #R0611) to the PCR products, until reaching 1X concentration. For 20 µL of PCR product use 4 µL of LD 6X.
8. Put the gel in the electrophoresis system and cover with TAE 1X. Load the samples in the gel and add 4 µL of loading marker (GeneRuler DNA Ladder mix, Thermo Scientific #SM0331). Run the electrophoresis for 30 minutes at 110V.
9. Reveal the bands with an ultraviolet (UV) transilluminator system.

The wild-type allele of *Herc1* gene produces a 708 bp band that will be visible in the gel under UV stimulation. In the knock-out allele, the 191 bp deletion provokes the reduction of the size of this band to 517 bp. Under these

electrophoretic conditions, both bands are well separated and distinguishable (Figure 19).

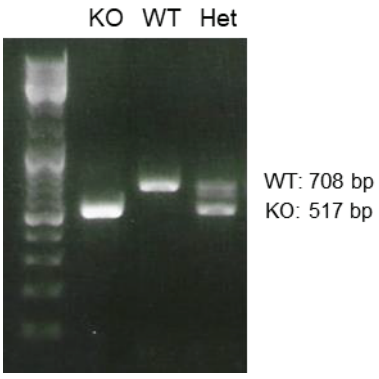

Figure 19. PCR analysis of a KO, a WT and a *Herc1*-heterozygous mouse. The Thermo Scientific (#SM0331) DNA Ladder mix was used as a molecular weight marker.

I.4. Diets

Two different diets were used in these studies: the standard chow diet (Teklad Global 14% Protein Rodent Maintenance Diet, Harlan Laboratories) and the high-fat diet (HFD) with 45% of energy content from fat (D12451, OpenSource Diets, Research Diets Inc; New Brunswick, NJ, USA). The nutritional composition of the different diet formulas is described in Table 3.

Table 4. Nutritional composition of the diet formulas used.

	Chow diet	HFD
Caloric Density (kcal/g)	2.9	4.7
Protein (%)	20	20
Carbohydrates (%)	67	35
Fat (%)	13	45

II. Tissue collection

For tissue collection, mice were all euthanized at the same time of the day. They were first anesthetized by intraperitoneal injection with 2% xylazine and 10% ketamine and sacrificed either by cardiac puncture or by cervical dislocation.

II.1. Blood

For blood collection, mice were sacrificed by cardiac puncture after being anesthetized. Blood was extracted using 1 mL syringes with a 23G needle. Subsequently, it was deposited in a sterile Eppendorf without any anticoagulant treatment. Coagulation phase must last from 10 to 15 minutes, and it should not pass more than 30 minutes at room temperature. After clotting, blood was centrifuged at 2000G for 15 minutes and serum was saved in a new sterile tube, that was immediately frozen in liquid nitrogen and afterwards stored at -80°C.

II.2. Bone

Upon death confirmation, both hindlimbs were isolated from the hip. Soft tissues were removed to expose the bone. Then, each hindlimb was processed differently:

- Left hindlimbs were fixed in PFA 4% for 24h. at 4°C. Then, they were washed three times with PBS and stored at 4°C in phosphate buffered saline (PBS) with 0.02% sodium azide.
- Femurs and tibiae from right hindlimbs were separated, and tibiae were measured using a vernier caliper. Then, the more distal parts of each bone were cut, and bones were centrifuged at 10000G for 15 seconds to eliminate the bone marrow. After that, tibiae and femurs were crumbled and immersed in TRIsure reagent (Bioline # BIO-38033), and subsequently frozen with liquid nitrogen and stored at -80°C.

II.3. Adipose tissues and liver

Adipose tissues were collected as described in Diaz-Martin *et al.*[329] First, 70% ethanol was sprayed on the abdomen of the mouse and a slight incision was made to

separate the skin from the peritoneum and collect the inguinal WAT from the subcutaneous space. After that, another incision was made to expose the peritoneum, and the gonadal adipose tissue and the liver were collected from the abdominal cavity. Finally, after spraying 70% ethanol on the back of the mouse, an incision was made at the level of the shoulders and brown adipose tissue was extracted by separating it from the WAT that surrounds it. All solid tissues were weighed after collection using a precision scale. Each tissue was then divided in 3 parts:

- One part to extract protein and analyze them by western blot. This tissue was frozen in liquid nitrogen and stored at -80°C.
- One part to extract RNA and perform quantitative RT-PCR. This tissue was immersed in TRIsure reagent and frozen and stored in the same way as the latter.
- The last part was fixed in 4% PFA at 4°C for 24h. and then processed for histological analysis.

III. Micro-computed tomography

The internal structure of the femurs was analyzed by micro-computed tomography (micro-CT) in the Barcelona Research Center in Multiscale Science and Engineering of the Universitat Politècnica de Catalunya. High-resolution images were acquired using a microtomograph Skyscan 1272 (Bruker microCT, Kontich), in accordance with the recommendations of the American Society of Bone and Mineral Research (ASBMR). Bones were scanned in air at 60 kV and 166 µA with an exposure time of 5600 ms, using a 1 mm aluminum filter and an 11 µm isotropic voxel size. Two-dimensional images were obtained every 1° for 180° total rotation.

Image reconstruction was performed with the NRecon v1.6 software (Bruker). An area comprising the tissue of interest was marked, and the output of the area selected as bone was stablished between 0.01 and 0.08 intensity units. The parameters were stablished as follows: smoothing 4, misalignment compensation 1.5, ring artefact correction 8, beam hardening correction 31%, defect pixel masking 5%. However, some of these parameters can be changed depending on the bone section to be analysed or

other variables like the age of the mice. In any case, it is important to maintain the same parameters between all the analysed mice to avoid variability.

Reconstructed images were analysed with CT-Analyser v1.13 (Bruker). For cortical measurements, manual Volumes of Interest (VOIs) of 100 slices delineating the femur medial cortex around the femoral midshaft were employed, and a binary threshold was established at 50-255. For trabecular measurements, manual VOIs starting 100 slices from distal growth plate of the femur and extending to the diaphysis for 150 slices were used, and a binary threshold was established at 15-255. However, the lower thresholds and the distance to the distal growth plate in the trabecular analysis can be altered depending on factors such as the age or the size of the mice, in order to better adjust the analysis to the target bone. In any case, once the parameters have been selected, they be maintained for all analysed mice in the experiment to allow comparison.

For visualization of the 3D reconstructions of the bone sections, CTVol v2.3 software (Bruker) was used. This program renders a 3D model from the 2D reconstructed data and display it.

IV. Histology

All histological procedures were performed in the Histology Platform of the Institut d'Investigació Biomèdica de Bellvitge (IDIBELL), with the aid of the histology technicians Lola Mulero and José Antonio Llamas.

IV.1. Bone decalcification

After fixation in 4% PFA, bones need to be decalcified in order to be histological processed and cut into sections. For decalcification, femurs were embedded in 16% EDTA in PBS 1X (pH=7.4) for 6 weeks, at 4°C. EDTA solution was replaced every 2-3 days. After the incubation time, the decalcified state must be manually checked: an elastic bone with no resistance to bending.

IV.2. Paraffin inclusion

The first step for histological processing of fixed adipose tissues and liver and decalcified femurs is paraffin embedding.

1. First, tissues are deposited in histology **cassettes** for individualization and identification. It is important to label the cassettes using a pencil, since ink would be removed in the next steps.
2. **Dehydration and paraffin embedding**. Samples must be dehydrated to promote paraffin embedding, replacing water with xylene which can mix better with paraffin. This process was performed automatically by the Leica TP1020 Tissue Processor. Each step takes 1 hour of incubation in the following solutions:
    i. Ethanol 30%
    ii. Ethanol 50%
    iii. Ethanol 70%
    iv. Ethanol 90%
    v. Ethanol 96%
    vi. Ethanol 100% 1
    vii. Ethanol 100% 2
    viii. Xylene 1
    ix. Xylene 2
    x. Paraffin 1
    xi. Paraffin 2
3. Formation of **paraffin blocks**. After paraffin inclusion, the cassettes are moved to a hot bath of paraffin at 65°C in a Leica EG 1150 H paraffin embedding station.
    i. The tissue is taken out of the cassette and placed in a metal mould. In the case of femurs, it is important to consider the orientation of the sample in this step.
    ii. Move the mould onto a cold surface with a bit of liquid paraffin, pressing mildly to put the sample horizontally.

iii. Add the identifier of the cassette onto the sample and fill it with liquid paraffin.

iv. Maintain the trapped sample on a cold surface until it is solidified (1 or 2 minutes).

v. Take the metal mould out and keep the blocks at 4°C until microtome sectioning.

IV.3. Microtome sectioning

Sectioning of the paraffin block was performed using a Leica RM 2255 microtome.

1. Paraffin surface must be refrigerated by placing the blocks on a cold surface (Leica EG 1150 C) for some hours prior to start processing in the microtome. Overnight refrigeration is recommended.
2. **Block trimming**. Before being able to get slices of the tissue, it must be exposed by removing the excess of paraffin in the surface of the block. This is accomplished by start cutting thicker sections of paraffin (~20 µm) until the sample is exposed. The final step of the trimming should be performed with a few thin sections to avoid the appearance of holes in the sample sections. After trimming the blocks should be cooled again for tissue sectioning.
3. **Tissue sectioning**. After trimming and cooling the block, tissue sections are obtained by cutting 5 µm sections. If the block gets warm, place it on the cold surface until it can be properly cut again.
4. When cutting the area of interest, place the cut sections in a warm water bath and pick up the sections with pre-treated glass microscope slides (StarFrost). Mark the slides with pencil before picking up the tissue sections to identify them. For adipose tissues, it is important not to let the sections in the water bath for a long time to prevent the breaking of the tissue.
5. Place the slides in a warm surface until water is evaporated. Then store them in a warm oven (37°C) overnight.

IV.4. Staining

Once the slides are dry, paraffin embedded sections must be deparaffinised and rehydrated to allow histological staining:

1. **Deparaffination**: Place slides in a bucket in the oven at 60°C for 30 to 60 minutes.
2. **Rehydration**: Samples must be rehydrated to allow the hydrophilic stains to attach to the tissue. This process is automatically performed in the Leica Auto Stainer XL. Each step takes 5 minutes of incubation in the following solutions:
    i. Xylene 1
    ii. Xylene 2
    iii. Xylene 3
    iv. Ethanol 100% 1
    v. Ethanol 100% 2
    vi. Ethanol 96% 1
    vii. Ethanol 96% 2
    viii. Ethanol 70%
    ix. Ethanol 50%
    x. Ethanol 30%
    xi. Distilled water (5 minutes to 24h.)

IV.4.1. Reactive preparation

Harris Haematoxylin

- Ready to use (Panreac #253949.1612)

Alcoholic Eosin

- 100ml ethanol 96%
- 25ml distilled H_2O (dH_2O).
- 1.25g Eosin (Panreac #131299.1606)
- Add 300ml ethanol 80%, mix and add 2ml glacial acetic acid to stabilise.

Weigert Haematoxylin

Mix these 2 solutions half and half in volume:

- Weigert's Haematoxylin solution A (Panreac #253453.1210)
- Weigert's Haematoxylin solution B (Panreac #253454.1210)

Acid alcohol or hydrochloric alcohol

- 1% hydrochloric acid in 70% ethanol.

Bouin

- Ready to use. Panreac #254102.1611.

Xilidine Ponceau/Fuchsin acid

- 300ml dH_2O
- 2.7g Briebrich Scarlet (Panreac #253986.1605).
- 0.3g Fuchsin acid (Panreac #251331.1605).
- Add 2ml glacial acetic acid to stabilise.

Phosphoacid solution

- 400ml dH_2O
- 10g phosphomolybdic acid (Sigma #79560-100G).
- 10g phosphotungstic acid (Sigma #79690-25G).

Aniline Blue

- 300ml dH_2O
- 7.2g aniline blue (Panreac #253708.1606).
- Mix and add 6ml glacial acetic acid to stabilise.

Fast Green

For 1:5000, 0,02%:

- 300ml dH_2O
- 0,06g Fast Green (Panreac #255668.1606).

TRAP Basic stock incubation medium (BI solution)

- 500 mL dH_2O
- 4.6g sodium acetate.
- 5.7g sodium tartrate.
- 2.8 mL glacial acetic acid.

Naphtol AS-BI phosphate substrate

- 0.1g Naphtol AS-BI Phosphate (Sigma #N2125).
- 5 mL 2-Ethoxiethanol (Sigma #128082).

Sodium nitrite

- 5 mL dH_2O
- 0.2g $NaNO_2$

Pararosaniline Dye

- 1g Pararosaniline.
- 20 mL 2M HCl

Mix well and filter before use. Store at room temperature in the dark.

IV.4.2. Haematoxylin and Eosin

Haematoxylin and eosin staining (H&E) allow the visualization of the histological structure of the tissues by contrasting the cytoplasmatic staining of the eosin (pink) with the nuclei staining of the haematoxylin (blue). First, prepare the dyes by filtering them. Then, 5 µm sections are stained:

1. 8 minutes in Harris Haematoxylin.
2. Wash with running tap water for 5 minutes.
3. In and out in hydrochloric acid for nuclear differentiation.
4. Wash with running tap water for 5 minutes.
5. 30 seconds in alcoholic eosin.
6. Dehydration:
    i. 5 dips in ethanol 70%
    ii. 5 dips in ethanol 96%

iii. 5 dips in ethanol 100% 1
iv. 5 dips in ethanol 100% 2
v. 5 minutes in xylol 1
vi. 5 minutes in xylol 2
vii. 5 minutes in xylol + eucalyptol

7. Mount the coverslide with DPX (Richard-Allan Scientific Cytoseal XYL).

IV.4.3. Masson's Trichrome

Masson's Trichrome staining is used for selectively stain collagen fibres in different tissues. Collagen will be stained in blue, nuclei in dark blue/black and the cytoplasm will be red. For 5 µm sections:

1. After rehydration, incubate in Bouin mordent overnight at room temperature.
2. Wash with running dH_2O for 10 minutes.
3. 5 minutes in Weigert Haematoxylin.
4. Wash with running tap water for 5 minutes.
5. Wash with ammoniacal water 3%
6. Wash with running dH_2O for 3 minutes.
7. 5 minutes in Xilidine-Ponceau-Acid Fuchsine.
8. Wash with running dH_2O for 5 minutes.
9. 5 minutes in phosphoacid solution mix.
10. 5 minutes in aniline blue.
11. 2 minutes in acetic acid 1%
12. Wash with running dH_2O for 3 minutes.
13. Dehydration:
    i. 5 dips in ethanol 70%
    ii. 5 dips in ethanol 96%
    iii. 5 dips in ethanol 100% 1
    iv. 5 dips in ethanol 100% 2
    v. 5 minutes in xylol 1
    vi. 5 minutes in xylol 2
    vii. 5 minutes in xylol + eucalyptol
14. Mount the coverslide with DPX (Richard-Allan Scientific Cytoseal XYL).

IV.4.4. Tartrate-resistant acid phosphatase

Tartrate-resistant acid phosphatase (TRAP) staining is used for the detection of osteoclasts in bone tissue sections. TRAP activity in these cells will produce a red stain, while the background will be green. For 5 µm sections:

1. Warm 500 mL of BI solution at 37°C. Use this pre-warmed solution to fill 2 staining buckets, each with 200 mL.
2. Take 1 bucket of BI solution and add 2 mL of Naphtol AS-BI phosphate substrate. Place slides into the bucket and incubate for 1h. at 37°C.
3. A few minutes before incubation time is up, mix 4 mL sodium nitrite solution with 4 mL pararosaniline dye. Mix gently by hand and let sit for 2 minutes, and then add this mix to the second pre-heated bucket of BI solution. Mix well.
4. Transfer the incubated slides from the first bucket to the second one without rinsing. Incubate at 37°C for 3-5 minutes. It is important to check periodically under the microscope the red staining and proceed immediately to next step if tissue shows any non-specific red stain.
5. Rinse 3 times with dH_2O
6. 45 seconds in 0.02% fast green.
7. Rinse with dH_2O
8. Dehydration:
    i. 5 dips in ethanol 70%
    ii. 5 dips in ethanol 96%
    iii. 5 dips in ethanol 100% 1
    iv. 5 dips in ethanol 100% 2
    v. 5 minutes in xylol 1
    vi. 5 minutes in xylol 2
    vii. 5 minutes in xylol + eucalyptol
9. Mount the coverslide with DPX (Richard-Allan Scientific Cytoseal XYL).

IV.5. Image obtention and quantification

Images were captured with a Brightfield Eclipse E800 (Nikon) microscope.

The diameter of white adipocytes and lipid droplets from BAT and liver was measured using the Adiposoft plugin for ImageJ[330] in 20x amplified pictures. Automatic mode was used and errors in the detection of adipocytes were manually corrected. The number of nuclei per field in BAT was quantified with ImageJ using three different 20x amplified pictures per animal. After splitting the colour channels, the threshold was adjusted in the red channel to select the cell nuclei. The number of nuclei was obtained using the tool "Analyse Particles" after the selection of the adequate size range.

Osteoclasts numbers were measured in isolated trabeculae from TRAP-stained sections. For each trabecula, the number of osteoclasts on its surface was divided by its perimeter. At least ten trabeculae from each animal were used.

V. Metabolic phenotyping

The metabolic phenotyping of the mice was performed in collaboration with the group of Dr. Rubén Nogueiras in Universidad de Santiago de Compostela (USC). Experiments were carried out by Dr. Begoña Porteiro.

V.1. Body composition determination

Whole body composition was measured using nuclear magnetic resonance (NMR) imaging (Whole Body Composition Analyzer; EchoMRI, Houston, TX). This method allows the determination of fat and lean mass.

V.2. Thermogenic imaging

Thermal images of the interscapular region of the animals were acquired using a E60bx: Compact-Infrared-Thermal-Imaging-Camera (FLIR; West Malling, Kent, Reino Unido). Images were analysed with FLIR-Tools software.

V.3. Indirect calorimetry

The indirect calorimetry system used (LAbMaster TSE Systems) is composed of individual metabolic cages with sensors for the registration of locomotor activity (LA), energy expenditure (EE), respiratory quotient (RQ) and food intake. Animals are acclimated to the cages for 48h. prior to the start of the measurements. Then, the

system performs measurements of food intake, O_2 consumption (vO_2), CO_2 production (vO_2) and locomotor activity every 30 minutes during 48h.

V.3.1. Locomotor activity

The cages incorporate infrared light beams in horizontal and vertical directions. The system detects every breaking point in the light beams (beam breaks) provoked by the motion of the animals.

V.3.2. Energy expenditure

In the indirect calorimetry system, the quantity of energy spent by the body is estimated from its oxygen consumption and carbon dioxide production[331]. For comparing groups, the energy expenditure of the organism must be normalized, since many factors such as adipose and lean mass affect this value. The most accepted method is performing a lineal regression plotting the body weight data of every individual together with its energy expenditure (in a X/Y graphic). Then, an analysis of covariance (ANCOVA) must be performed to eliminate the effect of body weight and assess whether there is a statistical difference in energy expenditure between the groups[331].

V.3.3. Respiratory quotient

It is calculated as the ratio between released CO_2 and consumed O_2 (vCO_2/ vO_2). It gives an approximation to the main energetic fuel used by the organism. The RQ value is close to 1 when glucose is predominantly used, as for every mol of O_2 consumed there is a release of 1 mol of CO_2. Conversely, the value is reduced to 0.8 and 0.7 if the main energetic source is amino acids or fat, respectively[332].

VI. Glucose and insulin tolerance tests

For glucose tolerance tests (GTT), animals were starved for 16h. and then injected intraperitoneally with 2g/Kg of D-Glucose (Sigma Aldrich #158968) in physiological saline solution. Glucose concentration in blood (mg/dL) was measured before the injection and after 15, 30, 60, 90 and 120 minutes, with a commercial strip (Glucocard G.Sensor, A.Menarini Diagnostics) and a glucometer (Glucocard G+meter, A. Menarini diagnostics).

For insulin tolerance tests (ITT), animals were starved for 6h. and then injected intraperitoneally with 0.35U/Kg of insulin (Actrapid, Novo Nordisk) in physiological saline solution. Glucose concentration in blood was measured in the same way as for GTT.

VII. β3-adrenergic stimulation

For β3-adrenergic stimulation, mice were placed in individual metabolic cages from the indirect calorimetry system. After an acclimatation time, they were injected intraperitoneally once with 1 mg/Kg of the β3-adrenergic receptor agonist CL 316243 (Sigma Aldrich). The oxygen consumption of the mice was measured during 24h: 18h prior to the stimulation and 6h after the injection.

VIII. Blood analysis

As described in section II.1. Blood, intracardiac blood was collected and serum was isolated for analysis.

VIII.1. Hormonal analysis

To determine sex steroids concentration in the serum, we used the following commercial ELISA kits: Testosterone ELISA kit (ADI-900-065, Enzo Life Sciences), 17β-Estradiol high sensitivity ELISA kit (ADI-900-174, Enzo Life Sciences) and Dihydrotestosterone ELISA kit (#KA1886, Abnova). All the kits were used according to manufacturer's instructions.

VIII.2. Detection of metabolites

For quantification of metabolites in the serum, the following kits were used, according to manufacturer guides: Triglycerides (GPO-POD; #41031), Cholesterol (CHOD-POD; #41021) and Total lipids (Sulfo-fosfo vanilline; #1001270). All of them were purchased from Spinreact.

IX. Cell culture

Cells were culture under sterile conditions and maintained in a cell incubator at 37 °C in a 5% CO_2 humidified atmosphere.

For passaging, cells were washed with PBS and detached from the plate using Trypsin-EDTA solution (0.25% Trypsin, 0.02% EDTA, Biological Industries #03-050-1A).

IX.1. Primary cell cultures

IX.1.1. Isolation of BM-MSCs

Under sterile conditions, C57BL/6N mice were anesthetized (ketamine 100 mg/kg and xylazine 50 mg/kg intraperitoneally) and then killed by cervical dislocation. Limbs (tibiae and femur) from three mice with the same genotype were pooled, and the marrow was extracted from the bones by centrifugation (10,000 × g for 15 s) at room temperature. After collecting all the marrow in sterile tubes, the pellet was resuspended using RPMI 1640 medium (Life Technologies) with 20% foetal bovine serum (FBS, Invitrogen), 100U/mL penicillin and 0.1 mg/mL streptomycin. 24 hours after initial plating, the media containing any non-adherent cells was carefully removed and replaced with fresh growth medium, and then replaced every 3–4 days. When MSCs reached the third pass, the basal medium was changed to Dulbecco's Modified Eagle's Medium (DMEM, Biological Industries #01-055-1A) supplemented with 20% FBS, 2 mM L-glutamine (L-Gln), 100U/mL penicillin and 0.1 mg/mL streptomycin.

IX.1.2. Osteocytes

IX.1.2.1. Culture plate coating

Prior to the isolation of osteocytes, culture plates must be coated with type I collagen, as these cells must grow in dished coated with 5 μg/cm^2 collagen to avoid losing their original phenotype. The protocol for the coating:

1. Incubate the cell dishes for 1h at room temperature or at 37°C with a 20 mM acetic acid solution containing 50 μg/mL of collagen type I from rat tail (Sigma, #08-115). For each 100 mm culture plate, 7.8 mL of this solution should be used to secure uniform coating. For 6-well plates, use 1 mL/well.
2. Remove the excess of collagen and keep the coated plates at 4°C. The collagen solution can be reused up to 5 times.

IX.1.2.2. Isolation of osteocytes

The isolation of osteocytes was performed as previously described by Sánchez-de-Diego *et al.*[333] It must be performed with newborn mice, between P0 and P3, since the yield from older mice is too poor. A minimum of 3 animals should also be pooled from each condition. In our conditions, for being able to separate WT and *Herc1*-KO osteocytes, the genotyping of the animals should be performed in parallel to the isolation of osteocytes, that will be executed individually for each mouse until the revealing of the genotypes, moment in which samples from the same genotypes will be pooled together. The genotyping can be performed as explained in sections I.2. DNA extraction from mice and I.3. Genotyping. Nevertheless, as these mice are too small to be identified by ear incisions, the tissue samples for DNA extraction and genotyping are taken from a small cut in the tail.

Two different solutions will be needed for the protocol of isolation. It is recommended to prepare and filter them with a 0.22 µm filter beforehand:

Table 5. Solutions for osteocyte isolation.

Solution	Recipe
Collagenase solution	For each animal, and for one digestion (there will be a total of 6 digestions): 0.6 mg collagenase II 0.2 mL trypsin (0.25% Trypsin-EDTA) Complete 1 mL volumen with alpha-MEM (Minimum Essential Medium Eagle Alpha Modification, Sigma #M8042) supplemented with 100U/mL penicillin and 0.1 mg/mL streptomycin
EDTA solution	For each animal, and for one digestion (there will be a total of 6 digestions): 5 mM EDTA dissolved in PBS 0.1% Bovine serum albumin (BSA) Adjust the pH to 7.4

First, surgical material that will be used must be properly sterilized. Then the mice are euthanized by decapitation inside a sterile culture hood. The calvaria and limbs of each mouse will be used for the protocol:

- Calvaria is extracted from the skull. It must be cleaned with PBS and 100U/mL penicillin and 0.1 mg/mL streptomycin, and the periosteum has to be carefully removed. The isolated calvaria is cut in small pieces for digestion.
- From the limbs we obtain the tibiae, femora, humeri, radius and ulna. These bones are also cleaned like calvaria and pooled with it in a 15 mL tube containing alpha-MEM with antibiotics. In our conditions, the bones from each mouse are processed individually. The tubes must be clearly labelled to identify each animal.

After pooling the calvaria and limb bones of each animal, the bones are rinsed three times with alpha-MEM with 100U/mL penicillin and 0.1 mg/mL streptomycin. Then, the subsequent digestions are started:

1. Add 1 mL collagenase solution and incubate for 25 minutes on a shaking/rotating platform at 37°C. Remove and discard the collagenase, rinse the bone pieces with 5 mL PBS and discard the liquid. Repeat this step 2 more times (digestions 1-3).
2. Incubate the bone pieces in 5 mL EDTA solution for 25 minutes on a shaking/rotating platform at 37°C. Remove and discard the EDTA, rinse with PBS and discard the liquid.
3. Repeat the digestion in the same conditions as in the first step (digestion 4). If we want to isolate osteoblast, instead of discarding the collagenase solution and the PBS rinse, we may transfer them to another tube for isolation (these digestions mainly contain osteoblasts).
4. Repeat the EDTA solution in the same conditions as step 2. Again, if we want osteoblasts we will save the solutions post incubation.
5. Repeat the digestion step (digestion 5). The solutions may be saved for osteoblast isolation.

6. Repeat the EDTA incubation. After this incubation, the EDTA solution and the posterior PBS rinse will be enriched in osteocytes. Save the solutions in a 50 mL centrifuge tube. If the genotyping is already finished, we may pool the solutions from animals sharing the same genotype.
7. Repeat the digestion process (digestion 6) and save the solutions, for they will also be enriched in osteocytes. Transfer them to the same 50 mL centrifuge tube used in the previous step.
8. Centrifuge the tube with the solutions from steps 6 and 7 at 1000G and resuspend the pellet in osteocyte culture medium composed of alpha-MEM with 5% heat-inactivated FBS, 5% heat-inactivated newborn calf serum (NBCS), 2 mM L-Gln, 100U/mL penicillin and 0.1 mg/mL streptomycin.
9. Seed the resuspended osteocytes in pre-coated dishes. Cells will attach in 24h and should be used within 7 days to prevent the loss of phenotype.

IX.2. Lentiviral particle production and target cell infection

Lentiviral vectors were produced in HEK 293T cells. Cells were transfected with 7 µg pMD2.G, 7 µg psPAX2 (VSV-G) and 7 µg of either empty pLKO.1-Puro or pLKO.1-shHERC1 by the calcium phosphate method. Media containing lentiviral particles were collected, filtered using polyvinyl difluoride filters (Millex-HV filter 0.45 µm, Millipore SLHV033RB) and stored in aliquots at -80°C. Target cells were seeded at a confluence of 50-60% in a 6-well plate before adding 300 µL of the medium containing the lentiviral vectors to each well. Fresh medium, supplemented with 5 µg/mL polybrene, was added to make a total volume of 1mL. Media with lentiviral vectors were removed the next day and after 24 hours, 5 µg/mL puromycin was added for selection.

MISSION shRNA clone of mouse HERC1 (TRCN0000087441) was purchased from Sigma-Aldrich. David Root gifted the plasmid vector pLKO.1–TRC control (Addgene plasmid #10879; http://n2t.net/addgene:10879; RRID:Addgene_10879)[334] and Didier Trono gifted the VSV-G envelope expressing plasmid pMD2.G (Addgene plasmid #12259; http://n2t.net/addgene:12259; RRID:Addgene_12259) and the lentivirus packaging plasmid psPAX2 (Addgene plasmid #12260; http://n2t.net/addgene:12260; RRID:Addgene_12260).

IX.3. Osteoblast differentiation from BM-MSCs

For osteoblast differentiation, BM-MSCs were seeded in six-well plates after reaching the fourth pass. When the seeded cells reached a confluence of 50-60%, they were infected with lentiviral particles containing shRNAs (control or against HERC1) as explained in the previous section. After the selection of infected cells with puromycin, they were cultured until reaching a confluence of 90%–100%. Then, the standard cell culture medium (DMEM with 20% FBS and penicillin/streptomycin) was changed for the differentiation medium composed of DMEM supplemented with:

- 20% FBS.
- 100U/mL penicillin and 0.1 mg/mL streptomycin.
- 8 mM β-glycerol phosphate.
- 1 mM ascorbic acid.

Cells were kept in the experiment for up to 21 days and the medium was changed for fresh differentiation medium every two days. The differentiation status of the cells was assessed at 3 time points: before the start of the culturing with differentiation medium and after 14 and 21 days of osteoblastic induction. Two methods for this assessment were alizarin red staining and detection of alkaline phosphatase activity.

IX.3.1. Alizarin Red staining

Alizarin Red S is an anthraquinone dye that has been widely used to evaluate calcium deposits in cell culture in a semi-quantitative way. It forms a complex with calcium giving rise to a bright red stain. The protocol for staining the cells is:

1. Remove the culture medium and rinse 3 times with PBS.
2. Fix the cells with 4% PFA for 15 minutes at room temperature with gentle shaking.
3. Remove PFA and rinse 3 times with milliQ H_2O.
4. Add 1 mL of 40 mM Alizarin Red-S (ARS Staining Quantification Assay, ScienCell #8678) per well. Incubate at room temperature for 45 minutes in the dark, with gentle shaking.

5. Remove the dye and rinse 5 times with milliQ H_2O.

After the staining, the results can be analysed by optical microscopy. The mineralization can be also quantified by extracting the staining with a 10% acetic acid solution and by measuring the absorbance at 405 nm.

IX.3.2. Alkaline phosphatase activity

Alkaline phosphatase activity is important for the mineralization of bone, and it is a good marker for bone formation, as it is characteristically elevated during osteoblast maturation. This activity was determined using an alkaline phosphatase detection kit (Sigma-Aldrich #SCR004) following the manufacturer's instructions:

1. Remove the culture medium and rinse 3 times with PBS.
2. Fix the cells with 4% PFA for 15 minutes at room temperature with gentle shaking.
3. Rinse the cells with milliQ running water for 45 seconds.
4. Add the mix of the Fast Red Violet solution with the Naphtol phosphate solution and incubate the cells for 30 minutes at room temperature in the dark.
5. Remove the reactives and rinse with milliQ H_2O.

The results can be evaluated by optical microscopy.

X. Gene expression analysis

For the analysis of gene expression, RNA was isolated from cells or tissues, it was retrotranscribed to cDNA and then the cDNAs were analysed by quantitative real time PCR (qRT-PCR).

X.1. RNA isolation

RNA was isolated from cells and tissues using TRIsure reagent (Bioline #BIO-38033) following the manufacturer instructions. During the whole protocol, it is **extremely important to use new gloves and autoclaved material**. It is also recommended to perform the protocol inside a fume hood, since phenols and alcohols will be used. Protocol:

1. **Lysis**. The first step is different for cells and tissues:
    a. **Cells**. Lyse the cells directly by adding 500 µL of TRIsure reagent per well of a 6-well plate. Plates can be then frozen or directly processed. For processing, cells are scraped with a 1 mL pipette tip. Then, the lysate is collected in a 1.5 mL tube.
    b. **Tissues**. Crumbled bones and adipose tissues were stored in TRIsure in 2 mL tubes at -80°C (tissue collection is described in sections II.2. Bone and II.3. Adipose tissues and liver). After thawing the samples on ice, they are homogenized with a Polytron for 45 seconds. This homogenization is also performed on ice to avoid sample overheating. Then, bone samples are ready for progressing with the protocol, but adipose tissues must repose for 5 minutes on ice in a vertical position. The fat cake that appears over the phenol phase must be removed, since it interferes with the posterior phase separation.
2. **Phase separation.** From this point, cell and tissue samples follow the same protocol. Incubate the samples for 5 minutes at room temperature. Add 100 µL of chloroform per 500 µL of TRIsure. Vortex the tubes for 15 seconds and let the samples rest at 3 room temperature for 3 minutes. Then, centrifuge the samples at 12000 G for 20 minutes at 4°C. The sample will split in two phases: a lower pale green organic phase and an upper colourless aqueous phase that contains the RNA.
3. **RNA precipitation.** Transfer the aqueous phase into a new 1.5 mL tube. Add 1 µL of glycogen to facilitate RNA precipitation. Then, add 250 µL of isopropanol for 500 µL of TRIsure used. Vortex the tubes for 15 seconds and incubate the samples for 10 minutes at room temperature. Then, centrifugate at 12000 G for 20 minutes at 4°C.
4. **RNA wash.** Remove the supernatant using a double tip: couple a 10 µL tip to a 1 mL tip to avoid pellet disturbance. Then, add 500 µL ethanol 75% to wash the pellet. Release the pellet from the wall of the tube and centrifuge again at 7500 G for 5 minutes.
5. **RNA drying and rehydration.** Remove the supernatant using a double tip again, and then air-dry the pellet. It can be done at room temperature, although

the process can be accelerated by placing the tubes in a thermoblock at 45°C, with the lids open. Then, dissolve the dry pellet in DEPC-treated water and incubate 10 minutes at 55°C to facilitate the dissolution.

6. **Quantification.** RNA samples can be quantified by using a Nanodrop.

After the isolation of the RNAs, they can be stored at -80°C.

X.2. Retrotranscription

For analysing the transcripts, RNAs must be retrotranscribed to cDNA. This was accomplished using the High-Capacity cDNA Reverse Transcription Kit (Applied Biosystems). The reactions were performed as follows:

Table 6. Volume of reagents for retrotranscription reaction.

Reagent	Volume for 30 µL reaction
RNA	1-2 µg contained in 15 µL
Buffer	3 µL
dNTP Mix	1.2 µL
Random primers	3 µL
Retrotranscriptase	1.5 µL
DEPC-treated water	Up to 15 µL

X.3. Quantitative Real Time PCR

Quantitative PCRs were performed with a QuantStudio 7 Pro Real-Time PCR system and a Taqman 5'-nuclease probe method (Applied Biosystems) with a SensiFAST Probe Hi-ROX Mix (Bioline). Designed Taqman assays from Applied Biosystems were used to quantify cDNA levels. The list of probes used in this thesis are listed in Table 7.

Table 7. List of probes used for qRT-PCR during the thesis.

Gene	Taqman probe ID
Acrp30	Mm00456425_m1
Alpl	Mm 00475834_m1
Bglap	Mm03413826_mH
Cebpa	Mm00514283_s1
Cidea	Mm00432554_m1
Col1a1	Mm 00801666_g1
Ctsk	Mm00484039_m1
Dlx5	Mm00438430_m1
Dmp1	Mm 01208363_m1
Fgf23	Mm 00445621_m1
Gapdh	Mm99999915_g1
Glut4	Mm00436615_m1
Lep	Mm00434759_m1
Npy	Mm00445771_m1
Opg	Mm00435454_m1
Pgc1a	Mm01208835_m1
Pparg	Mm01184322_m1
RankL	Mm00441906_m1
Runx2	Mm 03003491_m1
Sost	Mm 00470479_m1
Sp7	Mm00504574_m1
Tbp	Mm 01277042_m1
Trap	Mm00475698_m1
Ucp1	Mm01244861_m1

Reactions were carried out in 384 well plates, always in duplicates, and with a reaction mix detailed in Table 8.

Table 8. Volume of reagents for each qRT-PCR reaction.

Reagent	Volume for 11 µL reaction
cDNA	1 µL
Taqman probe	0.5 µL
SensiFAST	5.5 µL
MilliQ water	4.5 µL

XI. Protein analysis

For protein analysis, proteins were extracted from cells and separated by electrophoresis. Then, detection of specific proteins was performed by Western Blot.

XI.1. Protein extraction

For protein extraction, cells were lysed in a buffer composed of:

- 50 mM Tris-HCl, pH 7.5
- 150 mM NaCl
- 0.5%. NP40 detergent

Furthermore, this buffer was supplemented with protease and phosphatase inhibitors to avoid degradation of proteins and erasing of the phosphorylation marks:

- 50mM β-glicerophosphate
- 50 mM sodium fluoride
- 1 mM sodium vanadate
- 1 mM phenylmethylsulfonyl fluoride (PMSF)
- 5 µg/mL leupeptin
- 5 µg/mL aprotinin
- 1 µg/mL pepstatin A
- 100 µg/mL benzamidine

For protein extraction, the procedure must be performed on ice to minimise protein and phosphorylation degradation.

1. Discard the culture medium from the cells and rinse with PBS.
2. Add lysis buffer to the plate. For well from a 6 well plate, 100-150 µL should be used.
3. Detach the cells with a cell scraper and transfer the extracts to a 1.5 mL tube.
4. Incubate the samples for 15 minutes on ice with strong agitation to allow the total lysis of the cells.
5. Centrifuge at 13000 G for 10 minutes at 4°C. Then, transfer the supernatants to a new 1.5 mL tube and discard the pellets.
6. Quantify the protein concentration in the samples with the BCA Pierce protein assay (ThermoFisher #23227), following the manufacturer's intructions.
7. Add Lithium dodecyl sulphate (LDS) 4X buffer to the samples. This buffer is composed of:
    a. 250 mM Tris-HCl pH 8.5
    b. 2% LDS
    c. 0.4 mM EDTA
    d. 10% glycerol
    e. 0.2 mM phenol red
    f. 0.2 mM Coomassie Blue

After this, samples can be prepared for electrophoresis or stored at -20°C.

XI.2. Protein electrophoresis and western blot

Proteins were separated using a Tris-Acetate Polyacrylamide gel electrophoresis (PAGE) system. Before entering the PAGE system, protein samples must be supplemented with 100 mM DTT (dithiothreitol) and incubated for 10 minutes at 100°C, to denaturalise the proteins. The Tris-Acetate PAGE system used is a special recipe for a gradient gel, developed in our laboratory for the simultaneous analysis of high and low molecular weight proteins[335]. The gradient gel is elaborated by the continuous mixing of two different concentrations polyacrylamide gels in a two-vase communicating system. The recipes for the gels are detailed in Table 9.

Table 9. Recipe for 3% and 15% polyacrylamide gels.

Reagent	3% polyacrylamide gel	15% polyacrylamide gel
3M Tris-Acetate pH 7	0.47 mL	0.27 mL
40% Acrylamide	0.53 mL	1.5 mL
TEMED	8.75 µL	5 µL
Ammonium persulfate	33.25 µL	19 µL
MilliQ water	6 mL	2.23 mL

After polyacrylamide polymerization, protein samples are loaded into the wells within the gels and the electrophoresis is performed with a constant voltage of 130V. This electrophoresis is carried out inside a denaturalizing running buffer containing:

- 50 mM Tricine
- 50 mM Tris
- 0.1% Sodium dodecyl sulphate (SDS)
- 1.3 mM Sodium bisulphite

After the electrophoresis, the separated proteins in the gels are transferred to a polyvinylidene difluoride (PVDF) membrane. This transfer is performed inside an electrophoresis cuvette during 2h at 200 mA per gel, and at 4°C. For this, a transfer buffer is used, containing:

- 20% Methanol
- 25 mM Bicine
- 25 mM Bis-tris
- 1 mM EDTA
- 1.3 mM Sodium bisulphite

PVDF membranes with the proteins attached are blocked with 10% skimmed milk in TBS-T for 1h. Then, the membrane is incubated with primary antibodies against specific proteins at 4°C overnight. The list of the antibodies used during the thesis is listed in Table 10. The primary antibodies were prepared in a solution containing TBS-T with 3% BSA and 0.02% sodium azide.

Table 10. List of antibodies used during the thesis. The dilution to use in the TBS-T solution is also indicated.

Recognised protein	Dilution to use	Reference
CHC	1:1000	Santa Cruz Biotechnology #sc12734
C-RAF	1:1000	BD Biosciences #610151
ERK1/2	1:1000	Cell Signalling #9102
HERC1	1:500	Produced in the laboratory
p38	1:1000	Santa Cruz Biotechnology #sc-535
p-ERK1/2	1:5000	Sigma-Aldrich #M8159
p-p38	1:1000	Cell Signalling #9211
Vinculin	1:1000	Santa Cruz Biotechnology #sc-25336

The next day, primary antibodies are saved for reuse and the membranes are washed 3 times with TBS-T. Then, they are incubated for 1h with agitation with peroxidase-labelled secondary antibodies prepared in blocking solution (skimmed milk in TBS-T). After washing 3 more times the membranes, they are incubated for 1 minute with the Enhanced chemiluminescence (ECL) reactive to unchain the peroxidase reaction and the protein bands are visualized with a gel documentation system (LAS-3000, Fujifilm). Images are then processed with MultiGauge V3.0 software.

XII. Echocardiography

The analysis of the cardiac phenotype was performed in collaboration with the group of Dr. Javier Inserte from Vall d'Hebron Institut de Recerca (VHIR). Dr. David Aluja conducted the experiments.

Variations in cardiac morphology were measured by transthoracic echocardiography using a GE Vivid Q portable ultrasound machine (GE Healthcare) equipped with a i12L-RS probe of 13MHz. The thickness of the intraventricular septum wall (SWT) and of the posterior wall of the left ventricle (PWT) was measured using images taken in M mode.

XIII. Statistical analysis

The data were analysed using GraphPad Prism 8 software. Data are expressed as means ± standard error of the mean (SEM). Differences between groups were analysed using the student's t-test or one-way analysis of variance with Bonferroni's multiple comparison test. Differences were considered significant at three levels (*$p < 0.05$, **$p < 0.01$, and ***$p < 0.001$).

For the comparison of energy expenditure, ANCOVA was used to eliminate the effect of body weight differences between the groups.

RESULTS

CHAPTER I: HERC1 regulates bone homeostasis

The data from IMPC show that HERC1-KO mice could have decreased bone mineral content when compared to WT animals[75]. Nevertheless, despite this preliminary information and the evidence that many ubiquitin ligases are involved in the regulation of bone remodelling, no study to date had investigated the role of HERC1 in this process. In this thesis, we aim to unravel the role that this ubiquitin ligase plays in bone homeostasis.

I.1. HERC1 modulates osteoblastic differentiation

The first approach to investigate the role of HERC1 in bone formation was an *in vitro* model of osteoblastic differentiation. BM-MSCs isolated from WT mice were infected with mock lentivirus (plKO) or with a lentivirus carrying a shRNA against *Herc1* (shH1) and were cultured with the specific osteogenic medium for 3 weeks (Figure 20A). The analysis of protein expression by Western Blot showed that the silencing of *Herc1* caused by the shH1 was maintained after the 21 days (Figure 20B). Under these conditions, HERC1 depletion provokes an increase in the protein levels of C-RAF and in the phosphorylation of ERK and p38 (Figure 20B).

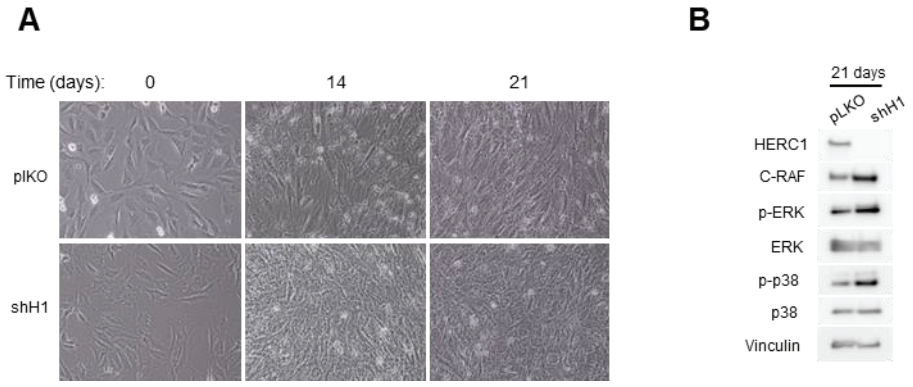

Figure 20. *Herc1* silencing is maintained for 21 days and increase ERK and p38 phosphorylation by the stabilization of C-RAF. BM-MSCs were infected with mock lentivirus or lentivirus carrying shRNA against HERC1 and cultured with osteogenic differentiation medium for 21 days. **A)** Representative images of differentiating MSCs at 0, 14 and 21 days, taken with optical microscopy. **B)** Lysates from cells after 21 days of differentiation were analysed by immunoblotting. Specific antibodies for the indicated proteins were used. Vinculin was used as a loading control. plKO was used as a control lentivirus. shH1: short hairpin RNA against *Herc1*.

To check the osteoblastic differentiation of these cells, the calcium deposits produced by them were evaluated by Alizarin Red staining after 14 and 21 days of differentiation. As expected, the calcium deposits increased during osteoblastogenesis. However, they were significantly increased in *Herc1*-depleted cells compared to control cells, both at 14 days and at 21 (Figure 21).

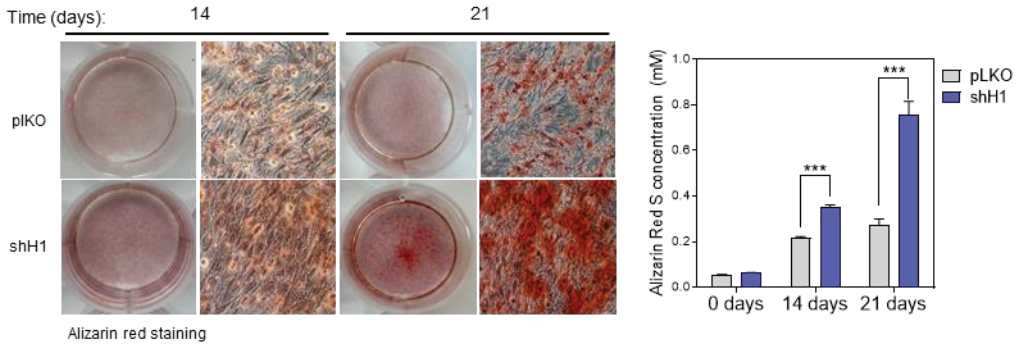

Figure 21. Alizarin red staining of control and Herc1-silenced MSCs after 14 and 21 days of differentiation. Left panel show representative images of Alizarin Red-stained cells after 14 and 21 days of culturing in differentiation medium, taken with optical microscopy. Right panel depicts the quantification of Alizarin Red S concentration. Data are expressed as mean ± SEM (n=5). ***p<0.001. pIKO was used as a control lentivirus. shH1: short hairpin RNA against *Herc1*.

To check whether the increase in the deposit of calcium was paired with enhanced osteoblastogenesis, we assessed the expression of osteoblast-specific genes by qRT-PCR. We observed that at 14 days of differentiation, *Herc1*-silenced cells expressed higher mRNA levels of early osteoblastogenesis marker *Runx2*, compared to control cells, with no changes in any other gene analysed. At 21 days, *Runx2* levels were matched between both genotypes, but *Herc1*-knockdown cells showed higher expression of other osteoblastic genes such as *Sp7*, *Col1a1* and *Alpl*. Moreover, there was also a significant rise in the expression of the mature osteoblast marker *Bglap* (Figure 22A). To further confirm these data, alkaline phosphatase activity was measured. Consistent with the increased expression of *Alpl* gene, we observed that alkaline phosphatase activity was greater in *Herc1*-depleted cells at 21 days of differentiation (Figure 22B).

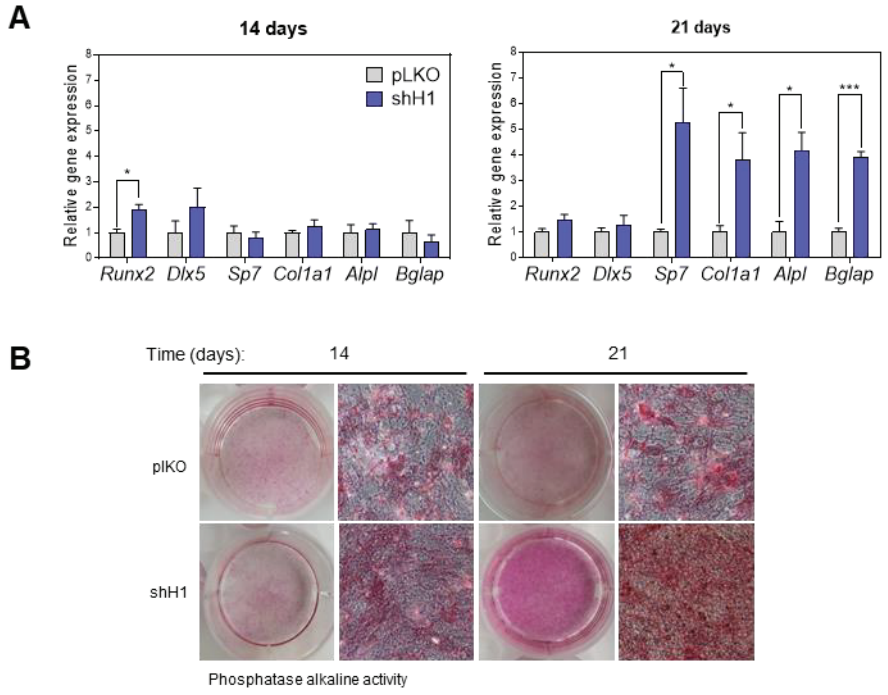

Figure 22. Herc1 regulates osteoblastic differentiation. A) Expression of osteoblast specific genes at 14 and 21 days of differentiation. The expression of each gene was normalized to *Tbp* expression. Data are expressed as mean ± SEM (n=4). *p < 0.05; **p < 0.01; ***p<0.001. **B)** Staining of alkaline phosphatase activity in 14 and 21-days differentiated cells. plKO was used as a control lentivirus. shH1: short hairpin RNA against *Herc1*.

I.2. *Herc1*-KO female mice display osteopenia at 8 weeks.

After the *in vitro* data suggesting a role for HERC1 in osteogenesis, we moved on to the *in vivo* model to check if *Herc1* gene has any physiological relevance in the regulation of bone homeostasis. With that purpose, we started by analysing the bone composition of the distal femurs of 8-week-old WT and *Herc1*-KO mice by micro-CT. By doing so, we discovered no differences in the cortical structure of femurs from male mice between WT and KO genotypes (Figure 23A). Focusing on the trabecular region of males, there was a trend towards a slight decrease in bone density of KO animals, although not reaching statistical significance (Figure 23A). The cortical results observed in males were replicated in females (Figure 23B). Nevertheless, in these female mice we

did find a statistically significant decrease in trabecular density, trabecular thickness and trabecular number in the KO compared to the WT littermates (Figure 23B).

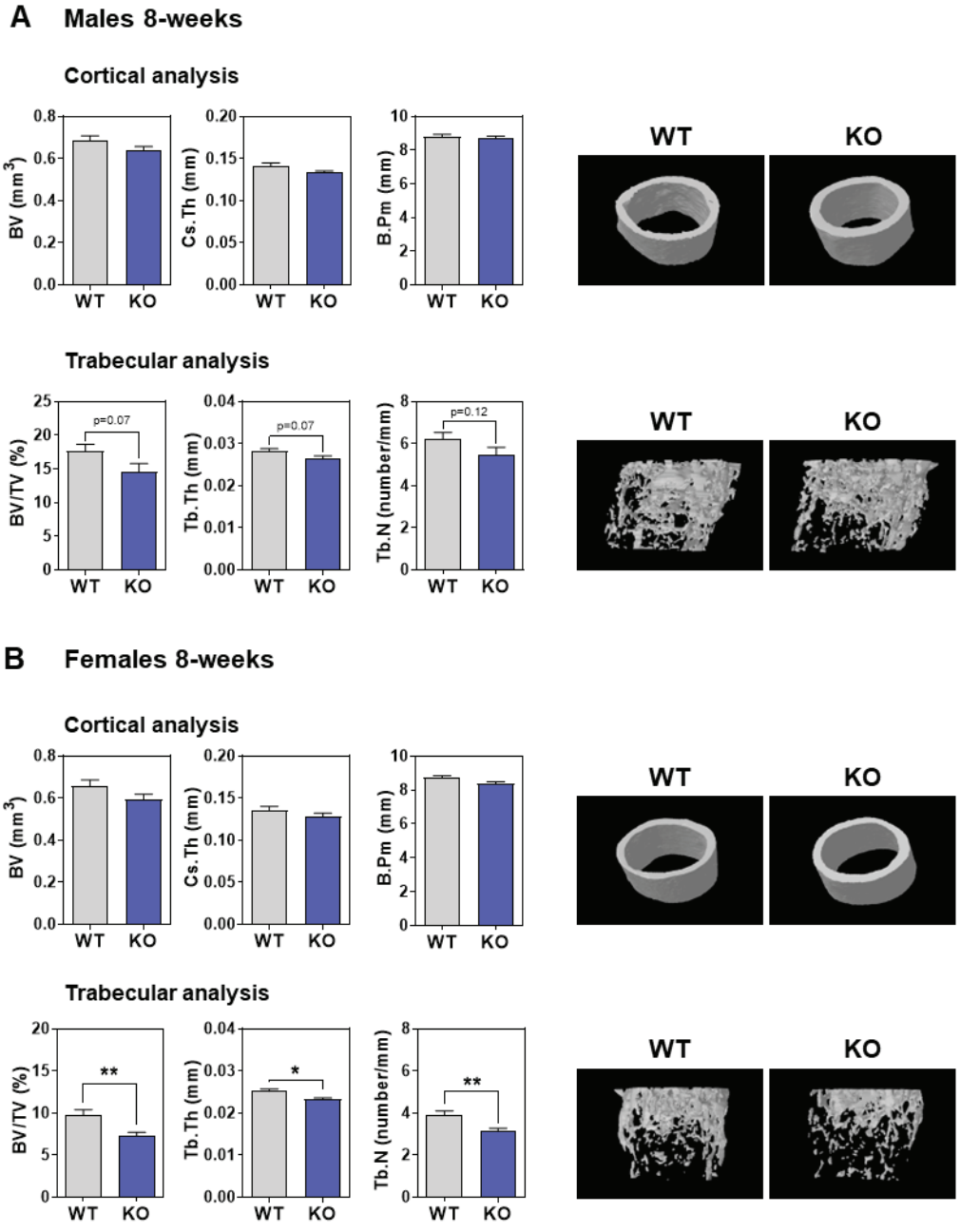

Figure 23. Bone composition by micro-CT analysis of 8-week-old mice. Cortical and trabecular analysis of distal femurs from male **(A)** and female **(B)** mice. Representative images are shown. Data are expressed as mean ± SEM (n = 8–12). Significant differences are relative to WT mice of the same sex. *p < 0.05; **p < 0.01.

Abbreviations: BV, bone volume; B.Pm, bone perimeter; BV/TV, Bone volume over tissue volume; Cs.Th, cortical thickness; Tb.N, trabecular number; Tb.Th, trabecular thickness; WT, wild-type; KO, *Hercl*-knock out.

I.3. Osteoclastogenesis is induced in female KO mice

To assess whether the osteopenia could be related to impairments in osteoblastogenesis, we extracted RNA from the femurs of 8-week-old mice after removing the bone marrow and performed qRT-PCR for key osteoblastic genes. However, despite the alterations in bone architecture, there were no clear changes in the expression of any of the studied genes between WT and *Herc1*-KO mice, neither in males nor females (Figure 24).

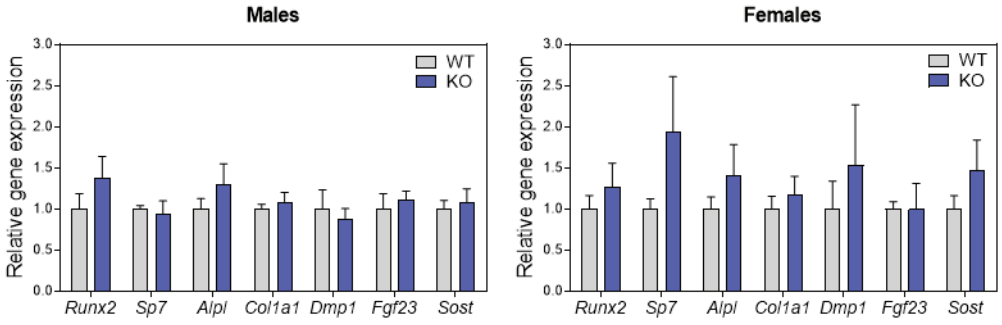

Figure 24. Expression of osteoblastic genes in femurs of male and female 8-week-old mice. The expression of each gene was normalized to *Tbp* expression. Data are expressed as mean ± SEM (n=4-8).

Discarding the alterations in osteoblastogenesis at this age, we wondered whether there was an imbalance in bone remodelling by increased bone resorption. For that, we analysed the mRNA levels of osteoclastic markers in the femurs of the same mice. We found that, while male mice did not express different levels of osteoclastic genes (Figure *25*A), female KO mice showed a strong trend for a rise in *RankL* expression, thus increasing the *RankL*/*Opg* ratio, although not reaching statistical significance (Figure *25*B). Besides, females had also higher expression of classical osteoclast markers *Trap* and *Ctsk* (Figure *25*B). After that, we performed histomorphometric measurements of TRAP-stained femoral sections, focusing on the trabecular region. We found that, while male mice did not show a significant difference in osteoclasts number in their trabeculae (Figure *25*C), *Herc1*-KO females had an increase in the quantity of osteoclasts per bone surface (Figure 25D).

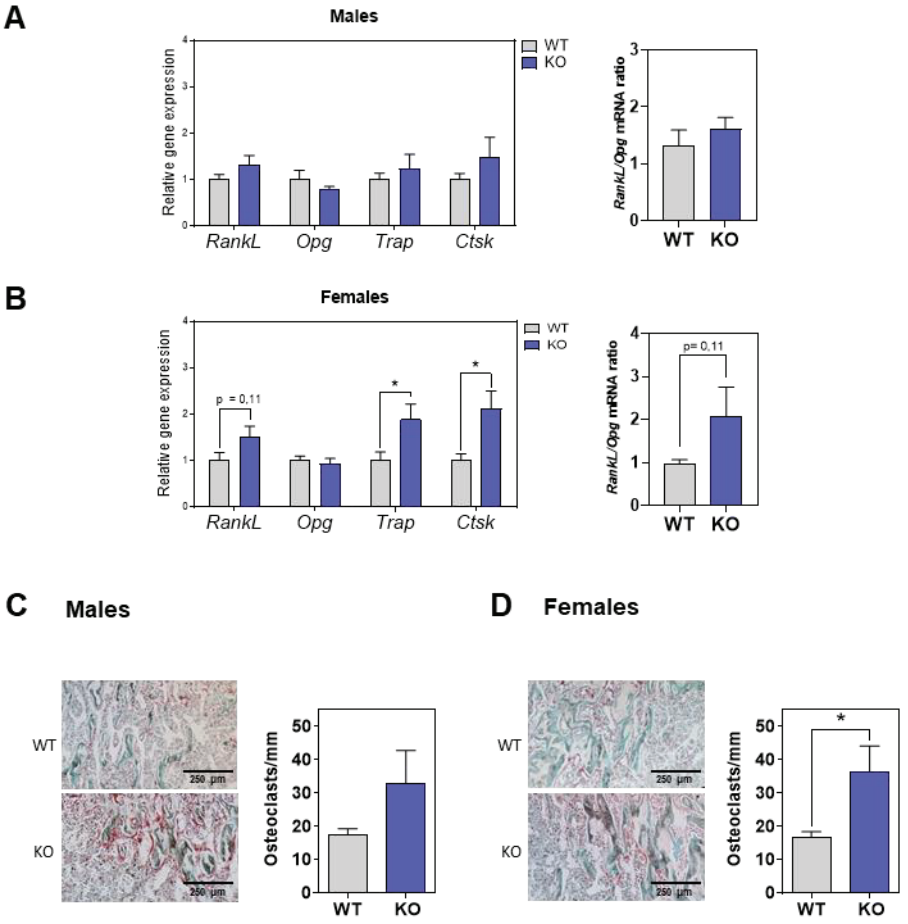

Figure 25. Osteoclastogenesis in femurs from 8-week-old WT and *Herc1*-KO mice. Expression of osteoclastic markers by qRT-PCR in **(A)** male and **(B)** female mice. The expression of each gene was normalized to *Gapdh* expression, and the *Rankl*/*Opg* mRNA ratio is depicted in the right panels (n = 5–9). **C)** Histological analysis of femurs obtained from male and **(D)** female mice. Representative images of longitudinal sections of femur from male and female KO mice stained with TRAP are shown in the left panels. Images were taken at 4x magnification. Right panels report the number of osteoclasts per surface of trabecular bone (n = 3–5). Data are expressed as mean ± SEM. Significant differences are relative to WT mice. *p < 0.05. Abbreviations: KO, *Herc1*-knockout; WT, wild-type.

I.4. KO females have lower androgen levels at 8 weeks

The regulation of bone metabolism by sex steroids have long been studied, and deficiencies in estrogens or androgens are strongly associated with osteoporosis[336]. Therefore, trying to elucidate the reason for the sex differences that we observe in bone phenotype, we measured by ELISA the levels of sex hormones in the serum of 8-week-old mice. This revealed that there were no differences in the concentration of estradiol

in the serum of WT and *Herc1*-KO mice, neither in males nor females (Figure 26A). Testosterone levels in males were also unchanged, but they were significantly reduced in female KO mice compared to WT controls (Figure 26B). This female-exclusive reduction in androgen levels was replicated with dihydrotestosterone (DHT), a more potent activator of androgen receptors (Figure 26C).

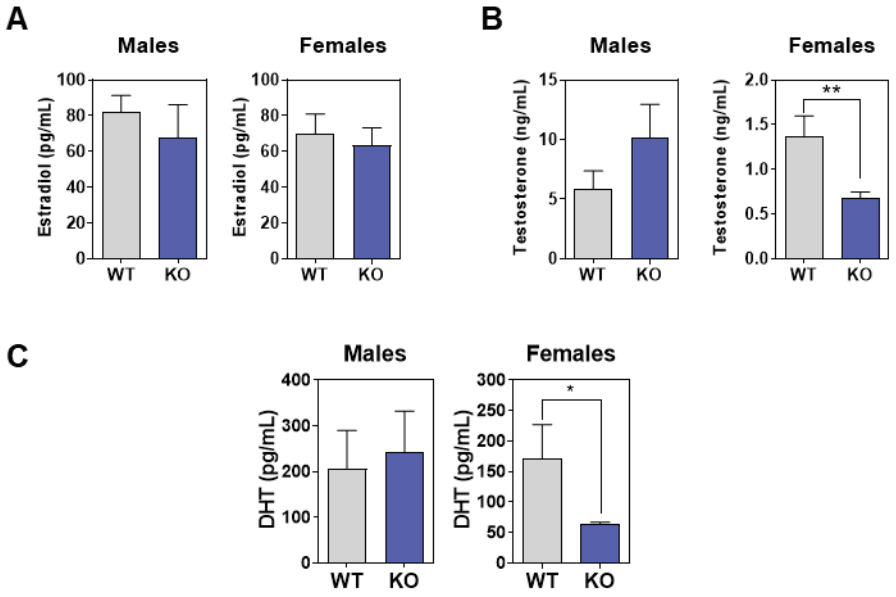

Figure 26. Sex steroids levels in the serum of 8-week-old mice. Quantification of the concentration of **(A)** estradiol **(B)** testosterone and **(C)** dihydrotestosterone in the serum of 8-week-old WT and *Herc1*-KO mice. The measurements were performed using ELISA commercial kits. Data are expressed as mean ± SEM (n=7-14). Significant differences are relative to WT mice. *p < 0.05; **p<0.01. Abbreviations: KO, *Herc1*-knockout; WT, wild-type.

I.5. *Herc1* loss provokes severe osteopenia in adult mice

Aging is a major cause of osteopenia due to disbalance in bone formation and resorption[337]. To investigate how the depletion of Herc1 could affect this age-dependent bone loss, we analysed distal femurs of 32 weeks-old mice by micro-CT. We discovered that the degradation of bone shown in young mice was enhanced with the age, as both male and female *Herc1*-KO mice showed a huge reduction in all trabecular morphometric values (Figure 27A-B). Regarding the cortical analysis, there was a slight decrease in the bone volume of KO males (Figure 27A), with no differences in females (Figure 27B).

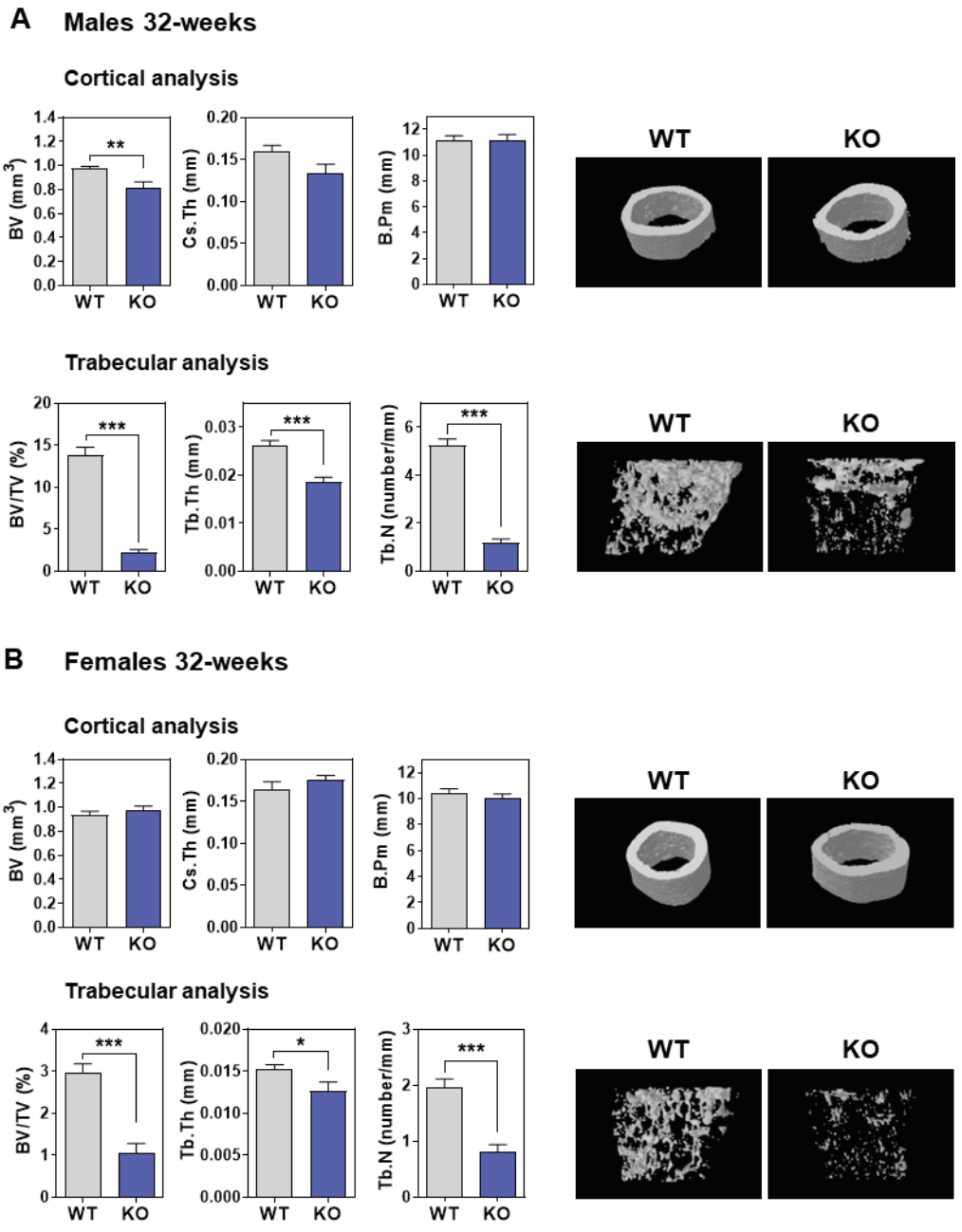

Figure 27. Bone composition by micro-CT analysis of 32-week-old mice. Cortical and trabecular analysis of distal femurs from male **(A)** and female **(B)** mice. Representative images are shown. Data are expressed as mean ± SEM (n = 6–12). Significant differences are relative to WT mice of the same sex. *p < 0.05; **p < 0.01; ***p<0.001. Abbreviations: BV, bone volume; B.Pm, bone perimeter; BV/TV, Bone volume over tissue volume; Cs.Th, cortical thickness; Tb.N, trabecular number; Tb.Th, trabecular thickness; WT, wild-type; KO, *Hercl*-knock out.

I.6. Osteoblastic and osteoclastic analysis in adult mice

After describing the severe osteopenia that *Hercl*-KO mice develop until 32 weeks of age, we wondered whether the bone remodelling balance is still altered at that age. For that, we isolated the RNA from the distal femurs of 32-week-old WT and KO mice and analysed the mRNA levels of osteoblastic markers by qRT-PCR. We found no differences between genotypes in the expression of neither the master regulators of osteoblastogenesis, (*Runx2* and *Sp7*) nor in the markers of early (*Alpl*) and late osteoblast maturation (*Dmp1* and *Sost*). This result was the same for males and females (Figure 28).

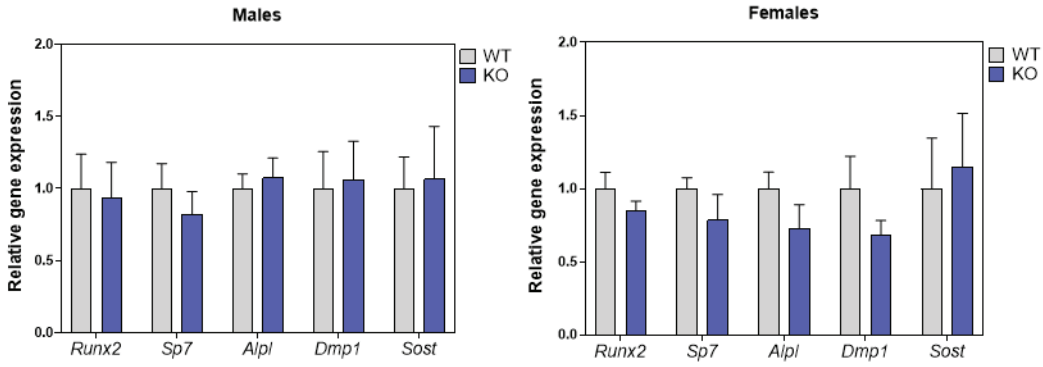

Figure 28. Expression of osteoblastic genes in femurs of male and female 32-week-old mice. The expression of each gene was normalized to *Tbp* expression. Data are expressed as mean ± SEM (n=3-7).

We then moved on to check if the alterations in osteoclast activity found at 8 weeks of age were still occurring in 32-week-old mice. We measured the expression of the osteoclastic markers in the femurs of these animals and found that WT and KO males still showed no differences in the mRNA levels of the key genes for osteoclastogenesis, *RankL* and *Opg*, nor in the genes encoding osteoclast-specific enzymes such as *Trap* and *Ctsk*. Consequently, the ratio between RankL and Opg was unchanged between genotypes (Figure *29*A). In females, conversely, there was a trend for a reduction in the expression of both *RankL* and *Opg* in *Hercl*-KO animals, that contrasts with the increase in *RankL* found at 8 weeks. As a result of the similar reduction of both genes expression, the ratio between *RankL* and *Opg* mRNA levels do not change between WT and KO 32-week-old female mice (Figure *29*B). Trap and Ctsk

gene expression was also unchanged, corroborating the equality in osteoclast activity between genotypes at 32 weeks of age (Figure *29*B). The analysis of the TRAP staining of the trabecular region of these animals revealed that there was not a significant difference in the number of osteoclasts per surface on the trabeculae of neither male nor female mice (Figure *29*C-D). However, it was clear that *Herc1*-KO animals, especially females, had such a reduced quantity of trabeculae that detection of osteoclasts on their surface was difficulted by the limited trabecular perimeter (Figure 29C-D).

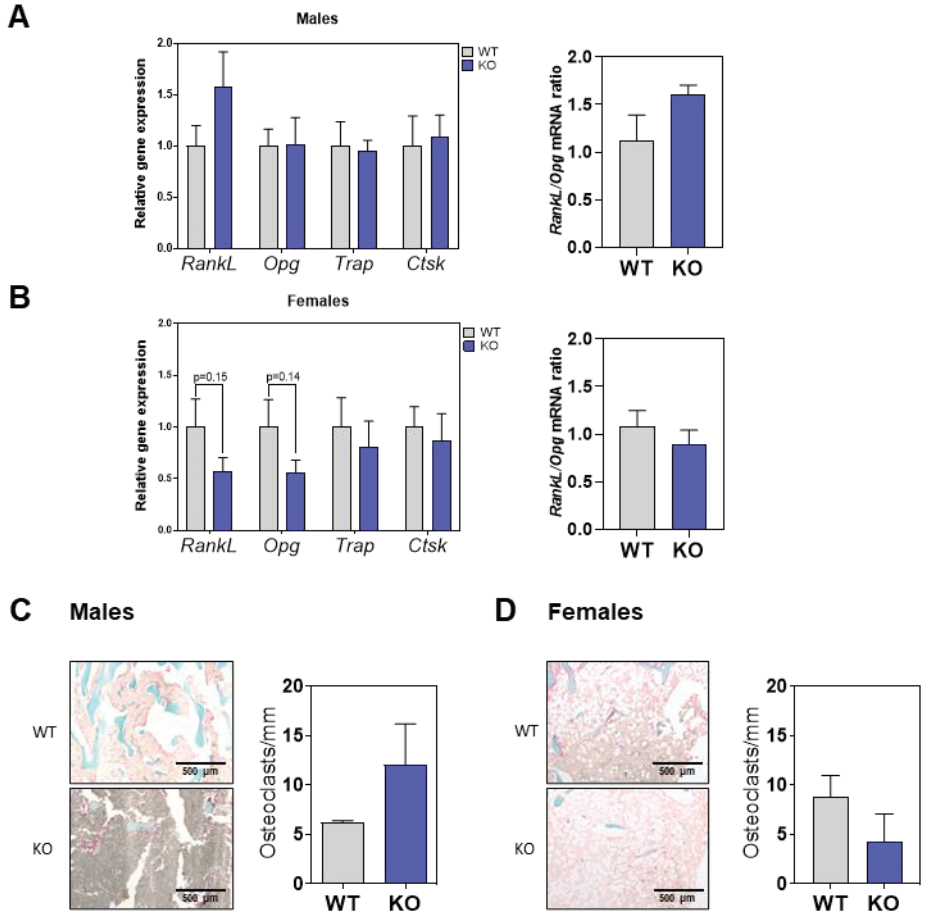

Figure 29. Osteoclastogenesis analysis in femurs from 32-week-old WT and *Herc1*-KO mice. Expression of osteoclastic markers by qRT-PCR in **(A)** male and **(B)** female mice. The expression of each gene was normalized to *Gapdh* expression, and the *Rankl*/*Opg* mRNA ratio is depicted in the right panels (n = 3–6). **C)** Histological analysis of femurs obtained from male and **(D)** female mice. Representative images of longitudinal sections of femur from male and female KO mice stained with TRAP are shown in the left panels. Images were taken with a 2x objective. Right panels report the number of osteoclasts per surface of trabecular bone (n = 2–4). Data are expressed as mean ± SEM. Abbreviations: KO, *Herc1*-knockout; WT, wild-type.

I.7. HERC1 regulates gene expression in osteocytes

Paracrine regulation is an important factor controlling bone homeostasis. As described in the Chapter II of the Introduction, osteocytes act as orchestrators of the bone remodeling process by secreting factors that influence both osteoblast and osteoclast differentiation. Thus, they are the main source of Sclerostin, inhibitor of osteoblastogenesis, and of RANKL, stimulator of osteoclastogenesis[104,105]. The production and secretion of these proteins by osteocytes modulates bone structure. Furthermore, osteocytes are also responsible for the secretion of endocrine factors such as FGF23 and NPY, that influence other organs kidney or adipose tissue[82,83]. For these reasons, we hypothesized that HERC1 could regulate the expression of some of these factors in a cell-autonomous way, which would explain at least part of the effects that the absence of *Herc1* gene has on bone remodeling.

To investigate the role of HERC1 in osteocytes, we isolated mature osteocytes from WT and KO mice and cultured them until confluence. Then, we extracted RNA from these cells and performed qRT-PCR to measure the expression of different osteocyte-specific genes. We observed that the mRNA levels of both *Runx2* and *Sp7* transcription factors were increased in *Herc1*-KO cells (**Figure 30**A). Inversely, the expression of the genes encoding collagen type 1 alpha chain 1 (*Col1a1*), osteocalcin (*Bglap*) and sclerostin (*Sost*) was not changed by the depletion of HERC1 (**Figure 30**A). However, KO cells did show an increase in the production of FGF23 and NPY factors (**Figure 30**A), which could also affect the homeostasis of other organs *in vivo*. Finally, the expression of *RankL* gene was greatly induced in *Herc1*-KO osteocytes, while *Opg* mRNA levels were significantly reduced (**Figure 30**A). Consequently, the ratio between *RankL* and *Opg* expression was considerably increased in KO cells (Figure 30B), which is consistent with the induction of osteoclast activity that we observed *in vivo* in young animals.

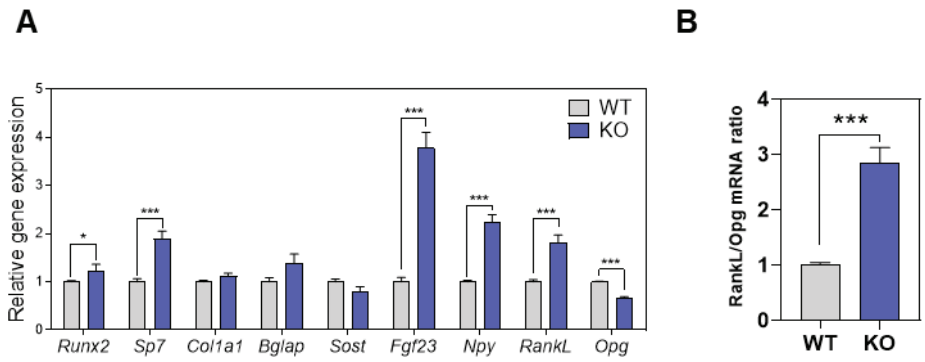

Figure 30. Gene expression in primary osteocytes. A) Expression of different osteocyte-specific genes in cultured primary osteocytes. The expression of each gene was normalized to *Tbp* expression (n=3-6). **B)** Ratio between *RankL* and *Opg* gene expression in primary osteocytes (n=4-6). Data are expressed as mean ± SEM *p<0.05; ***p<0.001. Abbreviations: KO, *Herc1*-knockout; WT, wild-type.

CHAPTER II: Regulation of energy balance and adipose tissue homeostasis by HERC1

Bone is a highly dynamic organ in constant communication with many other tissues throughout the body. Hence, alterations in bone homeostasis are often accompanied by several comorbidities affecting different organs. Among them, the crosstalk with adipose tissue has been extensively studied[338]. Taken this into account, and with the preliminary data from IMPC about *Herc1*-KO mice[75], we hypothesized that the loss of *Herc1* could also provoke important metabolic alterations.

II.1. HERC1 absence causes overweight in female mice

To assess the metabolic role of *Herc1* in the mouse model, we started monitoring the body weight of WT and *Herc1*-KO mice every week from 8 to 24 weeks of age. We observed that, while male mice did not show any difference in body weight between genotypes during the whole time, KO female mice had an accelerated rhythm of body weight increase. The differences in females started being statistically significant since the week 14 (Figure 31).

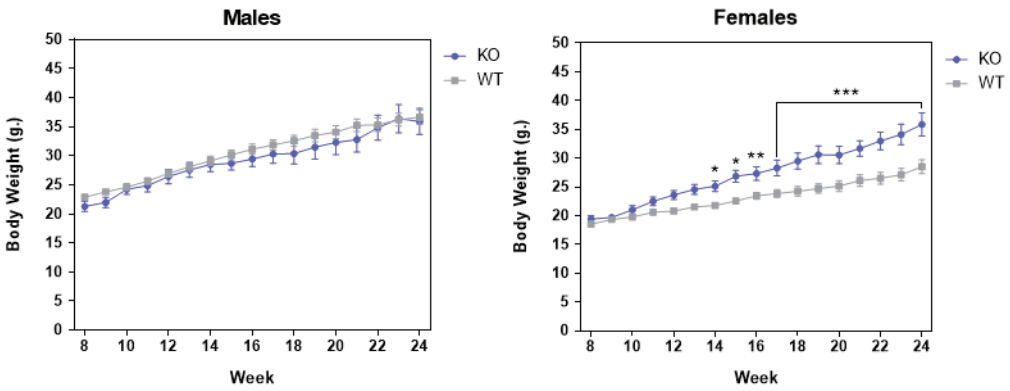

Figure 31. Body weight of male and female mice fed a normal diet from 8 to 24 weeks of age. Data are expressed as mean ± SEM (n = 7). *p < 0.05; **p < 0.01; ***p < 0.001. Abbreviations: KO, *Herc1*-knockout; WT, wild-type.

These changes in total body mass were easily noticeable at 24 weeks, when male WT and KO mice show the same body morphology, while female KO animals display a clear abdominal distension suggesting increased adipose tissue accumulation (Figure 32).

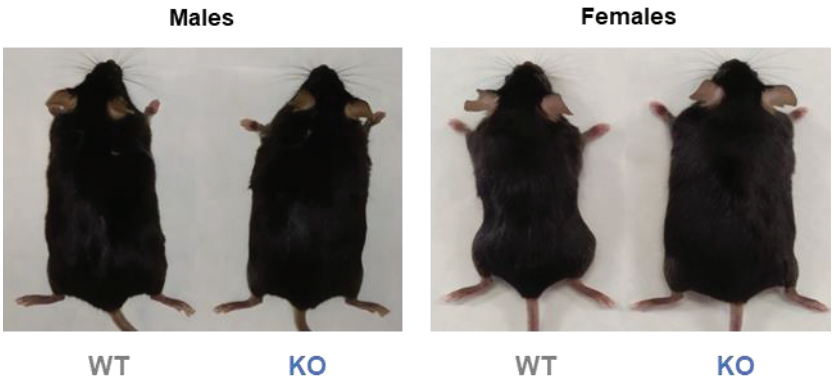

Figure 32. Body morphology of 24-week-old male and female mice. Images were taken with anesthetized animals. Abbreviations: KO, *Herc1*-knockout; WT, wild-type.

II.2. Increased weight in female mice is caused by an expansion of fat mass

After observing these sex-specific alterations, we focused our efforts on the characterization of the phenotype of females. With that purpose, the animals were first analyzed by NMR at 12 weeks. At this age, although the difference in body weight was still not significant, there was an important increase in the fat mass of KO animals compared to WT, with no changes in lean mass or free fluid mass (**Figure 33**A). Mice were scanned again at 19 weeks of age. At this stage, the differences of whole-body weight and fat mass between genotypes were enhanced (Figure 33B).

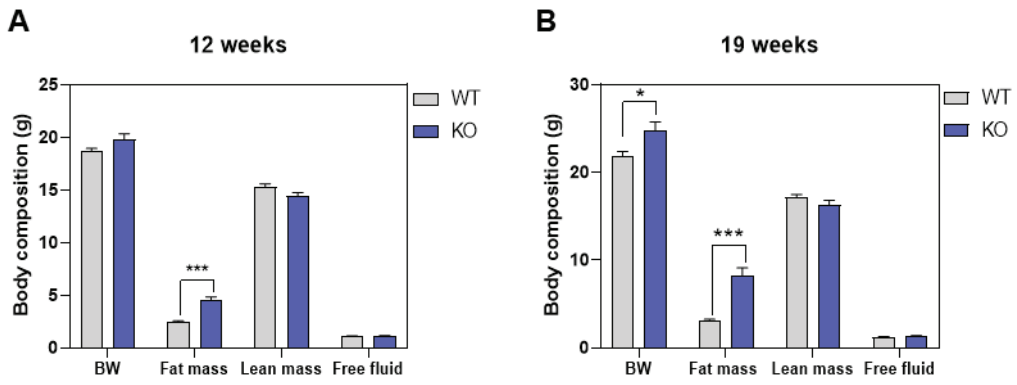

Figure 33. Body composition by NMR imaging of female mice at 12 weeks (A) and 19 weeks of age (B). Data are expressed as mean ± SEM (n = 5–8). *p < 0.05; ***p < 0.001. Abbreviations: BW, body weight; KO, *Herc1*-knockout; WT, wild-type.

II.3. The excess of fat is accumulated in inguinal and gonadal adipose tissues

Reporting the increase in adipose mass of KO female mice, we analysed two different adipose tissue depots after euthanizing the animals at 24 weeks of age: iWAT as the main subcutaneous fat depot and gWAT as a representation of visceral adipose tissue. We observed that both tissues were expanded in female *Herc1*-KO mice, as their mass, relativized to the total body weight of each animal, were considerably increased (**Figure 34**A-B). We then performed histological analysis to investigate the tissue's structure and adipocyte size and found that, while the average area of adipocytes from iWAT remained unchanged between genotypes, the adipose cells from gWAT were enlarged in the KO animals, although the difference did not reach statistical significance (Figure 34C-D). This suggest that, while iWAT expansion must be primarily due to hyperplasia, the gWAT depot also presents adipocyte hypertrophy.

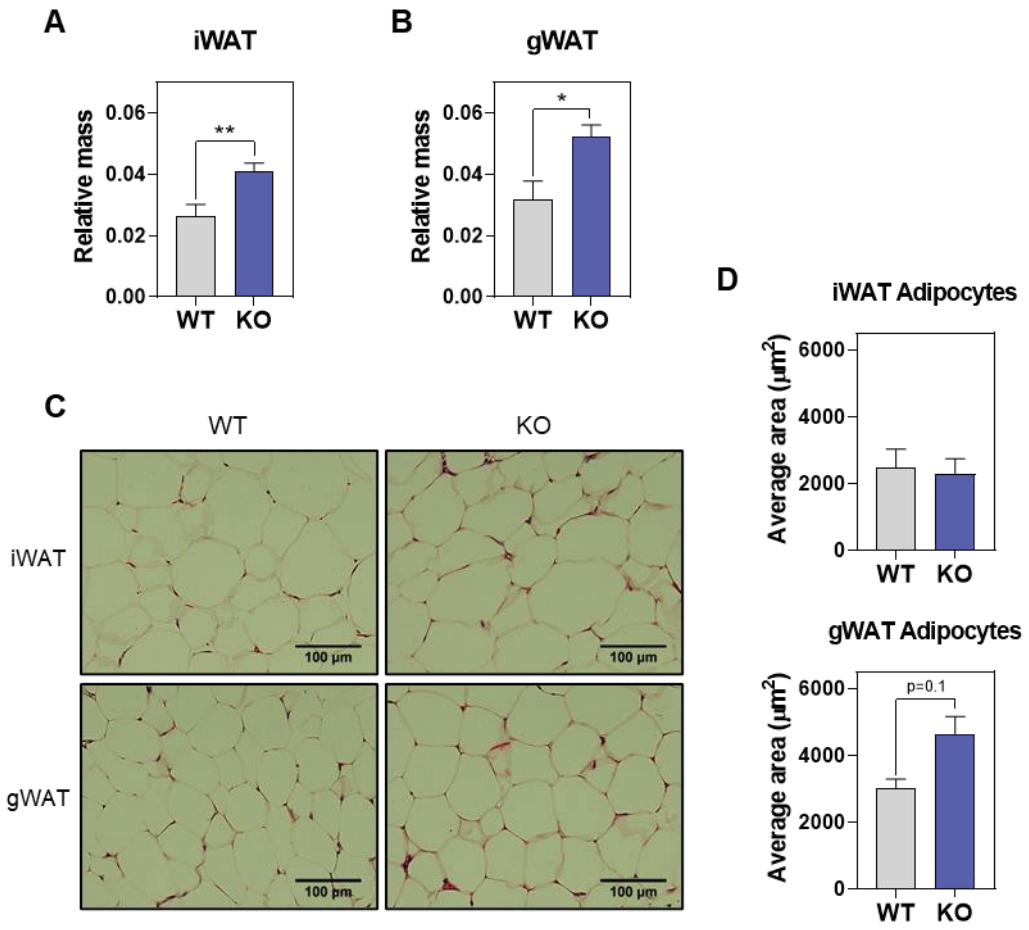

Figure 34. Mass and histological structure of white adipose tissues from 24-week-old female mice. Mass of the iWAT **(A)** and the gWAT **(B)** of each animal was relativized to its total body weight (n=7). **C)** H&E staining of 5 µm inguinal and gonadal adipose tissue slices. The images were taken with a 20x objective. **D)** Quantification of the average area of the adipocytes from 5 different 20x H&E images of each animal (n=3). Data are expressed as mean ± SEM. *p<0.05; **p<0.01. Abbreviations: iWAT, inguinal white adipose tissue; gWAT, gonadal white adipose tissue; KO, *Herc1*-knockout; WT, wild-type.

II.4. *Herc1* KO provokes light changes in the expression of adipose markers in female mice

We then moved to analyse the expression pattern of different genes involved in adipogenesis and adipose tissue function. For that, we isolated RNA from the iWAT and gWAT of 24 weeks old animals and performed qRT-PCR. We discovered a trend for an increase of *Cebpa* gene expression in iWAT from KO females, consistent with

enhanced differentiation of new adipocytes, although the levels of *Pparg* mRNA were equal between genotypes (Figure *35*A). Furthermore, in this tissue there was also a tendency for an increase in leptin (*Lep*) production in *Herc1*-null animals (Figure *35*A).

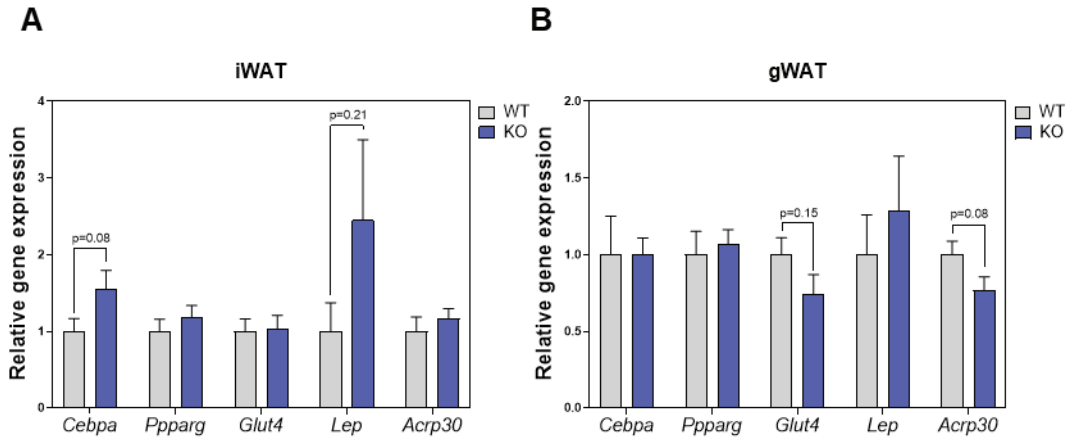

Figure 35. Expression of adipogenic genes in white adipose tissues of 24-week-old female mice. mRNA levels measured by qRT-PCR of cDNAs from **(A)** iWAT and **(B)** gWAT. The expression of each gene was normalized to *Gapdh* expression. Data are expressed as mean ± SEM (n=7). Abbreviations: iWAT, inguinal white adipose tissue; gWAT, gonadal white adipose tissue; KO, *Herc1*-knockout; WT, wild-type; *Lep*, leptin gene; *Acrp30*, adiponectin gene.

Conversely, in gWAT there was no change in the levels of *Cebpa* or *Pparg* mRNAs between WT and KO females (**Figure 35**B), suggesting that adipogenesis was not further induced by the absence of HERC1. However, KO animals presented a tendency towards the decrease of the expression of the insulin-sensitive glucose transporter *Glut4*, together with lower levels of *Acrp30* (adiponectin) mRNA (Figure 35B).

II.5. Increased fat accumulation in KO females correlates with a decrease in energy expenditure

To investigate the origin of the energy imbalance that leads to increased fat accumulation in *Herc1*-KO female mice, 19-week-old animals were put in individual metabolic cages that measured every 30 minutes the consumption of food and oxygen the production of carbon dioxide and the locomotor activity (LA) for 48h. Surprisingly, we found that food intake of KO females was significantly reduced (Figure *36*A). On the other hand, there was also a significant decrease in the energy expenditure of these

mice, independent of their body weight (Figure *36*B). The changes in energy expenditure were not explained by distinct locomotor activity, as it remained equal between genotypes in all conditions (Figure *36*C). Similarly, the total respiratory quotient was unchanged in KO females, although they presented a light decrease of this value during the night (Figure 36D).

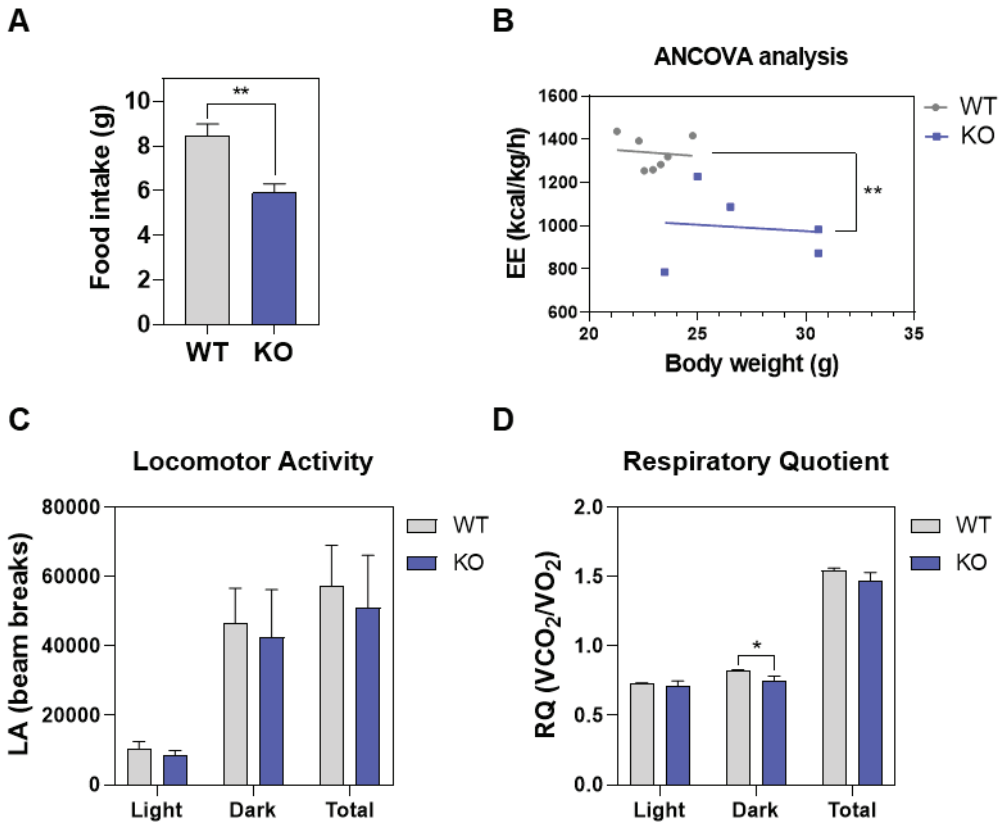

Figure 36. Metabolic phenotyping of 19 weeks-old female mice. Animals were put in individual metabolic cages that measured food and oxygen consumption, carbon dioxide production and locomotor activity during 48h. **A)** Food intake of the animals during 48h. **B)** ANCOVA of energy expenditure versus total body weight. This test allows the comparison of energy expenditure, measured with indirect calorimetry system, subtracting the effect of body weight. **C)** Locomotor activity measured with infrared light beams that register movements in horizontal and vertical directions. **D)** Respiratory quotient measured as the ratio between the CO_2 released and the O_2 consumed. Data are taken in light and dark conditions. Data are expressed as mean ± SEM (n=5-8). *p<0.05; **p<0.01. Abbreviations: KO, *Hercl*-knockout; WT, wild-type; EE, energy expenditure; LA, locomotor activity; RQ, respiratory quotient; ANCOVA, analysis of the covariance.

II.6. *Herc1*-KO female mice have impaired thermogenesis

Subsequently, we investigated the thermogenesis of the animals, another component of the energy expenditure. The interscapular temperature of 19 weeks-old female mice was measured at room temperature (~24ºC), a mild cold environment for the animals. We discovered that the temperature of the interscapular region of KO female mice was lower that the temperature found in WT mice (**Figure 37**A). When further analysing the interscapular brown adipose tissue of these animals by histology, we observed that brown adipocytes from KO females presented much larger lipid droplets that the ones found in WT animals (Figure 37B).

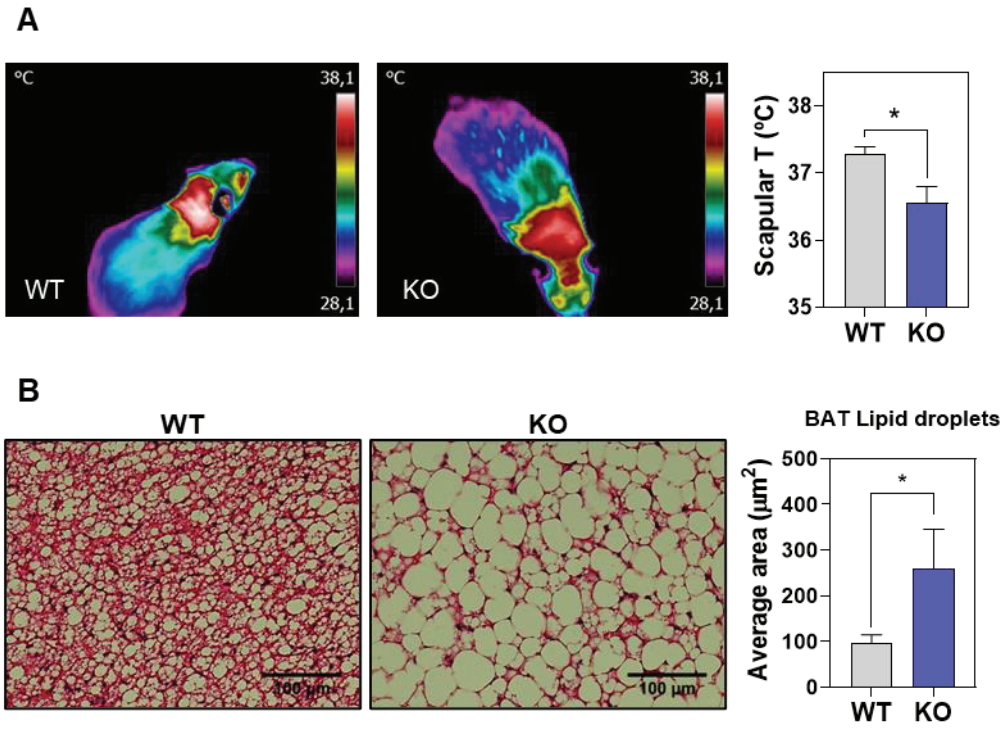

Figure 37. Interscapular thermal activity of 19-week-old female mice. A) Thermal images of WT and KO mice and quantification of the temperature of the interscapular region (n=5-8). Experiments were conducted at room temperature (~24ºC). **B)** H&E staining of brown adipose tissue (BAT) 5 µm slices from WT and KO mice. Images taken with a 20x objective. The graphic in the right depicts the average area of brown adipocytes lipid droplets, measured in 5 different 20x H&E images of each animal (n=3). Data are expressed as mean ± SEM. *p < 0.05. Abbreviations: KO, *Herc1*-knockout; WT, wild-type.

To deepen into the characterization of BAT, we extracted RNA from the tissues of 24-week-old animals and performed gene expression analysis by qRT-PCR. All the

animals were euthanized at room temperature (~24°C), so the thermogenic activity of the mice was slightly induced. In these conditions, we found reduced expression of the classical thermogenic genes *Ucp1* and *Pgc1a* in the BAT of Herc1-KO females, with no change in the mRNA levels of *Cidea*, another specific brown adipocyte marker, that code for a protein involved in the fusion of lipid droplets[287] (Figure 38A). Moreover, we also detected an increase in the expression of the *Lep* gene in the BAT from the KO animals (Figure 38B), suggesting increased production of leptin in this tissue, an adipokine mainly produced by white adipocytes. To check whether this thermogenic deficiency was restricted to BAT or also affected the browning potential in WAT, we also analysed the expression of brown cell markers in the iWAT and gWAT. We found that, in both tissues, there was a trend for a reduction of the mRNA levels of *Ucp1* and *Pgc1a* (Figure 38C-D).

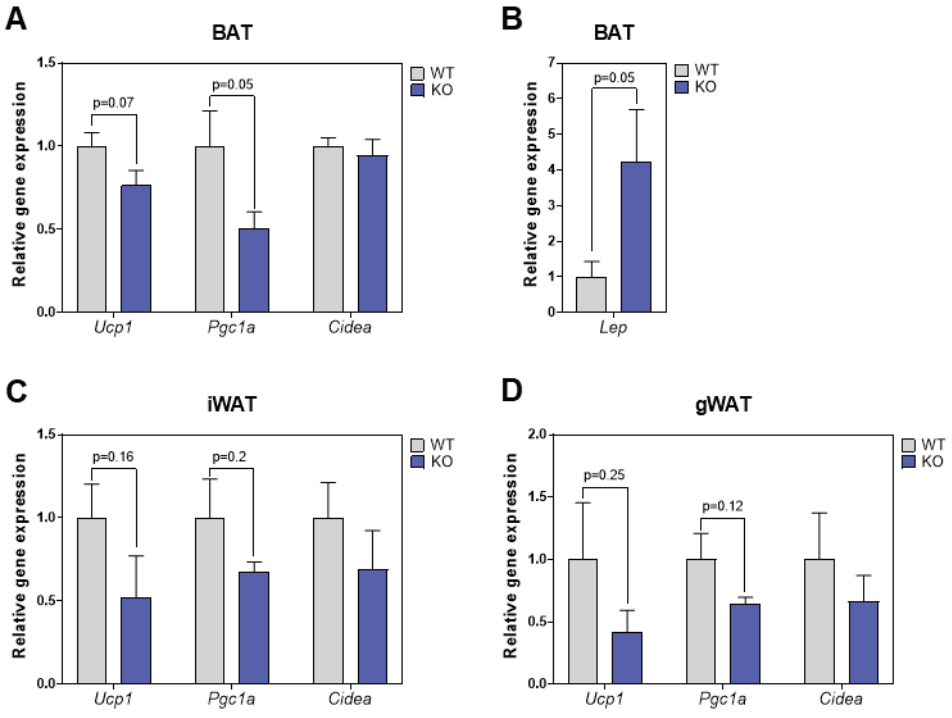

Figure 38. Expression of brown adipocyte genes in adipose tissues of 24-week-old female mice. mRNA levels measured by qRT-PCR of cDNAs from (A-B) BAT, (C) iWAT and (D) gWAT. The expression of each gene was normalized to *Gapdh* expression. Data are expressed as mean ± SEM (n=7). Abbreviations: iWAT, inguinal white adipose tissue; gWAT, gonadal white adipose tissue; KO, *Herc1*-knockout; WT, wild-type; *Lep*, leptin gene.

These results suggested an impairment in the response to adrenergic stimulation of KO female mice. To confirm that, 26-week-old animals were injected with an agonist of the β3-adrenergic receptor, and the volume of O_2 consumed by them was measured. We found that WT female mice had higher oxygen consumption that their KO littermates prior to the adrenergic stimulation, especially during the night (Figure *39*). Furthermore, after the β3 agonist injection there was a considerable increase in the volume of oxygen consumed by WT animals, while female KO mice had a reduced response, not being able to rise their oxygen consumption rate to the same extent (Figure 39).

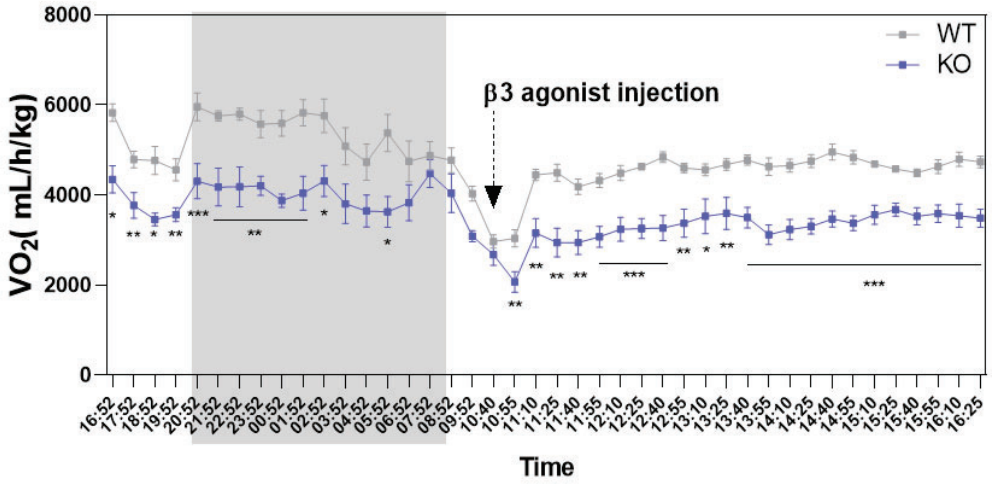

Figure 39. β3 adrenergic response of 26-week-old female mice. The volume of oxygen consumed by WT and *Herc1*-KO female mice was measured every hour during 24h. Halfway through the time, mice were injected with an agonist of the β3 adrenergic receptor, at 10:40h. *a.m.* The oxygen consumption was measured for 6h. more after the injection to assess the changes produced by the adrenergic stimulation. The grey zone indicates the dark time. Abbreviations: KO, *Herc1*-knockout; WT, wild-type.

The β3-adrenergic signalling from the SNS is the main responsible for the thermogenic induction of BAT and BgAT upon stimuli like cold exposure. To further characterize the role of HERC1 in adaptive thermogenesis, 30-week-old female mice were moved to a cold chamber, at 4°C, during 6h. and their scapular and internal temperatures were measured every hour. The thermogenic images clearly showed that the interscapular temperature of the *Herc1*-KO female mice was more reduced every hour in comparison with the scapular temperature of WT animals (Figure 40A-B).

Furthermore, we also found that, although WT and KO mice did not show any difference in the internal temperature prior to the cold exposure, the deficiency in the thermogenic ability of KO females provoked a severe hypothermia in these animals since the first hour of cold exposition, reaching an internal temperature of 35ºC after 6h in the cold chamber, while the rectal temperature of their WT littermates did not fall below 36.5ºC (Figure 40C).

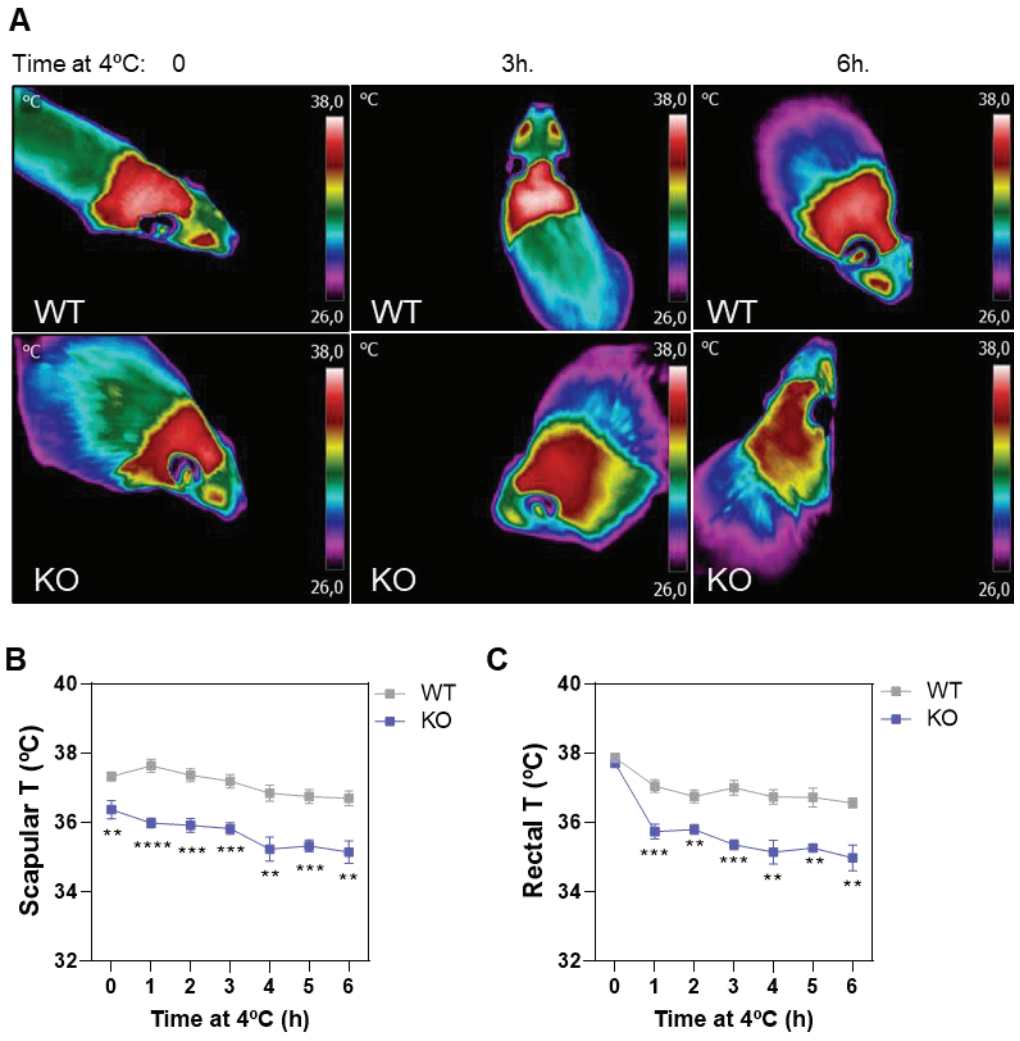

Figure 40. Adaptive thermogenesis of 30-week-old female mice. A) Thermal images of WT and KO mice after 0, 3 and 6h. of housing at 4ºC. **B)** Quantification of the interscapular region temperature detected with the thermogenic images every hour at 4ºC. **C)** Quantification of the internal temperature of the mice measured every hour at 4ºC with a rectal thermometer. Data are expressed as mean ± SEM (n=5-8). Significant differences are relative to the mean of WT mice at the same time point. **p<0.01; ***p<0.001. Abbreviations: KO, *Herc1*-knockout; WT, wild-type.

II.7. The levels of circulating lipids are increased in female *Herc1*-KO mice

Overloaded white adipose tissues do not retain the potential to store the excess of lipids inside their adipocytes, which also present enhanced lipolysis. This is correlated with an increase in the circulating levels of lipids[246]. To check if female KO mice presented this phenomenon, we measured the concentration of lipids in the serum of 32-week-old animals. We found that *Herc1*-KO females had increased levels of circulating total lipids, in comparison with WT females (Figure 41A). Nevertheless, the concentration of triglycerides and cholesterol in the serum was not altered between genotypes (Figure 41B-C), which points to the rise of the levels of another type of lipids, probably NEFA, as the responsible for the detection of increased circulating fat.

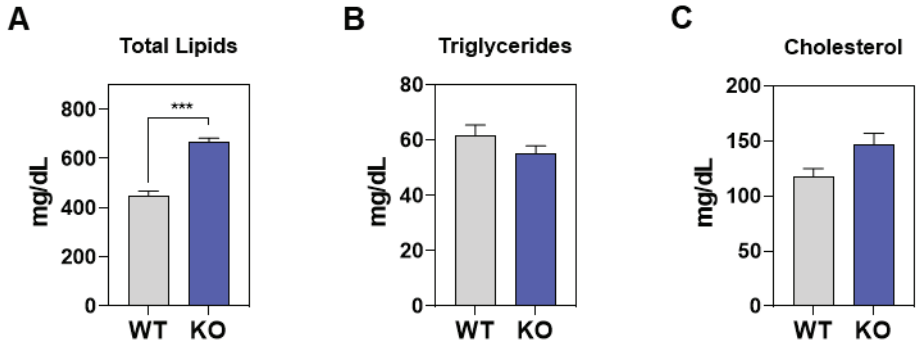

Figure 41. Concentration of lipids in the serum of 32-week-old female mice. The concentration of **(A)** total lipids, **(B)** triglycerides and **(C)** cholesterol was measured in the serum of the mice using commercial biochemical kits. Data are expressed as mean ± SEM (n=7-12). ***p < 0.001. Abbreviations: KO, *Herc1*-knockout; WT, wild-type.

II.8. *Herc1*-KO female mice develop ectopic fat accumulation in the liver and insulin resistance

Increased circulating lipids can be stored in non-adipose tissues, where their accumulation provokes lipotoxicity. One of the tissues most affected by this is the liver. In fact, the excessive accumulation of lipids in the liver leads to the non-alcoholic fatty liver disease (NAFLD), which is strongly associated with different components of the metabolic syndrome such as obesity or insulin resistance. Moreover, NAFLD can

progress to non-alcoholic steatohepatitis (NASH), characterized by the inflammation and damage of the liver, that may lead to fibrosis and finally to cirrhosis[339]. To assess the liver phenotype, we analysed this tissue from 24-week-old mice. We observed that the relative mass of the liver was not changed between WT and *Herc1*-KO female mice (Figure 42A). However, histological analysis of the tissue revealed that there was a light increase in the hepatic accumulation of lipids, although not reaching statistical significance (Figure 42B-C).

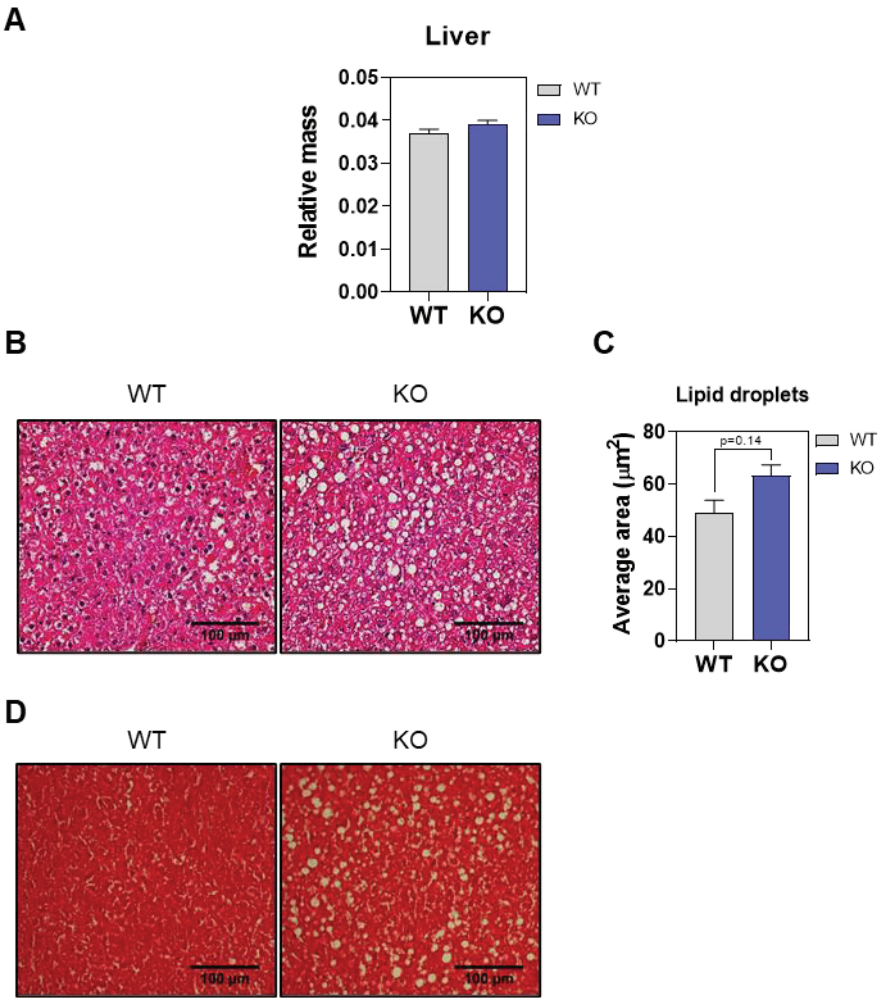

Figure 42. Mass and histological structure of livers from 24-week-old female mice. A) The mass of the liver of each animal was relativized to its total body weight (n=7). **B)** H&E staining of 5 µm liver slices. The images were taken with a 20x objective. **C)** Quantification of the average area of the adipocytes from 5 different 20x H&E images of each animal (n=3). **D)** Masson trichrome staining of 5 µm liver slices. Data are expressed as mean ± SEM. Abbreviations: KO, *Herc1*-knockout; WT, wild-type.

Masson's trichrome staining is useful for the detection of collagen fibres, which presence in the liver is characteristic of fibrosis[340]. Thus, we then performed this staining on liver sections to evaluate whether the hepatic steatosis found had pathological consequences. With this technique we did not detect any collagen staining, thus discarding severe hepatic damage at this stage (Figure 42D).

Having described the overweight phenotype and increased adiposity of female *Herc1*-KO mice, we then analysed glucose utilization and insulin function to assess if these animals presented more components of metabolic syndrome. For this, 22-week-old mice were subjected to a glucose tolerance test (GTT). After an intraperitoneal injection of glucose, KO female mice were not able to reduce the levels of circulating glucose at the same rhythm as their WT littermates, maintaining higher concentration for at least 120 minutes (**Figure 43**A). This was evidenced by the significant increase in the area under the curve (AUC) of the glucose levels of KO females during the experiment, in comparison with the AUC of the WT animals (**Figure 43**B). To elucidate the cause for the deficiency in glucose uptake, these mice were subjected to an insulin tolerance test (ITT) when they were 26 weeks old. Following the intraperitoneal injection of insulin, Herc1-KO females showed little reduction of glucose blood levels while WT animals presented an expected response to insulin action (Figure 43C). Likewise, the AUC of glucose levels from KO mice was increased compared to the AUC of WT animals (Figure 43D). These results are compatible with the insulin resistance in *Herc1*-KO female mice.

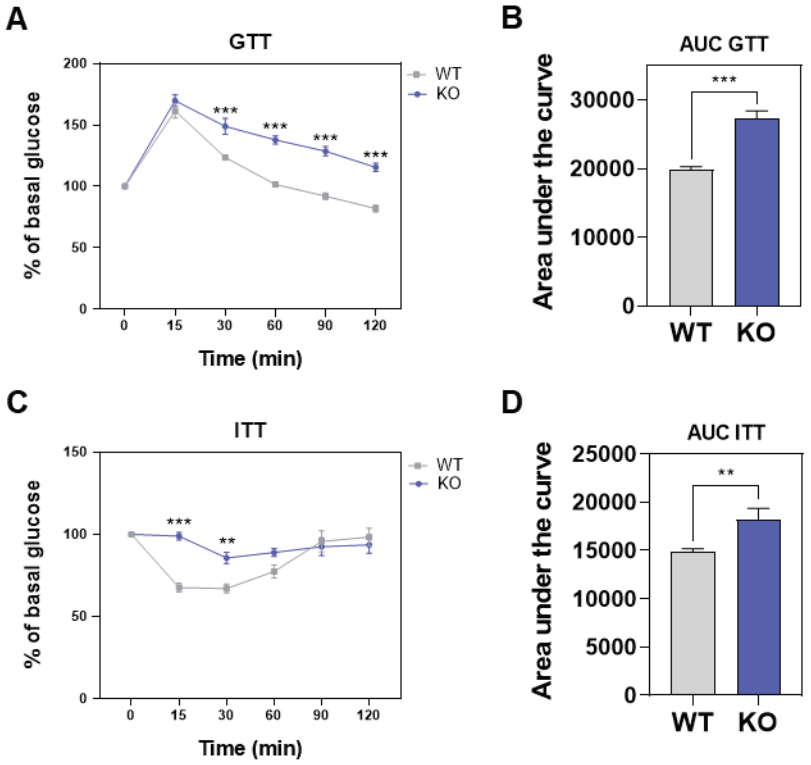

Figure 43. Glucose uptake in 22 and 26-week-old mice. A) GTT of 22-week-old female mice. Animals were starved for 16h. and intraperitoneally injected with 2g/Kg of D-Glucose. The glucose blood levels were measured before injection and 15, 30, 60, 90 and 120 minutes post-injection. All values were relativized to the glucose concentration of the animal at time 0 (basal glucose). **B)** Area under the curve of the variation of glucose concentration during the 120 minutes of monitoring the GTT. **C)** ITT of 26-week-old female mice. Animals were starved for 6h. and intraperitoneally injected with 0.35U/Kg insulin. The glucose blood levels were measured before injection and 15, 30, 60, 90 and 120 minutes post-injection. All values were relativized to the glucose concentration of the animal at time 0 (basal glucose). **D)** Area under the curve of the variation of glucose concentration during the 120 minutes of monitoring the ITT. Data are expressed as mean ± SEM (n=5-8) **p<0.01; ***p<0.001. Abbreviations: KO, Hercl-knockout; WT, wild-type; GTT, glucose tolerance test; AUC, area under the curve; ITT, insulin tolerance test

II.9. Knock-out of *Herc1* increases susceptibility to obesity in mice fed a high-fat diet

After stablishing the *Herc1*-KO as an overweight mouse model for females, we started an obesity model by switching the mice to a high-fat diet (HFD) for 16 weeks, starting at 8 weeks of age. With this approach, we monitored again the body weight of the animals every week and found that the differences reported in females were greatly enhanced (Figure 45A). Surprisingly, with this change of diet also KO male mice gained

more weight than their WT littermates, although the differences between genotypes were smaller (Figure 45B).

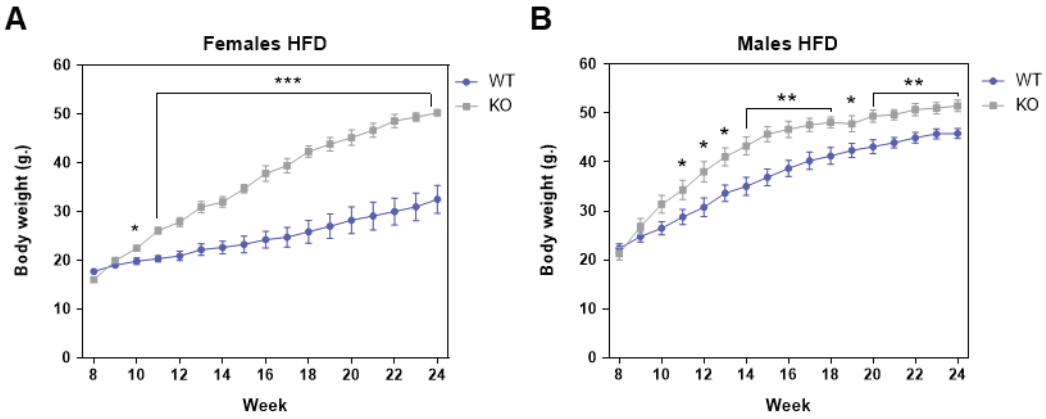

Figure 44. Body weight of mice fed a HFD diet from 8 to 24 weeks of age. **A)** Female and **(B)** male mice were weighted weekly. Data are expressed as mean ± SEM (n = 7). *p < 0.05; **p < 0.01; ***p < 0.001. Abbreviations: KO, *Hercl*-knockout; WT, wild-type.

The increase in body mass provoked by HFD feeding was clear when the animals reached 24 weeks, as the body morphology of both male and female mice was changed between WT and KO animals. Nevertheless, while the increased abdominal distension in female KO mice in comparison with their WT littermates was evident (Figure 45C), the difference in body morphology between WT and KO males was more subtle (Figure 45D).

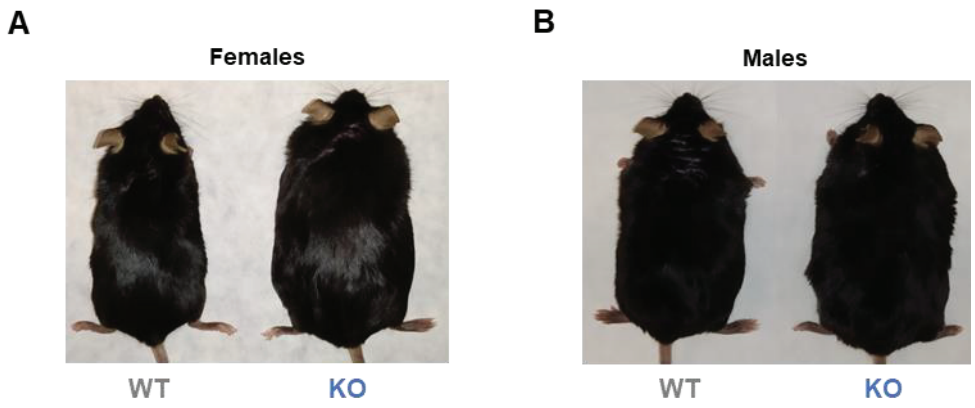

Figure 45. Body morphology of 24-week-old mice fed a HFD from 8 to 24 weeks of age. Images or **(A)** female and **(B)** male mice were taken with anesthetized animals. Abbreviations: KO, *Herc1*-knockout; WT, wild-type.

II.10. *Herc1*-KO female mice fed a HFD accumulate more fat in their white adipose tissues

The white adipose tissues of 24-week-old mice fed a HFD for 16 weeks were analysed. We observed that the differences in both iWAT and gWAT relative mass between KO and WT female mice that we found with a normal diet were enhanced by the HFD (Figure *46*A-B). However, male mice fed a HFD did not show any genotype-related difference in the relative mass of their WAT depots (Figure 46C-D). When analysing the histological structure of these tissues, we did not detect any significant difference in the size of the adipocytes between WT and KO females, neither in iWAT nor in gWAT (Figure 46E-F). Therefore, in this case the differences in adipose mass are due to hyperplasia, not to hypertrophy. Similar results were found in male mice (Figure 46G-H).

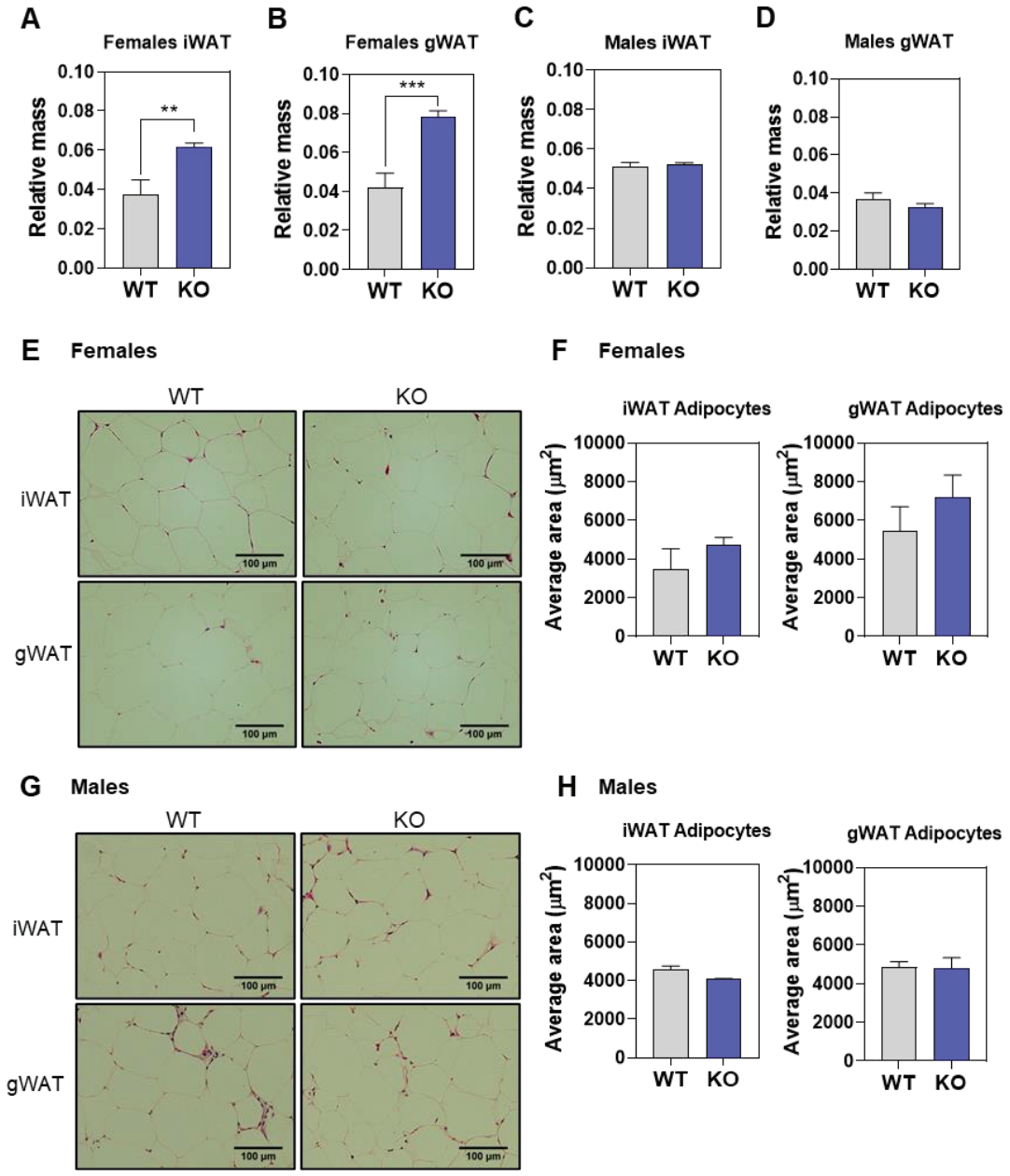

Figure 46. Mass and histological structure of white adipose tissues from 24-week-old animals fed a HFD. A) Relative mass of iWAT and **(B)** gWAT from female mice. **C)** Relative mass of iWAT and **(D)** gWAT from male mice. The mass of the adipose tissues of each animal was relativized to its total body weight (n=7). **E)** H&E staining of 5 µm inguinal and gonadal adipose tissue slices from female mice. The images were taken with a 20x objective. **F)** Quantification of the average area of the adipocytes from 5 different 20x H&E images of each female mouse (n=3). **G)** H&E staining of 5 µm inguinal and gonadal adipose tissue slices from male mice. The images were taken with a 20x objective. **H)** Quantification of the average area of the adipocytes from 5 different 20x H&E images of each female mouse (n=3). Data are expressed as mean ± SEM. **p<0.01; ***p<0.001. Abbreviations: iWAT, inguinal white adipose tissue; gWAT, gonadal white adipose tissue; KO, *Herc1*-knockout; WT, wild-type.

II.11. The absence of *Herc1* alters the expression of adipogenic genes in WAT depots from mice fed a HFD

After studying the structure of the white adipose tissues from the HFD-fed mice, we analysed the expression of genes involved in adipogenesis and adipose function. RNAs were isolated from the iWAT and gWAT of 24-week-old mice fed a HFD for 16 weeks, and the gene expression was assessed by qRT-PCR. Focusing on females, we found that there was a trend for an increase in the expression of *Pparg* in the iWAT of the KO animals (Figure 47A), result consistent with enhanced adipogenesis. Furthermore, the mRNA levels of *Lep* and *Acrp30*, the genes coding for the adipokines leptin and adiponectin, were both risen in this tissue (Figure 47A). Inversely, in the gWAT the expression of *Cebpa* was significantly reduced in the KO females, with no changes in the levels of *Pparg* (Figure 47B). In this tissue, there was also a great supress of the expression of *Glut4*, gene that codes for the insulin-sensitive glucose transporter type 4, and of *Acrp30* gene (Figure 47B). The production of leptin was also stimulated in the gWAT of Herc1-KO female mice (Figure 47B).

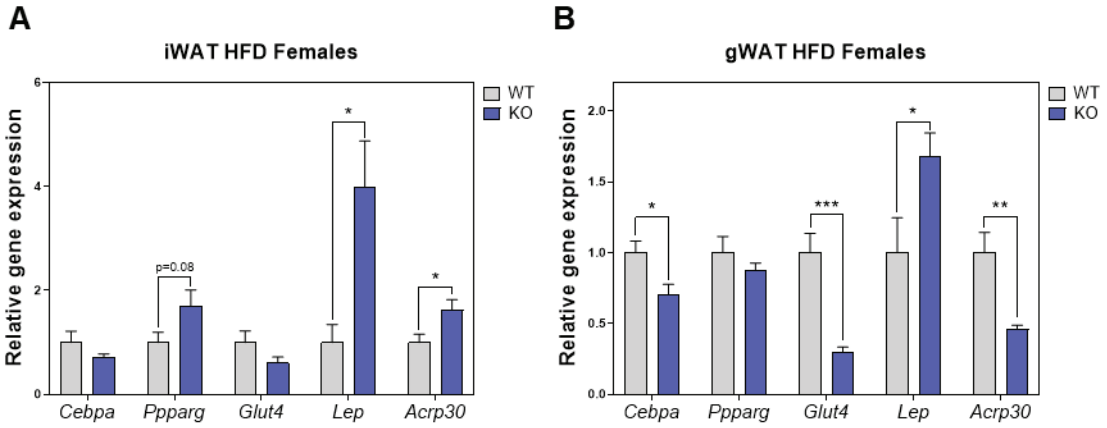

Figure 47. Expression of adipogenic genes in white adipose tissues of 24-week-old female mice fed a HFD for 16 weeks. mRNA levels measured by qRT-PCR of cDNAs from **(A)** iWAT and **(B)** gWAT. The expression of each gene was normalized to *Gapdh* expression. Data are expressed as mean ± SEM (n=7). *p<0.05; **p<0.01; ***p<0.001. Abbreviations: iWAT, inguinal white adipose tissue; gWAT, gonadal white adipose tissue; KO, *Herc1*-knockout; WT, wild-type; *Lep*, leptin gene; *Acrp30*, adiponectin gene.

Regarding the tissues from male mice, we detected a trend for a reduction in the expression of *Cebpa* in the iWAT of KO animals (Figure *48*A), and the mRNA levels of *Glut4* in this tissue were significantly reduced in the absence of Herc1 (Figure *48*A).

In gWAT, the expression of *Glut4* was also repressed in the KO males, although not reaching statistical significance, and there was also a significant reduction of the production of leptin (Figure 48B).

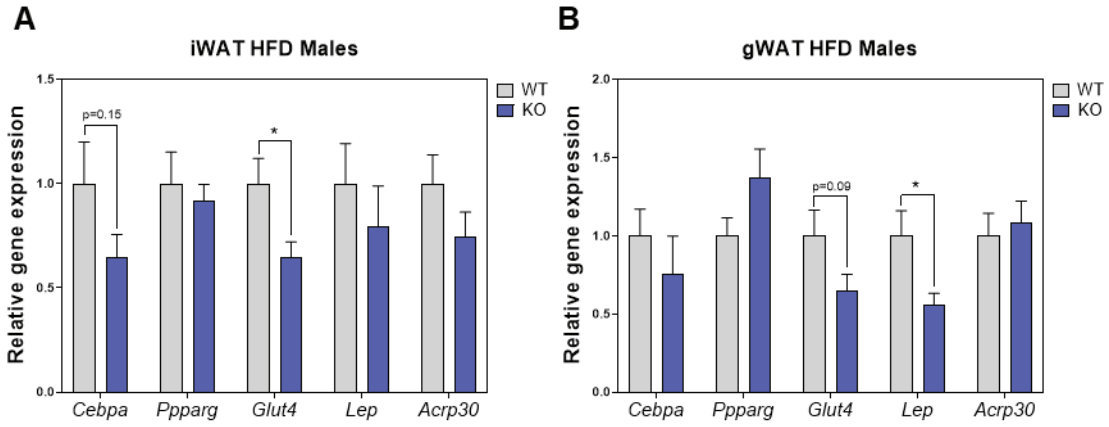

Figure 48. Expression of adipogenic genes in white adipose tissues of 24-week-old male mice fed a HFD for 16 weeks. mRNA levels measured by qRT-PCR of cDNAs from **(A)** iWAT and **(B)** gWAT. The expression of each gene was normalized to *Gapdh* expression. Data are expressed as mean ± SEM (n=7). *p<0.05. Abbreviations: iWAT, inguinal white adipose tissue; gWAT, gonadal white adipose tissue; KO, *Herc1*-knockout; WT, wild-type; *Lep*, leptin gene; *Acrp30*, adiponectin gene.

II.12. Knock-out of *Herc1* aggravates the BAT phenotype of HFD-fed mice

Given the fact that thermogenesis was impaired in KO female mice, we wondered whether BAT was more affected by the high fat diet in the *Herc1*-depleted animals compared to the WT, and if this was also the case for males under these diet conditions. The histological analysis of tissues from 24-week-old mice fed a HFD for 16 weeks revealed that, as expected, the diet change provoked the fusion of lipid droplets in brown adipocytes. The absence of *Herc1* gene stimulates this phenomenon, leading to larger lipid vacuoles in the BAT of both male and female KO mice (Figure 49A-B).

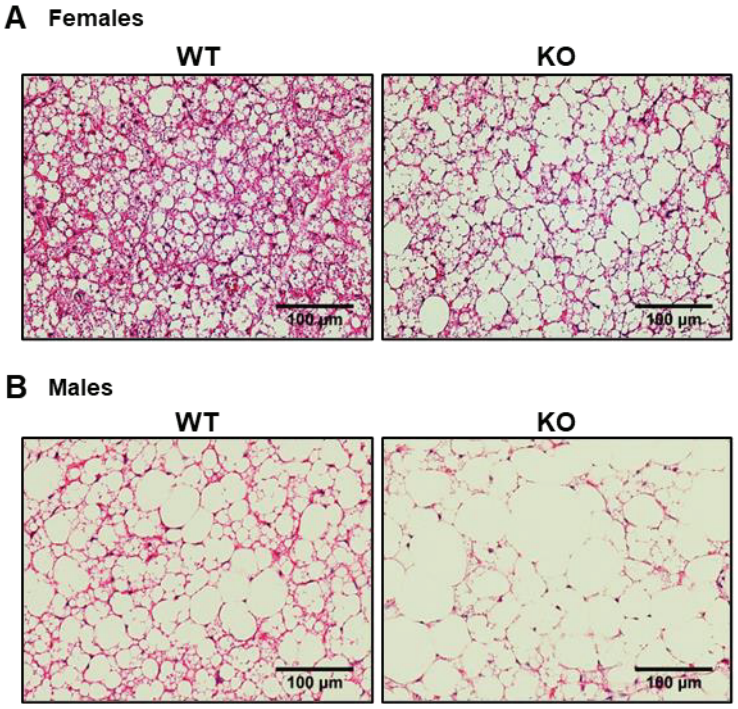

Figure 49. Tissular structure of BAT from 24-week-old mice fed a HFD for 16 weeks. H&E staining of brown adipose tissue (BAT) 5 µm slices from **(A)** female and **(B)** male WT and KO mice. Animals were euthanized at room temperature (~24°C). Images taken with a 20x objective. Abbreviations: KO, *Herc1*-knockout; WT, wild-type.

We also isolated the RNA from these tissues and analysed gene expression by qRT-PCR. By doing this, we did not detect any change between genotypes in the expression of classical thermogenic markers *Ucp1*, *Pgc1a* or *Cidea* in the BAT of females (Figure 50A). The mRNA levels of the master regulators of adipogenesis *Cebpa* and *Pparg* were also matched between WT and KO female mice, but there was a significant increase in the expression of the adipokine leptin in *Herc1*-null animals (Figure 50B), agreeing with the more "white-like" phenotype. Inversely, KO males did show a trend for an increase in the expression of *Pgc1a* (Figure 50C), and there was also a rise in the transcript levels of *Cebpa* and *Pparg* (Figure 50D), altogether suggesting enhanced brown adipogenesis in these conditions. Nevertheless, the expression of leptin was also stimulated in the KO male mice compared to their WT littermates (Figure 50D).

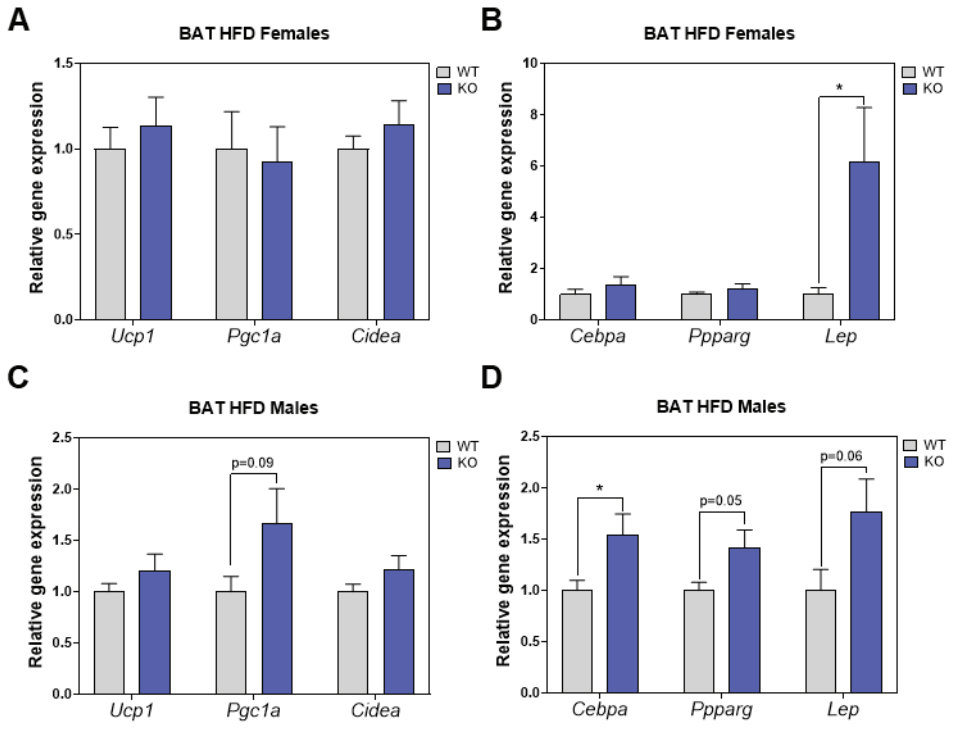

Figure 50. Expression of brown adipocyte genes in brown adipose tissue of 24-week-old mice fed a HFD for 16 weeks. mRNA levels measured by qRT-PCR of cDNAs from BAT of (A-B) female and (C-D) male mice. Animals were euthanized at room temperature (~24ºC). The expression of each gene was normalized to *Gapdh* expression. Data are expressed as mean ± SEM (n=7). *p<0.05. Abbreviations: BAT, brown adipose tissue; KO, *Herc1*-knockout; WT, wild-type; *Lep*, leptin gene.

II.13. *Herc1*-KO mice fed a HFD have altered expression of browning markers in WAT

The results of the analysis of BAT suggested that Herc1 KO could alter adaptive thermogenesis also under high fat diet conditions. To further investigate this, we also analysed the expression of browning markers in the iWAT and gWAT of these 24-week-old animals. We discovered that female KO mice fed a HFD did indeed present a decrease in the expression of *Ucp1*, *Pgc1a* and *Cidea* in both iWAT and gWAT, when compared to WT females (Figure 51A-B), which would support a deficiency of KO female mice for the induction of beige adipocytes. Conversely, male mice did not show any genotype-related difference in the expression of these markers in iWAT (Figure

51C), but KO males presented a trend for the increase of the transcript levels of the three genes in the gWAT (Figure 51D).

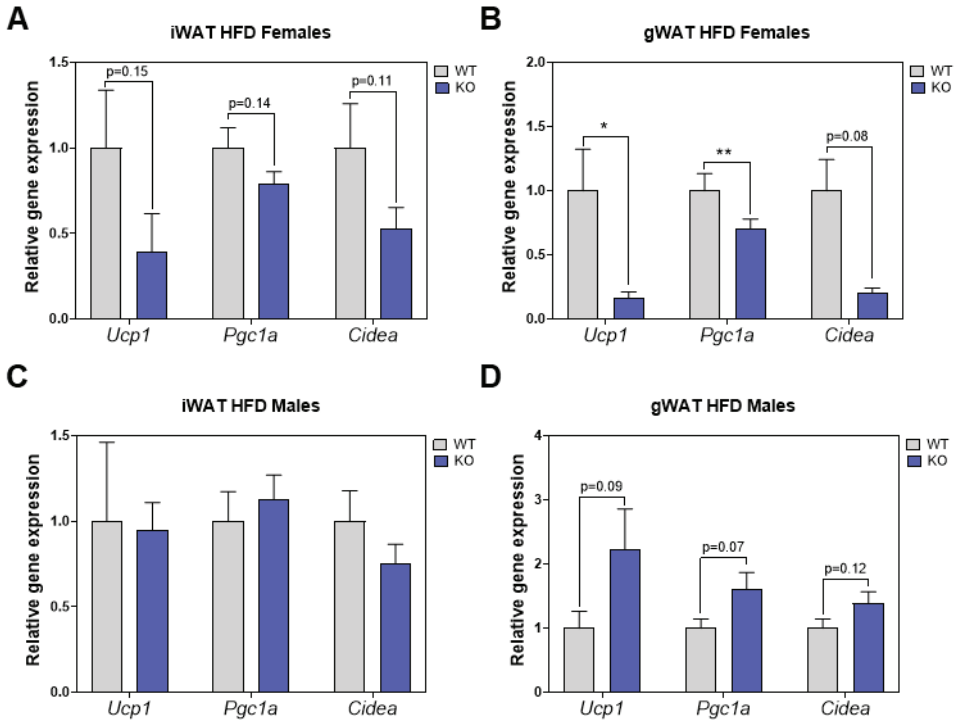

Figure 51. Expression of brown adipocyte genes in white adipose tissues of 24-week-old mice fed a HFD. mRNA levels measured by qRT-PCR of cDNAs from **(A)** iWAT and **(B)** gWAT from female mice, and **(C)** iWAT and **(D)** gWAT from male mice. The expression of each gene was normalized to *Gapdh* expression. Data are expressed as mean ± SEM (n=7). *p<0.05; **p<0.01. Abbreviations: iWAT, inguinal white adipose tissue; gWAT, gonadal white adipose tissue; KO, *Herc1*-knockout; WT, wild-type.

II.14. Hepatic steatosis provoked by HFD is enhanced by knock-out of Herc1.

The administration of a high-fat diet is the most widely used method for the induction of NAFLD in mouse models[341]. For this motive and considering the light induction of hepatic steatosis found in female *Herc1*-KO mice with a normal diet, we investigated whether the deficiency in *Herc1* could modulate the lipid accumulation in the liver caused by the HFD. First, we observed that livers from 24-week-old mice fed

a HFD for 16 weeks do not differ in relative mass between WT and KO animals, nor in females nor males (Figure 52A-B). However, when analysing these tissues by histology we did find a great increase in the size of the hepatic lipid droplets of KO male and female mice when compared to their WT littermates (Figure 52B). These differences were corroborated by the quantification of the size of the lipid droplets in the H&E images (Figure 52C). Nevertheless, although having increased steatosis, there was no indications of the presence of collagen fibres, as revealed by the Masson trichrome staining (Figure 52D).

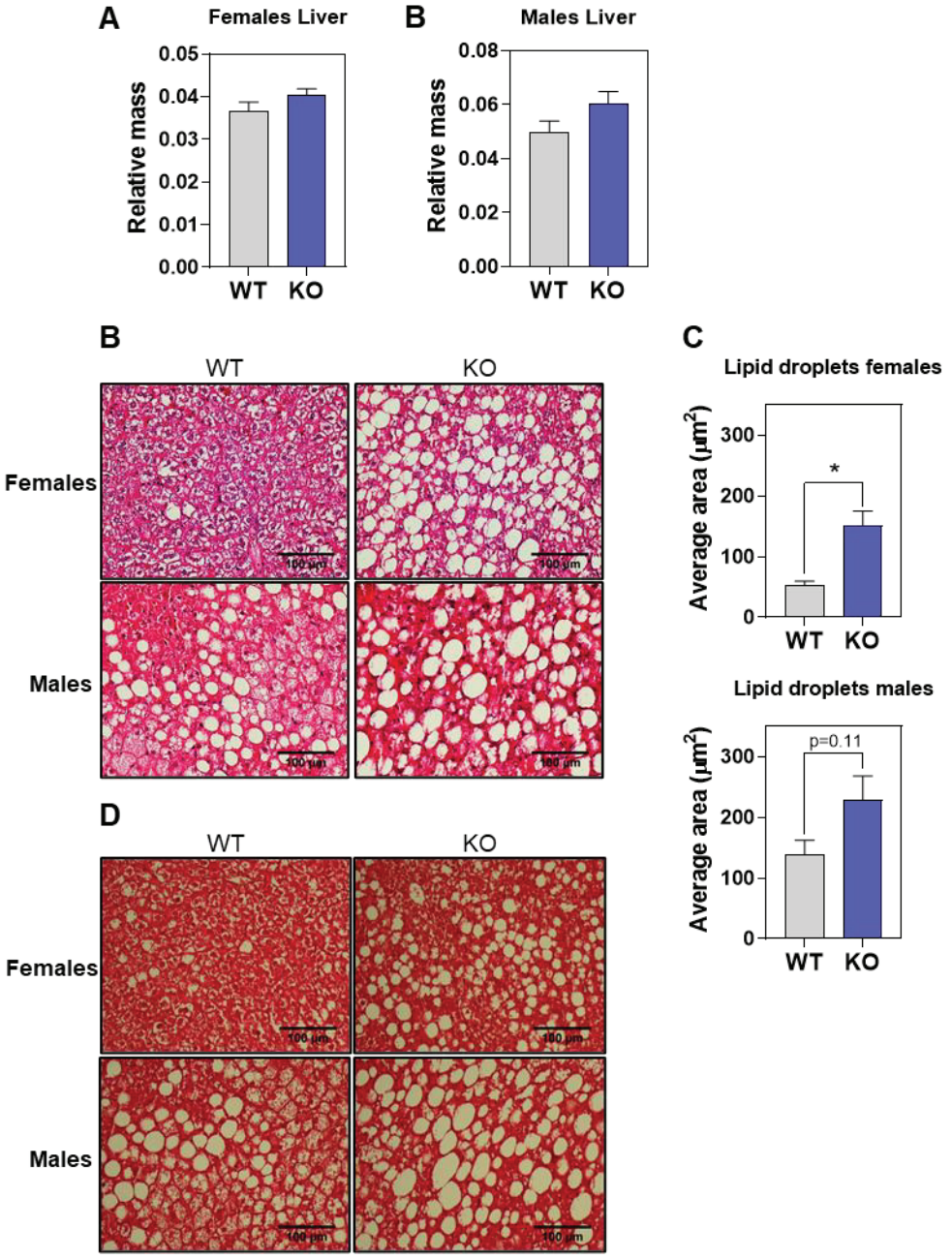

Figure 52. Mass and histological structure of livers from 24-week-old mice fed a HFD. Relative mass of the livers from **(A)** female and **(B)** male mice. The mass of the liver of each animal was relativized to its total body weight (n=7). **C)** H&E staining of 5 µm liver slices. The images were taken with a 20x objective. **C)** Quantification of the average area of the adipocytes from 5 different 20x H&E images of each animal (n=3). **D)** Masson trichrome staining of 5 µm liver slices. Data are expressed as mean ± SEM *p<0.05. Abbreviations: KO, *Herc1*-knockout; WT, wild-type.

DISCUSSION

Since *HERC1* discovery in 1996[17], this protein has been investigated using various kinds of models, ranging from studies in human patients to different cell lines[9,30]. Regarding mouse models, all the efforts had been focused on the study of the *tambaleante* mouse model. Nevertheless, while the neurological phenotype of these mice has been thoroughly researched[53], few data is available about other roles that *Herc1* could be playing *in vivo*. Besides, the mutation in *Herc1* that causes the *tambaleante* phenotype provokes an increment in HERC1 protein levels in brain, but it is not clear whether this protein conserve its original functions or not. Altogether, although the *tambaleante* model is still greatly useful, it also presents some limitations. Recently, a *Herc1*-knock out mouse model was generated, and these animals lack the expression of HERC1 protein in all tissues analysed. This makes this model a really powerful tool to investigate the physiological relevance of HERC1.

I. Gene knock-out models for the study of its physiological relevance

The characterization of the functions of a protein-coding gene and its product is a multi-step process that requires the combination of multiple approaches both *in vitro* and *in vivo*. Strategies using cell cultures allow the identification of molecular mechanisms by which the studied protein may modulate different cell processes such as differentiation, growth, migration or apoptosis, among many others. Furthermore, they facilitate the study of human genes by the utilization of cell lines derived from human tissues. However, it is important to consider that living organisms are complex systems composed of many interrelated organs that regulate each other, and the physiological relevance of each gene is not only restricted to a cell or a tissue but depends on the whole net of communications between organs. For this motive, the study of animal genetic models usually reveals new roles not previously expected for the studied gene[74].

Among the model animals used for determining gene function, the mouse has been considered one of the most optimal for extrapolating the conclusions to human biology. This is due to the conservation of most aspects of mammalian development, physiology and metabolism between human and mice. The conservation of gene

function between these species is also supported by the similar phenotypic consequences of most of the loss-of-function mutations in orthologous genes in both species[72].

For the study of gene function, one of the most direct approaches both *in vitro* and *in vivo* is the analysis of the consequences of the partial or complete loss of the gene expression[342]. Therefore, the use of gene knock-out models has enabled the uncovering of the role of specific genes in all types of physiological processes such as bone structure[343], adipose tissue and energy homeostasis[344] or brown adipose tissue phenotype[345]. In this line of research, the International Knockout Mouse Consortium started a global project with the aim of generate mice with mutations in every known coding gene. Among these mutant strains, most of them are conditional knock-outs, that allow the ablation of the gene in concrete tissues or developmental stages, but others are constitutive knock-outs, that globally supress the expression of the gene[72–74]. Interestingly, the mouse strains generated by this consortium are systematically phenotyped and the results are publicly available at the IMPC webpage[346]. It was in this project that the *Herc1*-KO mouse strain was generated by Dr. Chris Tyler-Smith and Dr. Michal Szpak at the Wellcome Trust Sanger Institute. The collaboration started between their group and our laboratory has enabled the further characterization of the phenotype of these animals, and this thesis represents the first effort in that direction.

II. HERC1 in bone homeostasis

The studies performed until date to characterise the pathophysiology of deficiencies in HERC1 can be classified in two groups. Studies that find somatic mutations in this gene have related them to cancer transformation or to a worse prognosis for oncological patients[30]. On the other hand, germline alterations in *HERC1* gene are strongly linked to neurological disorders, being responsible for the MDFPMR syndrome in humans and for the ataxic phenotype of the *tambaleante* mice[53]. This thesis provides the first evidence that HERC1 also controls bone homeostasis, and that the loss of its function leads to osteopenia.

MSCs are the raw material of bone. Their presence in bone marrow allows the regeneration of the tissue in the process of bone remodelling. Moreover, their pluripotency makes them very versatile, being able to become different cell types. Hence, the specification of their differentiation must be a tightly regulated process, in which many proteins may play a role. The self-renewal ability of these cells enables the utilization of primary cultures as a model for the analysis of their differentiation. Taking advantage of this feature, we started our study by analysing how the depletion of HERC1 affected the osteoblastic differentiation of MSCs. By doing this, we found that downregulation of HERC1 enhances the *in vitro* differentiation of these cells to osteoblasts, as proved by the increment in the secretion of calcium and in the alkaline phosphatase activity, as well as by the stimulation of the expression of genes like *Runx2*, *Sp7*, *Col1a1*, *Alpl* and *Bglap*. This increased osteoblastogenesis was paired with the upregulation of the phosphorylation of ERK and p38, phenomenon that was maintained even after 21 days of differentiation. The regulation of these MAPKs by HERC1 had already been described in other cellular contexts[25,29], but the replication of those results in this model could explain how HERC1 depletion may stimulate osteogenesis, as p38 and ERK pathways have been extensively proved as positive regulators of osteoblast differentiation by the phosphorylation of key transcription factors such as RUNX2, OSX or DLX5[169–175,177]. However, to stablish whether this regulation of osteogenesis by HERC1 is dependent of MAPK signalling more experiments will be necessary, using genetic or pharmacologic ablation of the activity of these proteins.

Despite the first evidence pointing towards HERC1 exerting a negative regulation of bone mass, the study of the *Herc1*-KO mouse proved the contrary. The analysis of the architecture of distal femurs from young mice revealed that these animals present an important osteopenia in their trabecular region, especially marked in the females. When we interrogated about the causes of this alteration, we found that mice at this age do not have any difference in the expression of osteoblastic genes in their femurs. However, the femurs of KO females did show an increase in the levels of osteoclastogenesis markers, having an increased ratio between *Rankl* and *Opg* expression. Furthermore, higher levels of the mRNAs of *Trap* and *Ctsk*, genes encoding two main osteoclastic enzymes, were also detected. In agreement with these data, there

were an increased number of osteoclasts in the trabeculae of KO females. Therefore, the osteopenia of these young animals seems to be due to a disbalance of bone remodelling, with bone resorption prevailing over bone creation (Figure 53). Furthermore, this imbalance must be maintained during the following months, for the bone loss is progressive and adult KO mice display a more severe osteopenia, with all the trabecular bone parameters dramatically affected in both sexes, and even a small reduction in the cortical bone volume of males. Nevertheless, at this age there was no difference neither in the osteoblastic nor the osteoclastic activity between genotypes.

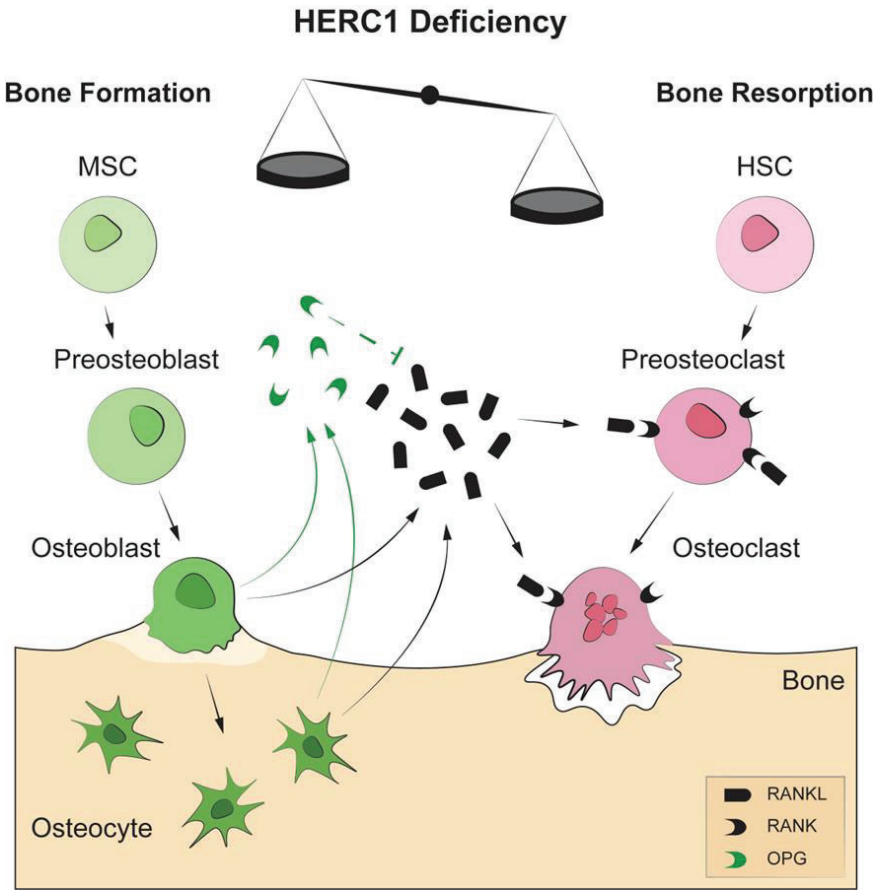

Figure 53. Schematic model of the role of HERC1 in bone remodelling. Osteoblasts and osteocytes produce RANKL, which then binds to its receptor (RANK) on the membranes of pre-osteoclasts/osteoclasts to increase osteoclastic differentiation and activation, resulting in bone resorption. Secreted OPG binds to RANKL, inhibiting RANK signalling and bone resorption. Femurs from *Herc1*-KO show increased *Rankl*/*Opg* ratio, causing an increase in osteoclast numbers that leads to osteopenia derived from the imbalance between bone formation and bone resorption. Abbreviations: HSC, hematopoietic stem cell; MSC, mesenchymal stem cells; OPG, osteoprotegerin; RANKL, RANK ligand; RANK, Receptor activator of nuclear factor κB.

The study of gene expression of osteocytes gave us another clue about how HERC1 depletion may regulate bone remodelling. Osteocytes are the orchestrators of this process, being responsible for the secretion of factors affecting osteoblast and osteoclast differentiation. Osteocytes from KO mice show greater expression of *Rankl* gene, while having a downregulation of *Opg*. Consequently, their paracrine action is presumably a potent inductor of osteoclastogenesis. Furthermore, this finding in cultured osteocytes proves that HERC1 affects the expression of these genes directly in these cells, and do not rely on an indirect regulation by modulating the secretion of other factors by other cell types.

The molecular mechanism proposed for the stimulation of osteogenesis by HERC1 depletion could also facilitate the enhanced osteoclastic activity. Both ERK and p38 MAPKs act as intermediates in the signalling cascades induced from M-CSF and RANKL, necessary for osteoclast differentiation and function[149,168,185–189,191,194]. Hence, their overactivation by the knock-out of *Herc1* may serve as a stimulator of osteoclastogenesis. Interestingly, the ablation of p38α in osteoclasts precursors mirrors the effects that *Herc1* knock-out has on osteoclastogenesis, but in the opposite direction: it decreases bone resorption at young age, but increases osteoclastogenesis in 6-months old mice[196]. This suggests that p38 activity may have age-dependent consequences in osteoclast function, and its constitutive overactivation by HERC1 loss could enhance osteoclastogenesis at 8 weeks of age, but repress it at 6 months, what would explain the changes in osteoclasts markers that we observe in *Herc1*-KO mice with aging. Nonetheless, more research is needed to assess whether there is a direct role of HERC1 in osteoclast biology.

Sex differences in the bone phenotype of young mice was also an intriguing discovery. Although both male and female KO mice develop a severe osteopenia at 32 weeks of age, this bone loss is started in females at a younger age. This made us wonder whether these differences could arise from alterations in sex hormones. Osteoporosis is a disease often related to deficiencies in androgen or estrogen signalling[336]. Furthermore, previous studies have shown that androgens suppress RANKL-induced osteoclast formation[347], that orchiectomy and androgen receptor deletions cause bone loss and that estrogens protect trabecular bone by promoting osteoclast apoptosis[348].

The KO mice did not show any alterations in estrogens levels. However, young females did have reduced circulating androgens. Given the protecting role of these hormones in bone architecture, this deficiency could explain at least some of the observed trabecular loss. Nevertheless, more studies directly aimed at unravelling the concrete role of androgens in our model and the molecular mechanisms by which HERC1 depletion downregulates their levels are necessary for confirming this hypothesis.

Bone is an organ with endocrine functions. Among the regulatory peptides produced by osteocytes, FGF23 is an important modulator of phosphate metabolism by its actions on kidney and the parathyroid gland[82]. Elevated circulating levels of FGF23 provoke the inhibition of phosphate transporters in the kidney, causing diseases like phosphaturia and hypophosphatemia[349]. With the parathyroid gland, FGF23 stablish a negative feedback loop: its signalling represses the expression of PTH, a hormone responsible for reacting to low levels of circulating calcium by of increasing its levels acting on bone and kidney. However, PTH action on bone also stimulates FGF23 production by the osteocytes (Figure 6)[82]. Higher levels of FGF23 in the blood have been linked to cardiovascular disease, being related to left ventricular hypertrophy, impaired vasoreactivity and increase arterial stiffness[350–352]. In the osteocytes from *Herc1*-KO mice, there is a significant upregulation of *Fgf23* gene. This suggest that loss of function of HERC1 could be a risk factor for renal and cardiovascular disease. Interestingly, a genome-wide association study identified a single nucleotide polymorphism in human *HERC1* gene (rs2228513) as a novel genetic marker for cardiovascular disease[353]. However, the residue affected by the change does not belong to any described domain and no functional evaluation has been reported[353].

Apart from the possible implication of HERC1 regulation of bone function in cardiovascular disease by the secretion of FGF23, other tissues may be also affected. Osteocytes are a source of NPY. This hormone has an important regulatory function on energy balance by the inhibition of the sympathetic stimulation of BAT, thus reducing energy expenditure[354]. It also controls feeding behaviour by modulating leptin signalling[355]. Furthermore, a study using a mouse conditional knock-out of *p38α* in the osteoblastic lineage found that these animals had reduced adiposity as a consequence of lower production of NPY by the bone[83]. Our results show that the osteocytes of

Herc1-KO mice have increased transcript levels of *Npy*. This suggests that the absence of HERC1 in osteocytes could affect energy balance by stimulating the production of NPY in the bone. Moreover, the study from Rodriguez-Carballo et al.[83] also suggests a molecular mechanism for this regulation of NPY expression by HERC1, as the loss of this ubiquitin ligase causes an overactivation of p38 through the stabilization of C-RAF protein[29]. The posterior results obtained in this thesis proving that *Herc1* knock-out does indeed cause an energy imbalance and increased adiposity by reducing energy expenditure make this line of investigation really promising, and further experiments should be performed to elucidate this relationship between bone and adipose phenotypes.

As a summary for this chapter, we have identified an important physiological role of HERC1 in bone homeostasis. Our data suggests that HERC1 is necessary for maintaining a correct balance in the process of bone remodelling by acting as a repressor of osteoclastogenesis. HERC1 could be a candidate for further evaluation in the efforts to identify the aetiology of osteopenia and related bone diseases like osteoporosis. Moreover, future research about the molecular mechanisms that mediate HERC1 regulation of bone mass is extremely interesting for the clinical implications that could arise from it. One example would be the confirmation of the role of MAPKs in HERC1 regulation of osteoclastic activity. In this case, specific inhibitors against these kinases could be good candidates for the treatment of HERC1-deficient patients with osteopenia. Some of them, like Sorafenib, have already been approved for humans and extensively used for the treatment of different cancers[356–358]. Furthermore, the regulation of bone homeostasis by HERC1 may affect other organs because of the endocrine functions that bone exerts, and these crosstalks should be further investigated.

III. HERC1 in energy balance

Obesity is characterized by an increased fat deposition provoked by sustained energy imbalance with energy intake prevailing over energy expenditure. This state is affected by a multitude of factors. Although many of them are related to the relationship of the individual with their environment, there is also a genetic basis, for

mutations in different genes have been related to an increased predisposition to obesity[294,359]. Alterations in these genes cause the dysregulation of energy balance by affecting food intake or one or more of the components of energy expenditure[290,359].

The relationship between HERC1 and energy balance had not been explored yet. The only evidence for the affectation of body mass by HERC1 alterations came from the study of the *tambaleante* mouse, which display a considerably reduced body weight[64]. Nevertheless, the aetiology of this was never addressed, and it is not clear whether it comes from energy disbalance or by other alterations affecting body size. The results regarding bone phenotype also suggested that energy balance and adipose tissue phenotype could be altered, due to the important regulatory crosstalk between these two tissues[83,316,338,354,355]. In this thesis, the first characterization of the role of HERC1 in the regulation of body mass is performed, and the results suggest that this ubiquitin ligase cooperates in the equilibrium of energy balance by the stimulation of energy expenditure in a sex-dependent manner. Hence, deficiency in HERC1 leads to increased body weight in females.

As stated before, changes in body mass are usually a consequence of metabolic alterations, and they can be easily measured in a non-invasive way. Therefore, *Herc1*-KO mice were systematically weighted every week. In this screening we soon realised that, although male mice showed an equal pattern of growth between genotypes, KO females started gaining weight faster than their WT littermates, until the differences were significative and easily noticeable. This evidence made us focus on the characterization of the female metabolic state. We discovered that these animals had reduced food intake but also reduced energy expenditure, and the energy balance seemed to be tilted towards a caloric surplus. The three main components of energy expenditure (locomotor activity, basal metabolic rate and adaptive thermogenesis) were then explored to search for the cause, and it was the thermogenetic activity of BAT what was clearly impaired in *Herc1*-KO females. Furthermore, this tissue showed a clear "whitening", with the fusion of lipid droplets, and a reduction in the expression of the thermogenic genes *Ucp1* and *Pgc1a*. Moreover, these brown adipocyte markers were also reduced in WAT depots, thus suggesting a repression of browning. Therefore, the depletion of HERC1 in female mice causes a decrease in the ability of generating heat

through adaptive thermogenesis, alteration that leads to a reduction of energy expenditure and tilts the energy balance towards caloric surplus (Figure 54).

Adaptive thermogenesis is a process mainly regulated by the adrenergic stimulation of the SNS under circumstances like cold exposure[281]. It has also been described that impairments in β-adrenergic signalling provoke the conversion of brown adipocytes to white-like unilocular cells[345]. The normal conditions in our animal facilities include maintaining a temperature between 22 and 24°C. However, this constitutes a mild cold environment for the animals, that hence have a slightly elevated sympathetic tone for maintaining a correct internal temperature[251]. Thus, the differences in thermogenesis, browning and BAT structure observed in KO females could be explained by a deficiency in the β-adrenergic signalling. This hypothesis was supported by the observation that the response of KO females to the stimulation with an agonist of the β3-adrenoreceptor was also reduced. Furthermore, the exposition of the mice to intense cold conditions at 4°C caused them a severe hypothermia, not being able to maintain neither scapular nor internal temperature. Altogether, these data show that *Herc1*-KO female mice are not able to properly stimulate thermogenesis via β-adrenergic signalling.

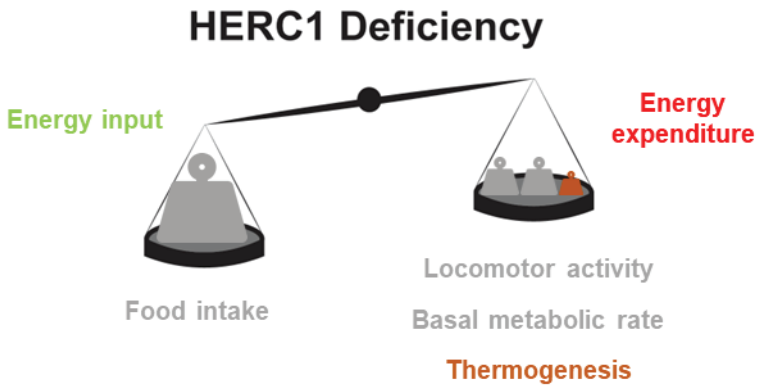

Figure 54. Schematic representation of the role of HERC1 deficiency in energy balance. Energy balance is the equilibrium between the energy input by the food intake, and the energy expenditure through locomotor activity, basal metabolic rate and adaptive thermogenesis. HERC1 deficiency provokes a reduction in the energy expenditure by thermogenesis, which inclines the balance towards caloric surplus.

The cellular regulation of β-adrenergic signalling is a plausible candidate to further investigate the molecular mechanisms altered by the depletion of HERC1. As

explained before, HERC1 has been linked to the regulation of MAPK pathways through the targeting of C-RAF for degradation[25,29]. Of them, p38 is a key modulator of the β-adrenergic signalling, being phosphorylated by PKA upon stimulation of the receptor, and acting as an enhancer of *UCP1* expression, thus activating browning and non-shivering thermogenesis[285,286,315]. Knock-down of HERC1 is described to cause a constitutive overactivation of p38[29], that is also observed in the BM-MSCs model (Figure 20). This would contradict the results showing that the absence of HERC1 leads to a repression of the thermal activity of the mice, since p38 overactivation is expected to stimulate the process. However, genetic studies in mice have found that the activation of different isoforms of p38 have distinct effects on BAT activity, since p38α deletion provokes an increase in the thermogenic programme, while p38δ phosphorylation rises energy expenditure through thermogenesis[360,361]. In fact, the authors of one of these works propose that p38α may block heat production in BAT by the inhibition of p38δ[361]. Another aspect of MAPK signalling cascades to consider is the fact that their activation must be finely regulated in a time-dependent manner. Hence, there are many works that show that both the loss and the prolonged phosphorylation of p38 and ERK MAPKs lead to the inhibition of cellular processes such as adipogenesis[305,306,309,310,362]. This could also be the case for thermogenesis, and the loss of HERC1 could be impairing the correct timely regulation of MAPK phosphorylation. Future experiments to elucidate the concrete isoforms of p38 affected by HERC1 regulation and the state of their phosphorylation during the whole process of non-shivering thermogenesis in the knock-out animals will be an interesting approach to unravel the role of HERC1 in energy balance.

III.1. HERC1 in white adipose tissue and metabolic health

Increased fat deposition by the sustained positive caloric balance is generally assumed by adipose tissues, that undergo structural and functional remodelling. The expansion of WATs by adipocyte hypertrophy allows the accumulation of TGs in their larger lipid droplets, but also impairs their functions. Thus, there is a positive correlation between adipocyte size and glucose intolerance, insulin resistance, hyperinsulinemia and inflammation of adipose tissue[363–366]. Furthermore, enlargement of visceral adipose depots has been related to more severe metabolic consequences that

the lipid accumulation in subcutaneous WAT. In fact, the distribution of fat deposition is considered a better marker for metabolic diseases than total fat mass[221,237].

The increases in body weight of KO female mice were proved to be due to increased adipose mass. Both iWAT and gWAT were enlarged but, while the expansion of the subcutaneous depot is mainly due to hyperplasia, the adipocytes in the visceral WAT presented light hypertrophy. Furthermore, iWAT showed a tendency for the increase of *Cebpa* expression, suggesting enhanced adipogenesis, and also for the increased production of leptin, indicating a good functioning of the endocrine action of this tissue for the control of energy homeostasis. This leptin overexpression could explain the reduction in food intake observed in the KO animals. Interestingly, BAT from KO females also showed increased levels of leptin, adding to a possible global hyperleptinemia in these animals. This adipokine is usually poorly expressed in BAT[266], but the whitening process that suffer this tissue due to HERC1 deficiency could stimulate the expression of white adipocyte genes, an hypothesis that should be thoroughly investigated in the future. On the other hand, the expression pattern of gWAT was more likely to support a malfunction of the tissue, for there was reduced levels of adiponectin, an insulin-sensitizer hormone, and of GLUT4. The deficiency in GLUT4 could suppose an impairment in the glucose uptake by this tissue due to insulin resistance.

Glucose intolerance and insulin resistance are hallmarks of the named metabolic syndrome, that is usually related to important risk factors such as obesity, dyslipidaemia, NAFLD or type 2 diabetes[297]. The overweight and the adipose phenotype of *Herc1*-KO females suggest that depletion of HERC1 could lead to these metabolic alterations. This hypothesis is supported by the presence of systemic glucose intolerance and insulin resistance in our model, together with the finding of some signs of dyslipidaemia with an increased concentration of circulating total lipids, and the detection of hepatic fat accumulation. Altogether, these results point to HERC1 as a sex-dependent regulator of metabolic health.

III.2. HERC1 and high-fat diet

The aforementioned results suggests that alterations in HERC1 could account for part of the genetic component of obesity and metabolic syndrome. However, the aetiology of these diseases is highly complex, and it is well known that environmental factors play an important role, and the interaction of the genotype with them is a key subject for study[294].

Diet-induced obesity (DIO) has been a standardized model for the study of obesity, adipose tissue remodelling and the metabolic complications related[367]. This approach has been used for the characterization of the role of many proteins in these processes[368,369]. For these reasons, we assessed how HERC1 deficiency affected the response of the mice to a high-fat diet. Our results show that DIO was importantly more severe in KO female mice that in their WT littermates, displaying a higher increase in body weight and inguinal and gonadal adipose mass. Furthermore, the pattern of gene expression in these tissues showed a clear alteration of metabolic health, especially in gWAT, where GLUT4 and adiponectin levels were dramatically reduced in the KO animals, suggesting a higher insulin resistance. Moreover, there was a consistent overexpression of leptin in all the adipose tissues, including WATs and BAT. Regarding this last tissue, the "whitening" induced by HFD was also enhanced by the absence of HERC1, although the expression of the genetic markers of thermogenesis were not changed. There was, however, a decrease in these markers in WATs, indicating that at least the browning process was more repressed in the KO females. Finally, the ectopic fat accumulation in the liver was also highly stimulated by the loss of HERC1, supporting the suggestion that HERC1 absence aggravates the consequences of DIO.

Despite not being affected in basal conditions, the stimulation of obesity by HFD also revealed a difference in body weight between WT and KO males. However, these differences were much smaller than the ones that we have described in females. In fact, they were not translated into an expansion of subcutaneous or gonadal adipose tissue depots, although they showed a reduction in the expression of the glucose transporter GLUT4, suggesting some type of metabolic alteration in males as well. In addition, the liver steatosis was also increased in male mice lacking HERC1.

Nevertheless, the expression of thermogenic markers was risen in the BAT and gWAT of KO males, a feature that should be further investigated. Hence, the knock-out of *Herc1* provokes alterations of DIO in both males and females, although there is still a strong sex-dependent component in this regulation.

IV. Final remarks on HERC1 physiological relevance

HERC1 has been thoroughly studied since 1996. At a cellular level, its activity has been related to the regulation of membrane trafficking through its interaction with phospholipids, CHC and ARF proteins, to migration and proliferation through the modulation of MAPK signalling and to the regulation of cell growth through the regulation of mTOR activity[9,11]. Physiologically, alterations of HERC1 have been linked to different types of cancers and neurological diseases[30,53]. In this thesis, we reveal the first evidence of HERC1 as a regulator of bone remodelling, energy balance and adipose tissue homeostasis.

As a final resume of this thesis, the results clearly show that HERC1 is necessary for bone and metabolic health in mice, and this postulates HERC1 as a good candidate for the study of the aetiology of diseases such as osteoporosis or obesity. The molecular mechanisms underlying this regulation are still to be elucidated, and hereinafter the use of complementary models will be useful for this research.

CONCLUSIONS

1. Downregulation of HERC1 stimulates osteoblastic differentiation of BM-MSCs *in vitro*.
2. Knock-out of *Herc1* gene causes progressive osteopenia in mice, starting at a younger age in females.
3. Osteopenia in *Herc1*-KO mice is caused by dysregulation of bone remodelling because of an increase in osteoclastogenesis.
4. HERC1 regulates gene expression in osteocytes in a cell autonomous way, and its deficiency leads to increased production of osteoclastic stimulators.
5. HERC1 deficiency causes overweight in female mice as a consequence of increased fat deposition.
6. Female mice lacking HERC1 have reduced energy expenditure and impaired adaptive thermogenesis.
7. *Herc1*-KO female mice display features of metabolic syndrome such as dyslipidaemia, hepatic fat accumulation and insulin resistance.
8. The absence of HERC1 aggravates diet-induced obesity.
9. There is an important sexual dimorphism in the physiological relevance of HERC1.

ADDENDUM

ADDENDUM RESULTS

During the course of the thesis, apart from the characterization of the bone and metabolic and adipose tissues phenotypes, we noticed other consequences of the knock-out of *Herc1* that affected the and survival of the mice and their cardiac phenotype. They are reported here for its interest for future investigation.

I. *Herc1*-KO mice have reduced survival

During the analysis of their phenotypes, all the mice were housed together, sharing the cage with their littermates. Although being subjected to the same conditions than WT mice and not reporting any clear difference in behaviour, *Herc1*-KO animals suffered spontaneous deaths at different ages, thus having reduced life expectancy than WT mice, that do not present mortality until the endpoint of the experiments. These deaths occurred in males and females with a similar proportion (Figure 55). Nonetheless, it was impossible to find the causes of these death by necropsy of the mice, so the mortality of *Herc1*-KO mice remains idiopathic and requires further research.

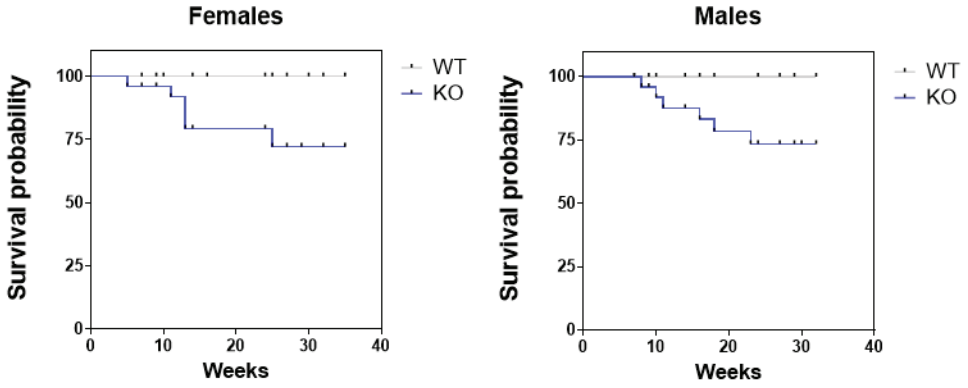

Figure 55. Survival of male and female WT and *Herc1*-KO mice. The Kaplan-Meier plots show the survival probability of WT and KO mice at any age until 35 weeks of age (n=48-53). Each step down is caused by a single death event. Abbreviations: KO, *Herc1*-knockout; WT, wild-type.

II. *Herc1*-KO male mice display ventricular atrophy

The spontaneous idiopathic deaths that suffer the KO mice made us explore other phenotypes that could explain these sudden phenomena, like alterations of the heart function. Heart failure (HF) is a chronic cardiovascular disease with a high prevalence, mortality and hospitalization rate in humans that is characterized by the imbalance between heart ability to pump blood and the organism necessities[370]. HF is preceded by ventricular remodelling, which is an alteration of cardiac structure and function as a result of myocardium response to a chronic pathologic stimulus[371]. Ventricular remodelling is a tightly regulated process, modulated by a plethora of molecular mechanisms. Interestingly, MAPK signalling and the ubiquitin-proteasome system (UPS) are among these mechanisms[372,373].

For studying the cardiac phenotype of the KO mice, animals were subjected to transthoracic echocardiography. We observed that females did not present any alterations in the septum and posterior walls of the ventricle (**Figure 56**A). However, male mice did show a significant reduction in the thickness of both the septum and the posterior walls, thus indicating ventricular atrophy that could be impairing the cardiac function (Figure 56B).

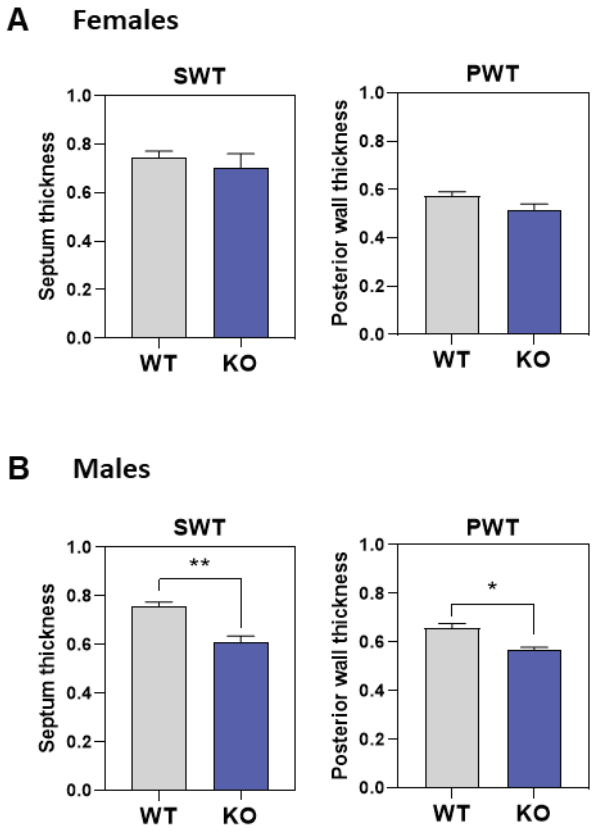

Figure 56. Septum and posterior wall thickness of the heart ventricle of WT and KO mice. A) Female and **(B)** male mice ventricles were measured by transthoracic echocardiography. Data (n = 4–8) are expressed as mean ± SEM. *p < 0.05; **p < 0.01; ***p < 0.001. Abbreviations: SWT, Septum wall thickness; PWT, Posterior wall thickness; KO, *Herc1*-knockout; WT, wild-type.

ADDENDUM DISCUSSION

At first, the severe affectations that *Herc1*-KO mice suffer regarding bone and metabolic phenotype were candidates for explaining the idiopathic mortality found in these animals. However, the sexual dimorphism found in these phenotypes was not correlated with the survival decline, as this seemed to be a sex-independent phenomenon. Reduced expression of HERC1 mRNAs had been linked before with reduced survival, but it was always related to oncological patients[49]. Nevertheless, we did not detect any tumour in any of the KO animals, at any life stage. In the search for a phenotype that could explain this reduced life expectancy, we found that *Herc1*-KO mice present a cardiac atrophy of the ventricular walls.

The relation of HERC1 alterations with cardiovascular disease is an unexplored field that is just now starting to be investigated. As explained before, there are some clues in the literature that point to HERC1 playing some role in heart function, since the single nucleotide polymorphism in human *HERC1* gene rs2228513 has been identified as a marker for cardiovascular disease[353]. In addition, the increase in *Fgf23* expression in *Herc1*-KO osteocytes is another factor that indicates a possible link between HERC1 deficiency and cardiovascular disease, because of the relationship between elevated FGF23 levels and cardiac alterations such as left ventricular hypertrophy, impaired vasoreactivity and increased arterial stiffness[350–352]. Furthermore, the components of the metabolic syndrome detected in the analysis of our mice also constitute a prevalent risk factor for the development of cardiovascular disease[374,375]. However, the results derived from the study of the heart phenotype of KO mice were intriguing. First, the cardiac atrophy is a phenomenon rarely described in the literature, although some works have found it linked to dysregulated autophagy[376], to cancer cachexia[377] or to the use of specific chemotherapies[378]. Most of the studies regarding cardiac dysfunction relate it with ventricular hypertrophy[379–382], including some of the works describing FGF23 role in cardiovascular disease[350]. Besides, sexual dimorphism appeared again, but in an opposite direction. The cardiac alterations in *Herc1*-KO mice were restricted to males, while females did not show any ventricular modification, despite presenting more severe alterations in bone and metabolic phenotypes than males.

Therefore, the causes of the alterations in ventricular morphology are still under investigation, as well as whether this phenomenon has any relation with the reduced life expectancy in the KO mice. Our hypothesis is that HERC1 could be necessary for the correct heart remodelling, and that deficiencies in HERC1 may difficult the expansion of the cardiomyocytes as a response to external stimuli.

BIBLIOGRAPHY

1. Komander, D. & Rape, M. The Ubiquitin Code. *Annu. Rev. Biochem.* **81**, 203–229 (2012).

2. Popovic, D., Vucic, D. & Dikic, I. Ubiquitination in disease pathogenesis and treatment. *Nat Med* **20**, 1242–1253 (2014).

3. Sluimer, J. & Distel, B. Regulating the human HECT E3 ligases. *Cell. Mol. Life Sci.* **75**, 3121–3141 (2018).

4. Buetow, L. & Huang, D. T. Structural insights into the catalysis and regulation of E3 ubiquitin ligases. *Nat Rev Mol Cell Biol* **17**, 626–642 (2016).

5. de Bie, P. & Ciechanover, A. Ubiquitination of E3 ligases: self-regulation of the ubiquitin system via proteolytic and non-proteolytic mechanisms. *Cell Death Differ* **18**, 1393–1402 (2011).

6. Scheffner, M. & Kumar, S. Mammalian HECT ubiquitin-protein ligases: Biological and pathophysiological aspects. *Biochimica et Biophysica Acta (BBA) - Molecular Cell Research* **1843**, 61–74 (2014).

7. Huibregtse, J. M., Sheneffer, M., Beaudenon, S. & Peter M., H. A family of proteins structurally and functionally related to the E6-AP ubiquitin-protein ligase. *Proc. Natl. Acad Sci USA* **92**, 2563–2567 (1995).

8. Streich, F. C. & Lima, C. D. Structural and Functional Insights to Ubiquitin-Like Protein Conjugation. *Annu. Rev. Biophys.* **43**, 357–379 (2014).

9. García-Cano, J., Martinez-Martinez, A., Sala-Gaston, J., Pedrazza, L. & Rosa, J. L. HERCing: Structural and Functional Relevance of the Large HERC Ubiquitin Ligases. *Front. Physiol.* **10**, 1014 (2019).

10. Marín, I. Animal HECT ubiquitin ligases: evolution and functional implications. *BMC Evol Biol* **10**, 56 (2010).

11. Sánchez-Tena, S., Cubillos-Rojas, M., Schneider, T. & Rosa, J. L. Functional and pathological relevance of HERC family proteins: a decade later. *Cell. Mol. Life Sci.* **73**, 1955–1968 (2016).

12. Hadjebi, O., Casas-Terradellas, E., Garcia-Gonzalo, F. R. & Rosa, J. L. The RCC1 superfamily: From genes, to function, to disease. *Biochimica et Biophysica Acta (BBA) - Molecular Cell Research* **1783**, 1467–1479 (2008).

13. Motoaki Otsubo *et al.* Isolation and characterization of the active cDNA.of the human cell cycle gene (RCC1) involved in the regulation of onset of chromosome condensation. *Genes & Dev.* **1**, 585–593 (1987).

14. Renault, L. *et al.* The 1.7 Å crystal structure of the regulator of chromosome condensation (RCC1) reveals a seven-bladed propeller. *Nature* **392**, 97–101 (1998).

15. Renault, L., Kuhlmann, J., Henkel, A. & Wittinghofer, A. Structural Basis for Guanine Nucleotide Exchange on Ran by the Regulator of Chromosome Condensation (RCC1). *Cell* **105**, 245–255 (2001).

16. Nemergt, M. E., Mizzen, C. A. & Allis, C. D. Chromatin Docking and Exchange Activity Enhancement of RCC1 by Histones H2A and H2B. **292**, 4 (2001).

17. Rosa, J. L., Casaroli-Marano, R. P., Buckler, A. J., Vilaro, S. & Barbacid, M. p619, a giant protein related to the chromosome condensation regulator RCC1, stimulates guanine nucleotide exchange on ARFi and Rab proteins. *EMBO J.* **15**, 4262–4273 (1996).

18. Cruz, C. *et al.* Assignment of the human P532 gene (HERC1) to chromosome 15q22 by fluorescence in situ hybridization. *Cytogenet Genome Res* **86**, 68–69 (1999).

19. Garcia-Gonzalo, F. R. & Rosa, J. L. The HERC proteins: functional and evolutionary insights. *CMLS, Cell. Mol. Life Sci.* **62**, 1826–1838 (2005).

20. Garcia-Gonzalo, F. R., Bartrons, R., Ventura, F. & Rosa, J. L. Requirement of phosphatidylinositol-4,5-bisphosphate for HERC1-mediated guanine nucleotide release from ARF proteins. *FEBS Letters* **579**, 343–348 (2005).

21. Rosa, J. L. & Barbacid, M. A giant protein that stimulates guanine nucleotide exchange on ARF1 and Rab proteins forms a cytosolic ternary complex with clathrin and Hsp70. *Oncogene* **15**, 1–6 (1997).

22. Garcia-Gonzalo, F. R. *et al.* The giant protein HERC1 is recruited to aluminum fluoride-induced actin-rich surface protrusions in HeLa cells. *FEBS Letters* **559**, 77–83 (2004).

23. Jacquemet, G. & Humphries, M. J. IQGAP1 is a key node within the small GTPase network. *Small GTPases* **4**, 199–207 (2013).

24. Schwarz, S. E., Rosa, J. L. & Scheffner, M. Characterization of Human hect Domain Family Members and Their Interaction with UbcH5 and UbcH7. *Journal of Biological Chemistry* **273**, 12148–12154 (1998).

25. Schneider, T. *et al.* The E3 ubiquitin ligase HERC1 controls the ERK signaling pathway targeting C-RAF for degradation. *Oncotarget* **9**, 31531–31548 (2018).

26. Lavoie, H. & Therrien, M. Regulation of RAF protein kinases in ERK signalling. *Nat Rev Mol Cell Biol* **16**, 281–298 (2015).

27. Dorard, C., Vucak, G. & Baccarini, M. Deciphering the RAS/ERK pathway *in vivo*. *Biochemical Society Transactions* **45**, 27–36 (2017).

28. Roberts, P. J. & Der, C. J. Targeting the Raf-MEK-ERK mitogen-activated protein kinase cascade for the treatment of cancer. *Oncogene* **26**, 3291–3310 (2007).

29. Pedrazza, L., Schneider, T., Bartrons, R., Ventura, F. & Rosa, J. L. The ubiquitin ligase HERC1 regulates cell migration via RAF-dependent regulation of MKK3/p38 signaling. *Sci Rep* **10**, 824 (2020).

30. Sala-Gaston, J. *et al.* HERC Ubiquitin Ligases in Cancer. *Cancers* **12**, 1653 (2020).

31. Zavodszky, E., Peak-Chew, S.-Y., Juszkiewicz, S., Narvaez, A. J. & Hegde, R. S. Identification of a quality-control factor that monitors failures during proteasome assembly. *Science* **373**, 998–1004 (2021).

32. Garcia-Gonzalo, F. R. *et al.* Interaction between HERC1 and M2-type pyruvate kinase. *FEBS Letters* **539**, 78–84 (2003).

33. Chong-Kopera, H. *et al.* TSC1 Stabilizes TSC2 by Inhibiting the Interaction between TSC2 and the HERC1 Ubiquitin Ligase. *Journal of Biological Chemistry* **281**, 8313–8316 (2006).

34. Orlova, K. A. & Crino, P. B. The tuberous sclerosis complex: Tuberous sclerosis complex. *Annals of the New York Academy of Sciences* **1184**, 87–105 (2010).

35. Diouf, B. *et al.* Somatic deletions of genes regulating MSH2 protein stability cause DNA mismatch repair deficiency and drug resistance in human leukemia cells. *Nat Med* **17**, 1298–1303 (2011).

36. Holloway, A., Simmonds, M., Azad, A., Fox, J. L. & Storey, A. Resistance to UV-induced apoptosis by β-HPV5 E6 involves targeting of activated BAK for proteolysis by recruitment of the HERC1 ubiquitin ligase: HERC1 mediates BAK degradation by E6. *Int. J. Cancer* **136**, 2831–2843 (2015).

37. Walz, C. *et al.* Atypical mRNA fusions in *PML-RARA* positive, *RARA-PML* negative acute promyelocytic leukemia. *Genes Chromosom. Cancer* NA-NA (2010) doi:10.1002/gcc.20757.

38. Opatz, S. *et al.* The clinical mutatome of core binding factor leukemia. *Leukemia* **34**, 1553–1562 (2020).

39. Neumann, M. *et al.* Mutational spectrum of adult T-ALL. *Oncotarget* **6**, 2754–2766 (2014).

40. Johansson, P. *et al.* SAMHD1 is recurrently mutated in T-cell prolymphocytic leukemia. *Blood Cancer Journal* **8**, 11 (2018).

41. Ping, Z. *et al. ERBB2* mutation is associated with a worse prognosis in patients with *CDH1* altered invasive lobular cancer of the breast. *Oncotarget* **7**, 80655–80663 (2016).

42. Craig, D. W. *et al.* Genome and Transcriptome Sequencing in Prospective Metastatic Triple-Negative Breast Cancer Uncovers Therapeutic Vulnerabilities. *Molecular Cancer Therapeutics* **12**, 104–116 (2013).

43. Rossi, F. A. *et al.* HERC1 Regulates Breast Cancer Cells Migration and Invasion. *Cancers* **13**, 1309 (2021).

44. Fan, X. *et al.* Genome profile in a extremely rare case of pulmonary sclerosing pneumocytoma presenting with diffusely-scattered nodules in the right lung. *Cancer Biology & Therapy* **19**, 13–19 (2018).

45. Zhu, D., Yang, D., Li, X. & Feng, F. Heterogeneous expression and biological function of SOX18 in osteosaroma. *J. Cell. Biochem.* **119**, 4184–4192 (2018).

46. Ali, M. S. *et al.* The Giant HECT E3 Ubiquitin Ligase HERC1 Is Aberrantly Expressed in Myeloid Related Disorders and It Is a Novel BCR-ABL1 Binding Partner. *Cancers* **13**, 341 (2021).

47. Quintás-Cardama, A. & Cortes, J. Molecular biology of bcr-abl1–positive chronic myeloid leukemia. *Blood* **113**, 1619–1630 (2009).

48. Uhlén, M. *et al.* Tissue-based map of the human proteome. *Science* **347**, 1260419 (2015).

49. Schneider, T. *et al.* Large HERCs Function as Tumor Suppressors. *Front. Oncol.* **9**, 524 (2019).

50. Chen, Z. *et al.* RNA-Associated Co-expression Network Identifies Novel Biomarkers for Digestive System Cancer. *Front. Genet.* **12**, 659788 (2021).

51. Yang, J. *et al.* Construction of circRNA-miRNA-mRNA network and identification of novel potential biomarkers for non-small cell lung cancer. *Cancer Cell Int* **21**, 611 (2021).

52. Guo, W. *et al.* NOTCH2NLA silencing inhibits ovarian carcinoma progression and oncogenic activity in vivo and in vitro. *Ann Transl Med* **9**, 1669–1669 (2021).

53. Pérez-Villegas, E. M. *et al.* The HERC proteins and the nervous system. *Seminars in Cell & Developmental Biology* (2021) doi:10.1016/j.semcdb.2021.11.017.

54. Ortega-Recalde, O. *et al.* Biallelic *HERC1* mutations in a syndromic form of overgrowth and intellectual disability: Biallelic *HERC1* mutations in a syndromic form. *Clin Genet* **88**, e1–e3 (2015).

55. Nguyen, L. S. *et al.* A nonsense variant in HERC1 is associated with intellectual disability, megalencephaly, thick corpus callosum and cerebellar atrophy. *Eur J Hum Genet* **24**, 455–458 (2016).

56. Utine, G. E. HERC1 mutations in idiopathic intellectual disability. *European Journal of Medical Genetics* 5 (2017).

57. Aggarwal, S., Bhowmik, A. D., Ramprasad, V. L., Murugan, S. & Dalal, A. A splice site mutation in *HERC1* leads to syndromic intellectual disability with macrocephaly and facial dysmorphism: Further delineation of the phenotypic spectrum. *Am. J. Med. Genet.* **170**, 1868–1873 (2016).

58. Schwarz, J. M. *et al.* A new homozygous HERC1 gain-of-function variant in MDFPMR syndrome leads to mTORC1 hyperactivation and reduced autophagy during cell catabolism. *Molecular Genetics and Metabolism* **131**, 126–134 (2020).

59. Hashimoto, R. *et al.* Whole-exome sequencing and neurite outgrowth analysis in autism spectrum disorder. *J Hum Genet* **61**, 199–206 (2016).

60. Lin, Y., Afshar, S., Rajadhyaksha, A. M., Potash, J. B. & Han, S. A Machine Learning Approach to Predicting Autism Risk Genes: Validation of Known Genes and Discovery of New Candidates. *Front. Genet.* **11**, 500064 (2020).

61. Wassef, M., Sotelo, C., Cholley, B., Brehier, A. & Thomasset, M. Cerebellar mutations affecting the postnatal survival of Purkinje cells in the mouse disclose a longitudinal pattern of differentially sensitive cells. *Developmental Biology* **124**, 379–389 (1987).

62. Rossi, F., Jankovski, A. & Sotelo, C. Target neuron controls the integrity of afferent axon phenotype: a study on the Purkinje cell-climbing fiber system in cerebellar mutant mice. *J. Neurosci.* **15**, 2040–2056 (1995).

63. Dusart, I., Guenet, J. L. & Sotelo, C. Purkinje cell death: Differences between developmental cell death and neurodegenerative death in mutant mice. *Cerebellum* **5**, 163–173 (2006).

64. Mashimo, T. *et al.* Progressive Purkinje Cell Degeneration in tambaleante Mutant Mice Is a Consequence of a Missense Mutation in HERC1 E3 Ubiquitin Ligase. *PLoS Genet* **5**, e1000784 (2009).

65. Porras-García, M. E., Ruiz, R., Pérez-Villegas, E. M. & Armengol, J. Á. Motor learning of mice lacking cerebellar Purkinje cells. *Front. Neuroanat.* **7**, (2013).

66. Bachiller, S. *et al.* The HERC1 E3 Ubiquitin Ligase is essential for normal development and for neurotransmission at the mouse neuromuscular junction. *Cell. Mol. Life Sci.* **72**, 2961–2971 (2015).

67. Ruiz, R., Pérez-Villegas, E. M., Bachiller, S., Rosa, J. L. & Armengol, J. A. HERC 1 Ubiquitin Ligase Mutation Affects Neocortical, CA3 Hippocampal and Spinal Cord Projection Neurons: An Ultrastructural Study. *Front. Neuroanat.* **10**, (2016).

68. Bachiller, S. *et al.* HERC1 Ubiquitin Ligase Is Required for Normal Axonal Myelination in the Peripheral Nervous System. *Mol Neurobiol* **55**, 8856–8868 (2018).

69. Pérez-Villegas, E. M. *et al.* Mutation of the HERC 1 Ubiquitin Ligase Impairs Associative Learning in the Lateral Amygdala. *Mol Neurobiol* **55**, 1157–1168 (2018).

70. Pérez-Villegas, E. M. *et al.* HERC1 Ubiquitin Ligase Is Required for Hippocampal Learning and Memory. *Front. Neuroanat.* **14**, 592797 (2020).

71. Montes-Fernández, M. A. *et al.* The HERC1 ubiquitin ligase regulates presynaptic membrane dynamics of central synapses. *Sci Rep* **10**, 12057 (2020).

72. Bradley, A. *et al.* The mammalian gene function resource: the international knockout mouse consortium. *Mamm Genome* **23**, 580–586 (2012).

73. Skarnes, W. C. *et al.* A conditional knockout resource for the genome-wide study of mouse gene function. *Nature* **474**, 337–342 (2011).

74. White, J. K. *et al.* Genome-wide Generation and Systematic Phenotyping of Knockout Mice Reveals New Roles for Many Genes. *Cell* **154**, 452–464 (2013).

75. https://www.mousephenotype.org/data/genes/MGI:2384589.

76. Clarke, B. Normal Bone Anatomy and Physiology. *CJASN* **3**, S131–S139 (2008).

77. Datta, H. K., Ng, W. F., Walker, J. A., Tuck, S. P. & Varanasi, S. S. The cell biology of bone metabolism. *Journal of Clinical Pathology* **61**, 577–587 (2008).

78. Florencio-Silva, R., Sasso, G. R. da S., Sasso-Cerri, E., Simões, M. J. & Cerri, P. S. Biology of Bone Tissue: Structure, Function, and Factors That Influence Bone Cells. *BioMed Research International* **2015**, 1–17 (2015).

79. Lee, N. K. & Karsenty, G. Reciprocal regulation of bone and energy metabolism. *Trends in Endocrinology & Metabolism* **19**, 161–166 (2008).

80. Karsenty, G. & Oury, F. Biology Without Walls: The Novel Endocrinology of Bone. *Annu. Rev. Physiol.* **74**, 87–105 (2012).

81. Oury, F. *et al.* Endocrine Regulation of Male Fertility by the Skeleton. *Cell* **144**, 796–809 (2011).

82. DiGirolamo, D. J., Clemens, T. L. & Kousteni, S. The skeleton as an endocrine organ. *Nat Rev Rheumatol* **8**, 674–683 (2012).

83. Rodríguez-Carballo, E. *et al.* p38α function in osteoblasts influences adipose tissue homeostasis. *FASEB j.* **29**, 1414–1425 (2015).

84. Shao, J. *et al.* Bone Regulates Glucose Metabolism as an Endocrine Organ through Osteocalcin. *International Journal of Endocrinology* **2015**, 1–9 (2015).

85. Sambrook, P. & Cooper, C. Osteoporosis. *Lancet* **367**, 2010–2018 (2006).

86. Meng Bao, C. L. *et al.* Advances in Bone Tissue Engineering. in *Regenerative Medicine and Tissue Engineering* (ed. Andrades, J. A.) (InTech, 2013). doi:10.5772/55916.

87. Cohen, A. *et al.* Assessment of trabecular and cortical architecture and mechanical competence of bone by high-resolution peripheral computed tomography: comparison with transiliac bone biopsy. *Osteoporos Int* **21**, 263–273 (2010).

88. Burr, D. B. & Akkus, O. Bone Morphology and Organization. in *Basic and Applied Bone Biology* 3–25 (Elsevier, 2014). doi:10.1016/B978-0-12-416015-6.00001-0.

89. Blair, H. C., Zaidi, M. & Schlesinger, P. H. Mechanisms balancing skeletal matrix synthesis and degradation. *Biochemical Journal* **364**, 329–341 (2002).

90. Brodsky, B. & Persikov, A. V. Molecular Structure of the Collagen Triple Helix. in *Advances in Protein Chemistry* vol. 70 301–339 (Elsevier, 2005).

91. Buehler, M. J. Molecular nanomechanics of nascent bone: fibrillar toughening by mineralization. *Nanotechnology* **18**, 295102 (2007).

92. Ricard-Blum, S. The Collagen Family. *Cold Spring Harbor Perspectives in Biology* **3**, a004978–a004978 (2011).

93. Vimalraj, S. Alkaline phosphatase: Structure, expression and its function in bone mineralization. *Gene* **754**, 144855 (2020).

94. Orimo, H. The Mechanism of Mineralization and the Role of Alkaline Phosphatase in Health and Disease. *J Nippon Med Sch* **77**, 4–12 (2010).

95. Rosset, E. M. & Bradshaw, A. D. SPARC/osteonectin in mineralized tissue. *Matrix Biology* **52–54**, 78–87 (2016).

96. Mizokami, A., Kawakubo-Yasukochi, T. & Hirata, M. Osteocalcin and its endocrine functions. *Biochemical Pharmacology* **132**, 1–8 (2017).

97. Otani, T. *et al.* The roles of osteocalcin in lipid metabolism in adipose tissue and liver. *Advances in Biological Regulation* **78**, 100752 (2020).

98. Staines, K. A., MacRae, V. E. & Farquharson, C. The importance of the SIBLING family of proteins on skeletal mineralisation and bone remodelling. *Journal of Endocrinology* **214**, 241–255 (2012).

99. Pittenger, M. F. *et al.* Multilineage Potential of Adult Human Mesenchymal Stem Cells. *Science* **284**, 143–147 (1999).

100. Almalki, S. G. & Agrawal, D. K. Key transcription factors in the differentiation of mesenchymal stem cells. *Differentiation* **92**, 41–51 (2016).

101. Saeed, H. *et al.* Mesenchymal stem cells (MSCs) as skeletal therapeutics–an update. *J Biomed Sci* **23**, 41 (2016).

102. Miller, S. C. Bone Lining Cells: Structure and Function. 11.

103. Franz-Odendaal, T. A., Hall, B. K. & Witten, P. E. Buried alive: How osteoblasts become osteocytes. *Dev. Dyn.* **235**, 176–190 (2006).

104. van Bezooijen, R. L. *et al.* Sclerostin Is an Osteocyte-expressed Negative Regulator of Bone Formation, But Not a Classical BMP Antagonist. *Journal of Experimental Medicine* **199**, 805–814 (2004).

105. Nakashima, T. *et al.* Evidence for osteocyte regulation of bone homeostasis through RANKL expression. *Nat Med* **17**, 1231–1234 (2011).

106. Bonewald, L. F. & Johnson, M. L. Osteocytes, mechanosensing and Wnt signaling. *Bone* **42**, 606–615 (2008).

107. Bonewald, L. F. The amazing osteocyte. *J Bone Miner Res* **26**, 229–238 (2011).

108. Asada, N. *et al.* Matrix-Embedded Osteocytes Regulate Mobilization of Hematopoietic Stem/Progenitor Cells. *Cell Stem Cell* **12**, 737–747 (2013).

109. Sato, M. *et al.* Osteocytes Regulate Primary Lymphoid Organs and Fat Metabolism. *Cell Metabolism* **18**, 749–758 (2013).

110. Ukita, M., Yamaguchi, T., Ohata, N. & Tamura, M. Sclerostin Enhances Adipocyte Differentiation in 3T3-L1 Cells. *J. Cell. Biochem.* **117**, 1419–1428 (2016).

111. Dallas, S. L., Prideaux, M. & Bonewald, L. F. The Osteocyte: An Endocrine Cell … and More. *Endocrine Reviews* **34**, 658–690 (2013).

112. Boyle, W. J., Simonet, W. S. & Lacey, D. L. Osteoclast differentiation and activation. *Nature* **423**, 337–342 (2003).

113. Bar-Shavit, Z. The osteoclast: A multinucleated, hematopoietic-origin, bone-resorbing osteoimmune cell. *J. Cell. Biochem.* **102**, 1130–1139 (2007).

114. Owen, R. & Reilly, G. C. In vitro Models of Bone Remodelling and Associated Disorders. *Front. Bioeng. Biotechnol.* **6**, 134 (2018).

115. Ducy, P., Zhang, R., Geoffroy, V., Ridall, A. L. & Karsenty, G. Osf2/Cbfa1: A Transcriptional Activator of Osteoblast Differentiation. *Cell* **89**, 747–754 (1997).

116. Nishio, Y. *et al.* Runx2-mediated regulation of the zinc finger Osterix/Sp7 gene. *Gene* **372**, 62–70 (2006).

117. Komori, T. *et al.* Targeted Disruption of Cbfa1 Results in a Complete Lack of Bone Formation owing to Maturational Arrest of Osteoblasts. 10.

118. Nakashima, K. & de Crombrugghe, B. Transcriptional mechanisms in osteoblast differentiation and bone formation. *Trends in Genetics* **19**, 458–466 (2003).

119. Ortuño, M. J., Susperregui, A. R. G., Artigas, N., Rosa, J. L. & Ventura, F. Osterix induces Col1a1 gene expression through binding to Sp1 sites in the bone enhancer and proximal promoter regions. *Bone* **52**, 548–556 (2013).

120. Marini, J. C. *et al.* Osteogenesis imperfecta. *Nat Rev Dis Primers* **3**, 17052 (2017).

121. Stein, G. S. & Lian, J. B. Molecular Mechanisms Mediating Proliferation/ Differentiation Interrelationships During Progressive Development of the Osteoblast Phenotype. **14**, 19 (1993).

122. Millán, J. L. & Whyte, M. P. Alkaline Phosphatase and Hypophosphatasia. *Calcif Tissue Int* **98**, 398–416 (2016).

123. Karsenty, G. Transcriptional Control of Skeletogenesis. *Annu. Rev. Genom. Hum. Genet.* **9**, 183–196 (2008).

124. Tu, Q., Valverde, P. & Chen, J. Osterix enhances proliferation and osteogenic potential of bone marrow stromal cells. *Biochemical and Biophysical Research Communications* **341**, 1257–1265 (2006).

125. Lee, M.-H., Kwon, T.-G., Park, H.-S., Wozney, J. M. & Ryoo, H.-M. BMP-2-induced Osterix expression is mediated by Dlx5 but is independent of Runx2. *Biochemical and Biophysical Research Communications* **309**, 689–694 (2003).

126. Nakashima, K. *et al.* The Novel Zinc Finger-Containing Transcription Factor Osterix Is Required for Osteoblast Differentiation and Bone Formation. *Cell* **108**, 17–29 (2002).

127. Sinha, K. M., Yasuda, H., Zhou, X. & deCrombrugghe, B. Osterix and NO66 Histone Demethylase Control the Chromatin of Osterix Target Genes During Osteoblast Differentiation: OSX AND NO66 CONTROL CHROMATIN ARCHITECTURE OF OSX TARGET GENES. *J Bone Miner Res* **29**, 855–865 (2014).

128. Baek, W.-Y., de Crombrugghe, B. & Kim, J.-E. Postnatally induced inactivation of Osterix in osteoblasts results in the reduction of bone formation and maintenance. *Bone* **46**, 920–928 (2010).

129. Frith, J. & Genever, P. Transcriptional Control of Mesenchymal Stem Cell Differentiation. *Transfus Med Hemother* **35**, 216–227 (2008).

130. Ryoo, H. M. *et al.* Stage-Specific Expression of Dlx-5 during Osteoblast Differentiation: Involvement in Regulation of Osteocalcin Gene Expression. **11**, 14 (1997).

131. Lee, M.-H. *et al.* Dlx5 Specifically Regulates Runx2 Type II Expression by Binding to Homeodomain-response Elements in the Runx2 Distal Promoter. *Journal of Biological Chemistry* **280**, 35579–35587 (2005).

132. Ulsamer, A. *et al.* BMP-2 Induces Osterix Expression through Up-regulation of Dlx5 and Its Phosphorylation by p38. *Journal of Biological Chemistry* **283**, 3816–3826 (2008).

133. Acampora, D. Craniofacial, vestibular and bone defects in mice lacking the Distal-lessrelated gene Dlx5. 15.

134. Lian, J. B. *et al.* Osteocalcin: Characterization and Regulated Expression of the Rat Gene. *Connective Tissue Research* **21**, 61–69 (1989).

135. Bellows, C. G., Reimers, S. M. & Heersche, J. N. M. Expression of mRNAs for type-I collagen, bone sialoprotein, osteocalcin, and osteopontin at different stages of osteoblastic differentiation and their regulation by 1,25 dihydroxyvitamin D. *Cell Tissue Res* **297**, 249 (1999).

136. Li, J., Zhang, H., Yang, C., Li, Y. & Dai, Z. An overview of osteocalcin progress. *J Bone Miner Metab* **34**, 367–379 (2016).

137. Komori, T. What is the function of osteocalcin? *Journal of Oral Biosciences* **62**, 223–227 (2020).

138. Feng, J. Q. *et al.* The Dentin Matrix Protein 1 (Dmp1) is Specifically Expressed in Mineralized, but not Soft, Tissues during Development. *J Dent Res* **82**, 776–780 (2003).

139. Qin, C., D'Souza, R. & Feng, J. Q. Dentin Matrix Protein 1 (DMP1): New and Important Roles for Biomineralization and Phosphate Homeostasis. *J Dent Res* **86**, 1134–1141 (2007).

140. Feng, J. Q. *et al.* Loss of DMP1 causes rickets and osteomalacia and identifies a role for osteocytes in mineral metabolism. *Nat Genet* **38**, 1310–1315 (2006).

141. Bonewald, L. F. & Wacker, M. J. FGF23 production by osteocytes. *Pediatr Nephrol* **28**, 563–568 (2013).

142. Shimada, T. *et al.* Targeted ablation of Fgf23 demonstrates an essential physiological role of FGF23 in phosphate and vitamin D metabolism. *J. Clin. Invest.* **113**, 561–568 (2004).

143. Poole, K. E. S. *et al.* Sclerostin is a delayed secreted product of osteocytes that inhibits bone formation. *FASEB j.* **19**, 1842–1844 (2005).

144. Semënov, M., Tamai, K. & He, X. SOST Is a Ligand for LRP5/LRP6 and a Wnt Signaling Inhibitor. *Journal of Biological Chemistry* **280**, 26770–26775 (2005).

145. Amrein, K. *et al.* Sclerostin and Its Association with Physical Activity, Age, Gender, Body Composition, and Bone Mineral Content in Healthy Adults. *The Journal of Clinical Endocrinology & Metabolism* **97**, 148–154 (2012).

146. Klangjareonchai, T. *et al.* Circulating Sclerostin and Irisin Are Related and Interact with Gender to Influence Adiposity in Adults with Prediabetes. *International Journal of Endocrinology* **2014**, 1–6 (2014).

147. Udagawa, N. *et al.* Osteoclast differentiation by RANKL and OPG signaling pathways. *J Bone Miner Metab* **39**, 19–26 (2021).

148. Ono, T. & Nakashima, T. Recent advances in osteoclast biology. *Histochem Cell Biol* **149**, 325–341 (2018).

149. Kong, Y.-Y. *et al.* OPGL is a key regulator of osteoclastogenesis, lymphocyte development and lymph-node organogenesis. *Nature* **397**, 315–323 (1999).

150. O'Brien, C. A. Control of RANKL gene expression. *Bone* **46**, 911–919 (2010).

151. Simonet, W. S. *et al.* Osteoprotegerin: A Novel Secreted Protein Involved in the Regulation of Bone Density. *Cell* **89**, 309–319 (1997).

152. Yasuda, H. *et al.* Identity of Osteoclastogenesis Inhibitory Factor (OCIF) and Osteoprotegerin (OPG): A Mechanism by which OPG/OCIF Inhibits Osteoclastogenesis in Vitro. **139**, 9 (1998).

153. Boyce, B. F. & Xing, L. Biology of RANK, RANKL, and osteoprotegerin. *Arthritis Res Ther* **9**, S1 (2007).

154. Hofbauer, L. C. Clinical Implications of the Osteoprotegerin/RANKL/RANK System for Bone and Vascular Diseases. *JAMA* **292**, 490 (2004).

155. Oddie, G. W. *et al.* Structure, function, and regulation of tartrate-resistant acid phosphatase. *Bone* **27**, 575–584 (2000).

156. Perez-Amodio, S. *et al.* Endogenous expression and endocytosis of tartrate-resistant acid phosphatase (TRACP) by osteoblast-like cells. *Bone* **36**, 1065–1077 (2005).

157. Nakamura, M., Aoyama, N., Yamaguchi, S. & Sasano, Y. Expression of tartrate-resistant acid phosphatase and cathepsin K during osteoclast differentiation in developing mouse mandibles. *Biomed. Res.* **42**, 13–21 (2021).

158. Hayman, A. R. Tartrate-resistant acid phosphatase (TRAP) and the osteoclast/immune cell dichotomy. *Autoimmunity* **41**, 218–223 (2008).

159. Burstone, M. S. HISTOCHEMICAL DEMONSTRATION OF ACID PHOSPHATASE ACTIVITY IN OSTEOCLASTS. *J Histochem Cytochem.* **7**, 39–41 (1959).

160. Hayman, A. R. *et al.* Mice lacking tartrate-resistant acid phosphatase (Acp 5) have disrupted endochondral ossification and mild osteopetrosis. 12.

161. Novinec, M. & Lenarčič, B. Cathepsin K: a unique collagenolytic cysteine peptidase. *Biological Chemistry* **394**, 1163–1179 (2013).

162. Lecaille, F., Brömme, D. & Lalmanach, G. Biochemical properties and regulation of cathepsin K activity. *Biochimie* **90**, 208–226 (2008).

163. Drake, F. H. *et al.* Cathepsin K, but Not Cathepsins B, L, or S, Is Abundantly Expressed in Human Osteoclasts. *Journal of Biological Chemistry* **271**, 12511–12516 (1996).

164. Troen, B. R. The Regulation of Cathepsin K Gene Expression. *Annals of the New York Academy of Sciences* **1068**, 165–172 (2006).

165. Motyckova, G. & Fisher, D. Pycnodysostosis: Role and Regulation of Cathepsin K in Osteoclast Function and Human Disease. *CMM* **2**, 407–421 (2002).

166. Gowen, M. *et al.* Cathepsin K Knockout Mice Develop Osteopetrosis Due to a Deficit in Matrix Degradation but Not Demineralization. *J Bone Miner Res* **14**, 1654–1663 (1999).

167. Greenblatt, M. B., Shim, J.-H. & Glimcher, L. H. Mitogen-Activated Protein Kinase Pathways in Osteoblasts. *Annu. Rev. Cell Dev. Biol.* **29**, 63–79 (2013).

168. Lee, K., Seo, I., Choi, M. & Jeong, D. Roles of Mitogen-Activated Protein Kinases in Osteoclast Biology. *IJMS* **19**, 3004 (2018).

169. Xiao, G. *et al.* MAPK Pathways Activate and Phosphorylate the Osteoblast-specific Transcription Factor, Cbfa1. *Journal of Biological Chemistry* **275**, 4453–4459 (2000).

170. Xiao, G., Jiang, D., Gopalakrishnan, R. & Franceschi, R. T. Fibroblast Growth Factor 2 Induction of the Osteocalcin Gene Requires MAPK Activity and Phosphorylation of the Osteoblast Transcription Factor, Cbfa1/Runx2. *Journal of Biological Chemistry* **277**, 36181–36187 (2002).

171. Ge, C. *et al.* Identification and Functional Characterization of ERK/MAPK Phosphorylation Sites in the Runx2 Transcription Factor. *Journal of Biological Chemistry* **284**, 32533–32543 (2009).

172. Artigas, N., Ureña, C., Rodríguez-Carballo, E., Rosa, J. L. & Ventura, F. Mitogen-activated Protein Kinase (MAPK)-regulated Interactions between Osterix and Runx2 Are Critical for the Transcriptional Osteogenic Program. *Journal of Biological Chemistry* **289**, 27105–27117 (2014).

173. Hu, E., Kim, J. B., Sarraf, P. & Spiegelman, B. M. Inhibition of Adipogenesis Through MAP Kinase-Mediated Phosphorylation of PPARγ. *Science* **274**, 2100–2103 (1996).

174. Ge, C. *et al.* Reciprocal Control of Osteogenic and Adipogenic Differentiation by ERK/MAP Kinase Phosphorylation of Runx2 and PPARγ Transcription Factors: MAPK CONTROL OF OSTEOGENESIS AND ADIPOGENESIS. *J. Cell. Physiol.* **231**, 587–596 (2016).

175. Matsushita, T. *et al.* Extracellular Signal-Regulated Kinase 1 (ERK1) and ERK2 Play Essential Roles in Osteoblast Differentiation and in Supporting Osteoclastogenesis. *Mol Cell Biol* **29**, 5843–5857 (2009).

176. Cuadrado, A. & Nebreda, A. R. Mechanisms and functions of p38 MAPK signalling. *Biochemical Journal* **429**, 403–417 (2010).

177. Rodríguez-Carballo, E., Gámez, B. & Ventura, F. p38 MAPK Signaling in Osteoblast Differentiation. *Front. Cell Dev. Biol.* **4**, (2016).

178. Greenblatt, M. B. *et al.* The p38 MAPK pathway is essential for skeletogenesis and bone homeostasis in mice. *J. Clin. Invest.* **120**, 2457–2473 (2010).

179. Ge, C. *et al.* Interactions between extracellular signal-regulated kinase 1/2 and P38 Map kinase pathways in the control of RUNX2 phosphorylation and transcriptional activity. *J Bone Miner Res* **27**, 538–551 (2012).

180. Ortuño, M. J. *et al.* p38 Regulates Expression of Osteoblast-specific Genes by Phosphorylation of Osterix. *Journal of Biological Chemistry* **285**, 31985–31994 (2010).

181. Czaplinska, D. *et al.* Phosphorylation of RSK2 at Tyr529 by FGFR2-p38 enhances human mammary epithelial cells migration. *Biochimica et Biophysica Acta (BBA) - Molecular Cell Research* **1843**, 2461–2470 (2014).

182. Siebel, A. *et al.* Contribution of S6K1/MAPK Signaling Pathways in the Response to Oxidative Stress: Activation of RSK and MSK by Hydrogen Peroxide. *PLoS ONE* **8**, e75523 (2013).

183. Yang, X. *et al.* ATF4 Is a Substrate of RSK2 and an Essential Regulator of Osteoblast Biology: Implication for Coffin-Lowry Syndrome. 12.

184. Rodríguez-Carballo, E. *et al.* The p38α MAPK Function in Osteoprecursors Is Required for Bone Formation and Bone Homeostasis in Adult Mice. *PLoS ONE* **9**, e102032 (2014).

185. Sherr, C. Colony-stimulating factor-1 receptor. *Blood* **75**, 1–12 (1990).

186. Mancini, A. *et al.* Identification of a second Grb2 binding site in the v-Fms tyrosine kinase. 8.

187. Weilbaecher, K. N. *et al.* Linkage of M-CSF Signaling to Mitf, TFE3, and the Osteoclast Defect in Mitfmi/mi Mice. *Molecular Cell* **8**, 749–758 (2001).

188. Bradley, E. W., Ruan, M. M. & Oursler, M. J. Novel Pro-survival Functions of the Kruppel-like Transcription Factor Egr2 in Promotion of Macrophage Colony-

stimulating Factor-mediated Osteoclast Survival Downstream of the MEK/ERK Pathway. *Journal of Biological Chemistry* **283**, 8055–8064 (2008).

189. Sundaram, K. *et al.* RANK ligand signaling modulates the matrix metalloproteinase-9 gene expression during osteoclast differentiation. *EXPERIMENTAL CELL RESEARCH* 11 (2007).

190. He, Y. *et al.* Erk1 Positively Regulates Osteoclast Differentiation and Bone Resorptive Activity. *PLoS ONE* **6**, e24780 (2011).

191. Matsumoto, M., Sudo, T., Saito, T., Osada, H. & Tsujimoto, M. Involvement of p38 Mitogen-activated Protein Kinase Signaling Pathway in Osteoclastogenesis Mediated by Receptor Activator of NF-κB Ligand (RANKL). *Journal of Biological Chemistry* **275**, 31155–31161 (2000).

192. Huang, H. *et al.* Osteoclast differentiation requires TAK1 and MKK6 for NFATc1 induction and NF-jB transactivation by RANKL. *Cell Death and Differentiation* **13**, 1879–1891 (2006).

193. Mansky, K. C., Sankar, U., Han, J. & Ostrowski, M. C. Microphthalmia Transcription Factor Is a Target of the p38 MAPK Pathway in Response to Receptor Activator of NF-κB Ligand Signaling. *Journal of Biological Chemistry* **277**, 11077–11083 (2002).

194. Matsumoto, M. *et al.* Essential Role of p38 Mitogen-activated Protein Kinase in Cathepsin K Gene Expression during Osteoclastogenesis through Association of NFATc1 and PU.1. *Journal of Biological Chemistry* **279**, 45969–45979 (2004).

195. Li, X. *et al.* p38 MAPK-Mediated Signals Are Required for Inducing Osteoclast Differentiation But Not for Osteoclast Function. *Endocrinology* **143**, 3105–3113 (2002).

196. Cong, Q. *et al.* p38α MAPK regulates proliferation and differentiation of osteoclast progenitors and bone remodeling in an aging-dependent manner. *Sci Rep* **7**, 45964 (2017).

197. Shen, J. *et al.* E3 Ubiquitin Ligase-Mediated Regulation of Osteoblast Differentiation and Bone Formation. *Front. Cell Dev. Biol.* **9**, 706395 (2021).

198. Sévère, N., Dieudonné, F.-X. & Marie, P. J. E3 ubiquitin ligase-mediated regulation of bone formation and tumorigenesis. *Cell Death Dis* **4**, e463–e463 (2013).

199. Zhao, M., Qiao, M., Oyajobi, B. O., Mundy, G. R. & Chen, D. E3 Ubiquitin Ligase Smurf1 Mediates Core-binding Factor α1/Runx2 Degradation and Plays A Specific Role in Osteoblast Differentiation. *Journal of Biological Chemistry* **278**, 27939–27944 (2003).

200. Zhao, M. *et al.* Smurf1 Inhibits Osteoblast Differentiation and Bone Formation in Vitro and in Vivo. *Journal of Biological Chemistry* **279**, 12854–12859 (2004).

201. Jones, D. C. *et al.* Regulation of Adult Bone Mass by the Zinc Finger Adapter Protein Schnurri-3. *Science* **312**, 1223–1227 (2006).

202. Li, X. *et al.* CHIP promotes Runx2 degradation and negatively regulates osteoblast differentiation. *Journal of Cell Biology* **181**, 959–972 (2008).

203. Thacker, G. *et al.* Skp2 inhibits osteogenesis by promoting ubiquitin–proteasome degradation of Runx2. *Biochimica et Biophysica Acta (BBA) - Molecular Cell Research* **1863**, 510–519 (2016).

204. Zhu, W. *et al.* The E3 ubiquitin ligase WWP2 facilitates RUNX2 protein transactivation in a mono-ubiquitination manner during osteogenic differentiation. *Journal of Biological Chemistry* **292**, 11178–11188 (2017).

205. Peng, Y. *et al.* Characterization of Osterix Protein Stability and Physiological Role in Osteoblast Differentiation. *PLoS ONE* **8**, e56451 (2013).

206. Xie, J. & Gu, J. Identification of C-terminal Hsp70-interacting protein as a mediator of tumour necrosis factor action in osteoblast differentiation by targeting osterix for degradation. *J. Cell. Mol. Med.* **19**, 1814–1824 (2015).

207. Choi, Y. H. *et al.* Cbl-b and c-Cbl negatively regulate osteoblast differentiation by enhancing ubiquitination and degradation of Osterix. *Bone* **75**, 201–209 (2015).

208. Hoshikawa, S. *et al.* Phosphorylation-dependent osterix degradation negatively regulates osteoblast differentiation. *FASEB j.* **34**, 14930–14945 (2020).

209. He, S. *et al.* LncRNA ODIRI inhibits osteogenic differentiation of hUC-MSCs through the FBXO25/H2BK120ub/H3K4me3/OSX axis. *Cell Death Dis* **10**, 947 (2019).

210. Kim, J. H. *et al.* Negative Feedback Control of Osteoclast Formation through Ubiquitin-mediated Down-regulation of NFATc1. *Journal of Biological Chemistry* **285**, 5224–5231 (2010).

211. Nakajima, A. *et al.* Loss of Cbl-b Increases Osteoclast Bone-Resorbing Activity and Induces Osteopenia. *Journal of Bone and Mineral Research* **24**, 1162–1172 (2009).

212. Purev, E., Neff, L., Horne, W. C. & Baron, R. c-Cbl and Cbl-b Act Redundantly to Protect Osteoclasts from Apoptosis and to Displace HDAC6 from □-Tubulin, Stabilizing Microtubules and Podosomes. *Molecular Biology of the Cell* **20**, 10 (2009).

213. Akiyama, T. Regulation of osteoclast apoptosis by ubiquitylation of proapoptotic BH3-only Bcl-2 family member Bim. *The EMBO Journal* **22**, 6653–6664 (2003).

214. Adapala, N. S. *et al.* The Loss of Cbl-Phosphatidylinositol 3-Kinase Interaction Perturbs RANKL-mediated Signaling, Inhibiting Bone Resorption and Promoting Osteoclast Survival. *Journal of Biological Chemistry* **285**, 36745–36758 (2010).

215. Lamothe, B. *et al.* TRAF6 ubiquitin ligase is essential for RANKL signaling and osteoclast differentiation. *Biochemical and Biophysical Research Communications* **359**, 1044–1049 (2007).

216. Zhou, J., Fujiwara, T., Ye, S., Li, X. & Zhao, H. Ubiquitin E3 Ligase LNX2 is Critical for Osteoclastogenesis In Vitro by Regulating M-CSF/RANKL Signaling and Notch2. *Calcif Tissue Int* **96**, 465–475 (2015).

217. Zhang, H. *et al.* Ubiquitin E3 Ligase Itch Negatively Regulates Osteoclast Formation by Promoting Deubiquitination of Tumor Necrosis Factor (TNF) Receptor-associated Factor 6. *Journal of Biological Chemistry* **288**, 22359–22368 (2013).

218. Zhang, Y. *et al.* Positional cloning of the mouse obese gene and its human homologue. *Nature* **372**, 425–431 (1994).

219. Trayhurn, P. & Beattie, J. H. Physiological role of adipose tissue: white adipose tissue as an endocrine and secretory organ. *Proc. Nutr. Soc.* **60**, 329–339 (2001).

220. Scheja, L. & Heeren, J. The endocrine function of adipose tissues in health and cardiometabolic disease. *Nat Rev Endocrinol* **15**, 507–524 (2019).

221. Lee, M.-J., Wu, Y. & Fried, S. K. Adipose tissue heterogeneity: Implication of depot differences in adipose tissue for obesity complications. *Molecular Aspects of Medicine* **34**, 1–11 (2013).

222. Lumish, H. S., O'Reilly, M. & Reilly, M. P. Sex Differences in Genomic Drivers of Adipose Distribution and Related Cardiometabolic Disorders: Opportunities for Precision Medicine. *ATVB* **40**, 45–60 (2020).

223. Carroll, J. F. *et al.* Visceral Fat, Waist Circumference, and BMI: Impact of Race/ethnicity. *Obesity* **16**, 600–607 (2008).

224. Frigolet, M. E. & Gutiérrez-Aguilar, R. The colors of adipose tissue. *GMM* **156**, 3932 (2020).

225. Ali, A. T., Hochfeld, W. E., Myburgh, R. & Pepper, M. S. Adipocyte and adipogenesis. *European Journal of Cell Biology* **92**, 229–236 (2013).

226. Crewe, C., An, Y. A. & Scherer, P. E. The ominous triad of adipose tissue dysfunction: inflammation, fibrosis, and impaired angiogenesis. *Journal of Clinical Investigation* **127**, 74–82 (2017).

227. Saely, C. H., Geiger, K. & Drexel, H. Brown versus White Adipose Tissue: A Mini-Review. *Gerontology* **58**, 15–23 (2012).

228. Fenzl, A. & Kiefer, F. W. Brown adipose tissue and thermogenesis. *Hormone Molecular Biology and Clinical Investigation* **19**, (2014).

229. Villarroya, F., Cereijo, R., Villarroya, J. & Giralt, M. Brown adipose tissue as a secretory organ. *Nat Rev Endocrinol* **13**, 26–35 (2017).

230. Giralt, M. & Villarroya, F. White, Brown, Beige/Brite: Different Adipose Cells for Different Functions? *Endocrinology* **154**, 2992–3000 (2013).

231. Cousin, B. *et al.* Occurrence of brown adipocytes in rat white adipose tissue: molecular and morphological characterization. *J Cell Sci* **103**, 931–942 (1992).

232. Barbatelli, G. *et al.* The emergence of cold-induced brown adipocytes in mouse white fat depots is determined predominantly by white to brown adipocyte transdifferentiation. *American Journal of Physiology-Endocrinology and Metabolism* **298**, E1244–E1253 (2010).

233. Lee, Y.-H., Petkova, A. P., Mottillo, E. P. & Granneman, J. G. In Vivo Identification of Bipotential Adipocyte Progenitors Recruited by β3-Adrenoceptor Activation and High-Fat Feeding. *Cell Metabolism* **15**, 480–491 (2012).

234. Rosenwald, M., Perdikari, A., Rülicke, T. & Wolfrum, C. Bi-directional interconversion of brite and white adipocytes. *Nat Cell Biol* **15**, 659–667 (2013).

235. Park, A. Distinction of white, beige and brown adipocytes derived from mesenchymal stem cells. *WJSC* **6**, 33 (2014).

236. Zwick, R. K., Guerrero-Juarez, C. F., Horsley, V. & Plikus, M. V. Anatomical, Physiological, and Functional Diversity of Adipose Tissue. *Cell Metabolism* **27**, 68–83 (2018).

237. Kwok, K. H. M., Lam, K. S. L. & Xu, A. Heterogeneity of white adipose tissue: molecular basis and clinical implications. *Exp Mol Med* **48**, e215–e215 (2016).

238. Rosen, E. D. & Spiegelman, B. M. What We Talk About When We Talk About Fat. *Cell* **156**, 20–44 (2014).

239. Tchkonia, T. *et al.* Mechanisms and Metabolic Implications of Regional Differences among Fat Depots. *Cell Metabolism* **17**, 644–656 (2013).

240. Ibrahim, M. M. Subcutaneous and visceral adipose tissue: structural and functional differences. *Obesity Reviews* **11**, 11–18 (2010).

241. Macotela, Y. *et al.* Intrinsic Differences in Adipocyte Precursor Cells From Different White Fat Depots. *Diabetes* **61**, 1691–1699 (2012).

242. Giordano, A., Smorlesi, A., Frontini, A., Barbatelli, G. & Cinti, S. White, brown and pink adipocytes: the extraordinary plasticity of the adipose organ. *European Journal of Endocrinology* **170**, R159–R171 (2014).

243. Nuttall, M. E. *et al.* Adipocytes and the Regulation of Bone Remodeling: A Balancing Act. *Calcif Tissue Int* **94**, 78–87 (2014).

244. Justesen, J. *et al.* Adipocyte tissue volume in bone marrow is increased with aging and in patients with osteoporosis. *Biogerontology* **2**, 165–171 (2001).

245. Horowitz, M. C. *et al.* Bone marrow adipocytes. *Adipocyte* **6**, 193–204 (2017).

246. Ghaben, A. L. & Scherer, P. E. Adipogenesis and metabolic health. *Nat Rev Mol Cell Biol* **20**, 242–258 (2019).

247. Lee, J.-E., Schmidt, H., Lai, B. & Ge, K. Transcriptional and Epigenomic Regulation of Adipogenesis. *Mol Cell Biol* **39**, e00601-18 (2019).

248. Huang, H. *et al.* BMP signaling pathway is required for commitment of C3H10T1/2 pluripotent stem cells to the adipocyte lineage. *Proc. Natl. Acad. Sci. U.S.A.* **106**, 12670–12675 (2009).

249. Sarjeant, K. & Stephens, J. M. Adipogenesis. *Cold Spring Harbor Perspectives in Biology* **4**, a008417–a008417 (2012).

250. Cereijo, R., Giralt, M. & Villarroya, F. Thermogenic brown and beige/brite adipogenesis in humans. *Annals of Medicine* **47**, 169–177 (2015).

251. Jung, S. M., Sanchez-Gurmaches, J. & Guertin, D. A. Brown Adipose Tissue Development and Metabolism. in *Brown Adipose Tissue* (eds. Pfeifer, A., Klingenspor, M. & Herzig, S.) vol. 251 3–36 (Springer International Publishing, 2018).

252. Puigserver, P. *et al.* A Cold-Inducible Coactivator of Nuclear Receptors Linked to Adaptive Thermogenesis. *Cell* **92**, 829–839 (1998).

253. Seale, P. *et al.* Transcriptional Control of Brown Fat Determination by PRDM16. *Cell Metabolism* **6**, 38–54 (2007).

254. Seale, P. *et al.* PRDM16 controls a brown fat/skeletal muscle switch. *Nature* **454**, 961–968 (2008).

255. Seale, P. *et al.* Prdm16 determines the thermogenic program of subcutaneous white adipose tissue in mice. *J Clin Invest* **121**, 96–105 (2011).

256. Bronnikov, G., Houstěk, J. & Nedergaard, J. Beta-adrenergic, cAMP-mediated stimulation of proliferation of brown fat cells in primary culture. Mediation via beta 1 but not via beta 3 adrenoceptors. *Journal of Biological Chemistry* **267**, 2006–2013 (1992).

257. Rosen, E. D. & Spiegelman, B. M. Adipocytes as regulators of energy balance and glucose homeostasis. **444**, 847–853 (2006).

258. Luo, L. & Liu, M. Adipose tissue in control of metabolism. *Journal of Endocrinology* 23 (2016).

259. Song, Z., Xiaoli, A. & Yang, F. Regulation and Metabolic Significance of De Novo Lipogenesis in Adipose Tissues. *Nutrients* **10**, 1–22 (2018).

260. Endemann, G. *et al.* CD36 is a receptor for oxidized low density lipoprotein. *Journal of Biological Chemistry* **268**, 11811–11816 (1993).

261. Wu, Q. *et al.* FATP1 Is an Insulin-Sensitive Fatty Acid Transporter Involved in Diet-Induced Obesity. *Mol Cell Biol* **26**, 3455–3467 (2006).

262. Jocken, J. W. E. & Blaak, E. E. Catecholamine-induced lipolysis in adipose tissue and skeletal muscle in obesity. *Physiology & Behavior* **94**, 219–230 (2008).

263. Fruhbeck, G., Mendez-Gimenez, L., Fernandez-Formoso, J.-A., Fernandez, S. & Rodrıguez, A. Regulation of adipocyte lipolysis. *Nutr. Res. Rev.* **27**, 63–93 (2014).

264. Jaworski, K., Sarkadi-Nagy, E., Duncan, R. E., Ahmadian, M. & Sul, H. S. Regulation of Triglyceride Metabolism.IV. Hormonal regulation of lipolysis in adipose tissue. *American Journal of Physiology-Gastrointestinal and Liver Physiology* **293**, G1–G4 (2007).

265. Qiao, L., Kinney, B., Schaack, J. & Shao, J. Adiponectin Inhibits Lipolysis in Mouse Adipocytes. *Diabetes* **60**, 1519–1527 (2011).

266. Gavaldà-Navarro, A., Villarroya, J., Cereijo, R., Giralt, M. & Villarroya, F. The endocrine role of brown adipose tissue: An update on actors and actions. *Rev Endocr Metab Disord* **23**, 31–41 (2022).

267. Fasshauer, M. & Blüher, M. Adipokines in health and disease. *Trends Pharmacol Sci* **36**, 461–470 (2015).

268. Boden, G., Chen, X., Mozzoli, M. & Ryan, I. Effect of fasting on serum leptin in normal human subjects. *J. Clin. Endocrinol. Metab.* **81**, 3419–3423 (1996).

269. Cowley, M. A. *et al.* Leptin activates anorexigenic POMC neurons through a neural network in the arcuate nucleus. *Nature* **411**, 480–484 (2001).

270. Friedman, J. The long road to leptin. *Journal of Clinical Investigation* **126**, 4727–4734 (2016).

271. Fischer, A. W., Cannon, B. & Nedergaard, J. Leptin: Is It Thermogenic? *Endocrine Reviews* **41**, 232–260 (2020).

272. Marroquí, L. *et al.* Role of leptin in the pancreatic β-cell: effects and signaling pathways. *Journal of Molecular Endocrinology* **49**, 9–17 (2012).

273. Moschos, S., Chan, J. L. & Mantzoros, C. S. Leptin and reproduction: a review. *Fertility and Sterility* **77**, 433–444 (2002).

274. Pérez-Pérez, A. *et al.* Role of leptin in female reproduction. *Clinical Chemistry and Laboratory Medicine (CCLM)* **53**, (2015).

275. Chen, X. X. & Yang, T. Roles of leptin in bone metabolism and bone diseases. *J Bone Miner Metab* **33**, 474–485 (2015).

276. Fang, H. & Judd, R. L. Adiponectin Regulation and Function. in *Comprehensive Physiology* (ed. Terjung, R.) 1031–1063 (Wiley, 2018). doi:10.1002/cphy.c170046.

277. Xin, X., Zhou, L., Reyes, C. M., Liu, F. & Dong, L. Q. APPL1 mediates adiponectin-stimulated p38 MAPK activation by scaffolding the TAK1-MKK3-p38 MAPK pathway. *American Journal of Physiology-Endocrinology and Metabolism* **300**, 103–110 (2011).

278. Deepa, S. S. *et al.* APPL1 Mediates Adiponectin-Induced LKB1 Cytosolic Localization Through the PP2A-PKCζ Signaling Pathway. *Molecular Endocrinology* **25**, 1773–1785 (2011).

279. Yamauchi, T. *et al.* Targeted disruption of AdipoR1 and AdipoR2 causes abrogation of adiponectin binding and metabolic actions. *Nat Med* **13**, 332–339 (2007).

280. Ryu, J. *et al.* APPL1 Potentiates Insulin Sensitivity by Facilitating the Binding of IRS1/2 to the Insulin Receptor. *Cell Reports* **7**, 1227–1238 (2014).

281. Lowell, B. B. & Spiegelman, B. M. Towards a molecular understanding of adaptive thermogenesis. *Nature* **404**, 652–660 (2000).

282. Townsend, K. L. & Tseng, Y.-H. Brown fat fuel utilization and thermogenesis. *Trends in Endocrinology & Metabolism* **25**, 168–177 (2014).

283. Mukherjee, S. & Ghosh, A. Molecular mechanism of mitochondrial respiratory chain assembly and its relation to mitochondrial diseases. *Mitochondrion* **53**, 1–20 (2020).

284. Mottillo, E. P. *et al.* Coupling of lipolysis and de novo lipogenesis in brown, beige, and white adipose tissues during chronic β3-adrenergic receptor activation. *Journal of Lipid Research* **55**, 2276–2286 (2014).

285. Cao, W., Medvedev, A. V., Daniel, K. W. & Collins, S. β-Adrenergic Activation of p38 MAP Kinase in Adipocytes. *Journal of Biological Chemistry* **276**, 27077–27082 (2001).

286. Cao, W. *et al.* p38 Mitogen-Activated Protein Kinase Is the Central Regulator of Cyclic AMP-Dependent Transcription of the Brown Fat Uncoupling Protein 1 Gene. *Mol Cell Biol* **24**, 3057–3067 (2004).

287. Barneda, D. *et al.* The brown adipocyte protein CIDEA promotes lipid droplet fusion via a phosphatidic acid-binding amphipathic helix. *eLife* **4**, e07485 (2015).

288. Son, Y. *et al.* Development of CIDEA reporter mouse model and its application for screening thermogenic drugs. *Sci Rep* **11**, 18429 (2021).

289. Hill, J. O., Wyatt, H. R. & Peters, J. C. Energy Balance and Obesity. *Circulation* **126**, 126–132 (2012).

290. Spiegelman, B. M. & Flier, J. S. Obesity and the Regulation of Energy Balance. *Cell* **104**, 531–543 (2001).

291. Johannsen, D. L. & Ravussin, E. Spontaneous physical activity: relationship between fidgeting and body weight control. *Current Opinion in Endocrinology, Diabetes & Obesity* **15**, 409–415 (2008).

292. Hulbert, A. J. & Else, P. L. Basal Metabolic Rate: History, Composition, Regulation, and Usefulness. *Physiological and Biochemical Zoology* **77**, 869–876 (2004).

293. López, M., Alvarez, C. V., Nogueiras, R. & Diéguez, C. Energy balance regulation by thyroid hormones at central level. *Trends in Molecular Medicine* **19**, 418–427 (2013).

294. González-Muniesa, P. *et al.* Obesity. *Nat Rev Dis Primers* **3**, 17034 (2017).

295. Okorodudu, D. O. *et al.* Diagnostic performance of body mass index to identify obesity as defined by body adiposity: a systematic review and meta-analysis. *Int J Obes* **34**, 791–799 (2010).

296. Blüher, M. Obesity: global epidemiology and pathogenesis. *Nat Rev Endocrinol* **15**, 288–298 (2019).

297. O'Neill, S. & O'Driscoll, L. Metabolic syndrome: a closer look at the growing epidemic and its associated pathologies. *Obes Rev* **16**, 1–12 (2015).

298. Lee, S.-H., Park, S.-Y. & Choi, C. S. Insulin Resistance: From Mechanisms to Therapeutic Strategies. *Diabetes Metab J* **46**, 15–37 (2022).

299. Greenfield, J. R. & Campbell, L. V. Insulin resistance and obesity. *Clinics in Dermatology* **22**, 289–295 (2004).

300. Longo, M. *et al.* Adipose Tissue Dysfunction as Determinant of Obesity-Associated Metabolic Complications. *IJMS* **20**, 2358 (2019).

301. Lair, B., Laurens, C., Van Den Bosch, B. & Moro, C. Novel Insights and Mechanisms of Lipotoxicity-Driven Insulin Resistance. *IJMS* **21**, 6358 (2020).

302. Bost, F., Aouadi, M., Caron, L. & Binétruy, B. The role of MAPKs in adipocyte differentiation and obesity. *Biochimie* **87**, 51–56 (2005).

303. Leiva, M., Matesanz, N., Pulgarín-Alfaro, M., Nikolic, I. & Sabio, G. Uncovering the Role of p38 Family Members in Adipose Tissue Physiology. *Front. Endocrinol.* **11**, 572089 (2020).

304. Sale, E. M., Atkinson, P. G. & Sale, G. J. Requirement of MAP kinase for differentiation of fibroblasts to adipocytes, for insulin activation of p90 S6 kinase and for insulin or serum stimulation of DNA synthesis. *The EMBO Journal* **14**, 674–684 (1995).

305. Prusty, D., Park, B.-H., Davis, K. E. & Farmer, S. R. Activation of MEK/ERK Signaling Promotes Adipogenesis by Enhancing Peroxisome Proliferator-activated Receptor γ (PPARγ) and C/EBPα Gene Expression during the Differentiation of 3T3-L1 Preadipocytes. *Journal of Biological Chemistry* **277**, 46226–46232 (2002).

306. Bost, F. *et al.* The Extracellular Signal–Regulated Kinase Isoform ERK1 Is Specifically Required for In Vitro and In Vivo Adipogenesis. *Diabetes* **54**, 402–411 (2005).

307. Carlson, C. J., Koterski, S., Sciotti, R. J., Poccard, G. B. & Rondinone, C. M. Enhanced Basal Activation of Mitogen-Activated Protein Kinases in Adipocytes From Type 2 Diabetes. *Diabetes* **52**, 634–641 (2003).

308. Tang, Q.-Q., Otto, T. C. & Lane, M. D. Mitotic clonal expansion: A synchronous process required for adipogenesis. *Proc. Natl. Acad. Sci. U.S.A.* **100**, 44–49 (2003).

309. Engelman, J. A., Lisanti, M. P. & Scherer, P. E. Specific Inhibitors of p38 Mitogen-activated Protein Kinase Block 3T3-L1 Adipogenesis. *Journal of Biological Chemistry* **273**, 32111–32120 (1998).

310. Aouadi, M. *et al.* p38MAP Kinase activity is required for human primary adipocyte differentiation. *FEBS Letters* **581**, 5591–5596 (2007).

311. Wang, X. & Ron, D. Stress-Induced Phosphorylation and Activation of the Transcription Factor CHOP (GADDI 53) by p38 MAP Kinase. *Science* **272**, 1347–1349 (1996).

312. Aouadi, M. *et al.* Inhibition of p38MAPK Increases Adipogenesis From Embryonic to Adult Stages. *Diabetes* **55**, 281–289 (2006).

313. Brunmeir, R. *et al.* Comparative Transcriptomic and Epigenomic Analyses Reveal New Regulators of Murine Brown Adipogenesis. *PLoS Genet* **12**, e1006474 (2016).

314. Whittle, A. J. *et al.* BMP8B Increases Brown Adipose Tissue Thermogenesis through Both Central and Peripheral Actions. *Cell* **149**, 871–885 (2012).

315. Xue, B., Coulter, A., Rim, J. S., Koza, R. A. & Kozak, L. P. Transcriptional Synergy and the Regulation of Ucp1 during Brown Adipocyte Induction in White Fat Depots. *MOL. CELL. BIOL.* **25**, 12 (2005).

316. Aparisi Gómez, M. P. *et al.* Fat and bone: the multiperspective analysis of a close relationship. *Quant Imaging Med Surg* **10**, 1614–1635 (2020).

317. Floyd, Z. E. & Stephens, J. M. Controlling a master switch of adipocyte development and insulin sensitivity: Covalent modifications of PPARγ. *Biochimica et Biophysica Acta (BBA) - Molecular Basis of Disease* **1822**, 1090–1095 (2012).

318. Hauser, S. *et al.* Degradation of the Peroxisome Proliferator-activated Receptor Is Linked to Ligand-dependent Activation. *J. Biol. Chem.* **275**, 18527–18533 (2000).

319. Lee, J. M. *et al.* The E3 ubiquitin ligase TRIM25 regulates adipocyte differentiation via proteasome-mediated degradation of PPARγ. *Exp Mol Med* **50**, 1–11 (2018).

320. Li, J. J. *et al.* Ubiquitin Ligase NEDD4 Regulates PPARγ Stability and Adipocyte Differentiation in 3T3-L1 Cells. *Sci Rep* **6**, 1–14 (2016).

321. Bengoechea-Alonso, M. T. & Ericsson, J. The ubiquitin ligase Fbxw7 controls adipocyte differentiation by targeting C/EBPα for degradation. *Proc. Natl. Acad. Sci. U.S.A.* **107**, 11817–11822 (2010).

322. Pal, P. *et al.* E3 Ubiquitin Ligase E6AP Negatively Regulates Adipogenesis by Downregulating Proadipogenic Factor C/EBPalpha. *PLoS ONE* **8**, e65330 (2013).

323. Willemsen, N., Arigoni, I., Studencka-Turski, M., Krüger, E. & Bartelt, A. Proteasome dysfunction disrupts adipogenesis and induces inflammation via ATF3. *Molecular Metabolism* **62**, 101518 (2022).

324. Dasuri, K. *et al.* Proteasome alterations during adipose differentiation and aging: links to impaired adipocyte differentiation and development of oxidative stress. *Free Radical Biology and Medicine* **51**, 1727–1735 (2011).

325. Wei, P., Pan, D., Mao, C. & Wang, Y.-X. RNF34 Is a Cold-Regulated E3 Ubiquitin Ligase for PGC-1α and Modulates Brown Fat Cell Metabolism. *Mol Cell Biol* **32**, 266–275 (2012).

326. Wang, Q. *et al.* Post-translational control of beige fat biogenesis by PRDM16 stabilization. *Nature* **609**, 151–158 (2022).

327. Wing, S. S. The UPS in diabetes and obesity. *BMC Biochem* **9**, S6 (2008).

328. The Jackson Laboratory - Quick DNA purification protocol.

329. Diaz Marin, R., Crespo-Garcia, S., Wilson, A. M. & Sapieha, P. RELi protocol: Optimization for protein extraction from white, brown and beige adipose tissues. *MethodsX* **6**, 918–928 (2019).

330. Galarraga, M. *et al.* Adiposoft: automated software for the analysis of white adipose tissue cellularity in histological sections. *Journal of Lipid Research* **53**, 2791–2796 (2012).

331. Shum, M., Zhou, Z. & Liesa, M. Determining Basal Energy Expenditure and the Capacity of Thermogenic Adipocytes to Expend Energy in Obese Mice. *JoVE* 63066 (2021) doi:10.3791/63066.

332. Even, P. C., Mokhtarian, A. & Pele, A. Practical aspects of indirect calorimetry in laboratory animals. *Neuroscience & Biobehavioral Reviews* **18**, 435–447 (1994).

333. Sánchez-de-Diego, C. *et al.* Glucose Restriction Promotes Osteocyte Specification by Activating a PGC-1α-Dependent Transcriptional Program. *iScience* **15**, 79–94 (2019).

334. Moffat, J. *et al.* A Lentiviral RNAi Library for Human and Mouse Genes Applied to an Arrayed Viral High-Content Screen. *Cell* **124**, 1283–1298 (2006).

335. Cubillos-Rojas, M. *et al.* Tris-Acetate Polyacrylamide Gradient Gels for the Simultaneous Electrophoretic Analysis of Proteins of Very High and Low Molecular Mass. in *Electrophoretic Separation of Proteins* vol. 1855 269–277 (Springer New York, 2019).

336. Khosla, S. & Monroe, D. G. Regulation of Bone Metabolism by Sex Steroids. *Cold Spring Harb Perspect Med* **8**, a031211 (2018).

337. Wei, Y. & Sun, Y. Aging of the Bone. in *Aging and Aging-Related Diseases* (ed. Wang, Z.) vol. 1086 189–197 (Springer Singapore, 2018).

338. Zhang, Y., Zhang, C., Wang, J., Liu, H. & Wang, M. Bone-Adipose Tissue Crosstalk: Role of Adipose Tissue Derived Extracellular Vesicles in Bone Diseases. *J Cell Physiol* **236**, 7874–7886 (2021).

339. Hardy, T., Oakley, F., Anstee, Q. M. & Day, C. P. Nonalcoholic Fatty Liver Disease: Pathogenesis and Disease Spectrum. *Annu. Rev. Pathol. Mech. Dis.* **11**, 451–496 (2016).

340. Iezzoni, J. C. Diagnostic histochemistry in hepatic pathology. *Seminars in Diagnostic Pathology* **35**, 381–389 (2018).

341. Recena Aydos, L. *et al.* Nonalcoholic Fatty Liver Disease Induced by High-Fat Diet in C57bl/6 Models. *Nutrients* **11**, 3067 (2019).

342. Alberts, B. *et al. Biology of the Cell. Chapter: Studying Gene Expression and Function*. (Garland Science, 2002).

343. Rowe, D. W. *et al.* Screening Gene Knockout Mice for Variation in Bone Mass: Analysis by µCT and Histomorphometry. *Curr Osteoporos Rep* **16**, 77–94 (2018).

344. Agudelo, L. Z. *et al.* Kynurenic Acid and Gpr35 Regulate Adipose Tissue Energy Homeostasis and Inflammation. *Cell Metabolism* **27**, 378-392.e5 (2018).

345. Kotzbeck, P. *et al.* Brown adipose tissue whitening leads to brown adipocyte death and adipose tissue inflammation. *Journal of Lipid Research* **59**, 784–794 (2018).

346. https://www.mousephenotype.org. https://www.mousephenotype.org.

347. Huber, D. M. *et al.* Androgens Suppress Osteoclast Formation Induced by RANKL and Macrophage-Colony Stimulating Factor. *Endocrinology* **142**, 3800–3808 (2001).

348. Manolagas, S. C., O'Brien, C. A. & Almeida, M. The role of estrogen and androgen receptors in bone health and disease. *Nat Rev Endocrinol* **9**, 699–712 (2013).

349. Arnold, A. *et al.* Hormonal regulation of biomineralization. *Nat Rev Endocrinol* **17**, 261–275 (2021).

350. Faul, C. *et al.* FGF23 induces left ventricular hypertrophy. *J. Clin. Invest.* **121**, 4393–4408 (2011).

351. Ky, B. *et al.* FGF23 Modifies the Relationship Between Vitamin D and Cardiac Remodeling. *Circ: Heart Failure* **6**, 817–824 (2013).

352. Mirza, M. A. I., Larsson, A., Lind, L. & Larsson, T. E. Circulating fibroblast growth factor-23 is associated with vascular dysfunction in the community. *Atherosclerosis* **205**, 385–390 (2009).

353. Kraus, W. E. *et al.* Metabolomic Quantitative Trait Loci (mQTL) Mapping Implicates the Ubiquitin Proteasome System in Cardiovascular Disease Pathogenesis. *PLoS Genet* **11**, e1005553 (2015).

354. Shi, Y.-C. *et al.* Arcuate NPY Controls Sympathetic Output and BAT Function via a Relay of Tyrosine Hydroxylase Neurons in the PVN. *Cell Metabolism* **17**, 236–248 (2013).

355. Kageyama, H. *et al.* Neuronal circuits involving neuropeptide Y in hypothalamic arcuate nucleus-mediated feeding regulation. *Neuropeptides* **46**, 285–289 (2012).

356. Gentile, M. *et al.* Sorafenib for the treatment of multiple myeloma. *Expert Opinion on Investigational Drugs* **25**, 743–749 (2016).

357. Bronte, G. *et al.* Sorafenib for the treatment of breast cancer. *Expert Opinion on Pharmacotherapy* **18**, 621–630 (2017).

358. Gounder, M. M. *et al.* Sorafenib for Advanced and Refractory Desmoid Tumors. *N Engl J Med* **379**, 2417–2428 (2018).

359. Singh, R. K., Kumar, P. & Mahalingam, K. Molecular genetics of human obesity: A comprehensive review. *Comptes Rendus Biologies* **340**, 87–108 (2017).

360. Zhang, S. *et al.* Metabolic benefits of inhibition of p38α in white adipose tissue in obesity. *PLoS Biol* **16**, e2004225 (2018).

361. Matesanz, N. *et al.* p38α blocks brown adipose tissue thermogenesis through p38δ inhibition. *PLoS Biol* **16**, e2004455 (2018).

362. Ferguson, B. S., Nam, H., Stephens, J. M. & Morrison, R. F. Mitogen-Dependent Regulation of DUSP1 Governs ERK and p38 Signaling During Early 3T3-L1 Adipocyte Differentiation. *J. Cell. Physiol* **231**, 1562–1574 (2016).

363. Reilly, S. M. & Saltiel, A. R. Adapting to obesity with adipose tissue inflammation. *Nat Rev Endocrinol* **13**, 633–643 (2017).

364. Strissel, K. J. *et al.* Adipocyte Death, Adipose Tissue Remodeling, and Obesity Complications. *Diabetes* **56**, 2910–2918 (2007).

365. Skurk, T., Alberti-Huber, C., Herder, C. & Hauner, H. Relationship between Adipocyte Size and Adipokine Expression and Secretion. *The Journal of Clinical Endocrinology & Metabolism* **92**, 1023–1033 (2007).

366. Weyer, C., Foley, J. E., Bogardus, C., Tataranni, P. A. & Pratley, R. E. Enlarged subcutaneous abdominal adipocyte size, but not obesity itself, predicts Type II diabetes independent of insulin resistance. *Diabetologia* **43**, 1498–1506 (2000).

367. Hariri, N. & Thibault, L. High-fat diet-induced obesity in animal models. *Nutr. Res. Rev.* **23**, 270–299 (2010).

368. Xu, L. *et al.* SGLT2 Inhibition by Empagliflozin Promotes Fat Utilization and Browning and Attenuates Inflammation and Insulin Resistance by Polarizing M2 Macrophages in Diet-induced Obese Mice. *EBioMedicine* **20**, 137–149 (2017).

369. Teijeiro, A., Garrido, A., Ferre, A., Perna, C. & Djouder, N. Inhibition of the IL-17A axis in adipocytes suppresses diet-induced obesity and metabolic disorders in mice. *Nat Metab* **3**, 496–512 (2021).

370. Ziaeian, B. & Fonarow, G. C. Epidemiology and aetiology of heart failure. *Nat Rev Cardiol* **13**, 368–378 (2016).

371. Konstam, M. A., Kramer, D. G., Patel, A. R., Maron, M. S. & Udelson, J. E. Left Ventricular Remodeling in Heart Failure. *JACC: Cardiovascular Imaging* **4**, 98–108 (2011).

372. Muslin, A. J. MAPK signalling in cardiovascular health and disease: molecular mechanisms and therapeutic targets. *Clinical Science* **115**, 203–218 (2008).

373. Pagan, J., Seto, T., Pagano, M. & Cittadini, A. Role of the Ubiquitin Proteasome System in the Heart. *Circ Res* **112**, 1046–1058 (2013).

374. Lasheras, J. *et al.* Gene expression profiling in hearts of diabetic mice uncovers a potential role of estrogen-related receptor γ in diabetic cardiomyopathy. *Molecular and Cellular Endocrinology* **430**, 77–88 (2016).

375. Tune, J. D., Goodwill, A. G., Sassoon, D. J. & Mather, K. J. Cardiovascular consequences of metabolic syndrome. *Translational Research* **183**, 57–70 (2017).

376. Vanhoutte, D. *et al.* Thbs1 induces lethal cardiac atrophy through PERK-ATF4 regulated autophagy. *Nat Commun* **12**, 3928 (2021).

377. Murphy, K. T. The pathogenesis and treatment of cardiac atrophy in cancer cachexia. *American Journal of Physiology-Heart and Circulatory Physiology* **310**, H466–H477 (2016).

378. Xia, P. *et al.* Doxorubicin induces cardiomyocyte apoptosis and atrophy through cyclin-dependent kinase 2–mediated activation of forkhead box O1. *Journal of Biological Chemistry* **295**, 4265–4276 (2020).

379. Inserte, J. *et al.* Left ventricular hypertrophy in rats with biliary cirrhosis. *Hepatology* **38**, 589–598 (2003).

380. Aluja, D. *et al.* Calpains mediate isoproterenol-induced hypertrophy through modulation of GRK2. *Basic Res Cardiol* **114**, 21 (2019).

381. Yáñez-Bisbe, L. *et al.* Aging Impairs Reverse Remodeling and Recovery of Ventricular Function after Isoproterenol-Induced Cardiomyopathy. *IJMS* **23**, 174 (2021).

382. Aluja, D., Delgado-Tomás, S., Ruiz-Meana, M., Barrabés, J. A. & Inserte, J. Calpains as Potential Therapeutic Targets for Myocardial Hypertrophy. *IJMS* **23**, 4103 (2022).